


POSTLAUNCH REPORT FOR
APOLLO MISSION A-101 (u)
(BP-13)

TO UNCLASSIFIED
CLASSIFICATION CHANGE
By authority of *DDJ - E9 116*
Changed by *DDJ - E9 116*
Classified Document Master Control Station, NASA
Scientific and Technical Information Facility
Date *11/1/72*

CLASSIFIED DOCUMENT - TITLE UNCLASSIFIED

NATIONAL AERONAUTICS AND SPACE ADMINISTRATION
MANNED SPACECRAFT CENTER
HOUSTON, TEXAS
June 18, 1964

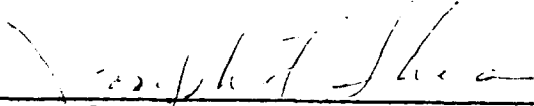


POSTLAUNCH REPORT FOR

APOLLO MISSION A-101

(BP-13)

Approved for Distribution:




Dr. Joseph F. Shea
Manager, Apollo Spacecraft Program Office

NATIONAL AERONAUTICS AND SPACE ADMINISTRATION

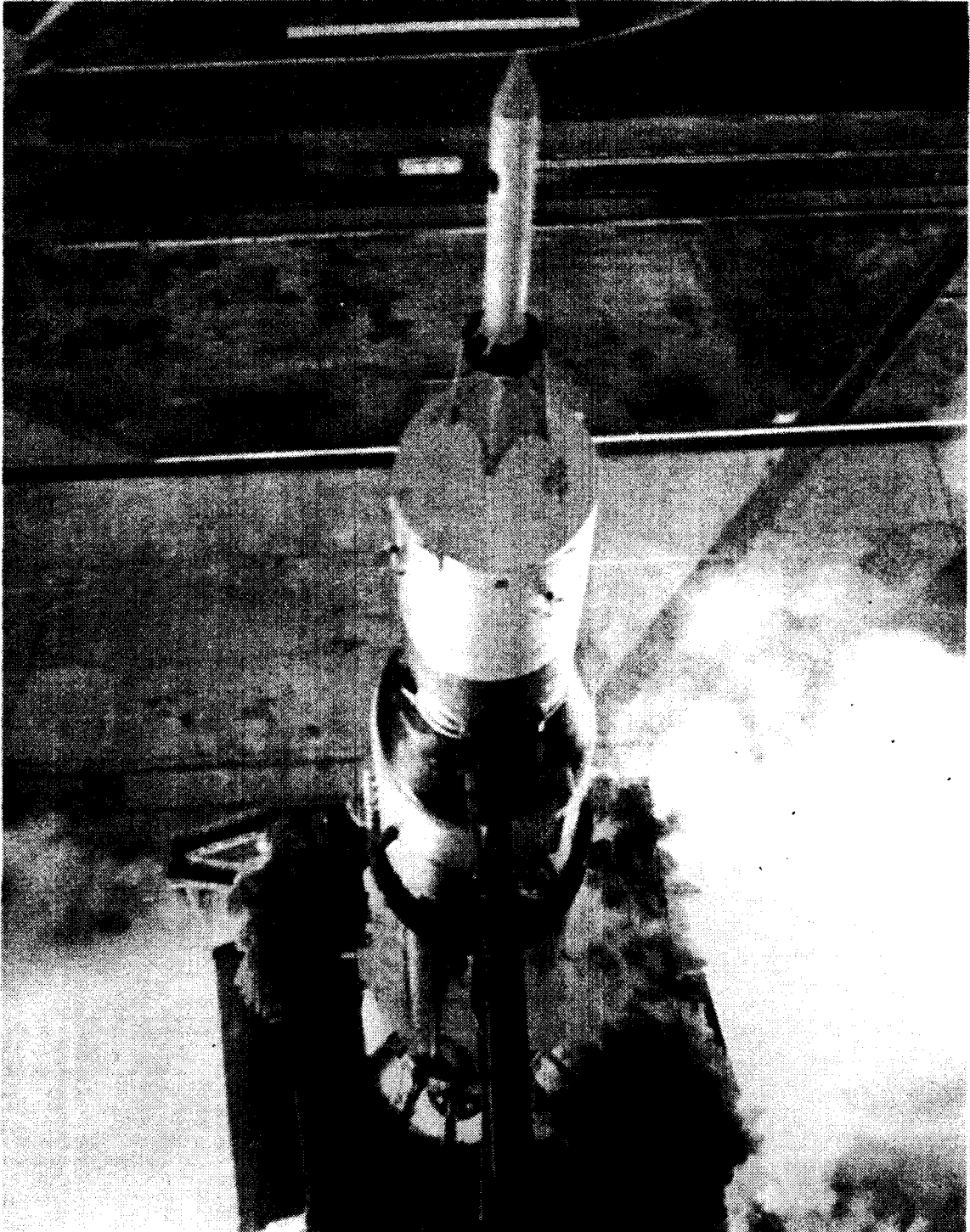
MANNED SPACECRAFT CENTER

HOUSTON, TEXAS

JUNE 18, 1964



10



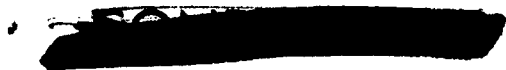
Apollo spacecraft BP-13 at time of Saturn SA-6 ignition.

CONTENTS

Section	Page
FRONTISPIECE	i
ABBREVIATIONS AND SYMBOLS	v
TABLES	viii
FIGURES	ix
1.0 SUMMARY	1-1
2.0 INTRODUCTION	2-1
3.0 FLIGHT TRAJECTORY	3-1
4.0 SPACECRAFT DESCRIPTION AND PERFORMANCE	4-1
4.1 Spacecraft Description	4-1
4.2 Instrumentation	4-13
4.3 Communications	4-34
4.4 Electrical and Sequential	4-39
4.5 Propulsion and Pyrotechnics	4-44
4.6 Structures	4-50
4.7 Heat Protection	4-111
4.8 Aerothermodynamics	4-114
4.9 Equipment Cooling	4-134
4.10 Acoustics	4-143
5.0 LAUNCH VEHICLE DESCRIPTION AND PERFORMANCE	5-1
6.0 MISSION OPERATIONS	6-1
6.1 Prelaunch Operations	6-1
6.2 Launch Operations	6-15




Section	Page
6.3 Range Operations	6-20
6.4 Data Coverage and Availability	6-24
7.0 CONCLUDING REMARKS	7-1
8.0 REFERENCES	8-1



ABBREVIATIONS AND SYMBOLS

Abbreviations


ATO	Apollo Test and Operations
BP	boilerplate
BW	bandwidth
cal	calorimeter
CM	command module
DOD	Department of Defense
EBW	exploding bridgewire
ECS	environmental control subsystem
EMI	electromagnetic interference
ETR	Eastern Test Range
g.e.t.	ground elapsed time
G.m.t.	Greenwich mean time
GSE	ground support equipment
GSFC	Goddard Space Flight Center
IECO	inboard engine cutoff (S-I stage)
IU	instrument unit (Saturn vehicle)
KSC	John F. Kennedy Space Center
LES	launch escape subsystem
LH ₂	liquid hydrogen
lox	liquid oxygen
MISTRAM	missile trajectory measurement
MSC	Manned Spacecraft Center
MSFC	Marshall Space Flight Center
OECO	outboard engine cutoff (S-I stage)
OSPPO	Operations Support, Plans, and Programs Office (MSC Florida Operations)
OTP	Operational Test Procedure
prf	pulse repetition frequency
PSD	power spectral density




PSTL-1	Static and fluctuating pressure wind-tunnel test model (0.055 scale) of Saturn SA-6 launch vehicle with Apollo spacecraft
RCS	reaction control subsystem
RF	radio frequency
RFI	radio frequency interference
RMS	root-mean-square
SA	Saturn-Apollo
SAD	special adapter devices
SM	service module
SMD	special measuring device
s/s	samples per second
S-I	Saturn launch vehicle first stage
S-IV	Saturn launch vehicle second stage

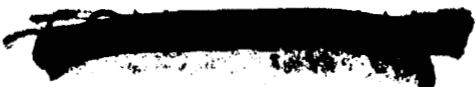
Symbols

F	flight day
g	gravitational constant
I_{XX}	moment of inertia around the X-axis, slug-ft ²
I_{YY}	moment of inertia around the Y-axis, slug-ft ²
I_{ZZ}	moment of inertia around the Z-axis, slug-ft ²
M	Mach number
p	pressure, lb/sq in.
q	dynamic pressure, lb/sq ft
q_{max}	maximum dynamic pressure, lb/sq ft
\dot{q}	heat flux, Btu/ft ² /sec
Re_D	Reynolds number, based on maximum body diameter D
T	launch time, sec
X	longitudinal axis of the spacecraft and launch vehicle
X_A	longitudinal location, referenced to the overall spacecraft, in. (fig. 4.1-3)





X_C	longitudinal location, referenced to the command module, in. (fig. 4.1-3)
X_L	longitudinal location, referenced to the launch escape subsystem, in. (fig. 4.1-3)
X_{LV}	longitudinal location, referenced to the launch vehicle S-I stage, in. (fig. 4.1-3)
X_S	longitudinal location, referenced to the service module, in. (fig. 4.1-3)
Y	plane of the Y-axis passes through the X-axis and is perpendicular to the plane of the Z-axis, in. (fig. 4.1-2)
Z	plane of the Z-axis passes through the X-axis and through the center of the CM hatch and of fins I and III of the SA-6 launch vehicle, in. (fig. 4.1-2)
α	angle of attack, deg
αq	product of angle of attack and dynamic pressure, (deg) (lb/sq ft)
ΔP	Q-ball pressure measurement
ϕ	angular clockwise distance from +Z looking aft (fig. 4.1-2)



TABLES

Table		Page
3.0-I	MISSION EVENT TIMES	3-3
3.0-II	COMPARISON OF PLANNED AND ACTUAL TRAJECTORY PARAMETERS	3-4
4.1-I	SPACECRAFT BP-13 MASS CHARACTERISTICS	4-4
4.2-I	APOLLO MISSION A-101 MEASUREMENTS REQUIREMENTS SUMMARY	4-16
4.2-II	MEASUREMENT LIST FOR BOILERPLATE 13	4-17
4.2-III	FLIGHT EQUIPMENT FOR BP-13 SPACECRAFT INSTRUMENTATION SUBSYSTEM	4-26
4.3-I	TELEMETRY RF PACKAGE	4-37
4.6-I	FLIGHT LOADS COMPARISON	4-61
4.9-I	COOLING SUBSYSTEM PARAMETERS	4-137
4.9-II	DIRECT CURRENT SUMMARY	4-138
6.1-I	OPERATIONAL TEST PROCEDURES AT DOWNEY (ATO)	6-5
6.1-II	OPERATIONAL TEST PROCEDURE AT FLORIDA OPERATIONS	6-7
6.3-I	TELEMETRY COVERAGE	6-22
6.3-II	C-BAND RADAR COVERAGE	6-23
6.4-I	DATA AVAILABILITY	6-27

FIGURES

Figure		Page
2.0-1	Saturn-Apollo space vehicle for mission A-101 at lift-off	2-3
2.0-2	Sequence of major events for Apollo mission A-101 . .	2-4
3.0-1	Ground track for the Apollo A-101 orbital mission for the first three orbital passes	3-6
3.0-2	Altitude-longitude profile for Apollo mission A-101 for the first three orbital passes	3-7
3.0-3	Time histories of trajectory parameters for the Apollo mission A-101 launch phase	
	(a) Altitude and range	3-8
	(b) Space-fixed velocity and flight-path angle . . .	3-9
	(c) Earth-fixed velocity and flight-path angle . . .	3-10
	(d) Dynamic pressure and Mach number	3-11
	(e) Longitudinal acceleration along spacecraft X-axis	3-12
3.0-4	Time histories of trajectory parameters for Apollo mission A-101 for first three passes of orbital phase	
	(a) Latitude, longitude, and altitude	3-13
	(b) Space-fixed velocity and flight-path angle . . .	3-14
4.1-1	Apollo BP-13 spacecraft	4-5
4.1-2	Y- and Z-axis and angular coordinate system used for designating locations within the BP-13 spacecraft. .	4-6
4.1-3	X-axis systems used for designating longitudinal locations of BP-13 spacecraft and SA-6 launch vehicle	4-7
4.1-4	Launch escape subsystem for BP-13 spacecraft	4-8

Figure		Page
4.1-5	Command module interior equipment layout for BP-13 spacecraft (view through hatch).	4-9
4.1-6	Command module interior equipment layout (view to right of hatch)	4-10
4.1-7	Command module exterior of BP-13 spacecraft	4-11
4.1-8	Cutaway view of BP-13 spacecraft service module, insert, and adapter	4-12
4.2-1	Instrumentation and communications subsystems on BP-13 spacecraft	4-27
4.2-2	Locations of vibration, acoustic, and acceleration transducers for BP-13 spacecraft	4-28
4.2-3	Strain gage locations on BP-13 spacecraft	4-29
4.2-4	Fluctuating pressure transducer locations on BP-13 spacecraft	4-30
4.2-5	Static pressure locations in the command module on BP-13 spacecraft	4-31
4.2-6	Heat-flux calorimeter locations on BP-13 spacecraft. .	4-32
4.2-7	Launch-escape tower temperature transducer locations on BP-13 spacecraft	4-34
4.3-1	Location of telemetry transmitters and C-band transponders on BP-13 spacecraft	4-37
4.3-2	Location of telemetry omniantenna on command module of BP-13 spacecraft	4-38
4.4-1	Electrical power subsystem for BP-13 spacecraft . . .	4-41
4.4-2	Electrical power subsystem components for BP-13 spacecraft	4-42
4.4-3	Launch escape sequencer subsystem for BP-13 spacecraft	4-43

Figure		Page
4.5-1	Bonding electrical wire harness to LES motor case for BP-13 spacecraft	4-46
4.5-2	BP-13 spacecraft launch escape tower jettison motor .	4-47
4.5-3	BP-13 spacecraft LES jettison motor ignition locations	4-48
4.5-4	BP-13 spacecraft launch escape tower separation system	4-49
4.6-1	Apollo BP-13 spacecraft launch escape subsystem structure	4-62
4.6-2	Detail of command module-service module interface (BP-13 spacecraft)	4-63
4.6-3	Rawinsonde atmospheric wind data at Cape Kennedy, Fla., May 28, 1964	4-64
4.6-4	Comparison of predicted α_q and Q-ball α_q (Apollo mission A-101)	4-65
4.6-5	Variation of angle of attack with altitude (Apollo mission A-101)	4-66
4.6-6	Static pressure flight measurement on BP-13 spacecraft compared with wind-tunnel measurements on model PSTL-1 (ref. 1)	
	(a) $\phi = 0^\circ$	4-67
	(b) $\phi = 90^\circ$	4-68
	(c) $\phi = 180^\circ$	4-69
4.6-7	Static pressure coefficient over the command module conical surface (BP-13 spacecraft)	
	(a) Angular location, approximately 90°	4-70
	(b) Angular location, 180°	4-71
	(c) Angular location, 357°	4-72

Figure		Page
4.6-8	Pressure venting scheme for BP-13 spacecraft service module, insert, and adapter compartment	4-73
4.6-9	Service module internal pressure (BP-13 spacecraft). .	4-74
4.6-10	Axial force (compression) at interface of BP-13 spacecraft adapter and Saturn SA-6 instrument unit (station X _A 722)	4-75
4.6-11	Flight measured acceleration (BP-13 spacecraft)	
	(a) Launch escape subsystem at Q-ball interface . . .	4-76
	(b) Command module	4-77
4.6-12	Digital spectrum estimation of X-axis acceleration (BP-13 spacecraft)	4-78
4.6-13	Digital spectrum estimation of lateral bending acceleration (BP-13 spacecraft)	
	(a) LES Y-axis at Q-ball interface	4-79
	(b) LES Z-axis at Q-ball interface	4-80
	(c) Command module Y-axis	4-81
	(d) Command module Z-axis	4-82
4.6-14	First bending mode acceleration of BP-13 spacecraft at ignition of S-IV stage	4-83
4.6-15	Digital spectrum estimation of first bending mode acceleration of BP-13 spacecraft after ignition of S-IV stage	
	(a) LES Z-axis at Q-ball interface	4-84
	(b) LES Y-axis at Q-ball interface	4-85
4.6-16	Development view of BP-13 spacecraft service module, insert, and adapter wall showing transducer locations	4-86

Figure		Page
4.6-17	RMS of fluctuating pressure no. 7 on BP-13 service module	4-87
4.6-18	Static pressure at BP-13 spacecraft CM-SM shoulder . .	4-88
4.6-19	RMS estimation of BP-13 spacecraft service module radial vibration	4-89
4.6-20	Digital spectrum estimation of BP-13 spacecraft service module radial vibration	
	(a) Instrument SA0086D	4-90
	(b) Instrument SA0087D	4-91
4.6-21	BP-13 spacecraft adapter load trend comparison	4-92
4.6-22	RMS of fluctuating pressures over BP-13 spacecraft	
	(a) Fluctuating pressure 1 (CA0179P)	4-93
	(b) Fluctuating pressure 2 (CA0180P)	4-94
	(c) Fluctuating pressure 3 (CA0181P)	4-95
	(d) Fluctuating pressure 4 (SA0182P)	4-96
	(e) Fluctuating pressure 6 (SA0184P)	4-97
	(f) Fluctuating pressure 7 (SA0185P)	4-98
	(g) Fluctuating pressure 8 (SA0186P)	4-99
	(h) Fluctuating pressure 9 (SA0187P)	4-100
	(i) Fluctuating pressure 10 (SA0188P)	4-101
4.6-23	Comparison of BP-13 spacecraft fluctuating pressures for longitudinal locations at 357° with wind tunnel data using model PSTL-1 (ref. 1)	
	(a) M = 0.80 and M = 0.85	4-102
	(b) M = 0.90 and M = 0.95	4-103
	(c) M = 1.00 and M = 1.50	4-104
	(d) M = 2.00 and M = 2.50	4-105

Figure		Page
4.6-24	Fluctuating pressure trends for circumferential locations on BP-13 spacecraft service module at $X_A 974$	
	(a) $M = 0.80$ and $M = 0.85$	4-106
	(b) $M = 0.90$ and $M = 0.95$	4-107
	(c) $M = 1.00$ and $M = 1.50$	4-108
	(d) $M = 2.00$ and $M = 2.50$	4-109
4.6-25	Spectrogram of BP-13 spacecraft service module fluctuating pressures ($\frac{1}{3}$ octave band analysis)	4-110
4.7-1	Command module heat protection for BP-13 spacecraft. .	4-112
4.7-2	Bond-line LES tower temperatures measured during flight (BP-13 spacecraft)	4-113
4.8-1	Top view of BP-13 spacecraft command module showing calorimeter locations	4-119
4.8-2	Development view of BP-13 spacecraft service module, insert, and adapter compartment showing calorimeter locations	4-120
4.8-3	Launch configuration environment in terms of Mach number (M) and Reynolds number (Re_D) for BP-13 spacecraft	4-121
4.8-4	Heating rates measured on BP-13 spacecraft command module during flight	
	(a) Calorimeters 1, 5, and 10	4-122
	(b) Calorimeters 2, 4, and 11	4-123
	(c) Calorimeters 3, 9, and 12	4-124
	(d) Calorimeters 6, 7, and 8	4-125
4.8-5	Comparison of heating rate histories at $X_C = 74$ for three circumferential locations on BP-13 spacecraft.	4-126

Figure		Page
4.8-6	Comparison of heating rate histories at $X_C = 52$, for six circumferential locations on BP-13 spacecraft	4-127
4.8-7	Comparison of heating rate histories at $X_C = 27$ for two circumferential locations on BP-13 spacecraft	4-128
4.8-8	Comparison of heating rate histories at $\phi = 180^\circ$ for three longitudinal locations on BP-13 spacecraft	4-129
4.8-9	Comparison of heating rate histories at $\phi = 319^\circ$ for three longitudinal locations on BP-13 spacecraft . .	4-130
4.8-10	Comparison of heating rate histories at $\phi = 3^\circ$ for three longitudinal locations on BP-13 spacecraft . .	4-131
4.8-11	Heating rates measured on the BP-13 spacecraft service module during flight	4-132
4.8-12	Heating rates measured on the BP-13 spacecraft adapter during flight	4-133
4.9-1	Environmental control subsystem schematic for BP-13 spacecraft	4-139
4.9-2	Sectional view of coolant-pump assembly for BP-13 spacecraft	4-140
4.9-3	Command module cabin air temperature (BP-13 spacecraft)	4-141
4.9-4	Command module cabin pressure (BP-13 spacecraft) . . .	4-142
5.0-1	Apollo mission A-101 space vehicle showing cutaway views of launch vehicle	5-4
6.1-1	Schedule milestones for BP-13 spacecraft at Downey, California, ATO	6-10
6.1-2	Schedule milestones for BP-13 spacecraft in Hangar AF, Cape Kennedy, Florida	6-11

Figure		Page
6.1-3	BP-13 spacecraft mating in Hangar AF, Cape Kennedy, Florida	6-12
6.1-4	BP-13 spacecraft loaded on vertical transport prior to mating with the launch vehicle	6-13
6.1-5	Schedule milestones for BP-13 spacecraft at launch complex 37B, Cape Kennedy, Florida	6-14
6.2-1	Apollo mission A-101 precount activities on F-1 day, May 25, 1964	6-17
6.2-2	Apollo mission A-101 countdown activities on postponed launch day, May 26, 1964	6-18
6.2-3	Apollo mission A-101 final countdown activities, F day, May 28, 1964	6-19

1.0 SUMMARY

The Apollo spacecraft mission A-101 was successfully accomplished on May 28, 1964. The unmanned boilerplate spacecraft (BP-13) was launched at 12:07 p.m. e.s.t. into earth orbit from complex 37B of the Eastern Test Range, Cape Kennedy, Florida, by the Saturn I Block II vehicle SA-6.

The purpose of the test was to demonstrate the compatibility of the spacecraft with the launch vehicle in the launch and exit trajectory and environment for Apollo earth orbital flights.

All mission test objectives were fulfilled by the time of orbital insertion, and additional data were obtained by telemetry through the Manned Space Flight Network until the end of effective battery life in the fourth orbital pass. Radar skin tracking was continued by the network until the spacecraft reentered on the 54th orbital pass over the Pacific Ocean near Canton Island.

During the launch countdown there were no holds caused by the spacecraft. All spacecraft subsystems fulfilled their specified functions throughout the countdown and planned flight test period. Engineering data were received through telemetry from all but 6 of the 112 instrumented spacecraft measurements for the full flight test period of the mission.

Although improper running was indicated for the pump in the onboard equipment and cabin cooling subsystem, the subsystem performed its function satisfactorily.

The actual launch trajectory during the S-I stage powered flight and part of the S-IV stage powered flight was slightly slow in velocity and low in altitude and flight-path angle; however, the actual trajectory did provide the launch environment required for the spacecraft mission. The three spacecraft telemetry transmitters performed satisfactorily. Telemetry reception was continuous during launch and exit except for about 3 seconds at the time of launch vehicle staging. The C-band transponders and C telemetry link operated until approximately 3:08 g.e.t.^a Telemetry A and B links operated until approximately 5:21 g.e.t.

The instrumentation subsystem was successful in determining the launch and exit environment. Aerodynamic heating produced a maximum truss-member bond-line temperature on the LES tower of less than 20 percent of the design limit (550° F).

^aUnless otherwise specified, all times shown in this report are taken from the instant of vehicle lift-off (12:07:00.42 p.m. e.s.t.)

[REDACTED]

Postflight examination of strain gage, pressure, and acceleration data indicated that the spacecraft structure performed adequately in the flight environment encountered. Values of angle of attack and dynamic pressure encountered during the powered phase of flight were within allowable limits and compare well with those predicted before launch. The wind-tunnel static-pressure measurements used in loads analyses were in agreement with the flight-measured static pressures. The internal pressures within the SM were within an allowable range and verified the venting method. Examination of the available acceleration data revealed no evidence of severe dynamic loads.

The ground service equipment performed satisfactorily during pre-launch and countdown operations.

[REDACTED]

2.0 INTRODUCTION

Apollo mission A-101 was the first flight of the Apollo spacecraft configuration with a Saturn launch vehicle. The unmanned flight test vehicle consisted of the BP-13 boilerplate spacecraft and the SA-6 Saturn I Block II launch vehicle. The space vehicle, shown in figure 2.0-1 was launched from complex 37B of the Eastern Test Range, Cape Kennedy, Florida, on May 28, 1964.

The BP-13 spacecraft was the first of two boilerplate spacecraft planned to be used in demonstrating the compatibility of the Apollo spacecraft configuration with the Saturn I Block II launch vehicle in a launch and exit environment similar to that expected for Apollo-Saturn V orbital flights with production spacecraft.

The spacecraft flight configuration consisted of a production type launch escape subsystem (LES), boilerplate command module (CM), and boilerplate service module (SM) assembly, insert, and adapter. Boilerplate flight test spacecraft are development vehicles which simulate production spacecraft only in external size and shape and mass characteristics. Boilerplate flight test spacecraft are equipped with instrumentation to obtain flight data for engineering analysis and evaluation. These data are used to confirm or determine the design criteria for the production spacecraft.

The flight sequence of major events during the BP-13 flight into orbit is given in figure 2.0-2. Spacecraft separation from the launch vehicle was not planned for this flight; therefore, the second stage (S-IV) and instrument unit (IU) of the launch vehicle together with the attached spacecraft (without the jettisoned LES) were inserted into orbit as a single unit. There were no provisions for recovery of the spacecraft.

The first-order spacecraft test objectives of this flight were as follows:

- (1) Demonstrate the physical compatibility of the spacecraft with the launch vehicle under preflight and flight conditions.
- (2) Obtain data to verify design criteria for the launch environment.
- (3) Demonstrate the primary mode of the launch escape tower jettison using the escape tower jettison motor.

The second-order test objectives were as follows:

(1) Demonstrate the structural integrity of the launch escape subsystem under flight-loading conditions.


(2) Demonstrate the compatibility of the BP-13 communications and instrumentation subsystem with the launch vehicle system.

(3) Demonstrate the adequacy of ground support handling equipment and procedures.

All of the first- and second-order objectives were satisfactorily fulfilled.

An evaluation has been made of all flight data^a, and the results of the evaluation are presented in this report.

^aAcoustic data reduction not complete at the time of publication. Acoustic data analysis will be reported at a later date.



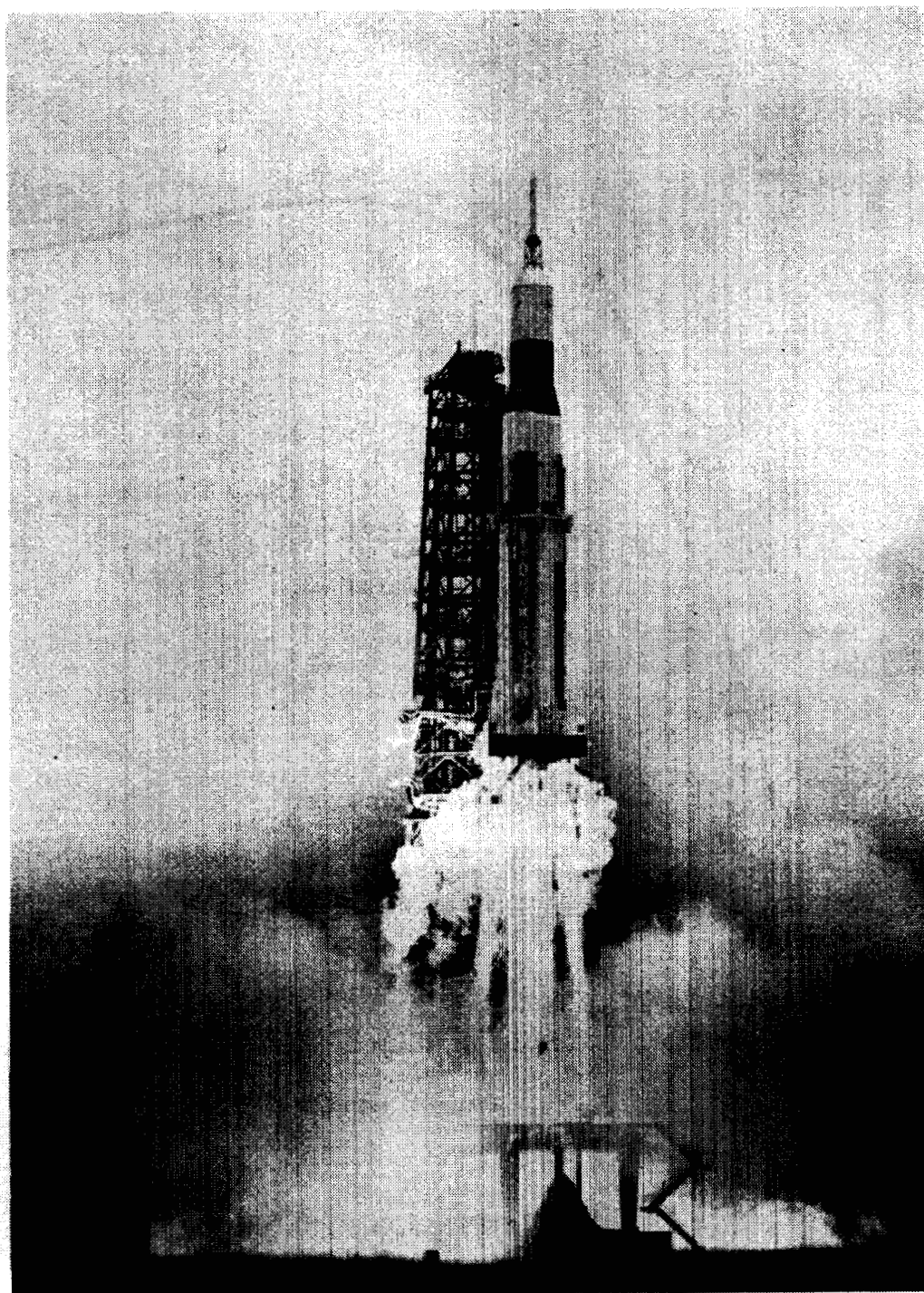


Figure 2.0-1.- Saturn-Apollo space vehicle for mission
A-101 at lift-off.

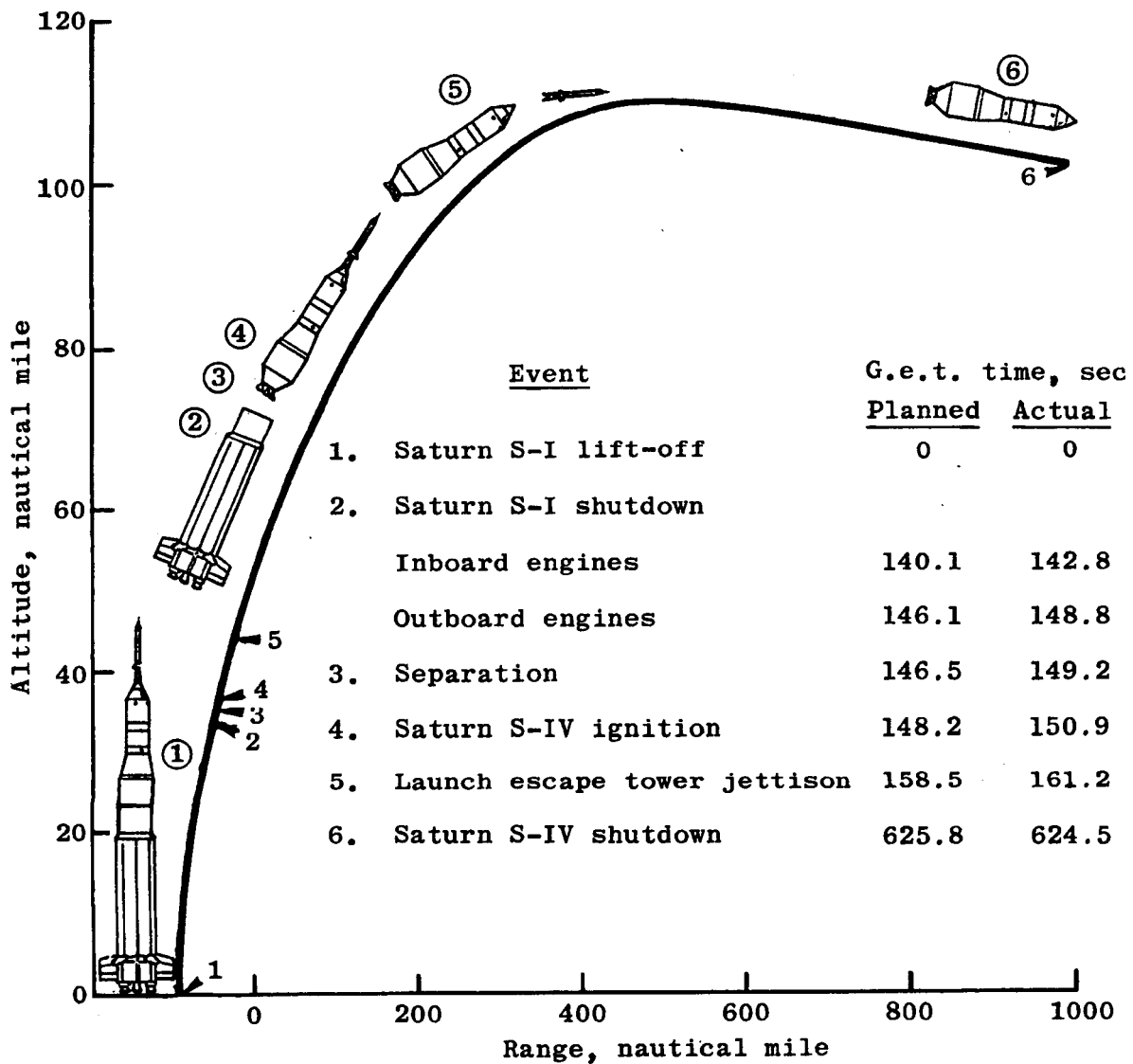


Figure 2.0-2.- Sequence of major events for Apollo mission A-101.

3.0 FLIGHT TRAJECTORIES

The trajectories referred to as "planned" were preflight-calculated nominal trajectories supplied by Marshall Space Flight Center, and the trajectories referred to as "actual" were based on the Manned Space Flight Network tracking data. In both the planned and actual trajectories, the Patrick model atmosphere for altitudes below 25 nautical miles and the 1959 ARDC model for altitudes above 25 nautical miles were used. The earth model used was the Fischer Ellipsoid. The ground track for the first three orbital passes of the Apollo mission A-101 is presented in figure 3.0-1. The altitude-longitude profile for the launch and three orbital passes is presented in figure 3.0-2. These two figures show that the actual profile was close to the nominal.

A comparison of the actual and planned mission event times for the launch phase is given in table 3.0-I. It can be seen from the table that the actual S-I cutoff events were approximately 3 seconds later than planned, and the actual S-IV cutoff was approximately 1 second earlier than planned. The launch trajectory data shown in figure 3.0-3 were based on the real-time output of the Range Safety Impact Predictor Computer (IP-7094) which used FPS-16, Azusa, missile trajectory measurement (MISTRAM) system, and the FPQ-6 radars. The data from these tracking facilities were used during the time periods listed in the following table:

Radars used	g.e.t., min:sec
FPS-16	0 to 01:00
Azusa	01:00 to 05:28
MISTRAM	05:28 to 07:42
FPQ-6	07:42 to 08:31
MISTRAM	08:31 to 09:34
FPQ-6	09:34 to 11:09

[REDACTED]

The actual launch trajectory is compared with the planned launch trajectory in figure 3.0-3. It can be seen from the figure that the actual launch trajectory did provide the launch environment required for the spacecraft mission. The actual trajectory parameters were slightly low in velocity, altitude, and flight-path angle during the S-I stage powered flight and part of the S-IV stage powered flight and resulted in an insertion into the planned orbit at a point somewhat nearer perigee than planned.

The orbital portion of the trajectory is shown in figure 3.0-4. The planned orbital trajectory was obtained by starting with the nominal insertion conditions supplied by Marshall Space Flight Center and integrating forward for three orbital passes. The actual orbital portion of the trajectory was derived by starting with the orbital configuration position and velocity vector obtained at the end of the first pass over Patrick Air Force Base, as determined by Goddard Computer using the Manned Space Flight Network tracking data. The Patrick vector was integrated backward along the flight trajectory to orbital insertion (defined as S-IV cutoff plus 5 seconds) and forward for three orbital passes. These integrated values were in good agreement with the position and velocity vectors determined by the Goddard Computer for passes near Carnarvon, Australia, during the first pass and Pretoria, South Africa, during the second pass. Thus, the validity of the integrated orbital portion of the flight trajectory was established. It can be seen in figure 3.0-4 that the actual orbital flight trajectory was in very close agreement with the planned.

A comparison of the actual and planned trajectory parameter is given in table 3.0-II. The table shows that the actual insertion conditions and orbital parameters were in good agreement with the planned. As based on the Patrick velocity vector, the estimated lifetime of the orbital configuration, consisting of the BP-13 spacecraft, the instrument unit, and the Saturn S-IV stage, was calculated to be 42 orbital passes. The actual reentry of the orbital configuration was reported during the 54th orbital pass near Canton Island.

[REDACTED]

TABLE 3.0-I.- MISSION EVENT TIMES

Event	Planned, sec	Actual, sec	Difference, sec
Lift-off	0	0	0
Tilt arrest	134.0	134.0	0
IECO	140.1	142.8	2.7
OECO	146.1	148.8	2.7
Ullage rockets ignition	146.4	149.1	2.7
Separation of S-I and S-IV	146.5	149.2	2.7
S-IV ignition	148.2	150.9	2.7
Ullage rocket jettison	158.5	161.2	2.7
Launch escape tower jettison	158.5	161.2	2.7
S-IV cutoff	625.76	624.5	-1.26

TABLE 3.0-II.- COMPARISON OF PLANNED AND ACTUAL
TRAJECTORY PARAMETERS

Condition	Planned	Actual	Difference
S-IV cutoff			
Time from lift-off, sec	625.76	624.5	-1.26
Time from lift-off, min:sec	10:25.76	10:24.5	-00:01.26
Geodetic latitude, deg North	21.8277	21.9780	0.1503
Longitude, deg West	-61.0872	-61.4660	0.3788
Altitude, feet	607,466	600,335	-7,131
Altitude, nautical miles	100.0	98.8	-1.2
Range, nautical miles	1,133.0	1,110.0	-23
Space-fixed velocity, ft/sec	25,610.1	25,621.5	11.4
Space-fixed flight-path angle, deg	0.12985	0.08255	-0.04730
Space-fixed heading angle, deg East of North	113.7869	113.6775	-0.1094
S-IV cutoff +5 sec			
Time from lift-off, sec	630.76	629.5	-1.26
Time from lift-off, min:sec	10:30.76	10:29.5	-00:01.26
Geodetic latitude, deg North	21.6892	21.8407	0.1515
Longitude, deg West	-60.7727	-61.1522	-0.3795
Altitude, feet	607,621	600,408	-7,213
Altitude, nautical miles	100.0	98.8	-1.2
Range, nautical miles	1,152.5	1,129.4	-23.1
Space-fixed velocity, ft/sec	25,616.8	25,628.2	11.4
Space-fixed flight-path angle, deg	0.13067	0.08349	-0.04718
Space-fixed heading angle, deg East of North	113.9109	113.8020	-0.1089

TABLE 3.0-II.- COMPARISON OF PLANNED AND ACTUAL
TRAJECTORY PARAMETERS - Concluded

Condition	Planned	Actual	Difference
Orbital parameters			
Perigee altitude, statute miles . . .	113.1	113.2	0.1
Perigee altitude, nautical miles . .	98.3	98.4	0.1
Apogee altitude, statute miles . . .	140.2	141.0	0.8
Apogee altitude, nautical miles . . .	121.8	122.5	0.7
Period, min	88.59	88.62	0.03
Inclination angle, deg	31.76	31.78	0.02
Maximum conditions			
Altitude, statute miles	140.2	141.0	0.8
Altitude, nautical miles	121.8	122.5	0.7
Space-fixed velocity, ft/sec	25,634.2	25,633.5	-0.7
Earth-fixed velocity, ft/sec	24,301.0	24,303.8	2.8
Exit acceleration, g	5.80	4.89	-0.91
Exit dynamic pressure, lb/sq ft . . .	805.0	808.8	3.8

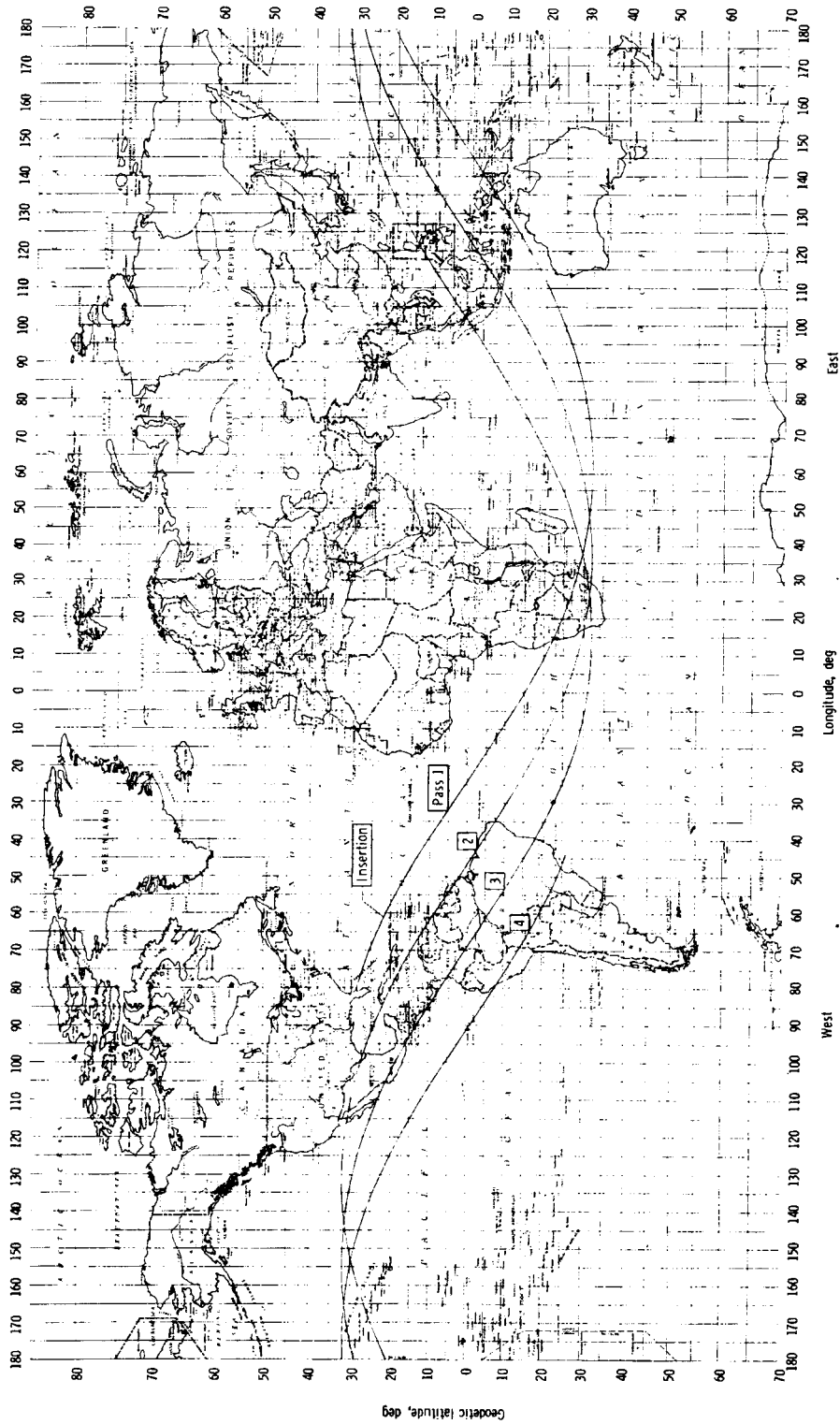


Figure 3.0-1.- Ground track for the Apollo A-101 orbital mission
for the first three orbital passes.

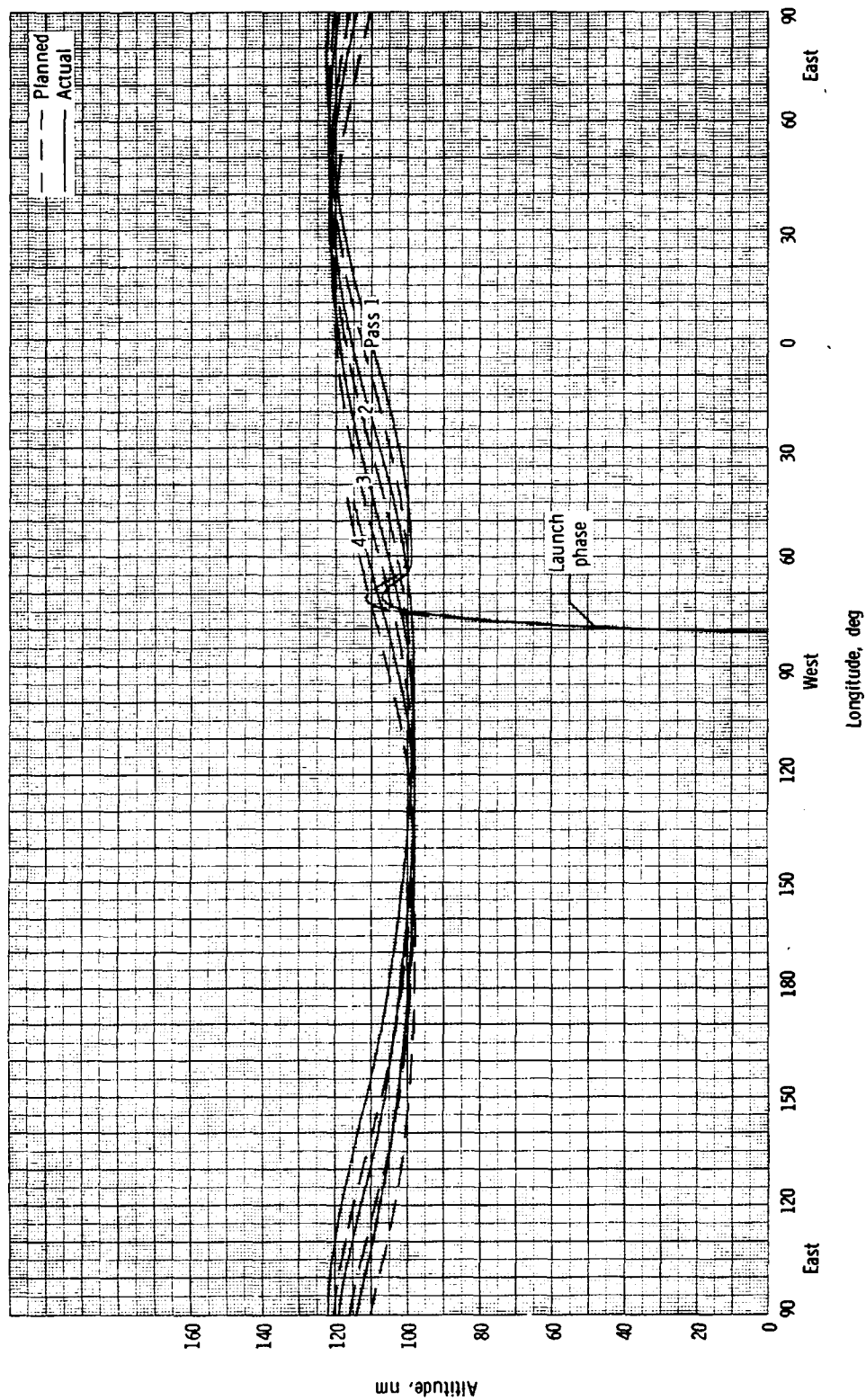
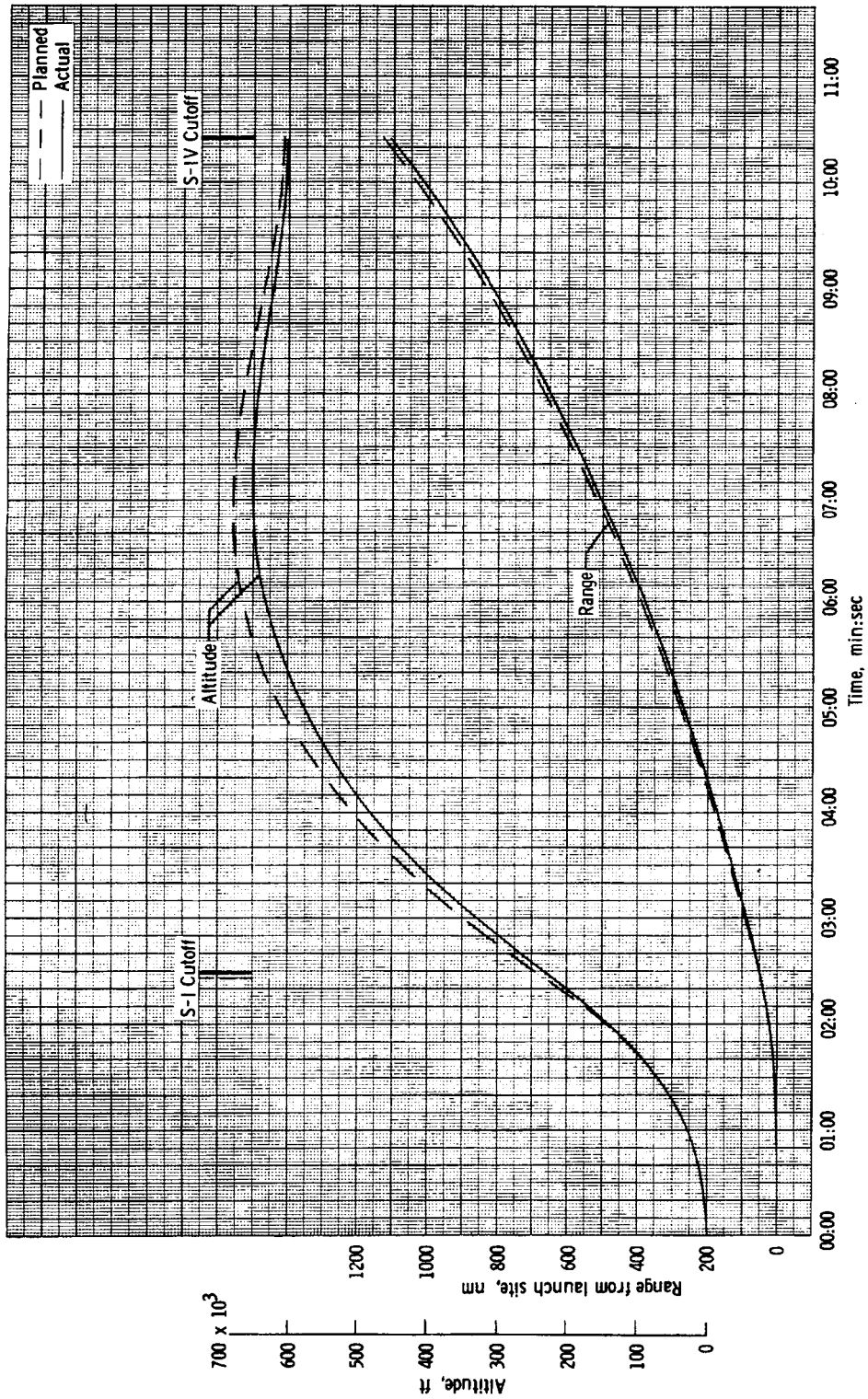
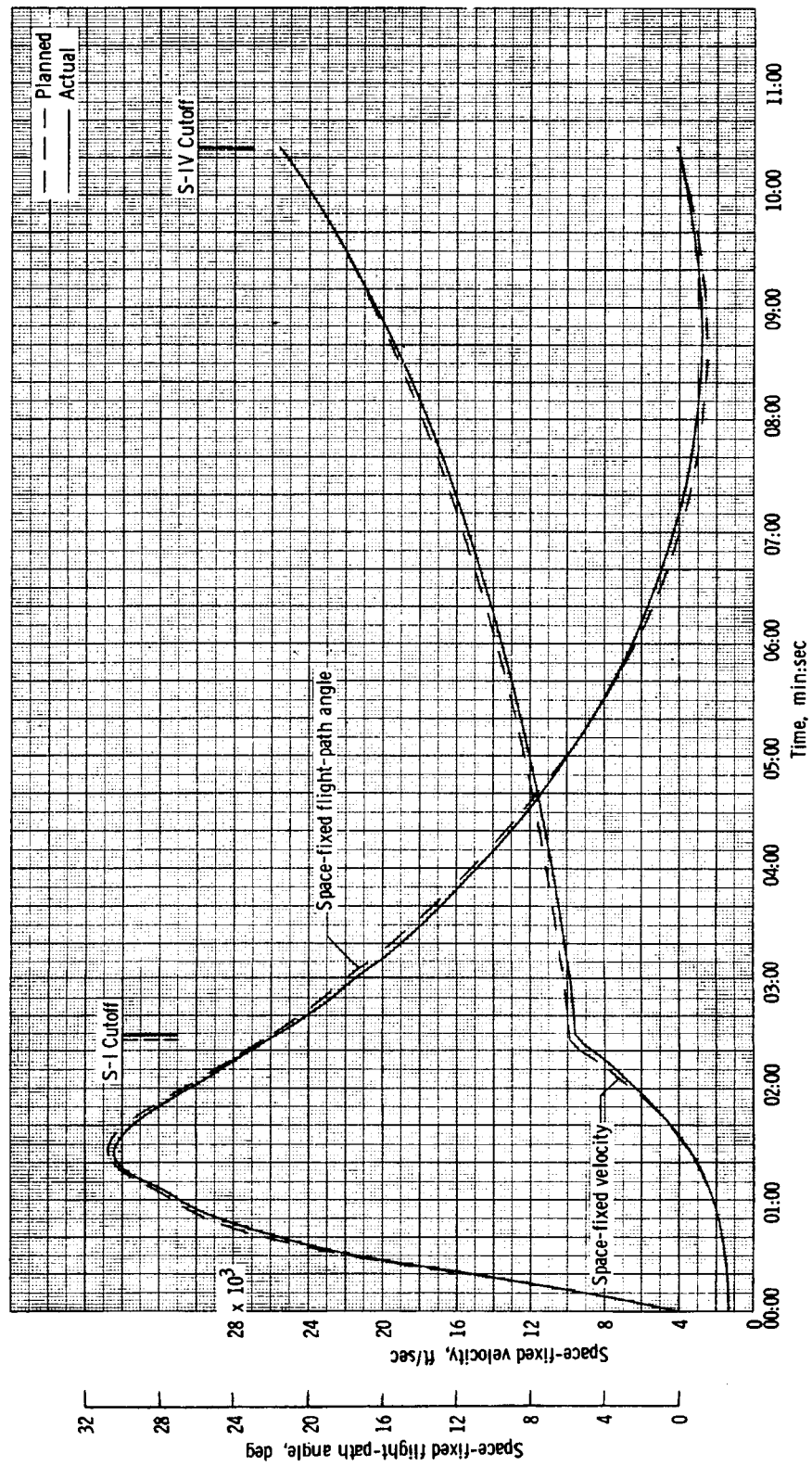


Figure 3.0-2.- Altitude-longitude profile for Apollo mission A-101 for the first three orbital passes.



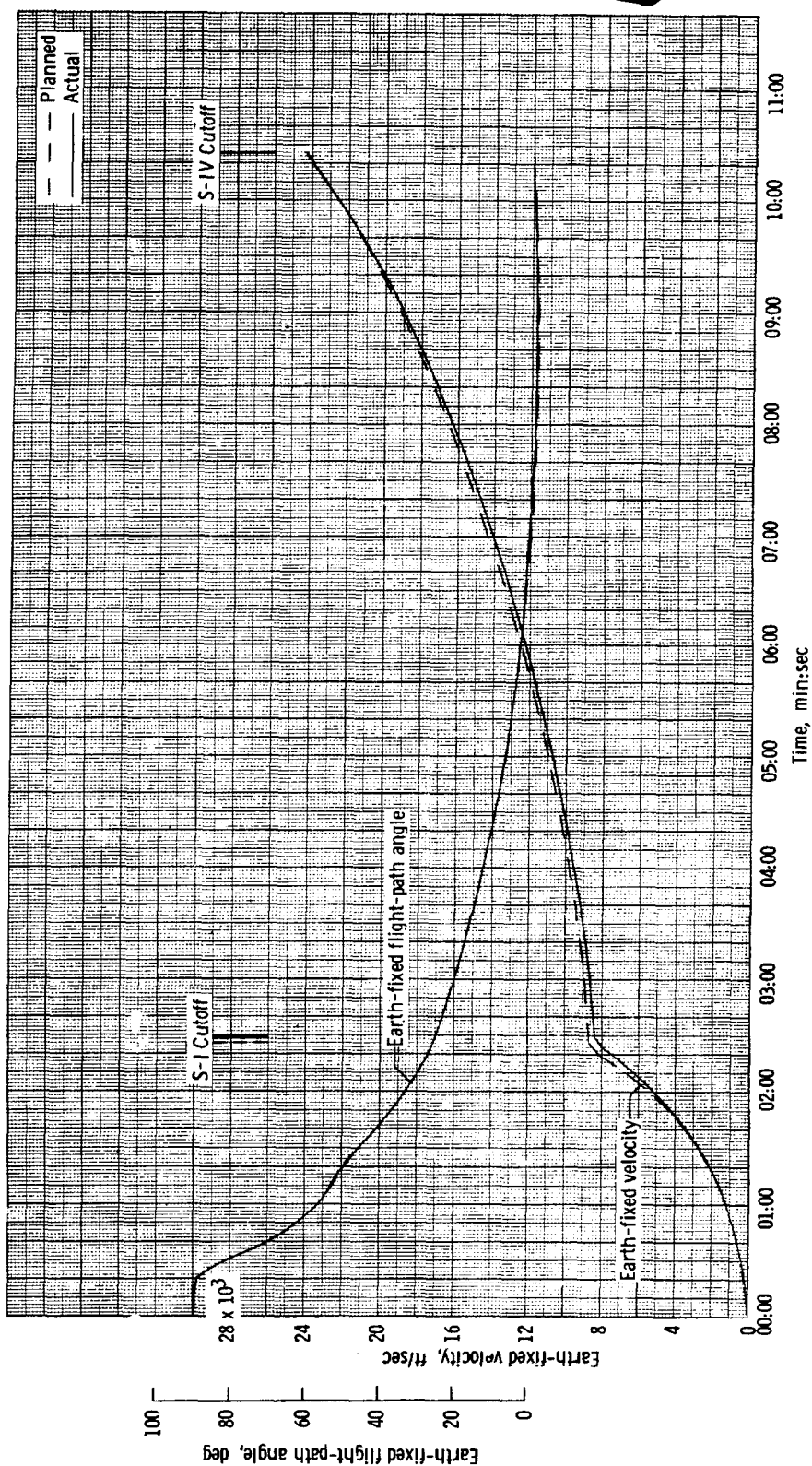
(a) Altitude and range.

Figure 3.0-3.- Time histories of trajectory parameters for the Apollo mission A-101 launch phase.



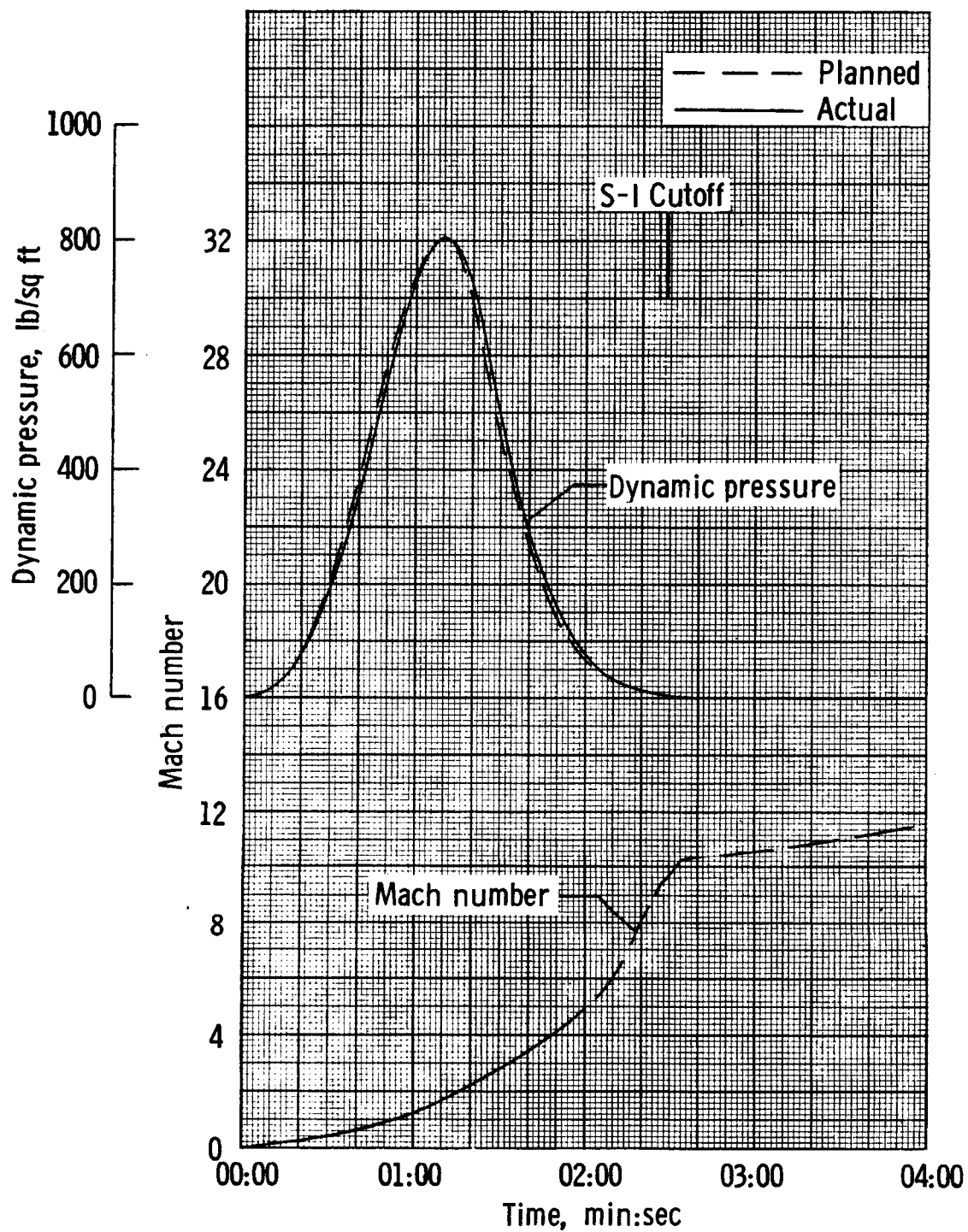
(b) Space-fixed velocity and flight-path angle.

Figure 3.0-3.- Continued.



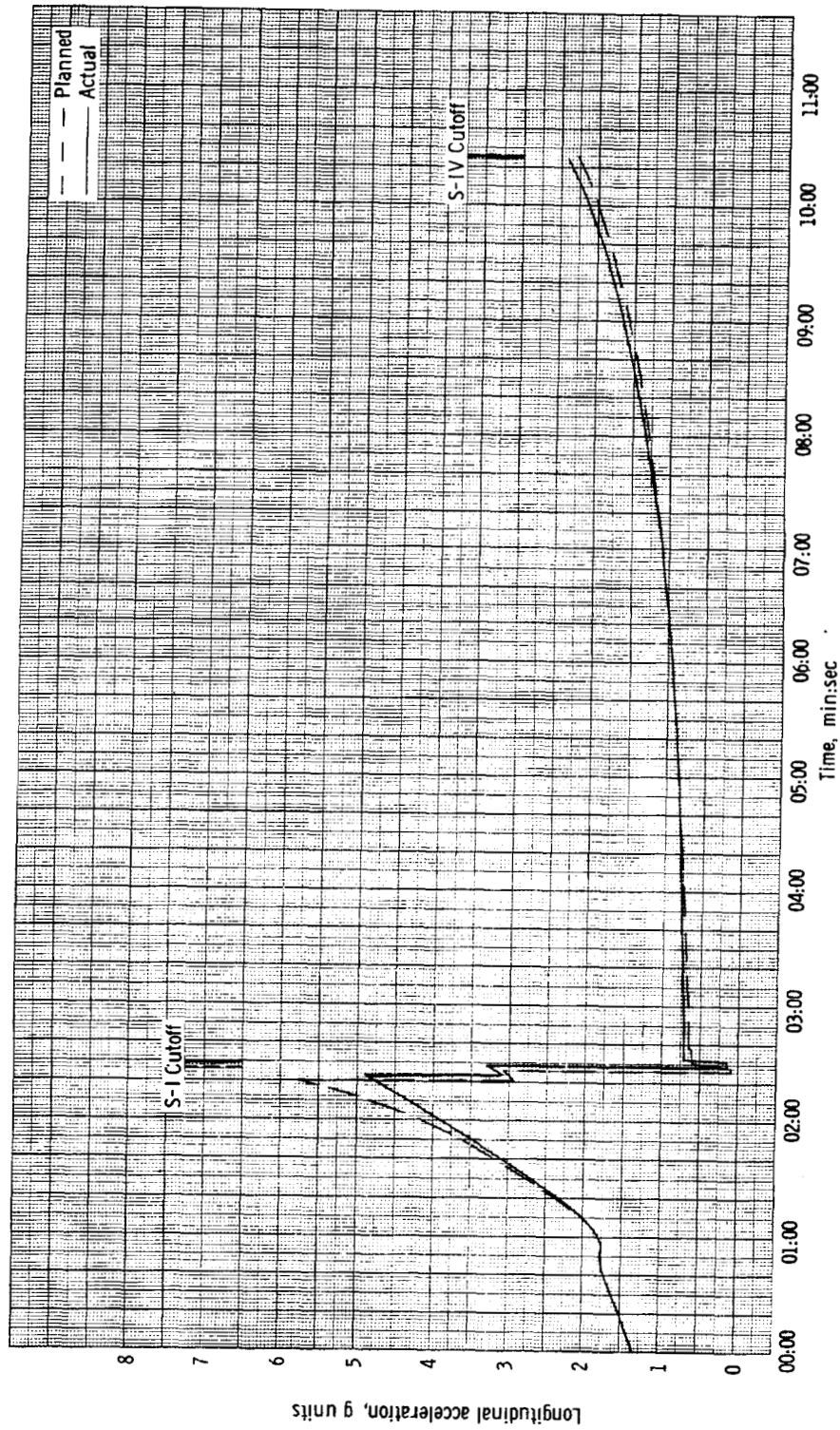
(c) Earth-fixed velocity and flight-path angle.

Figure 3.0-3.- Continued.



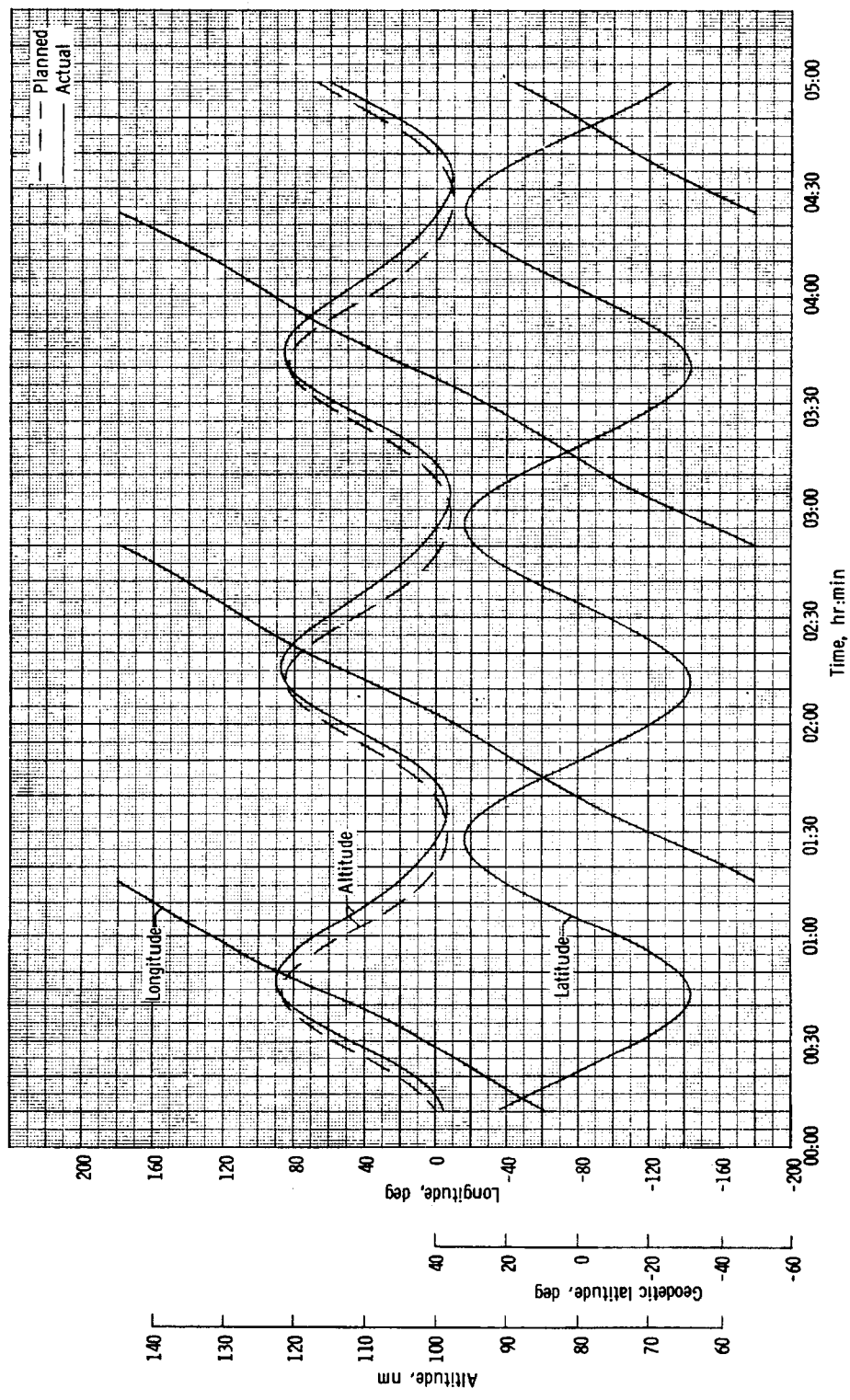
(d) Dynamic pressure and Mach number.

Figure 3.0-3.- Continued.



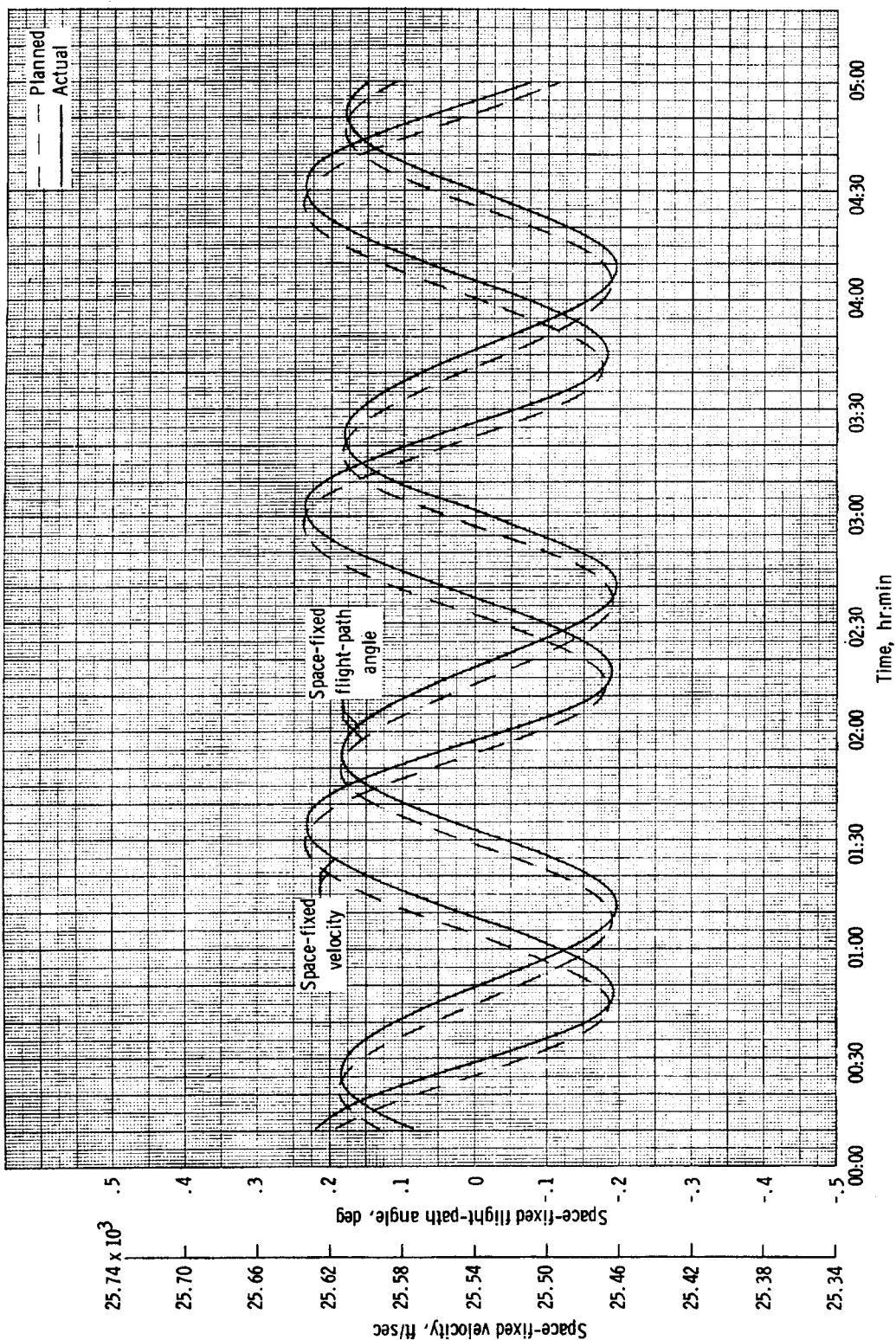
(e) Longitudinal acceleration along spacecraft X-axis.

Figure 3.0-3.- Concluded.



(a) Latitude, longitude, and altitude.

Figure 3.0-4.- Time histories of trajectory parameters for Apollo mission A-101 for first three passes of orbital phase.



(b) Space-fixed velocity and flight-path angle.

Figure 3.0-4.- Concluded.

4.0 SPACECRAFT DESCRIPTION AND PERFORMANCE

4.1 Spacecraft Description

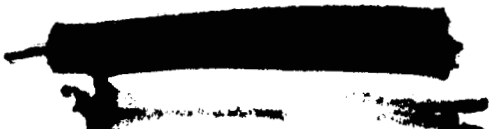
Apollo spacecraft boilerplate 13 (BP-13) was composed of four major assemblies: the prototype launch escape subsystem (LES), the boilerplate command module (CM), the boilerplate service module (SM) with fairing and SM insert, and the boilerplate adapter. These major assemblies were designed to be similar in external configuration to the production Apollo spacecraft. The major assemblies and exterior dimensions of each are shown in figure 4.1-1, the spacecraft reference axis system is given in figure 4.1-2, the coordinate systems for X-axis stations of the overall spacecraft and individual assemblies are given in figure 4.1-3.

The launch escape subsystem (LES) is shown in figure 4.1-4. The truss-type tower structure was a welded titanium tubular frame, and the exposed surfaces were covered with silica-filled Buna-N rubber for thermal insulation. Each of the four legs was attached to the command module by a single-mode explosive bolt. A structural skirt was mounted between the top of the tower structure and the launch escape motor. The bolt attachments at the interface between the tower and the skirt provided LES alignment capability. Two sequencers which provided firing signals to the LES pyrotechnics were attached to the underside of the skirt.

The tower jettison motor and the tower release mechanism were live, but the launch escape and pitch control motors were inert although they simulated the mass and other physical characteristics of the production spacecraft motors.

A conical section of welded Inconel sheet was mounted to the forward end of the pitch-control motor housing. The section contained 184 pounds of sheet lead ballast to provide the proper LES mass characteristics. The ballast enclosure also provided the interface plane for mounting the Q-ball assembly. The operation of the LES is described in section 4.5.

The command module was conical with a convex base and rounded apex. The sides were semimonocoque aluminum structures terminating in the forward and aft heat shields. The exterior was covered with cork for protection against aerodynamic heating. Section 4.7 presents a description of the cork insulation configuration. The inner side walls and top of the cabin were insulated with a quilted fiber-glass material. The major components of the subsystems were mounted on shelves and brackets located along portions of the inner wall as shown in figures 4.1-5 and 4.1-6.



A tubular aluminum structure was welded to the forward bulkhead to simulate the egress tunnel of the production spacecraft. A main hatch of aluminum alloy provided access to the cabin. Prior to launch, the hatch was bolted to the CM exterior structure and sealed with epoxy.

External protuberances of the production spacecraft configuration, including the air vent, umbilical fairing, and two scimitar antennas, shown in figure 4.1-7, were simulated for a better definition of aerodynamic parameters.

The CM aft heat shield was similar in size and shape to the operational heat shield. It was composed of an inner and outer layer of laminated fiber glass over an aluminum honeycomb core and was attached to the CM by four adjustable struts. No ablative material was used because the aft heat shield was not exposed to the launch environment and no recovery of the spacecraft was planned.

The lower portion of the forward compartment was constructed of aluminum covered with cork insulation, and the upper portion was a fiber-glass honeycomb radome containing the VHF telemetry omniantenna. (See figs. 4.3-2 and 4.7-1.)

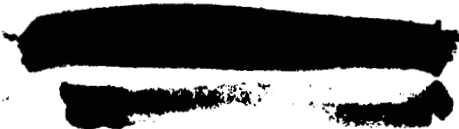
The boilerplate service module assembly consisted of the fairing, service module structure, and SM insert which were bolted together. The boilerplate adapter was bolted to the SM insert. The SM assembly and the insert, shown in figure 4.1-8, were of semimonocoque aluminum construction. For further structural details, see section 4.6.


A pneumatically actuated umbilical assembly was located approximately 18 inches below the top of the SM and 58° from the -Z-axis toward the +Y-axis. External electrical power, GSE signals, and coolant fluid were obtained through this assembly prior to launch.

Dummy quadrant packages for the reaction control subsystem (RCS) were attached to the upper portion of the SM exterior, 90° apart. In order to duplicate the aerodynamic characteristics of the production units, the dummy packages were the same size and shape and were arranged on the SM in the same location as that of the operative units on the production spacecraft.

In addition, the SM and adapter contained instrumentation transducers and associated components and wiring and electrical wire harnesses that interfaced with the launch vehicle instrument unit for the Q-ball signals, the two tower jettison command signals, and GSE signals.

The total weight inserted into orbit was 17,023 pounds. Due to a restriction in the launch vehicle payload capability, the original





BP-13 spacecraft weight of 18,600 pounds was reduced by approximately 1,600 pounds after the spacecraft was delivered at Cape Kennedy. The resultant mass characteristics are shown in table 4.1-I. The weights, as shown in this table, include 2,014 pounds of ballast in the CM, no ballast in the SM, and 245 pounds of ballast in the adapter.




TABLE 4.1-I.- SPACECRAFT BP-13 MASS CHARACTERISTICS

	Weight, lb	Center of gravity, inches (a)			Moment of inertia, slug-feet ² (b)		
		X _A	Y _A	Z _A	Roll I _{XX}	Pitch I _{YY}	Yaw I _{ZZ}
Command module	9,300	1,041.2	2.4	5.1	5,664	3,982	3,906
Service module	4,172	951.1	1.4	-0.8	5,019	4,187	4,148
SM insert and adapter	3,551	785.5	-3.2	-1.5	4,369	3,733	3,752
Total in orbit	17,023	965.8	1.0	2.3	15,105	48,464	48,350
Launch escape system	6,520	1,294.7	^b 0.0	^b -0.2	252	8,778	8,781
Total at launch	23,543	1,056.9	0.7	1.6	15,364	167,350	167,233

^aSee figure 4.1-2 for reference axis system and figure 4.1-3 for X_A reference point.

^bCalculated.

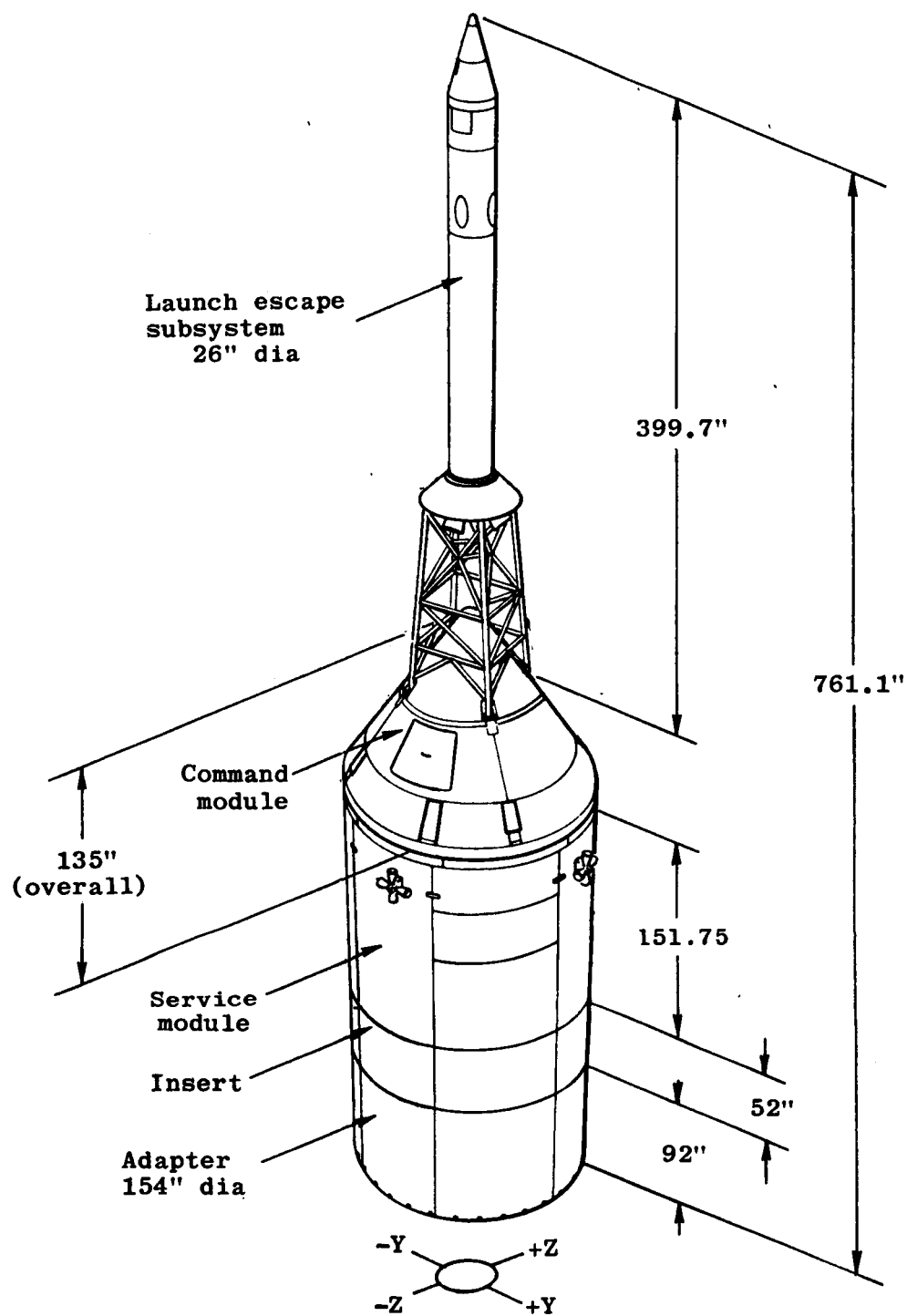
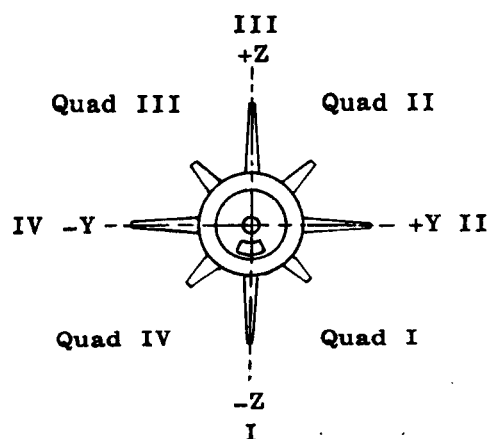
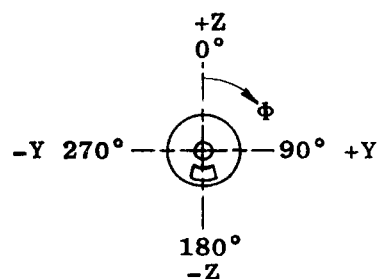


Figure 4.1-1. - Apollo BP-13 spacecraft.



Total space vehicle
component locations
(MSC and MSFC)



Spacecraft instrumentation
locations^a (MSC only)

Both views looking aft

^aSee table 4.2-II

Figure 4.1-2.- Y- and Z-axis and angular coordinate system used for
designating locations within the BP-13 spacecraft.

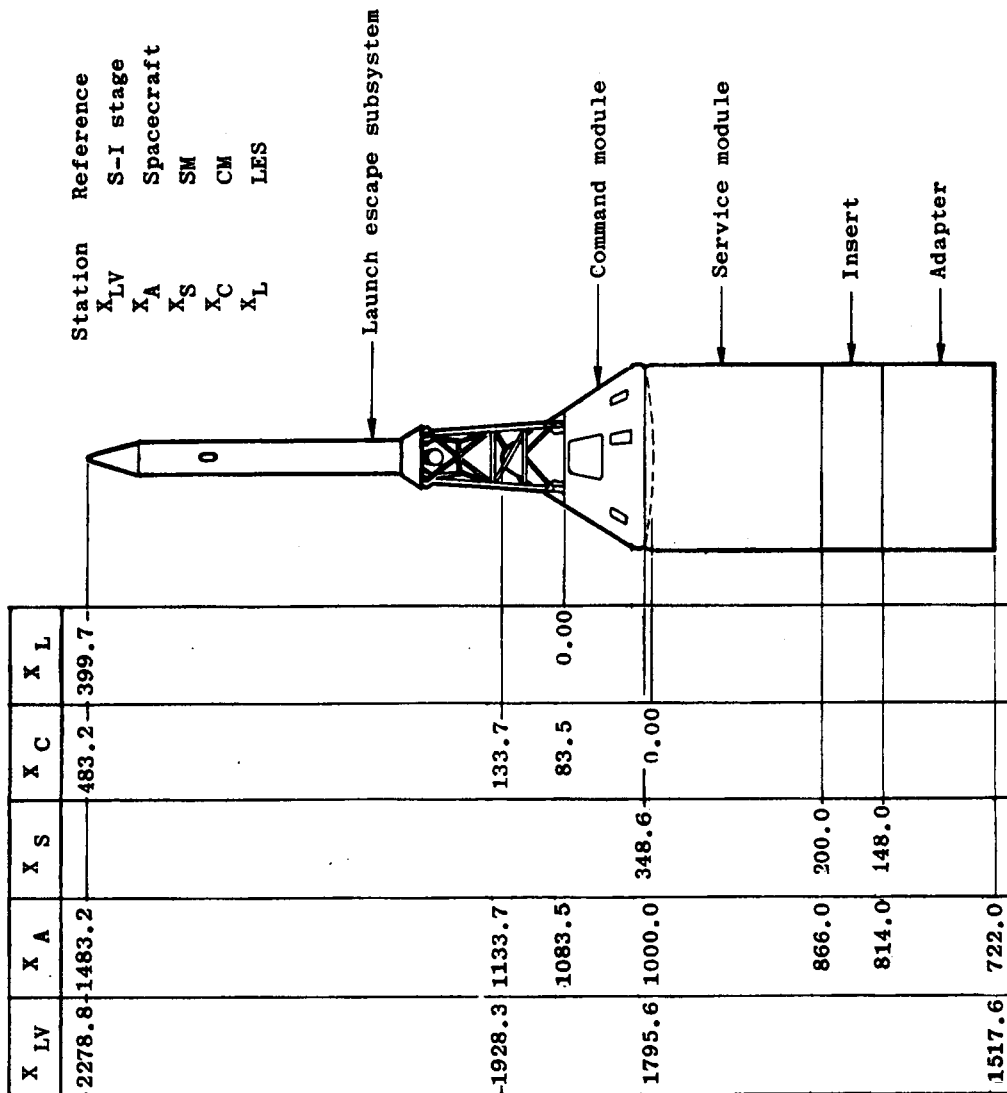


Figure 4.1-3. - X-axis systems used for designating longitudinal locations of BP-13 spacecraft and SA-6 launch vehicle.

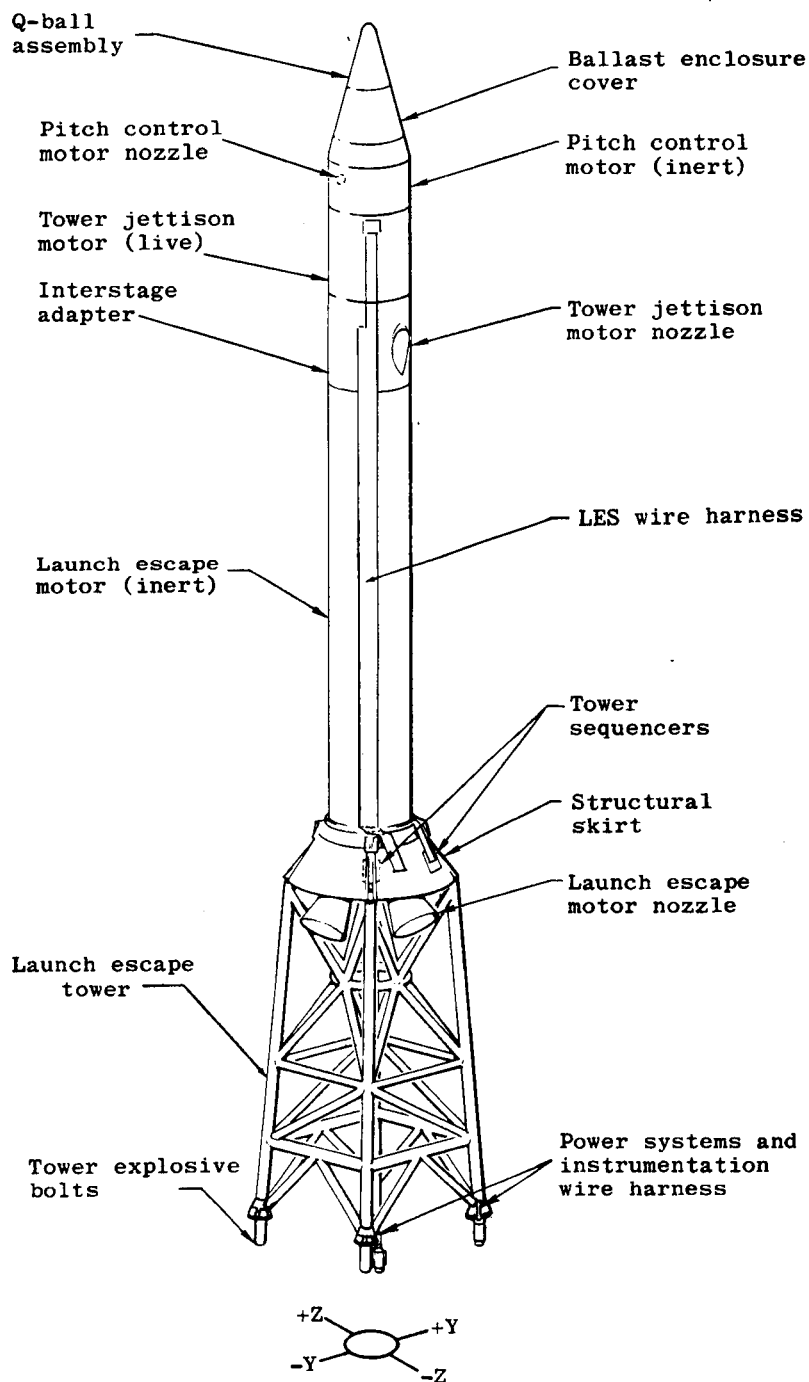


Figure 4.1-4.- Launch escape subsystem for BP-13 spacecraft.

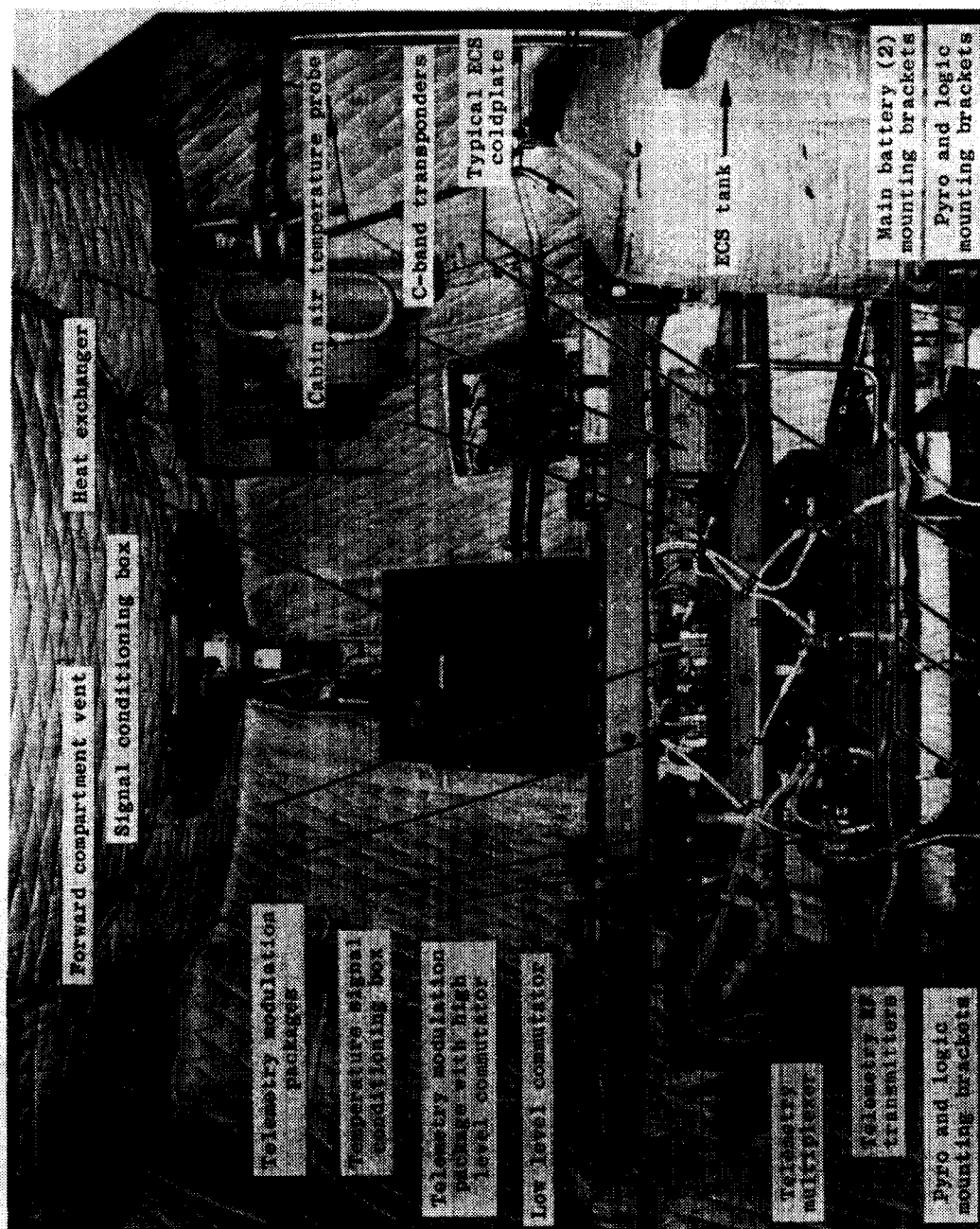


Figure 4.1-5.- Command module interior equipment layout for BP-13 spacecraft (view through hatch).

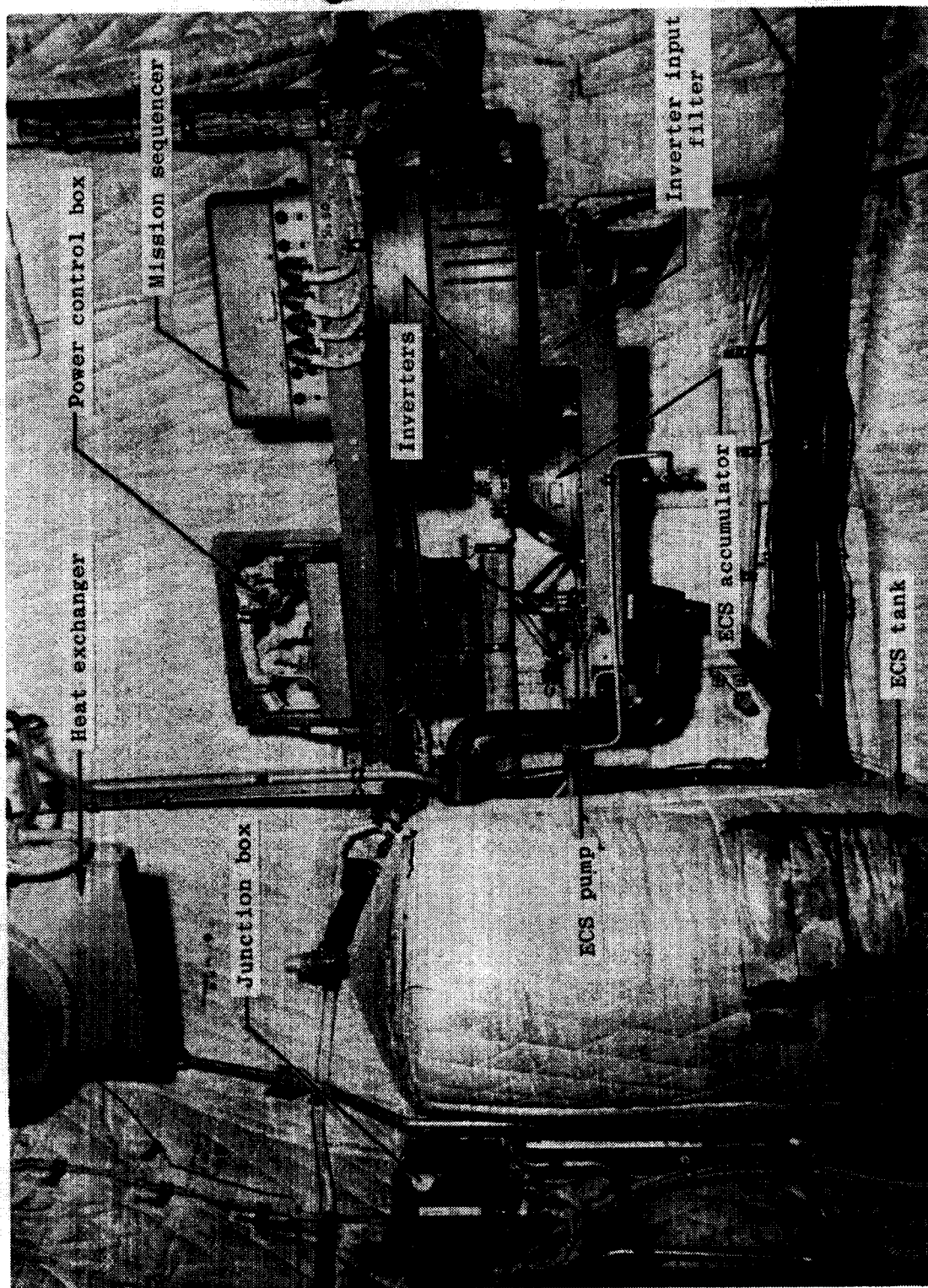


Figure 4.1.1-6. - Command module interior equipment layout (view to right of hatch).

TABLE 4.6-I. - FLIGHT LOADS COMPARISON

Location, X_A , in.	Time from lift-off, sec	Bending moment, in.-lb	Axial force (compression), lb	Source
^a 722	50	732,000	51,900	Flight measured parameters and predicted angle of attack for T-0 winds.
		1,755,000	52,200	Flight measured parameters and flight measured Q-ball angle of attack.
		856,000	53,400	Preflight calculations with programed angle of attack with no winds.
^a 722	60	1,550,000	73,000	Flight measured parameters and predicted angle of attack for T-0 winds.
		2,570,000	74,000	Flight measured parameters and flight measured Q-ball angle of attack.
		2,100,000	73,000	Preflight calculations with programed angle of attack with no winds.
^a 722	70	4,360,000	92,100	Flight measured parameters and calculated angle of attack for T-0 winds.
		6,380,000	94,400	Preflight calculations with programed angle of attack with no winds.
		4,160,000	78,000	Preflight calculations with programed angle of attack with no winds.
^a 722	72	5,570,000	94,200	Flight measured parameters and calculated angle of attack for T-0 winds.
^b 1008.5	72	311,000	88,000	Flight measured parameters and calculated angle of attack for T-0 winds.
^c 1084	72	205,000	18,000	Flight measured parameters and calculated angle of attack for T-0 winds.

^a X_A Sta. 722 - Adapter-IU interface^b X_A Sta. 1008.5 - CM-SM interface^c X_A Sta. 1084 - LES-CM interface

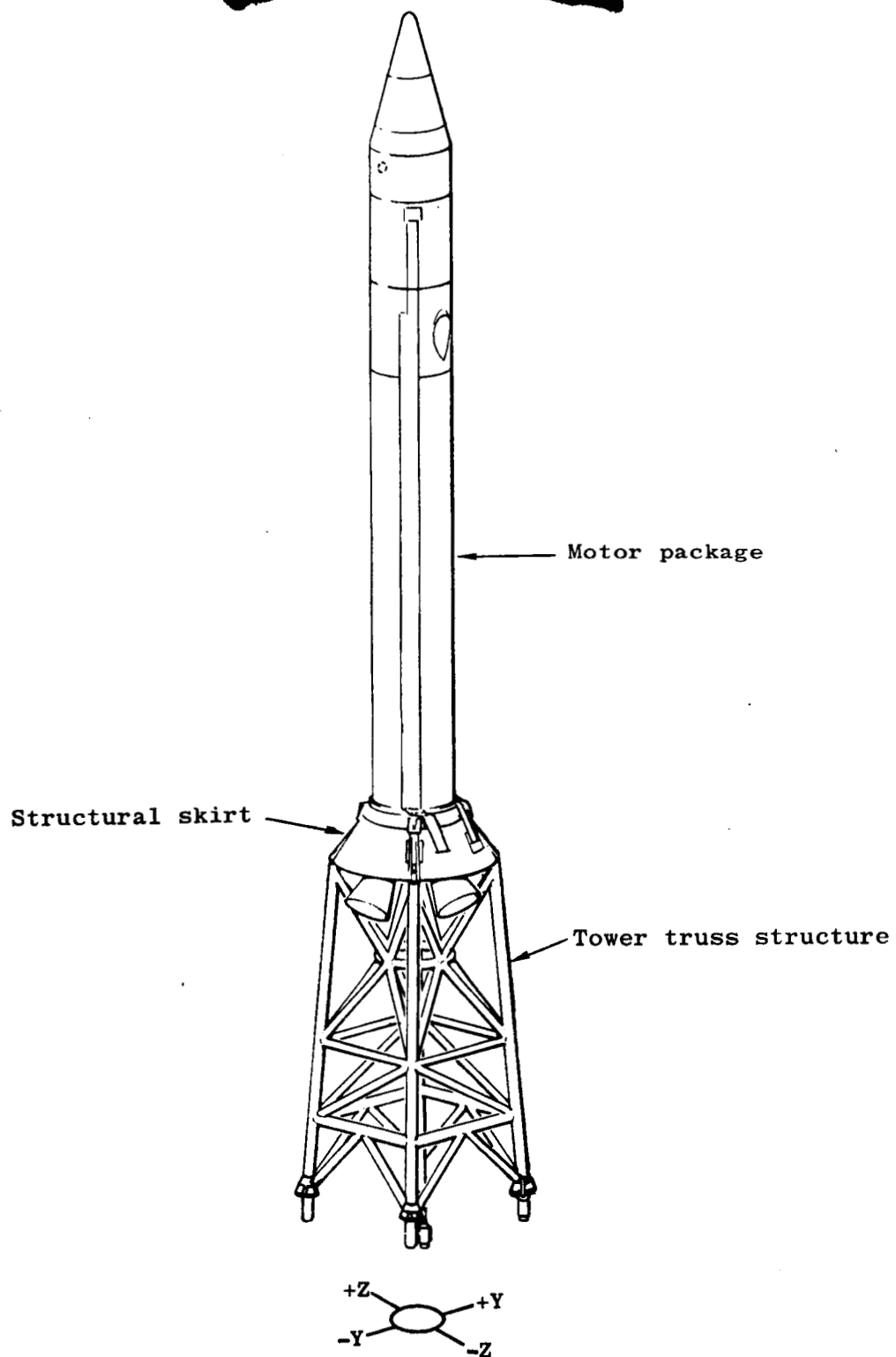


Figure 4.6-1.- Apollo BP-13 spacecraft launch escape subsystem structure.

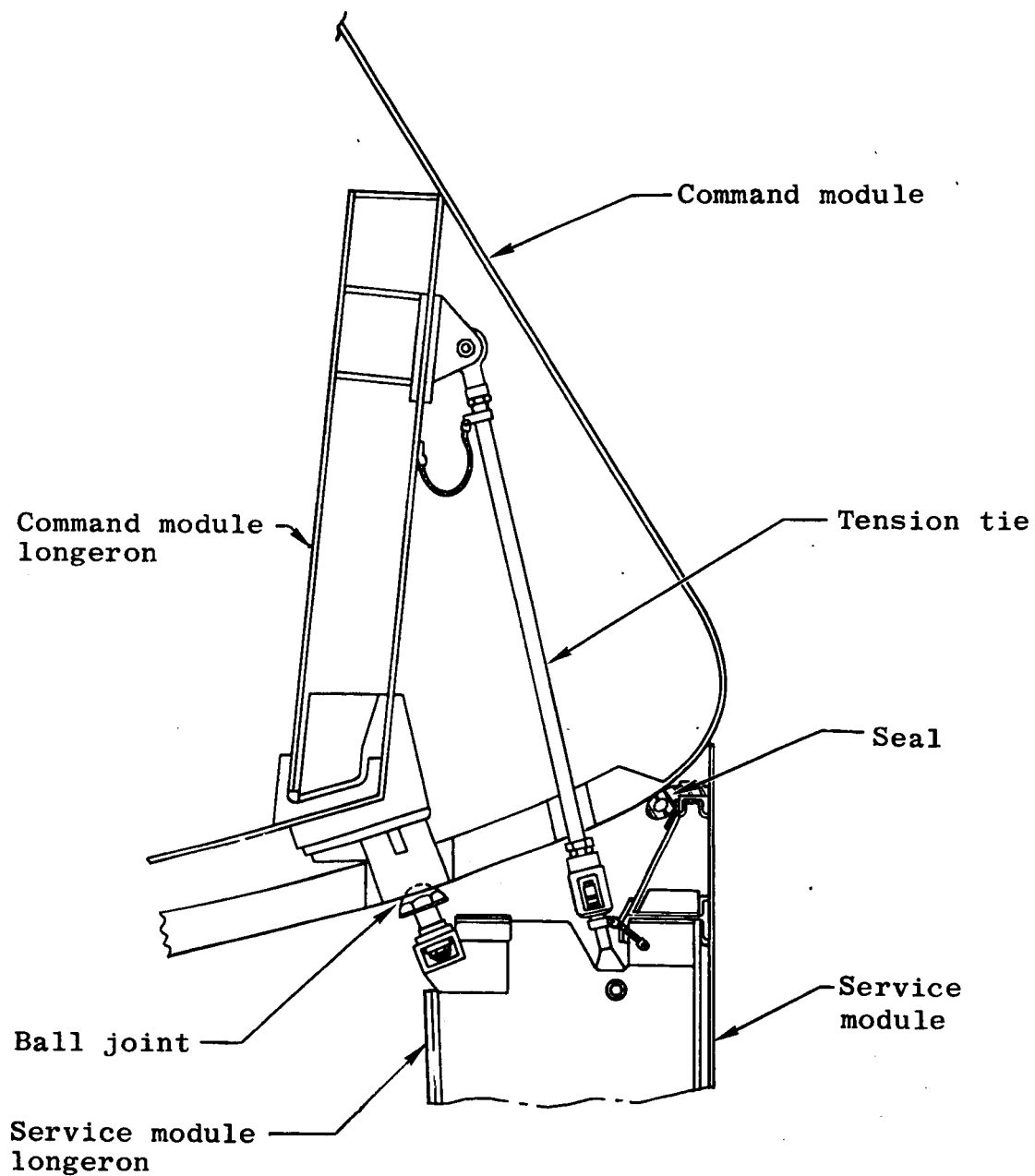


Figure 4.6-2.- Detail of command module-service module interface (BP-13 spacecraft).

4-64

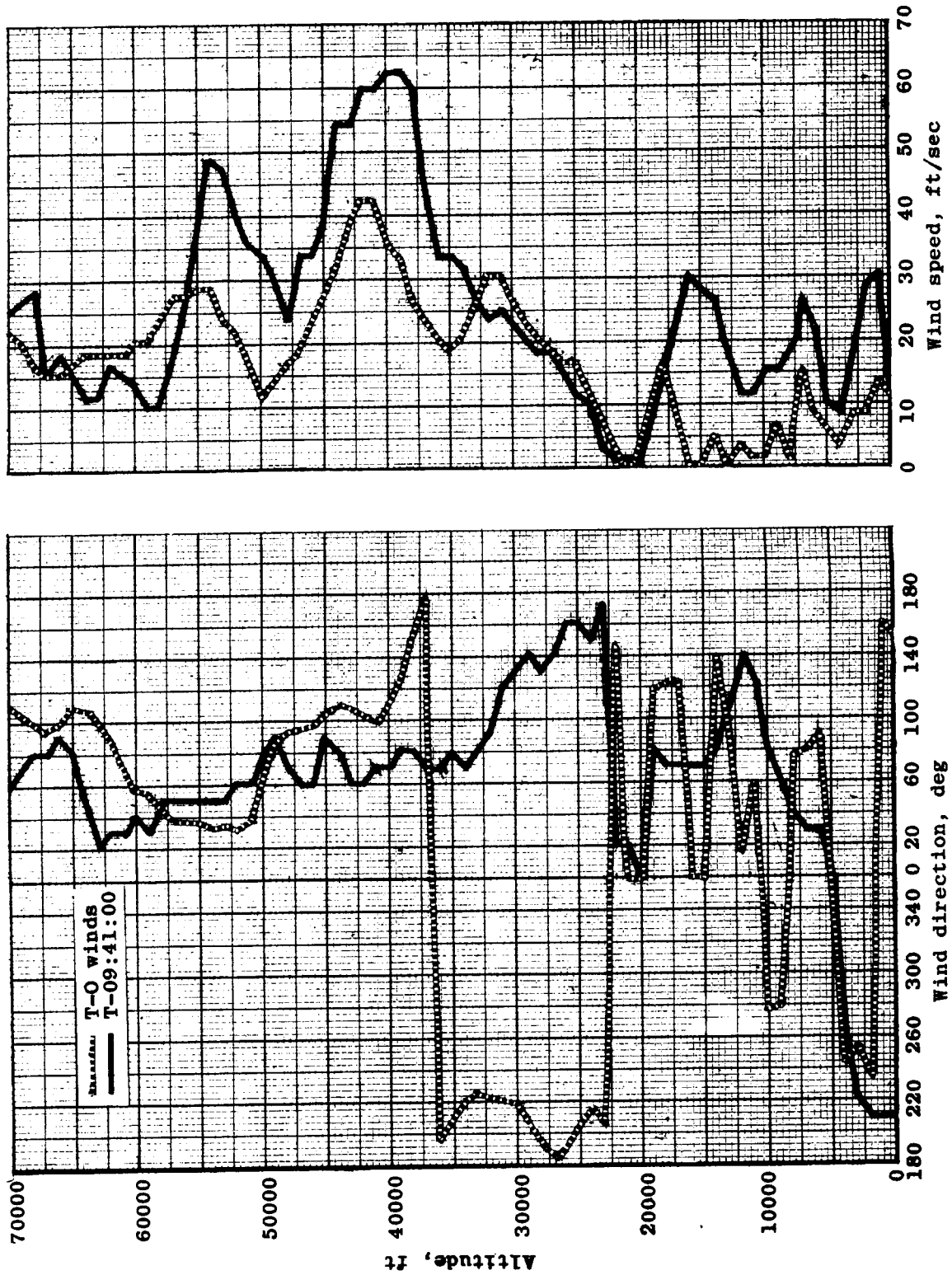


Figure 4.6-3.- Rawinsonde atmospheric wind data at Cape Kennedy, Fla., May 28, 1964.

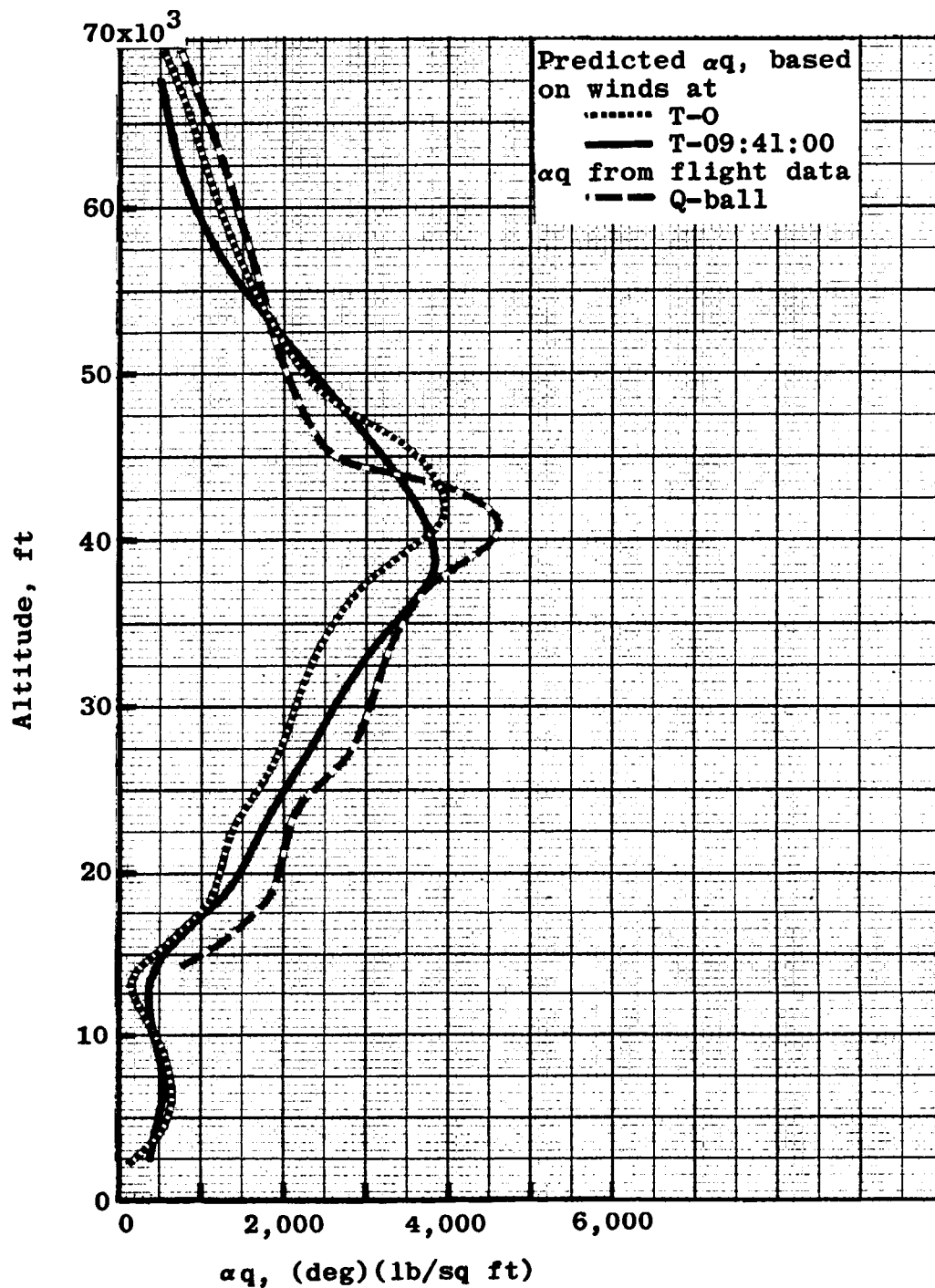


Figure 4.6-4.- Comparison of predicted αq and Q-ball αq (Apollo mission A-101).

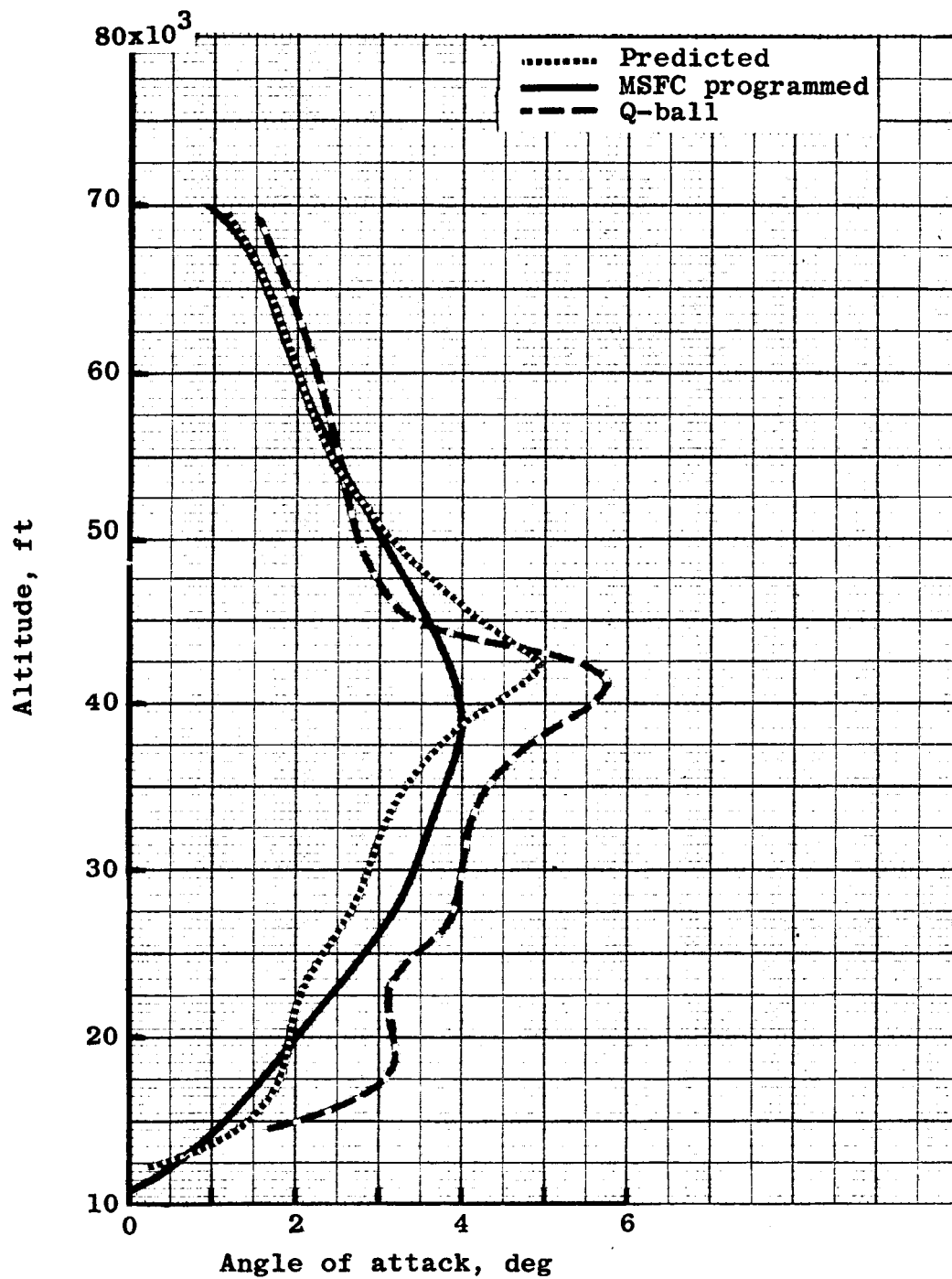


Figure 4.6-5.- Variation of angle of attack with altitude (Apollo mission A-101).

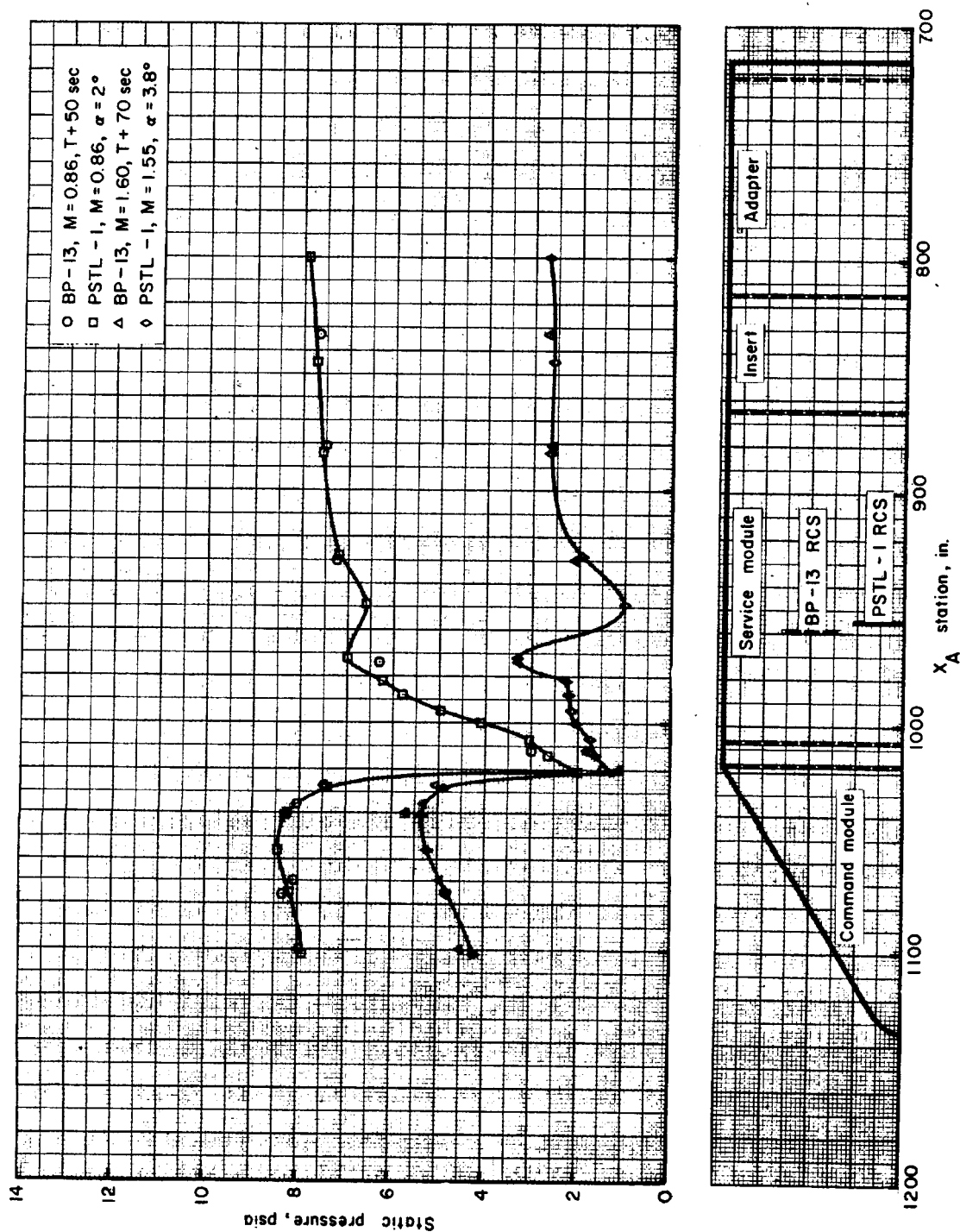
(a) $\phi = 0^\circ$

Figure 4.6-6.- Static pressure flight measurement on BP-13 spacecraft compared with wind-tunnel measurements on model PSTL-1 (ref. 1).

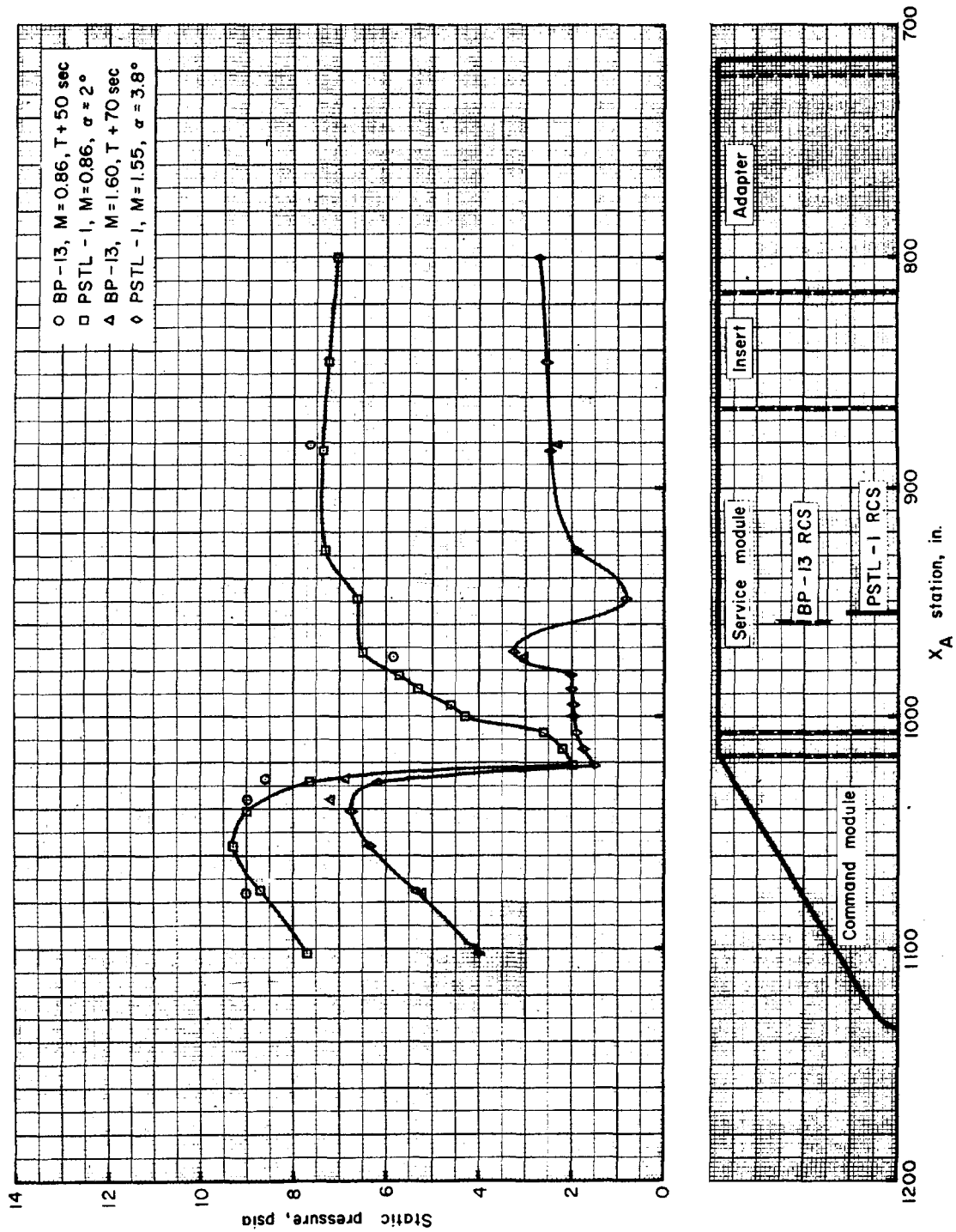
(b) $\phi = 90^\circ$

Figure 4.6-6.- Continued.

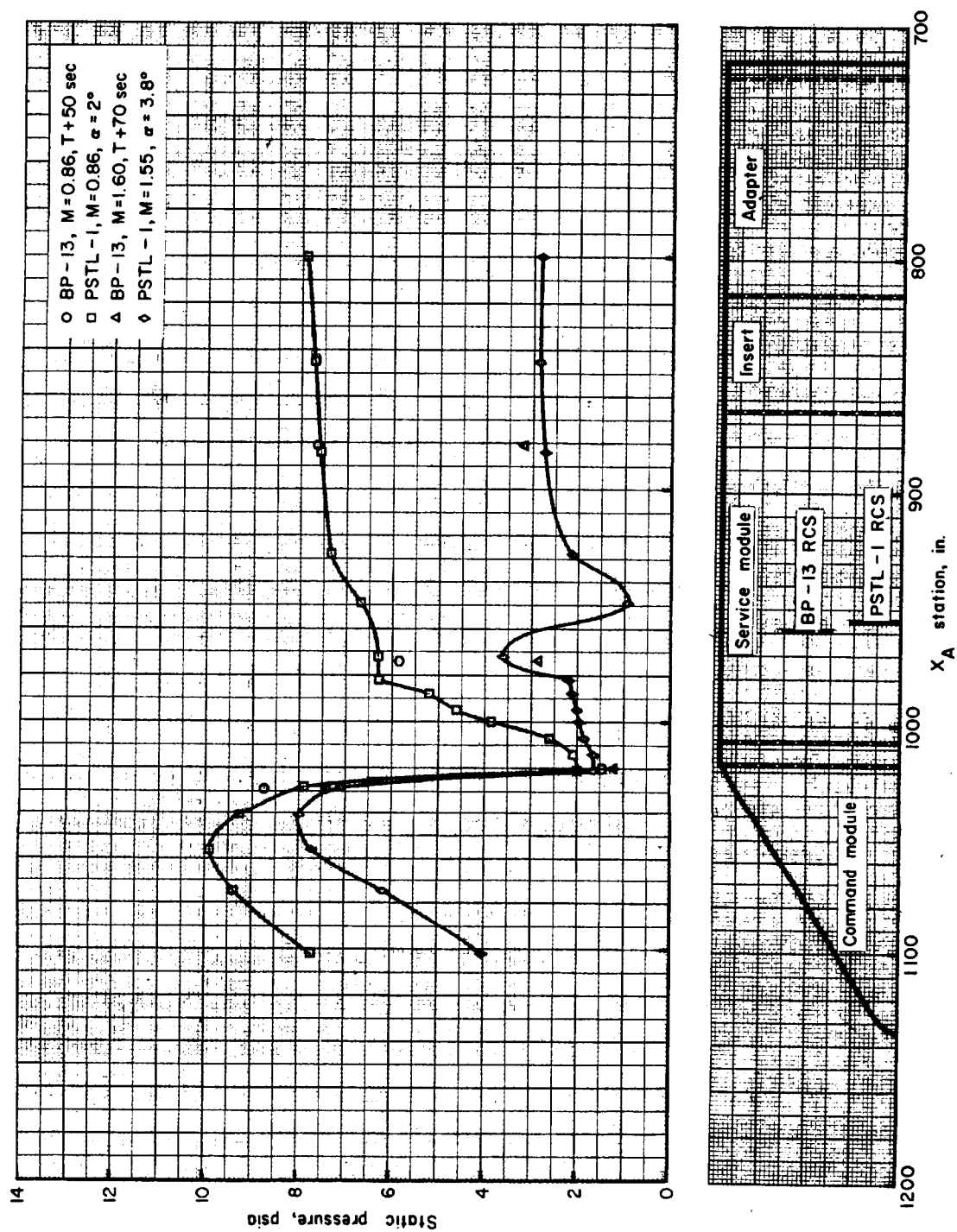
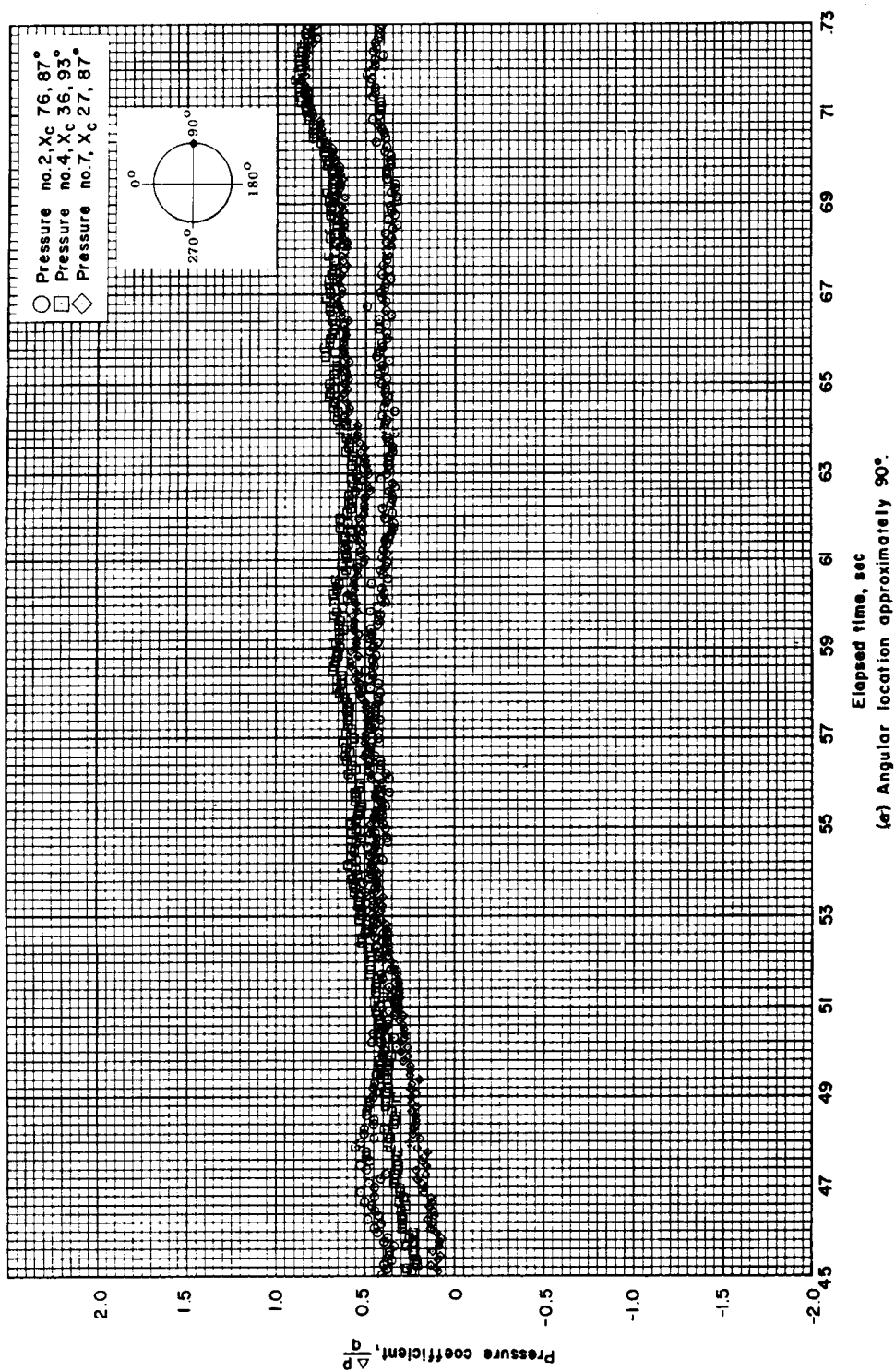
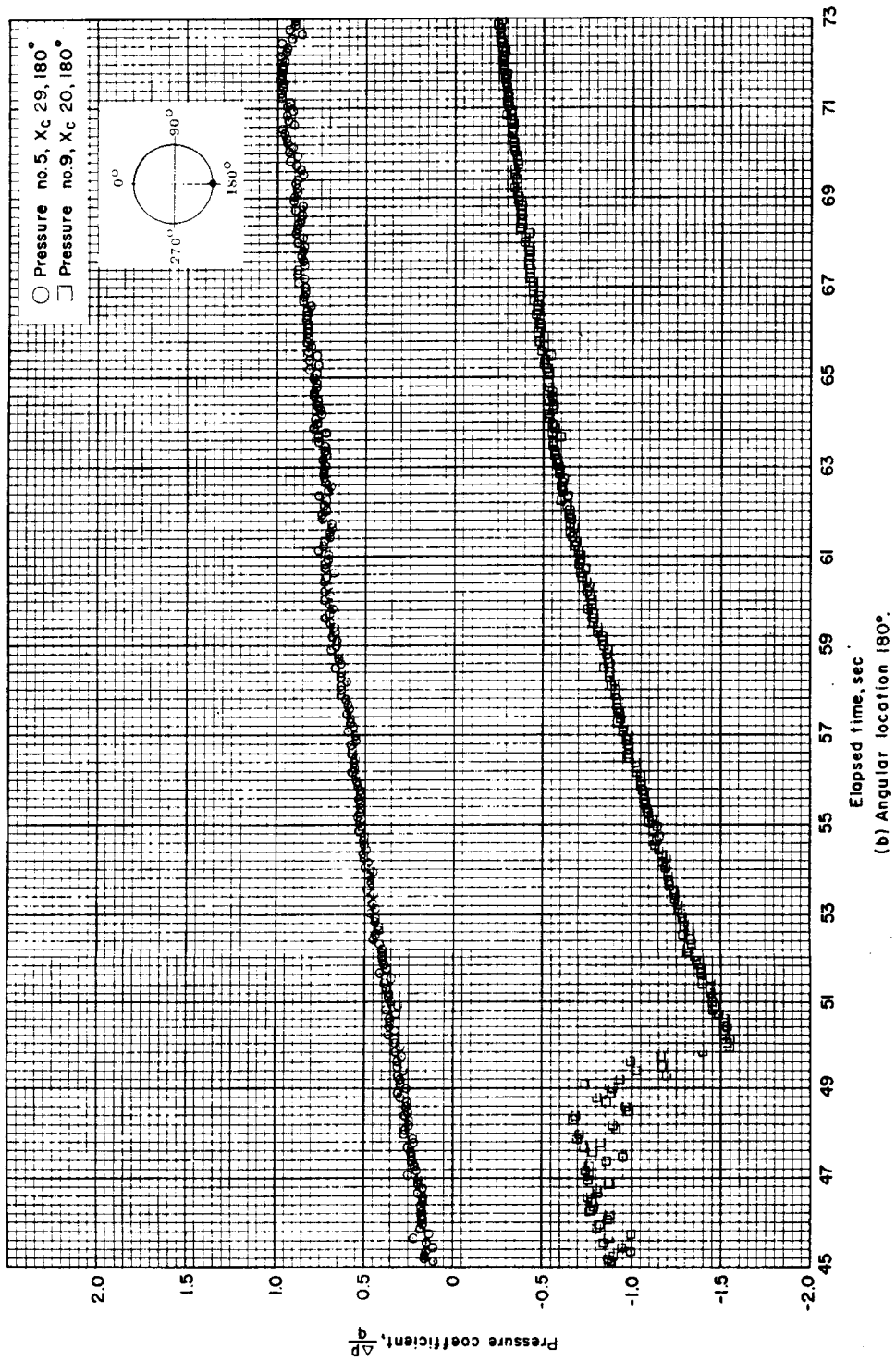
(c) $\phi = 180^\circ$

Figure 4.6-6.- Concluded.



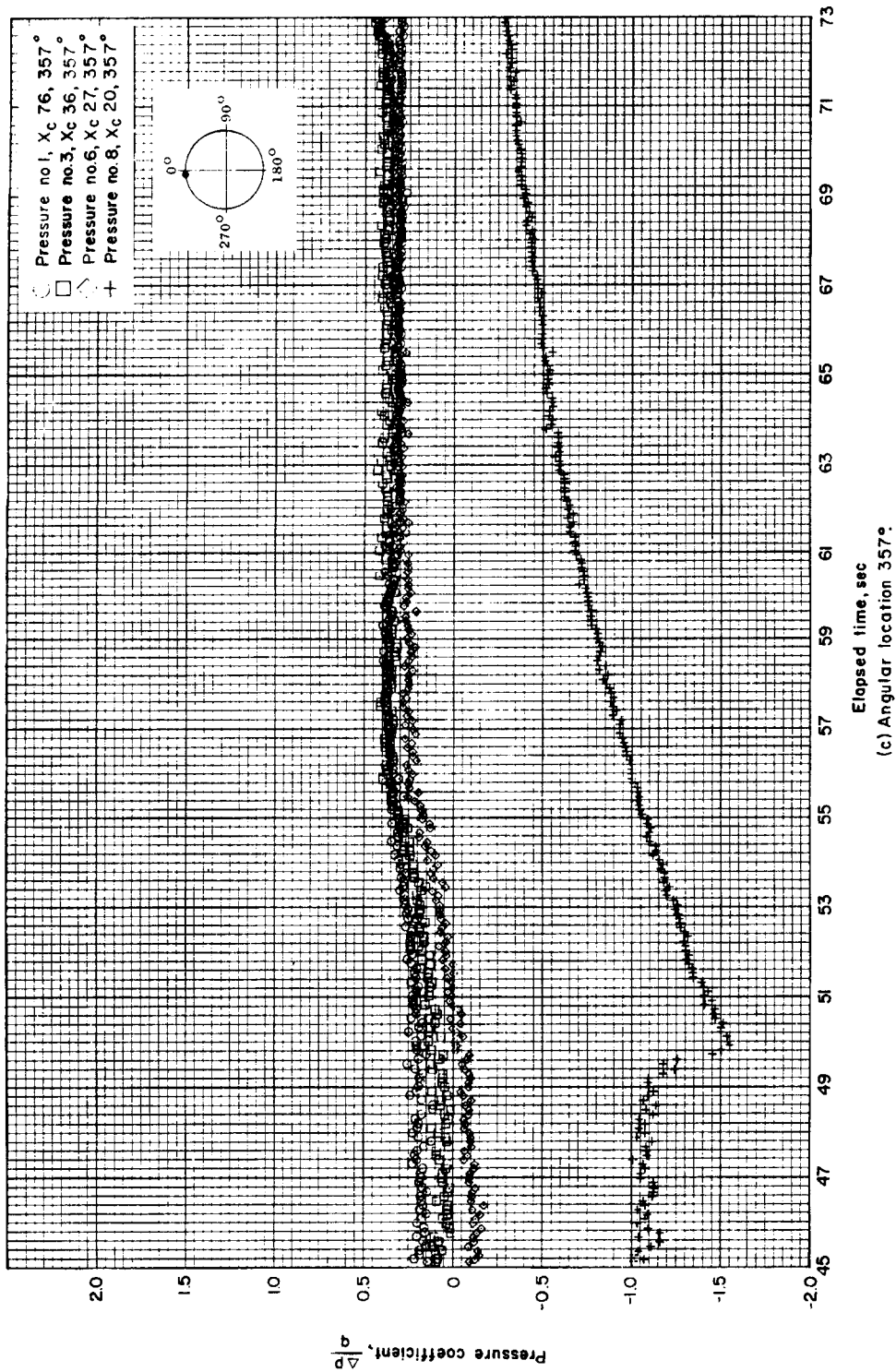
(a) Angular location, approximately 90°

Figure 4.6-7.- Static pressure coefficient over the command module conical surface (BP-13 spacecraft).



(b) Angular location, 180°

Figure 4.6-7.- Continued.



(c) Angular location, 357°

Figure 4.6-7.- Concluded.

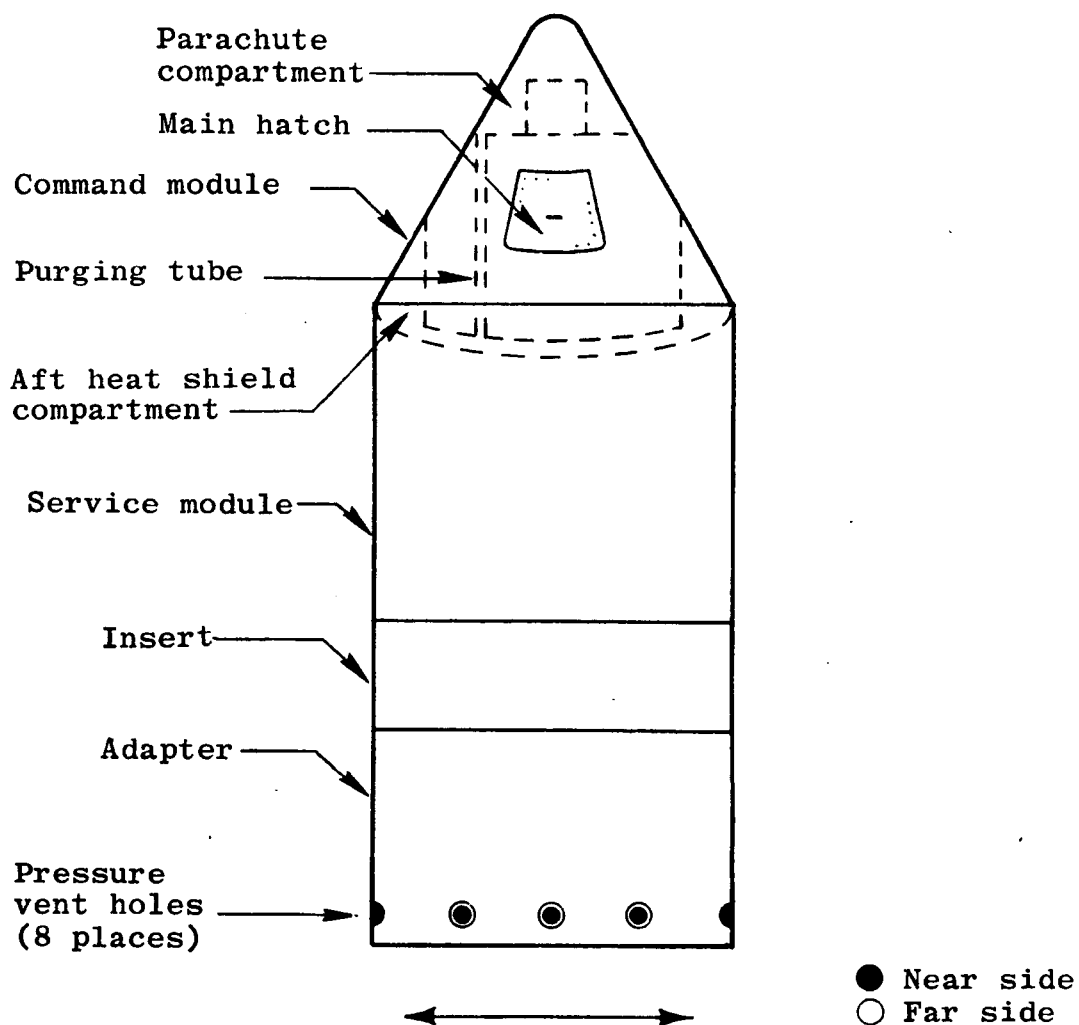


Figure 4.6-8.- Pressure venting scheme for BP-13 spacecraft service module, insert, and adapter compartment.

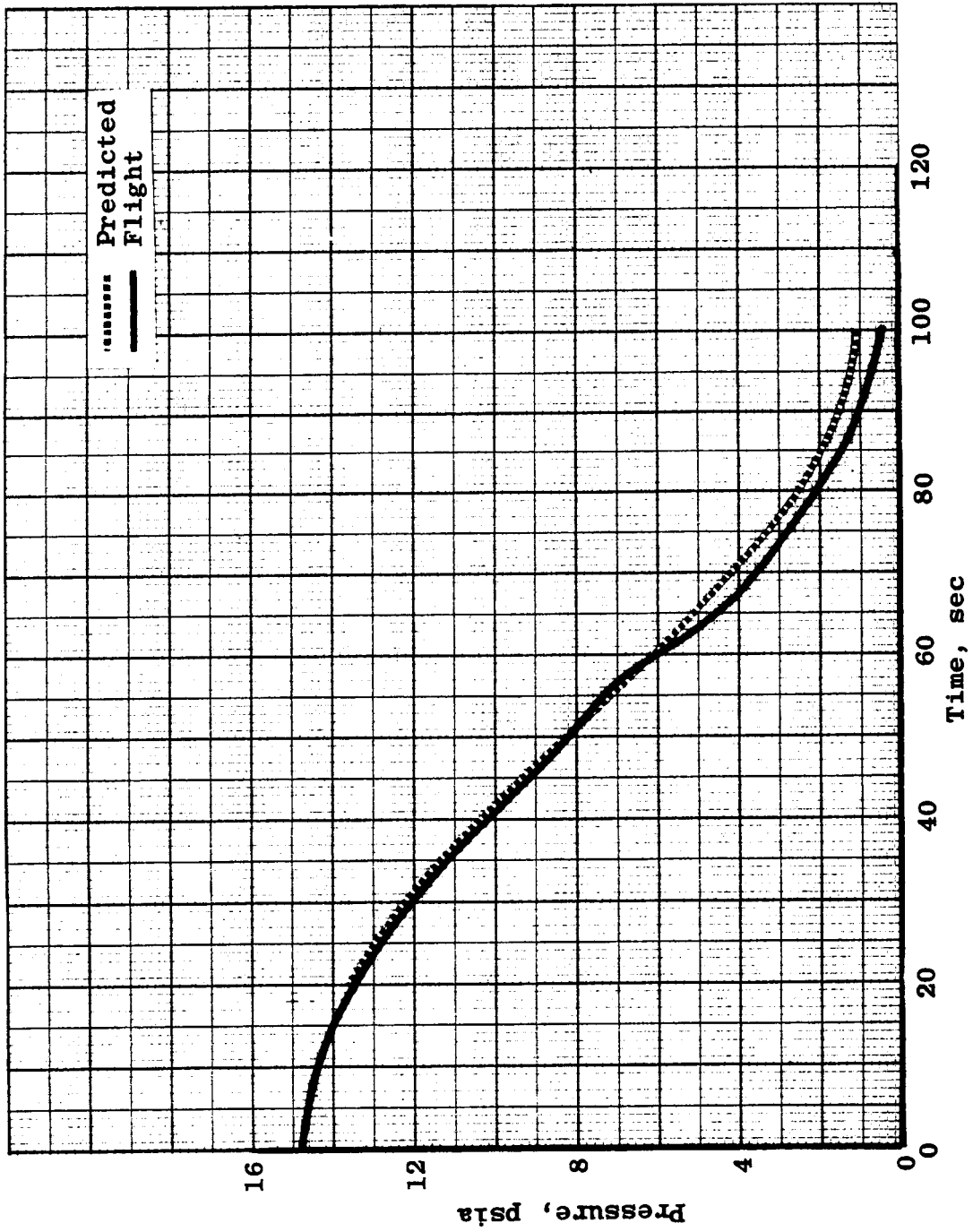


Figure 4.6-9.- Service module internal pressure (BP-13 spacecraft).

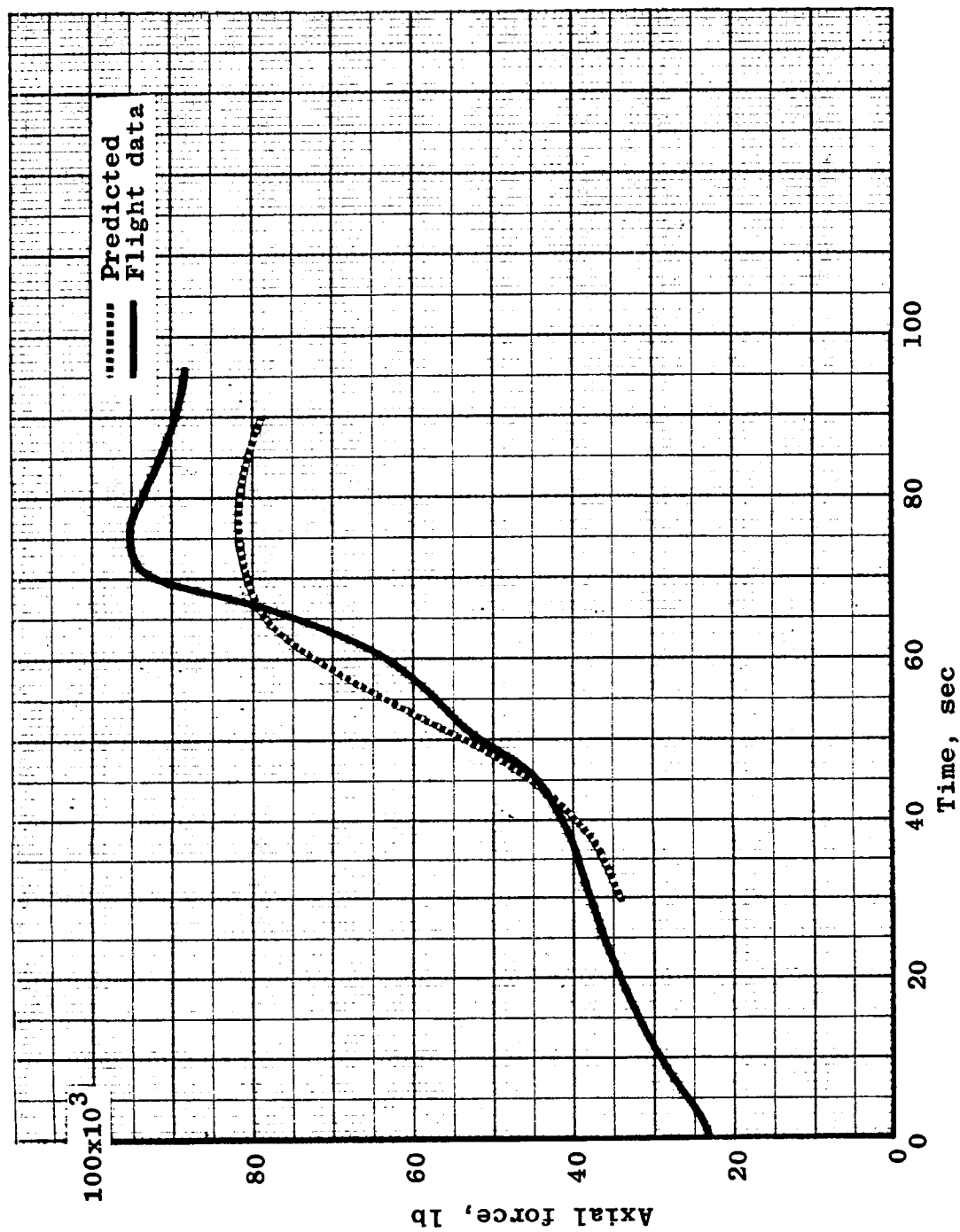
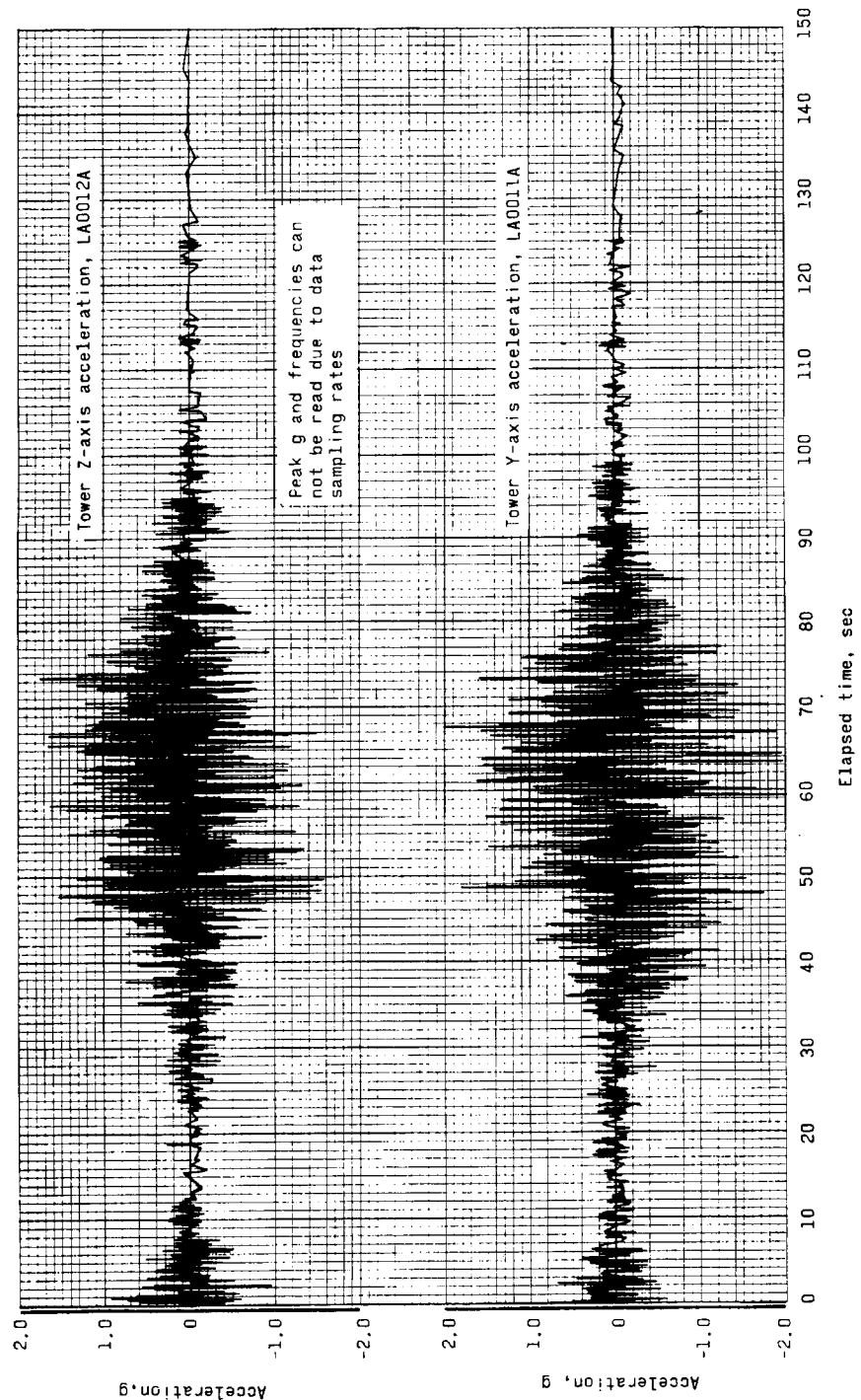
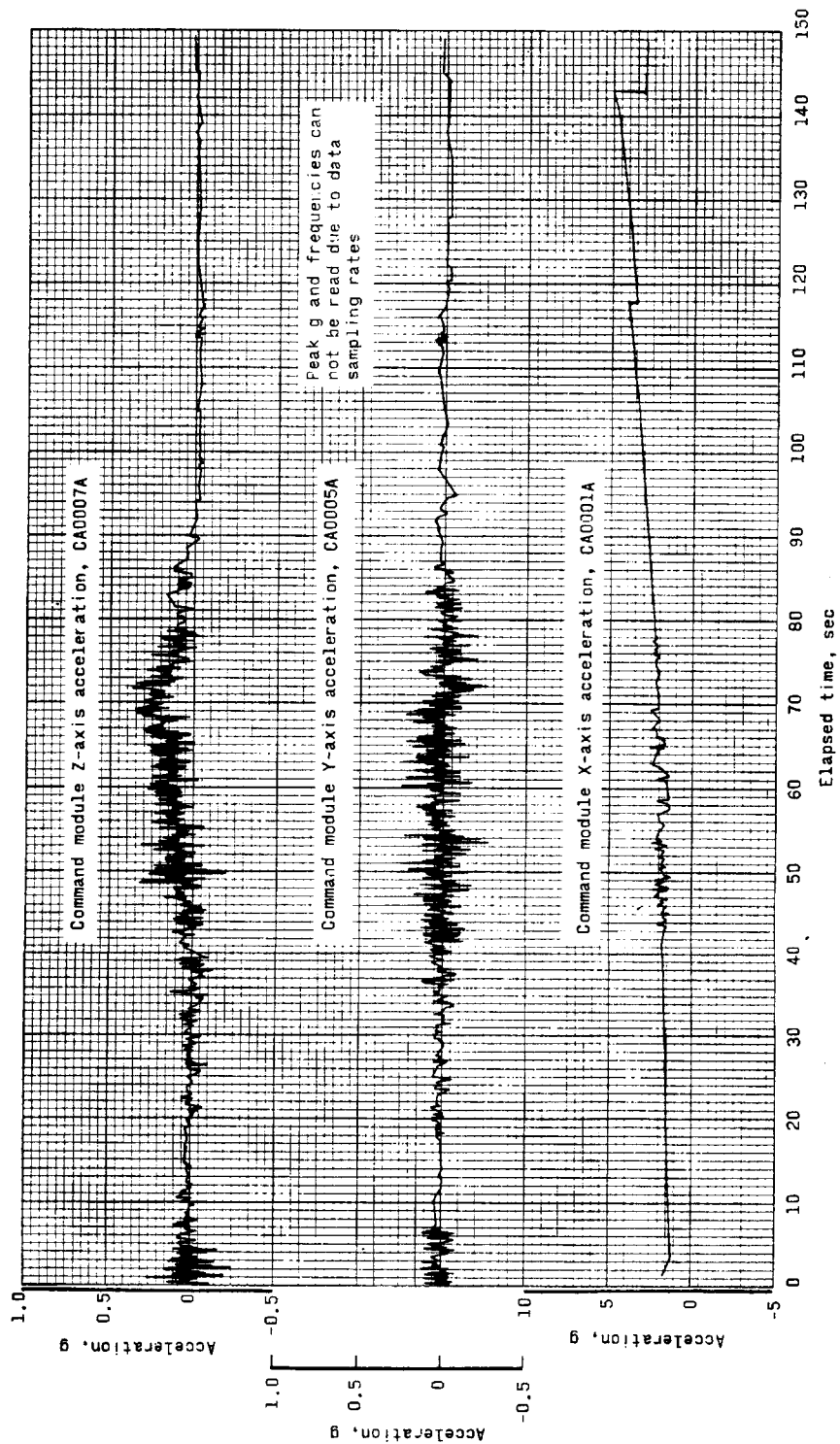


Figure 4.6-10.- Axial force (compression) at interface of BP-13 spacecraft adapter and Saturn SA-6 instrument unit (station X_A 722).



(a) Launch-escape subsystem at Q-ball interface.

Figure 4.6-11.--Flight measured acceleration (BP-13 spacecraft).



(b) Command module.

Figure 4.6-11.- Concluded.

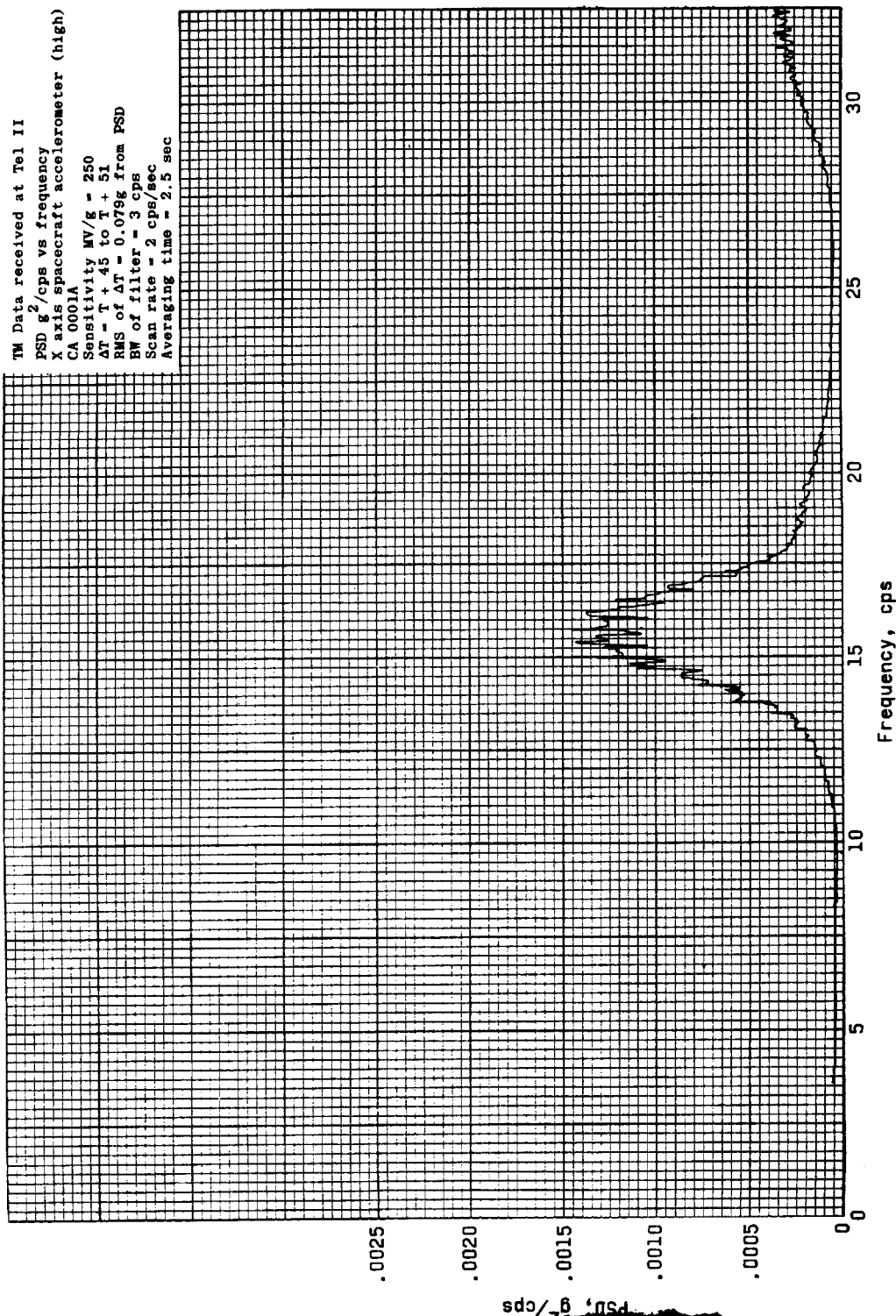
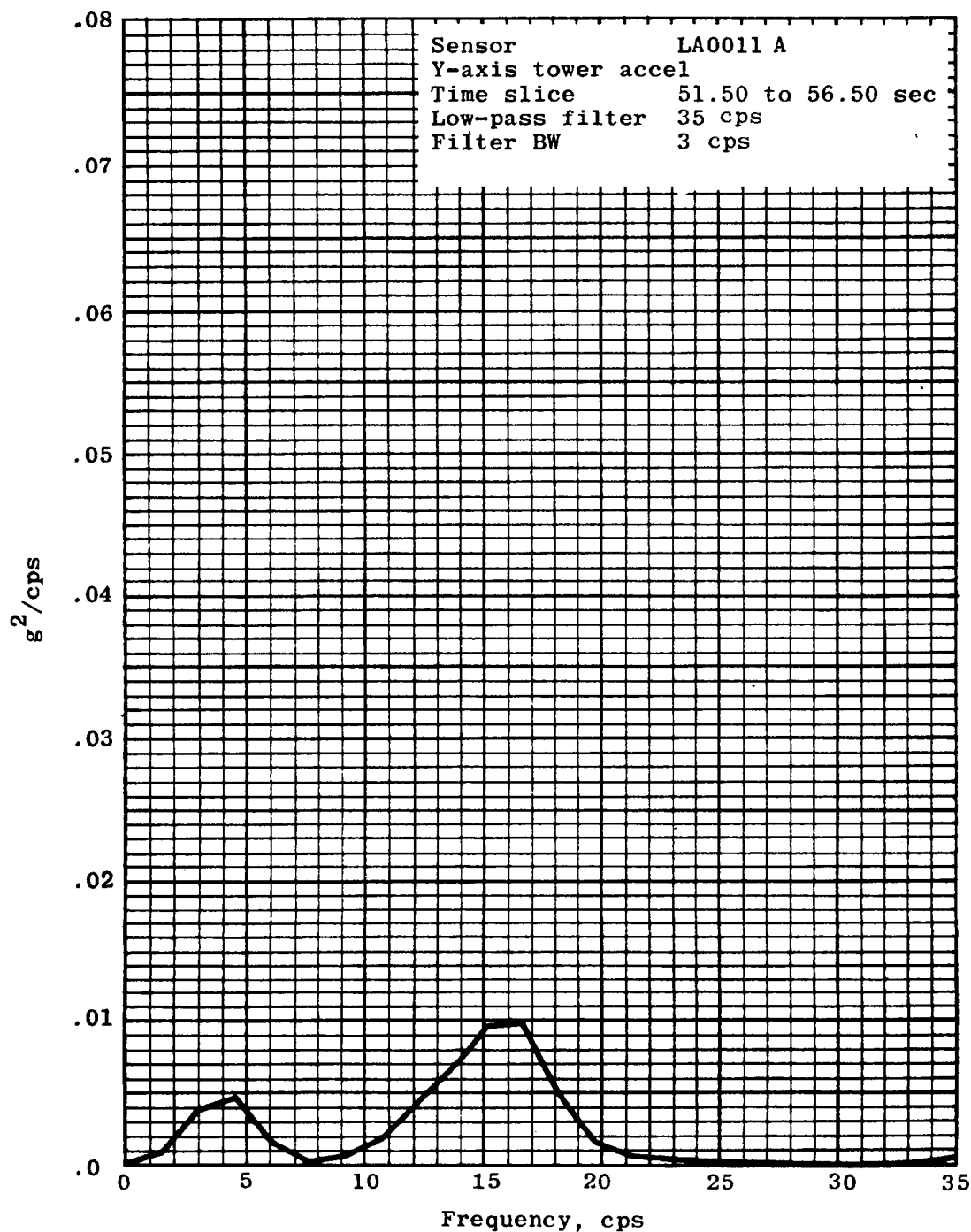
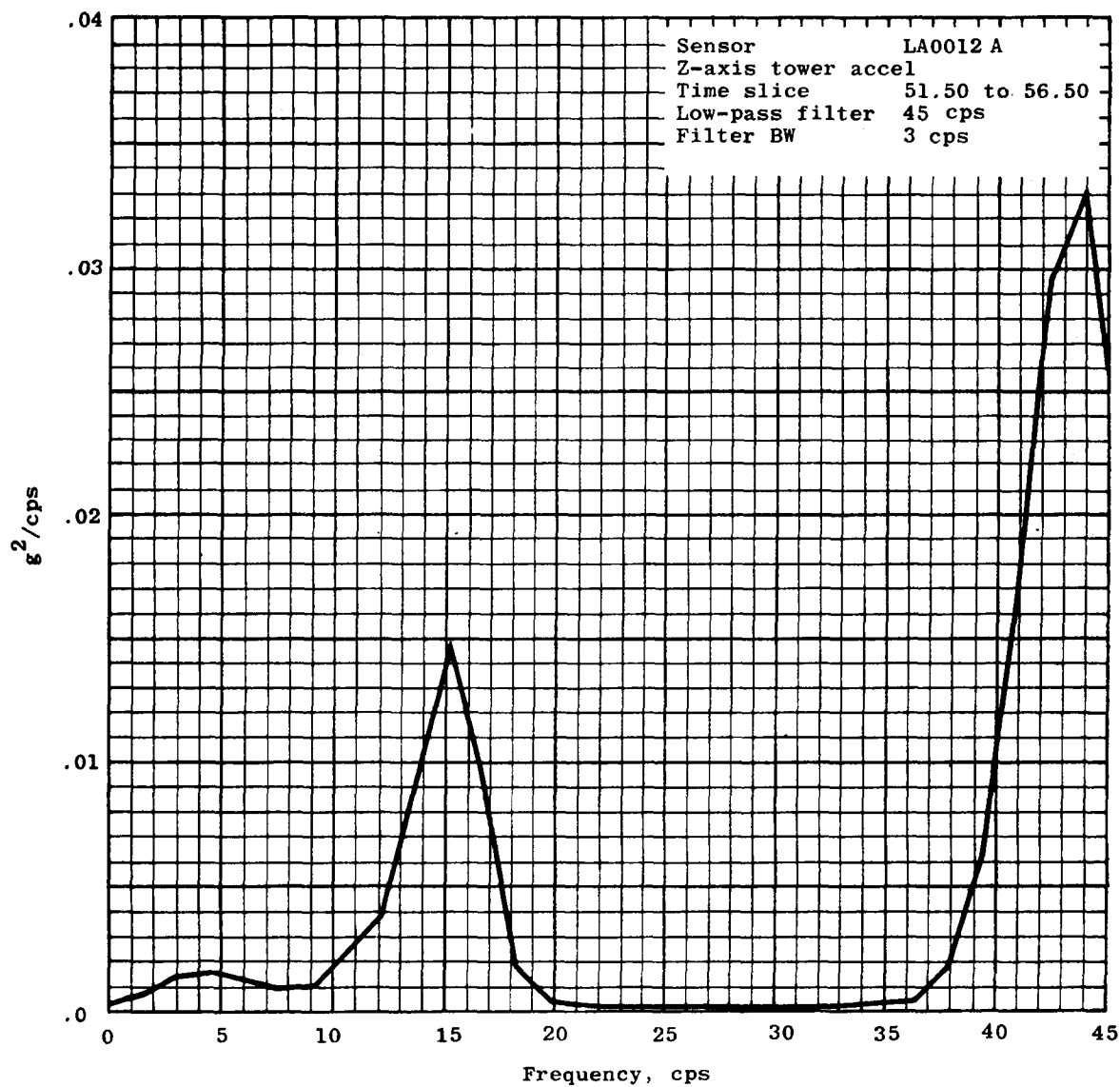


Figure 4.6-12.- Digital spectrum estimation of X-axis acceleration (BP-13 spacecraft).



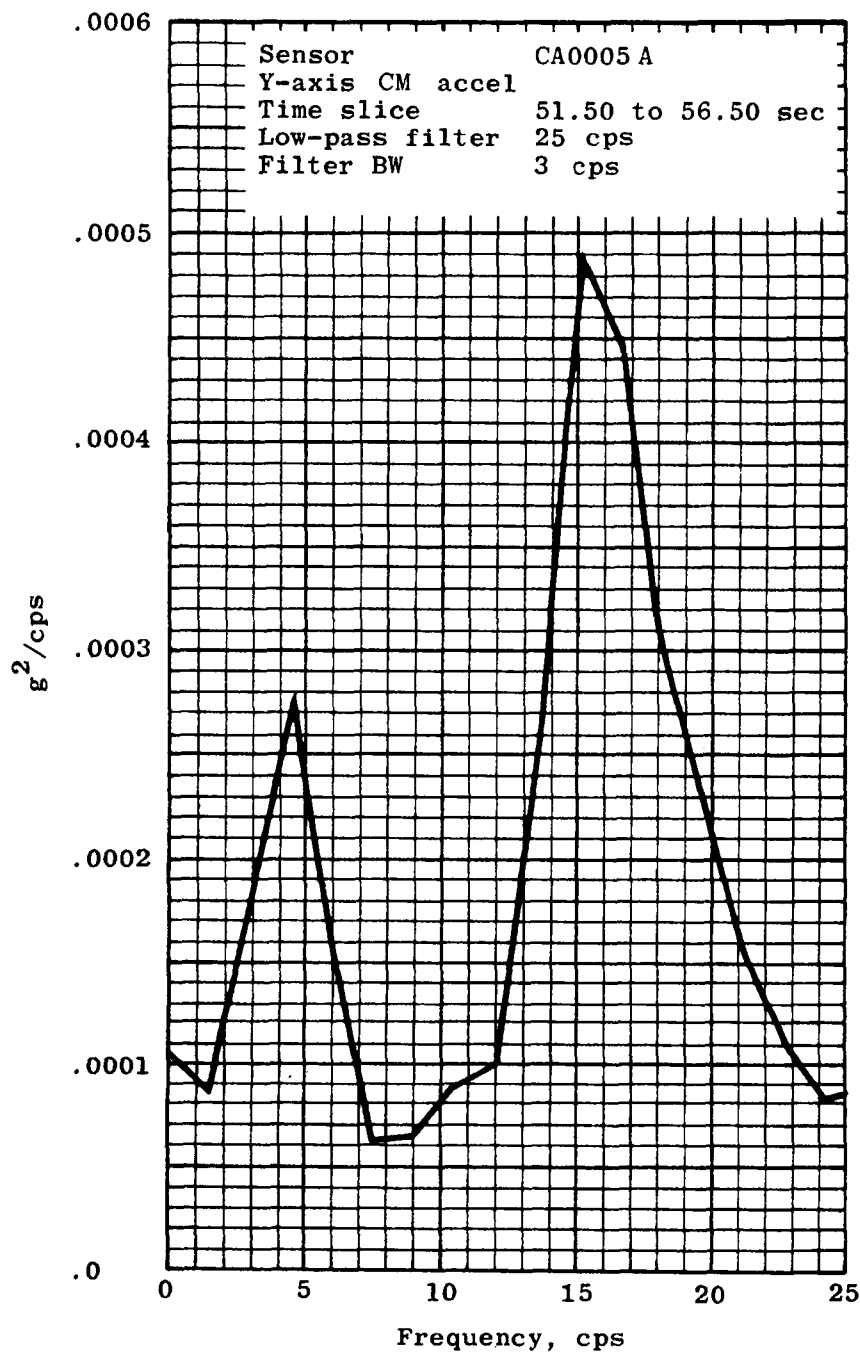
(a) LES Y-axis at Q-ball interface

Figure 4.6-13.- Digital spectrum estimation of lateral bending acceleration (BP-13 spacecraft).



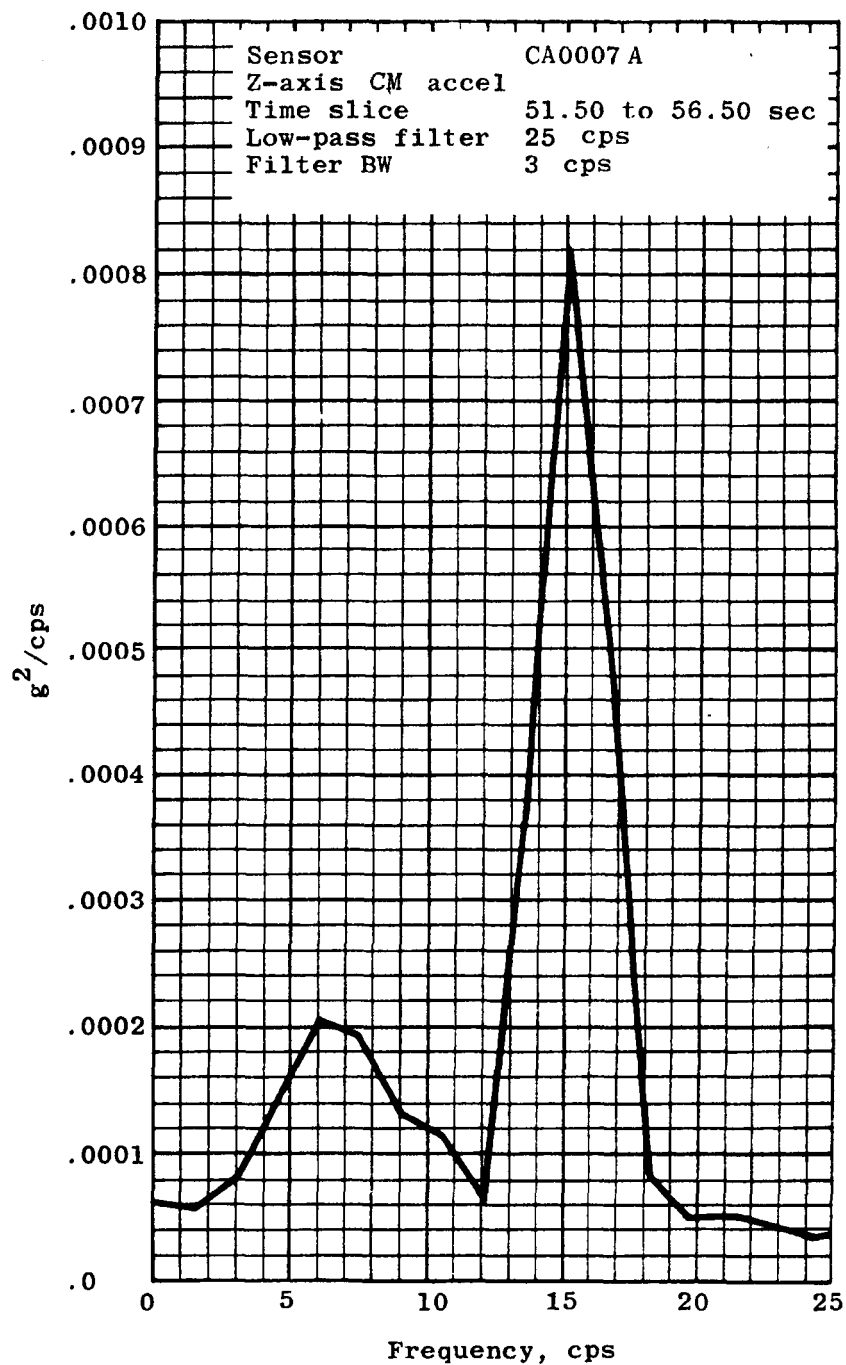
(b) LES Z-axis at Q-ball interface.

Figure 4.6-13.- Continued



(c) Command module Y-axis.

Figure 4.6-13.- Continued.



(d) Command module Z-axis.

Figure 4.6-13.- Concluded.

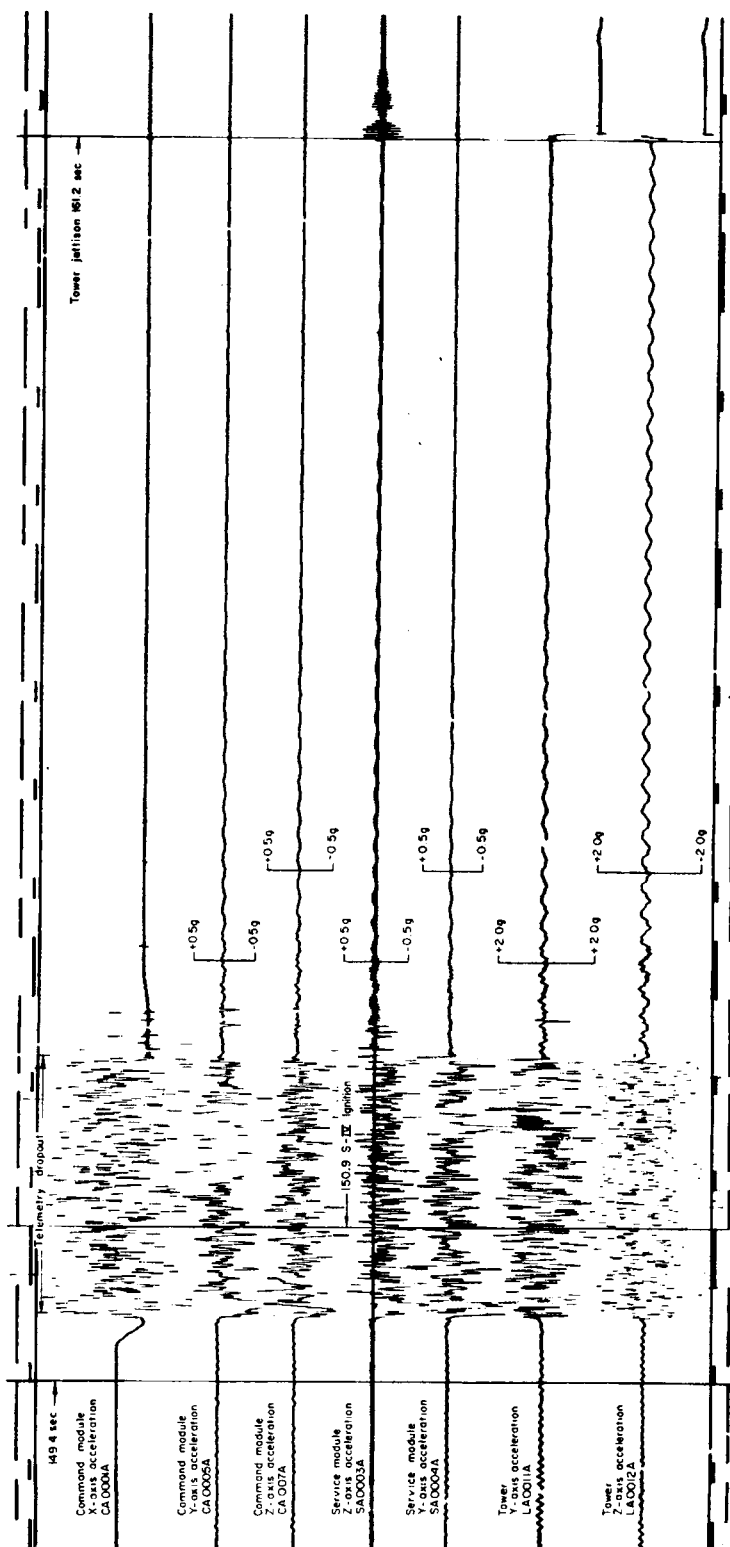
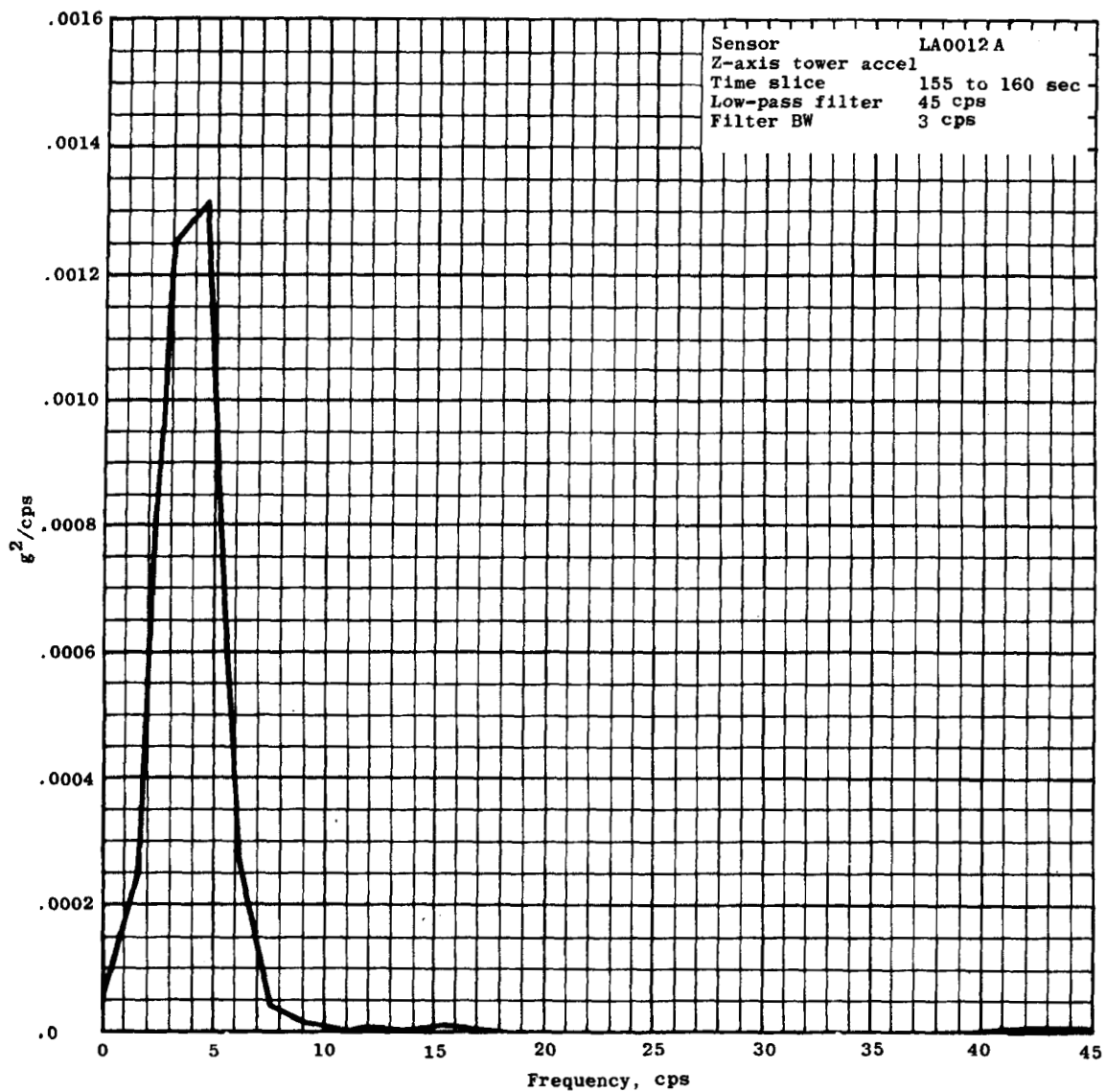
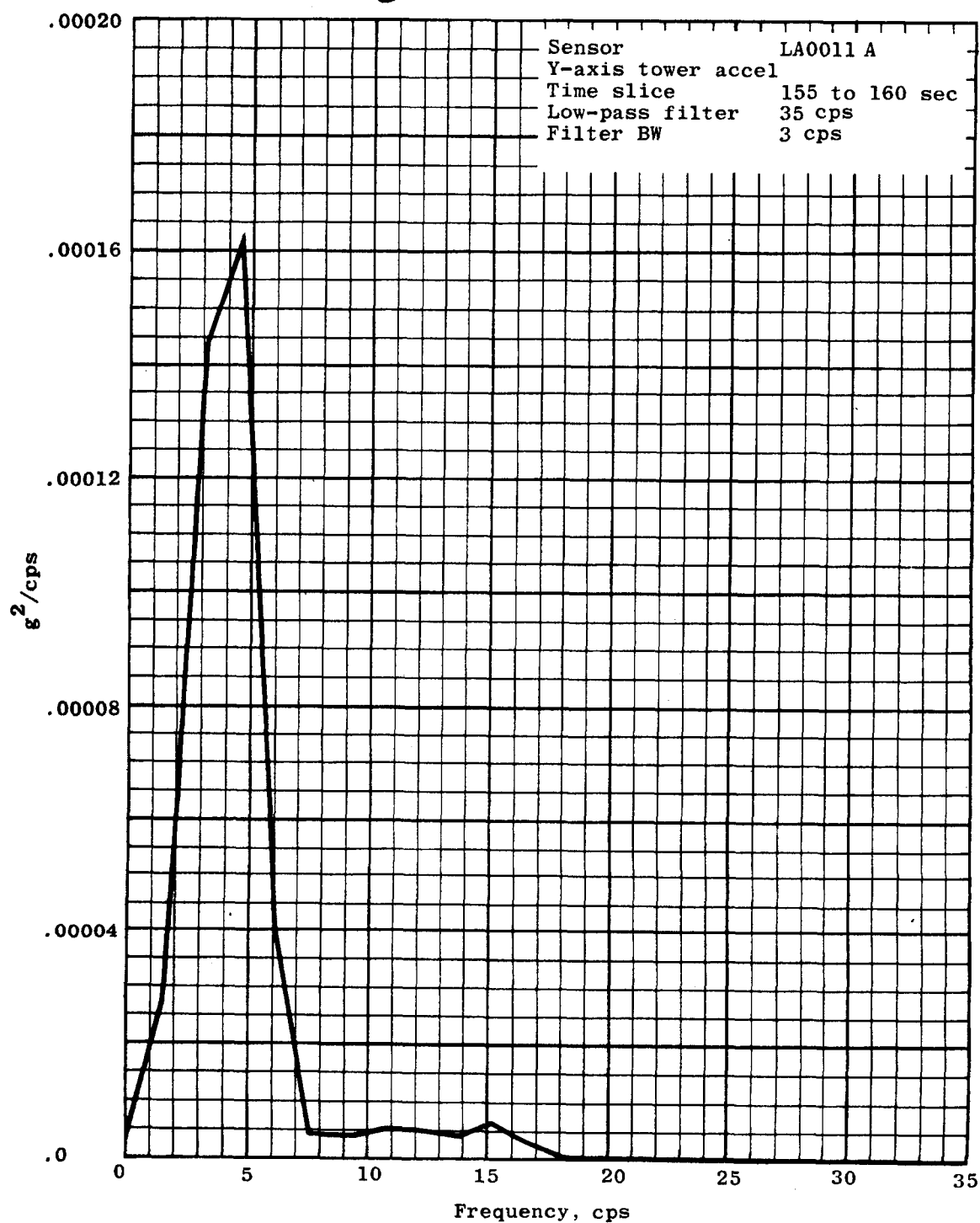


Figure 4.6-14.- First bending mode acceleration of BP-13 spacecraft at ignition of S-IV stage.



(a) LES Z-axis at Q-ball interface

Figure 4.6-15.- Digital spectrum estimation of first bending mode acceleration of BP-13 spacecraft after ignition of S-IV stage.



(b) LES Y-axis at Q-ball interface.

Figure 4.6-15.- Concluded.

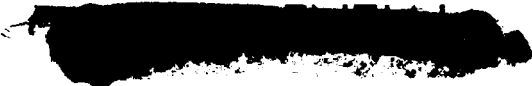


Figure 4.6-16.- Development view of BP-13 spacecraft service module, insert, and adapter wall showing transducer locations.

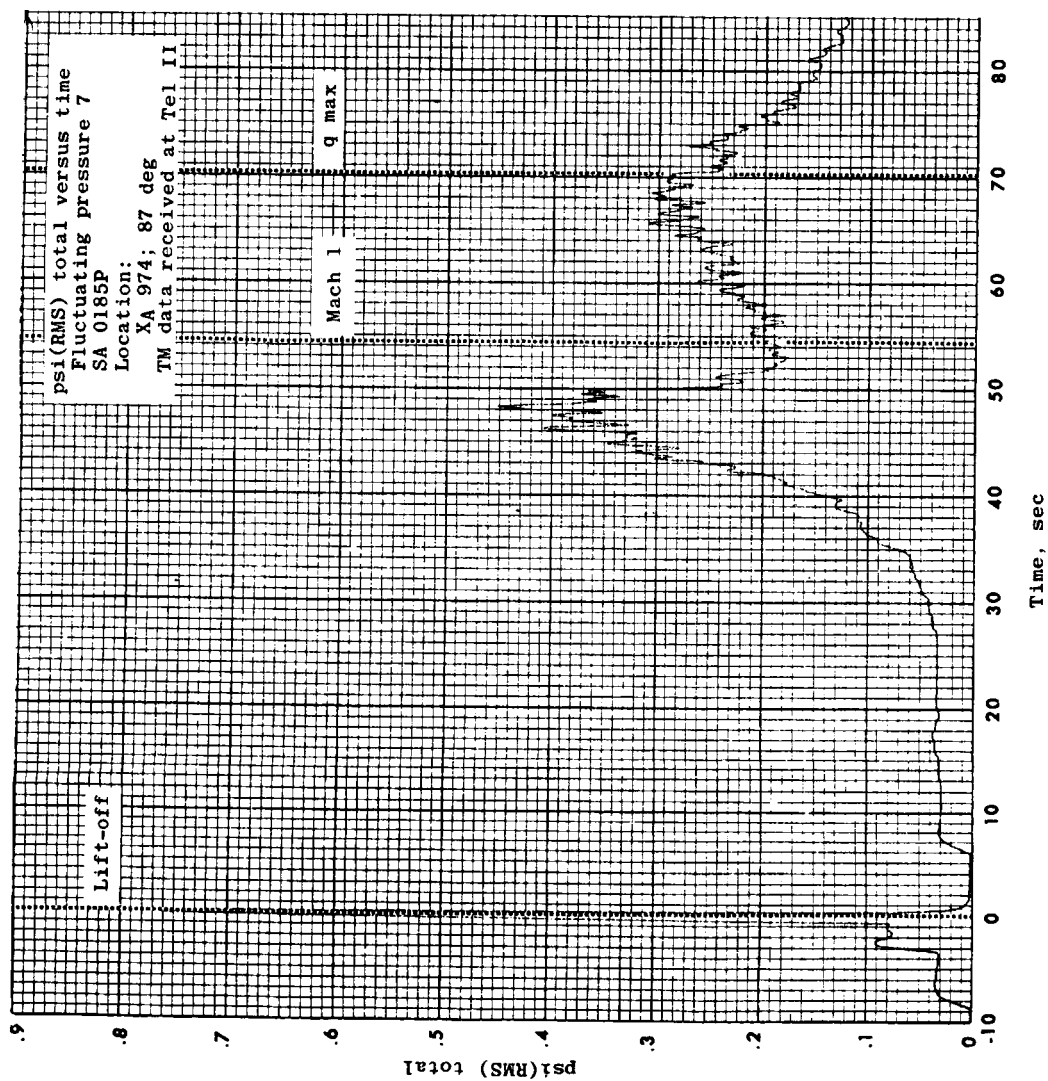


Figure 4.6-17.- RMS of fluctuating pressure no. 7 on BP-13 service module.

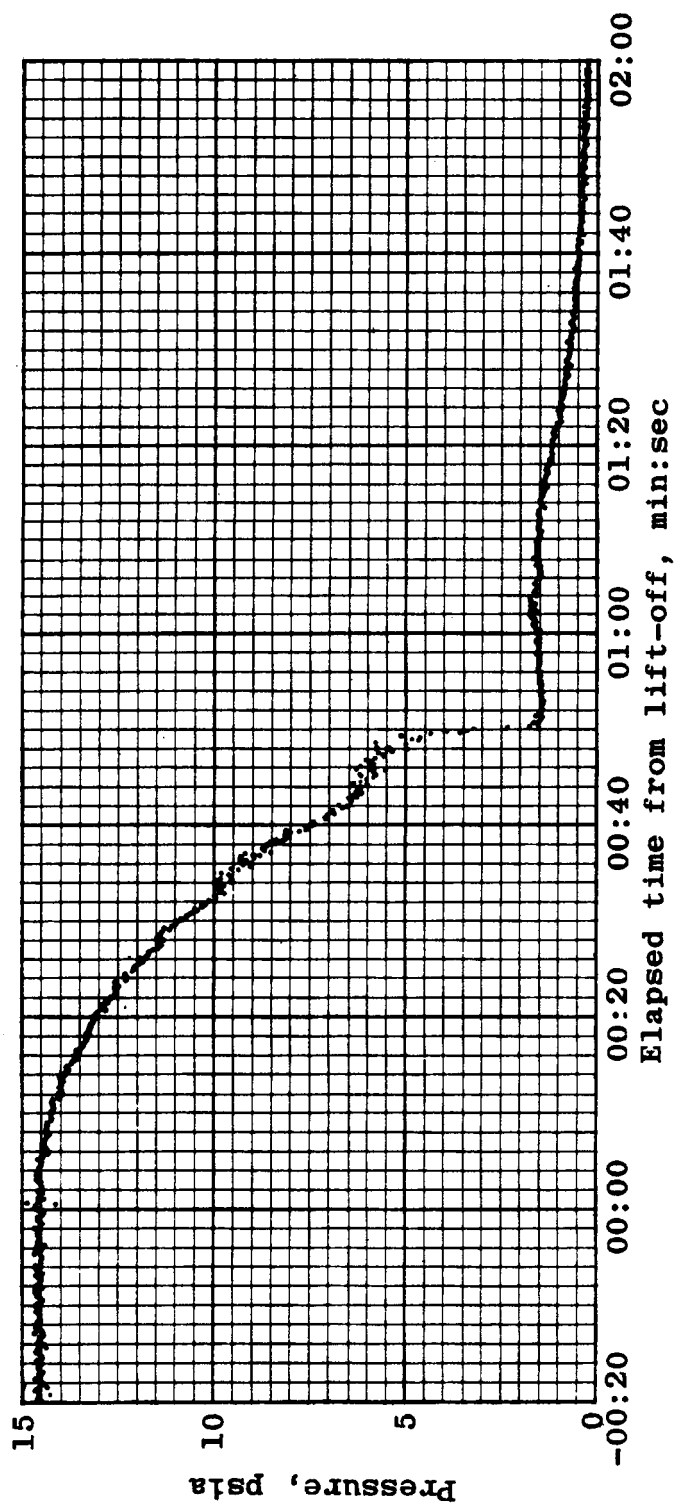


Figure 4.6-18.- Static pressure at BP-13 spacecraft CM-SM shoulder.

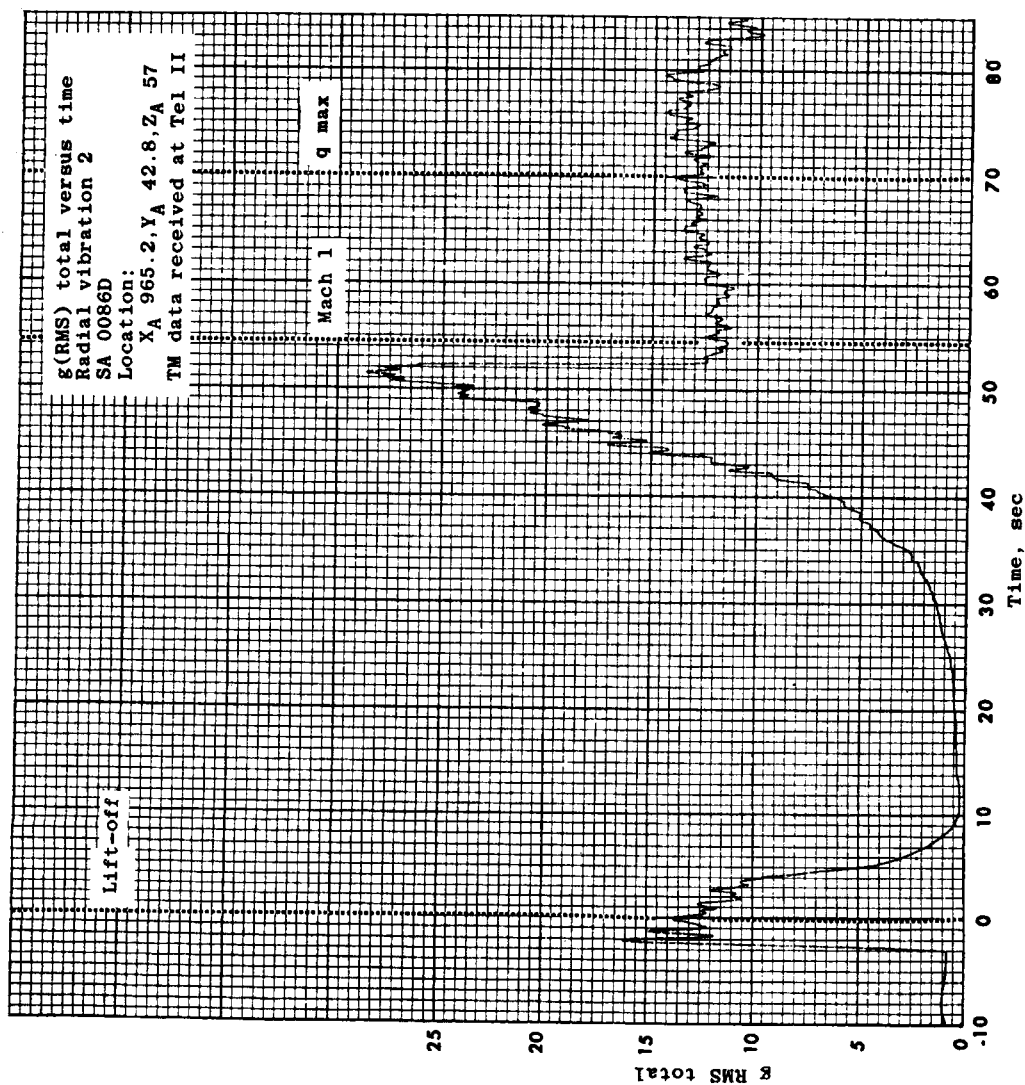
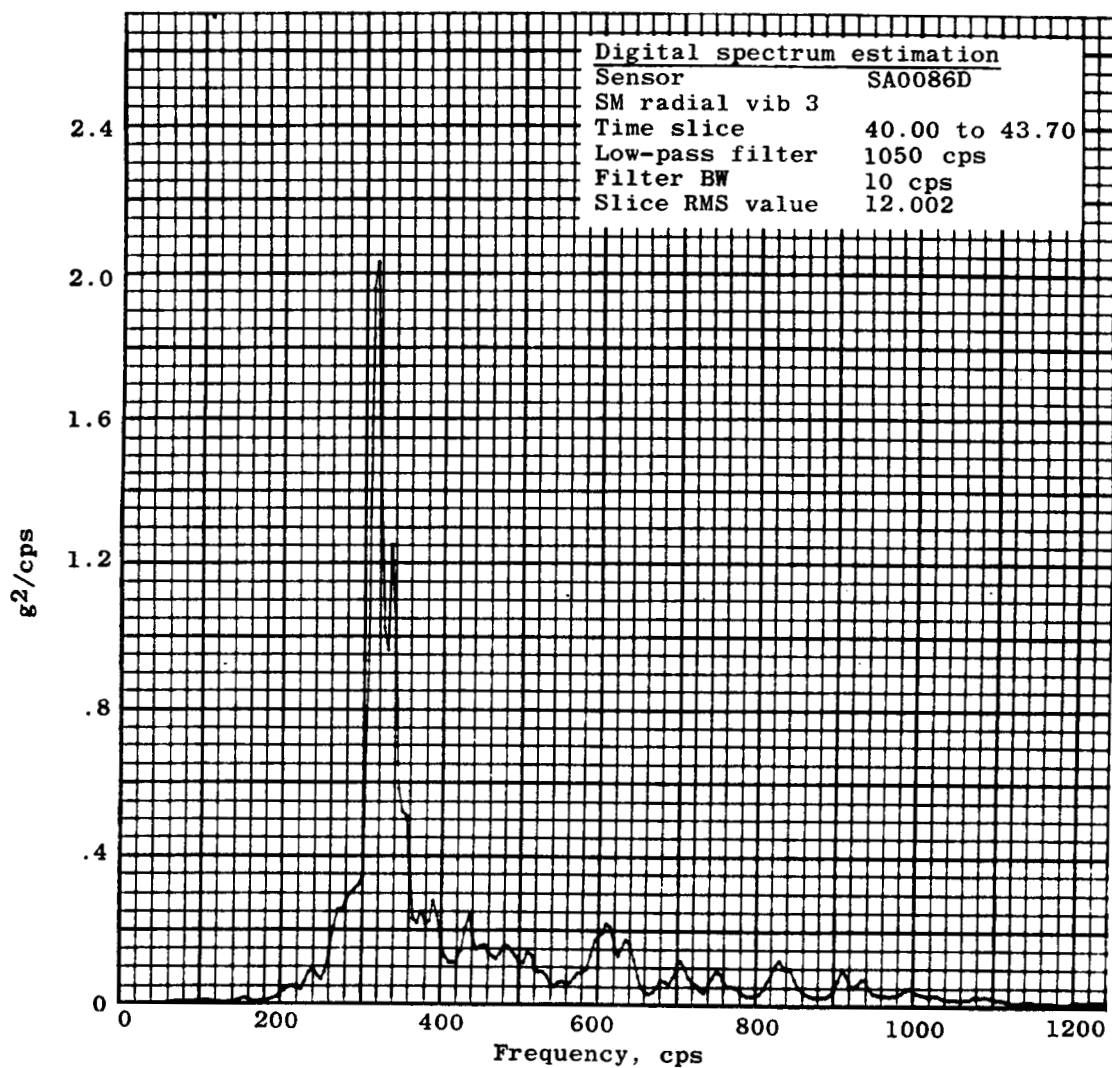
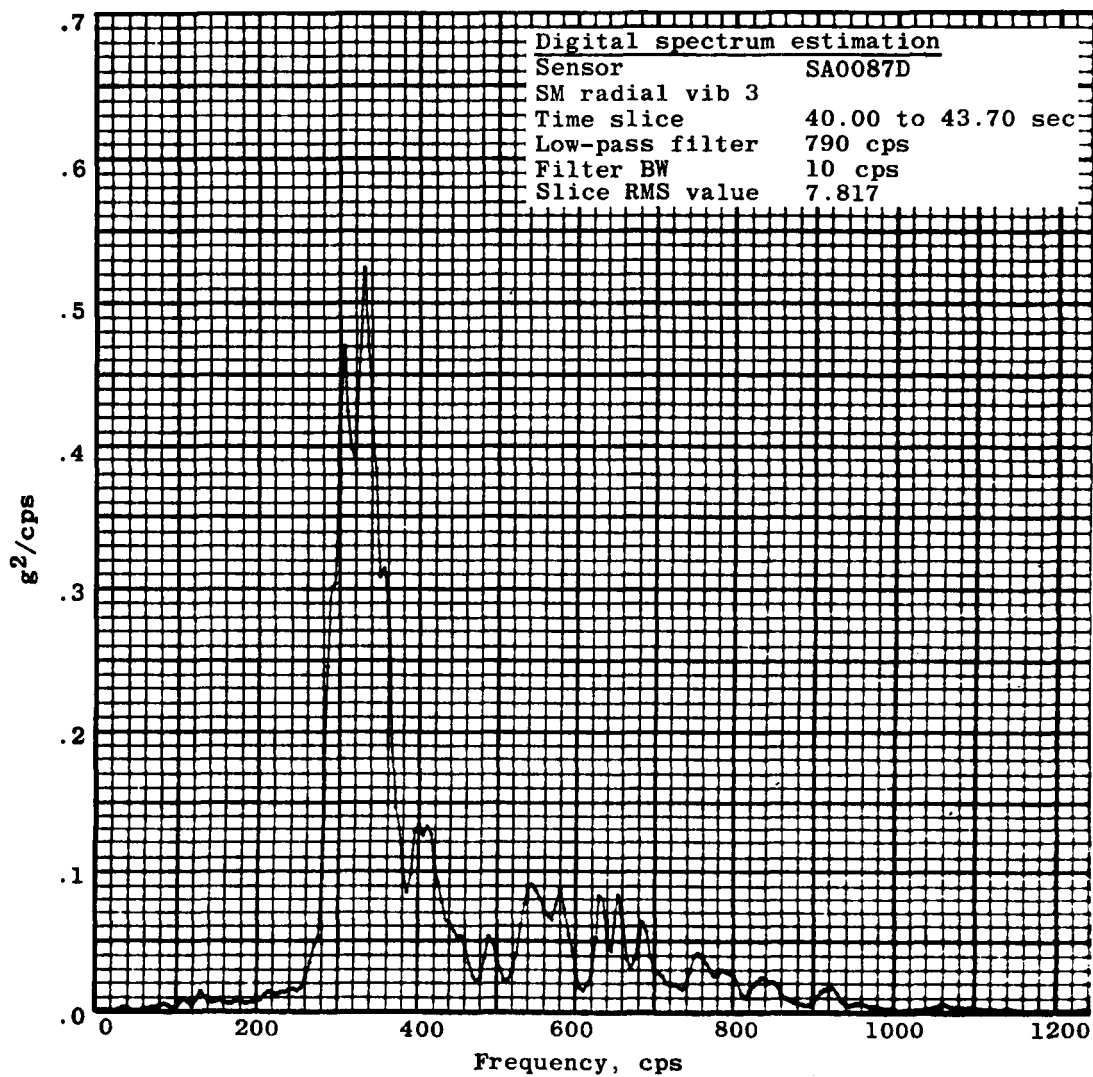


Figure 4.6-19.- RMS estimation of BP-13 spacecraft service module radial vibration.



(a) Instrument SA0086D

Figure 4.6-20.- Digital spectrum estimation of BP-13 spacecraft service module radial vibration.



(b) Instrument SA0087D

Figure 4.6-20.- Concluded.

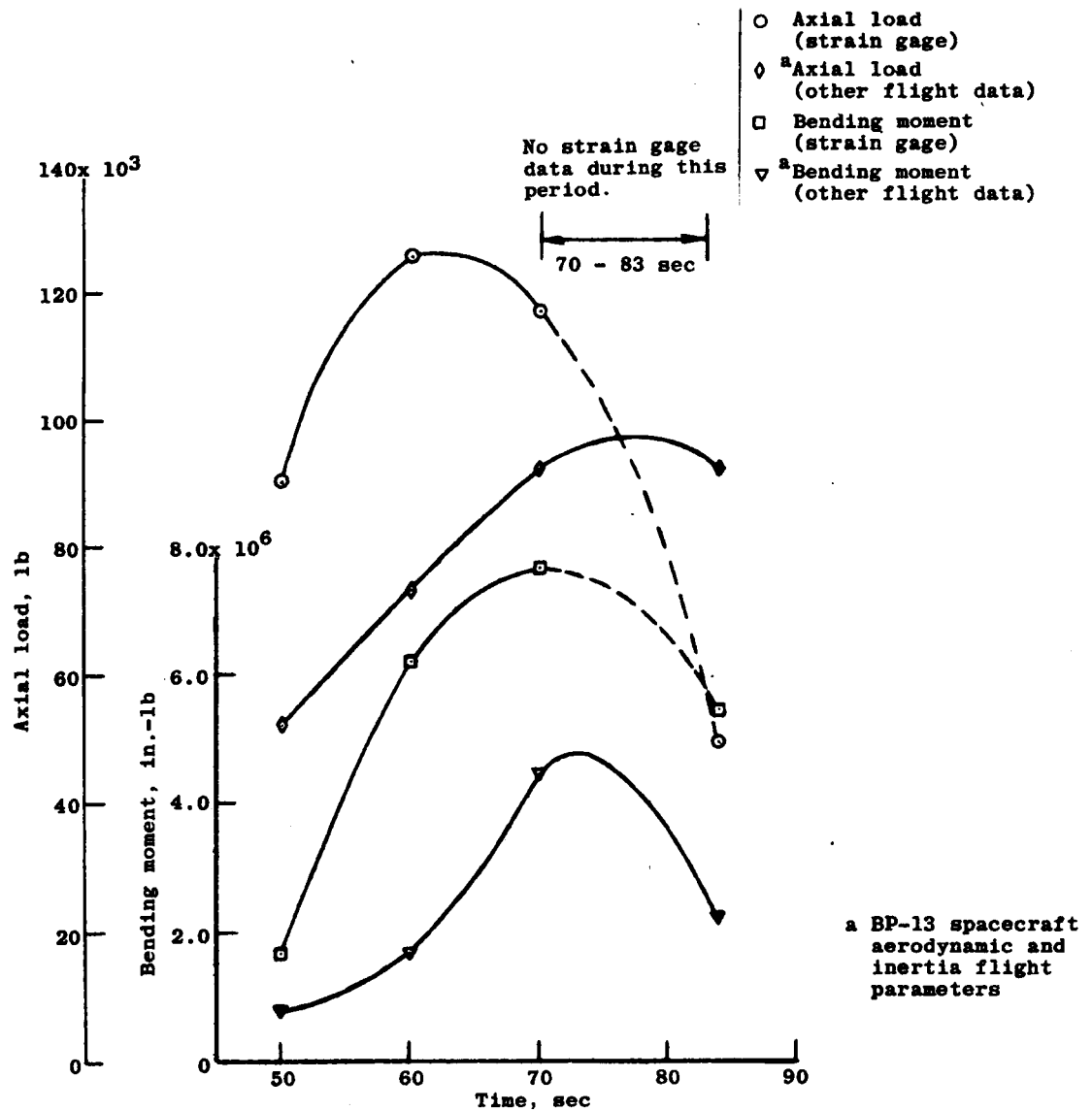
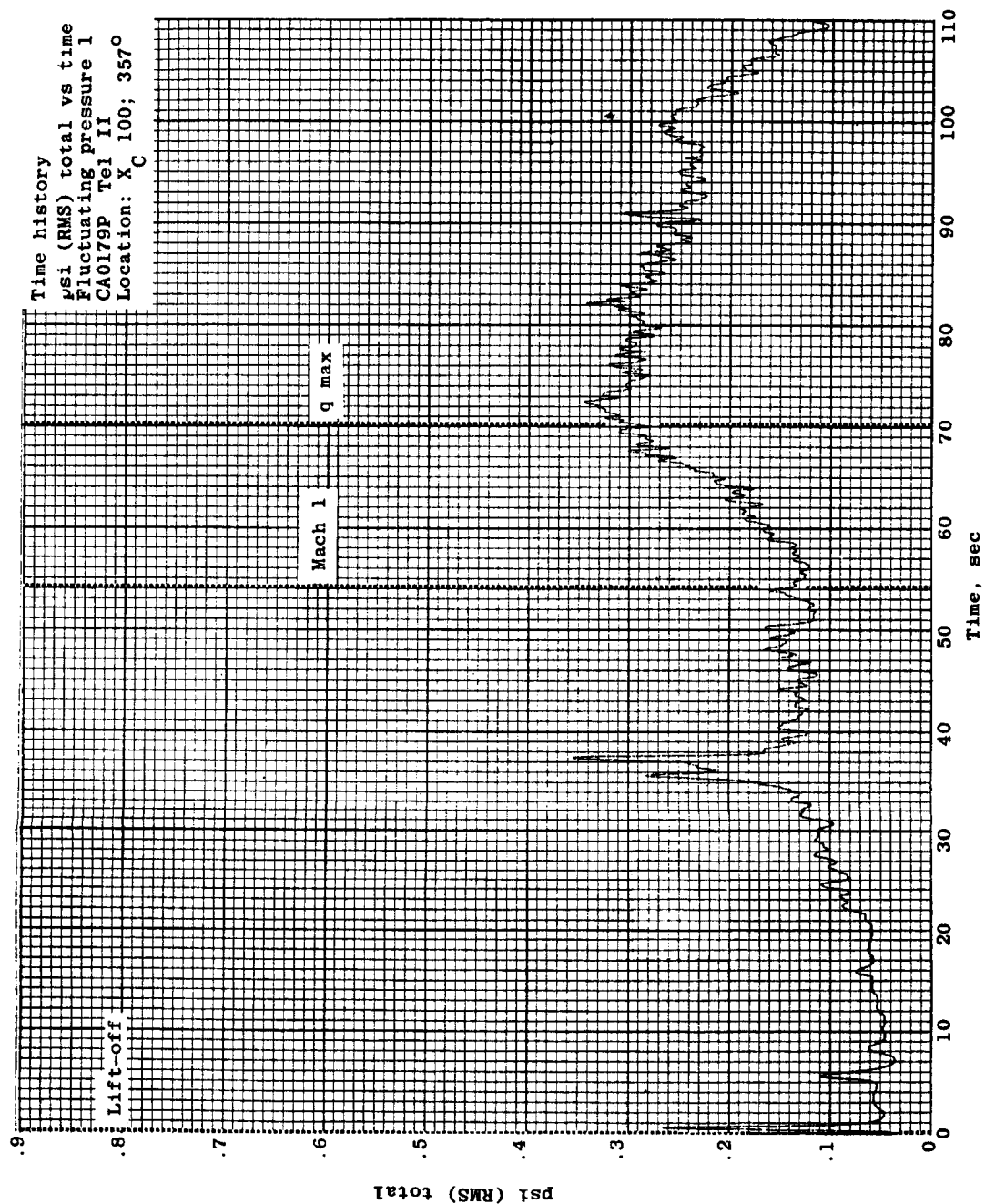
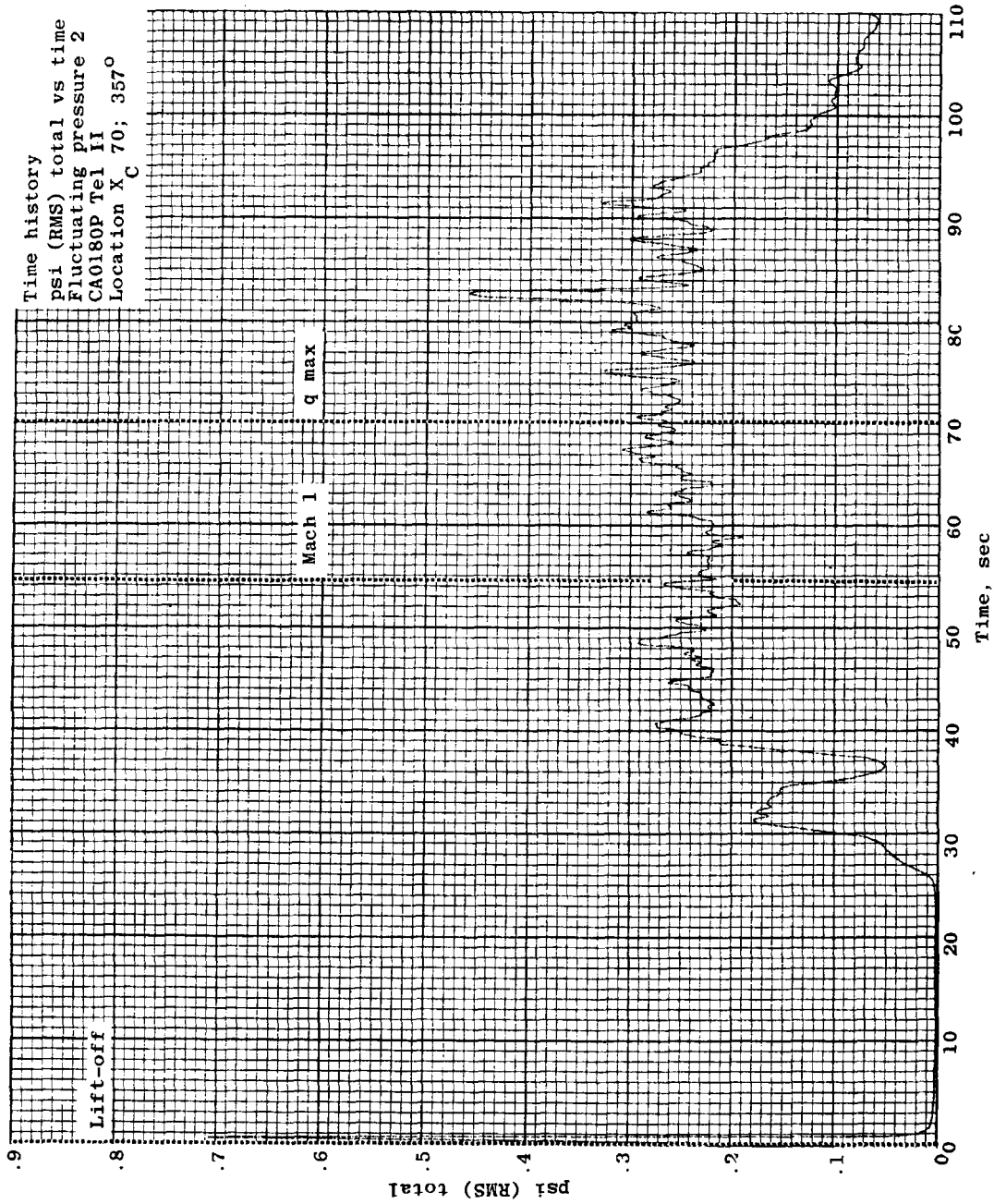


Figure 4.6-21.- BP-13 spacecraft adapter load trend comparison.



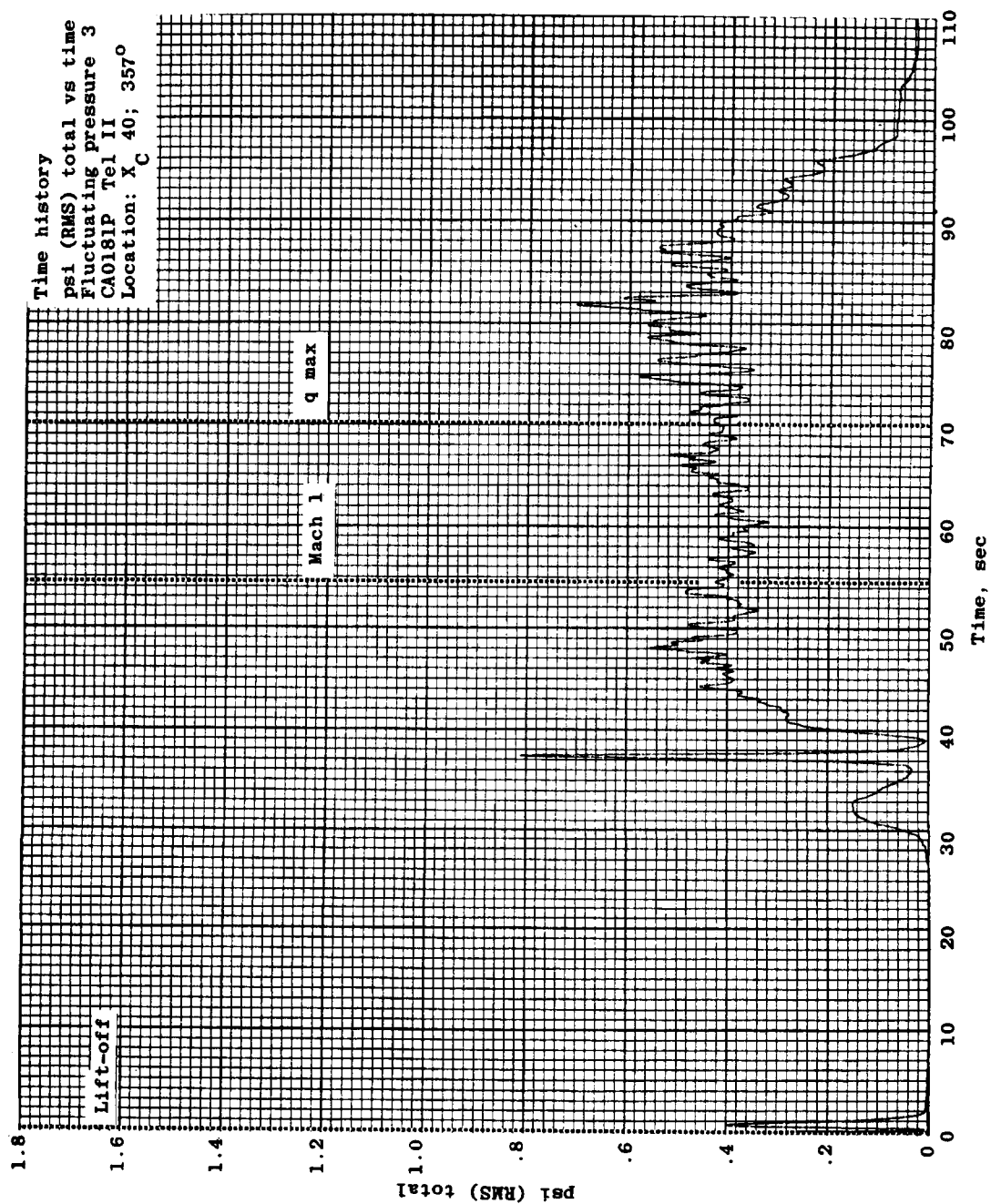
(a) Fluctuating pressure 1 (CA0179P)

Figure 4.6-22.- RMS of fluctuating pressures over BP-13 spacecraft.



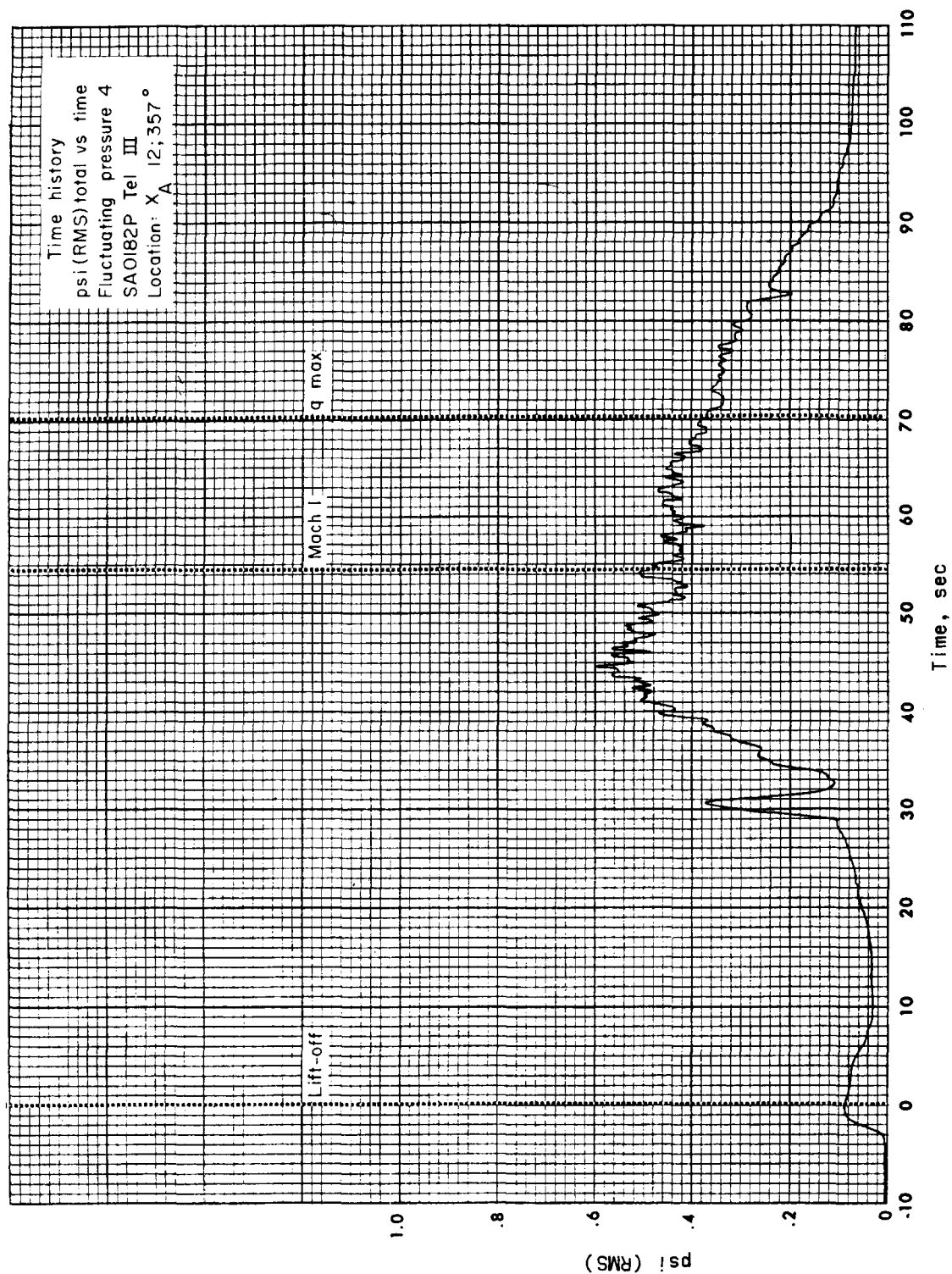
(b) Fluctuating pressure 2 (CA0180P)

Figure 4.6-22.- Continued.



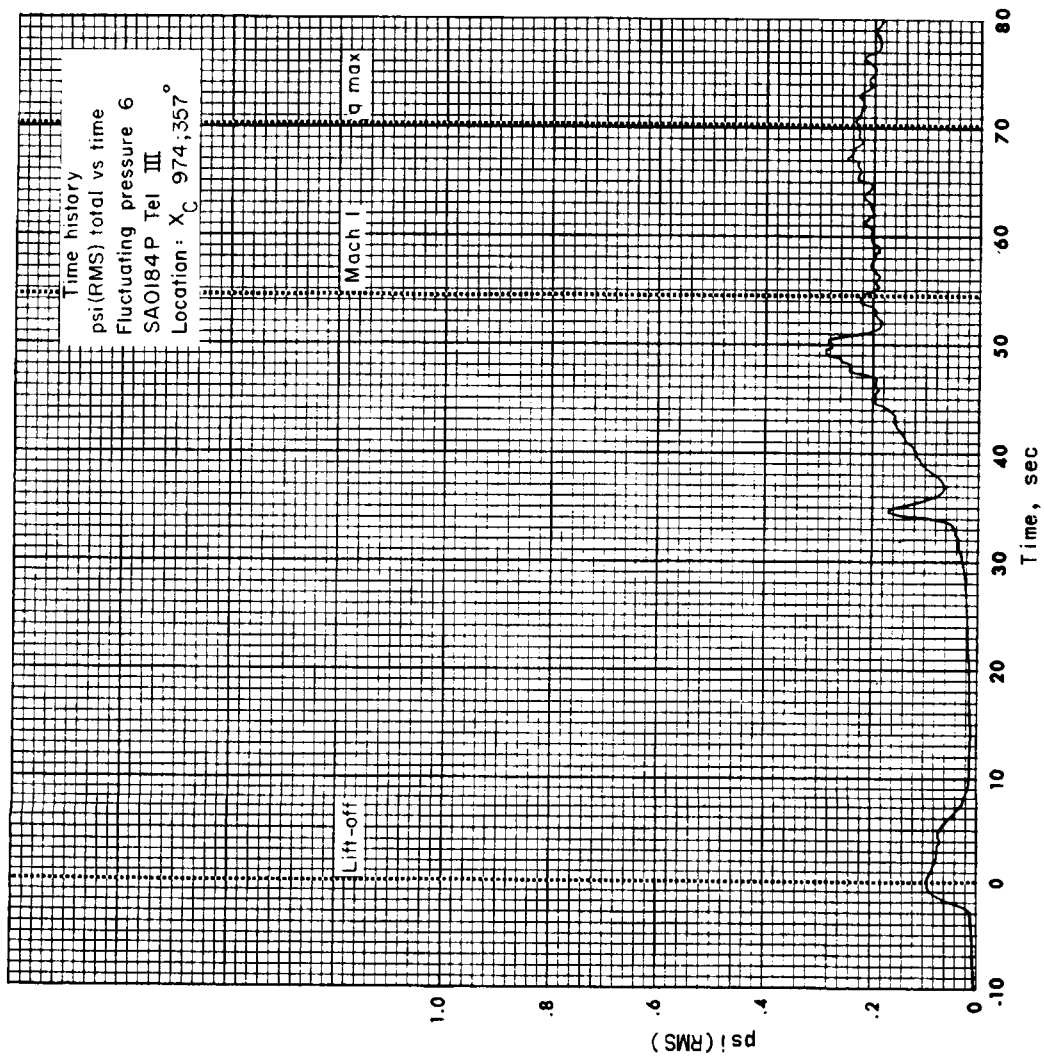
(c) Fluctuating pressure 3 (CA0181P)

Figure 4.6-22.- Continued.



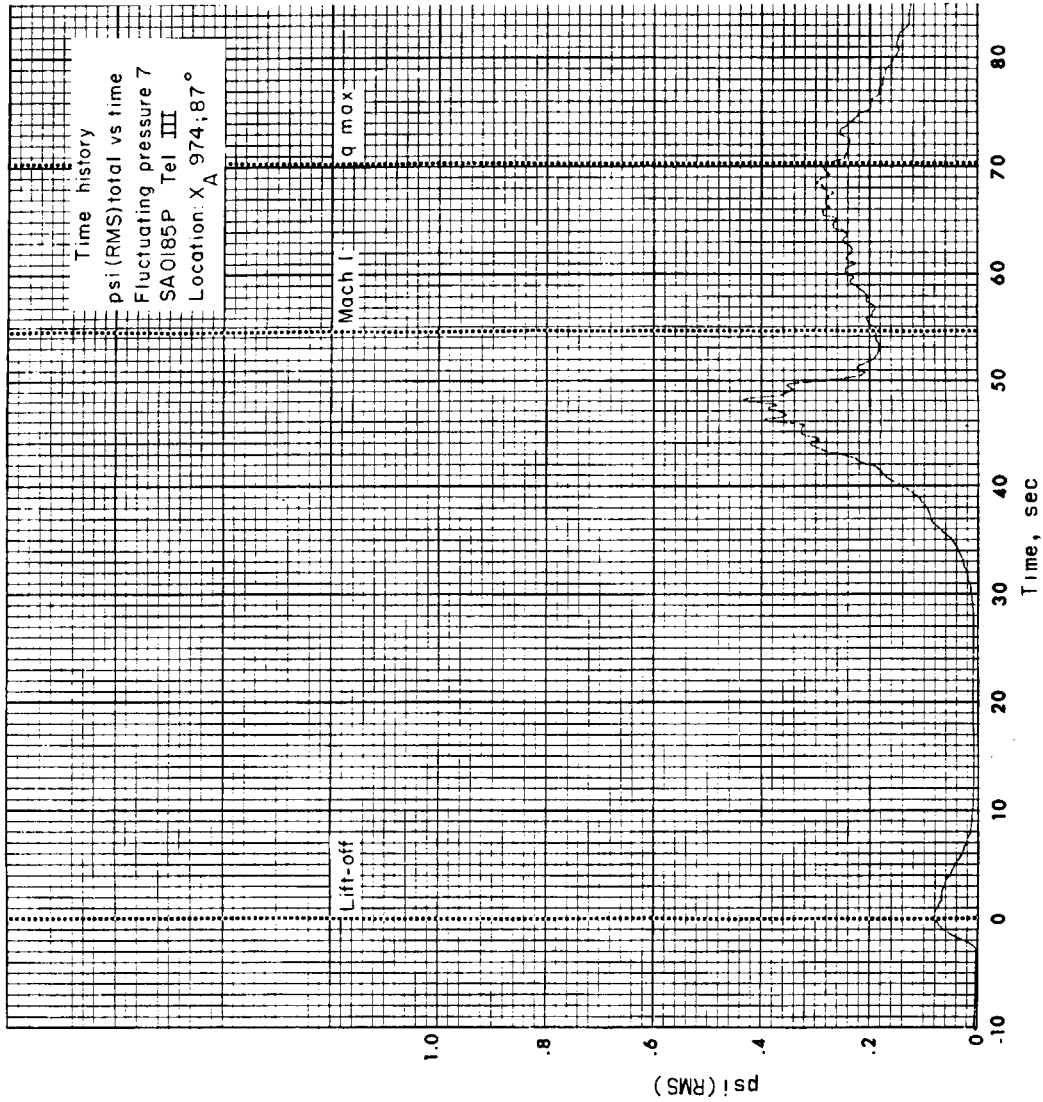
(d) Fluctuating pressure 4 (SAOI82P)

Figure 4.6-22.- Continued.



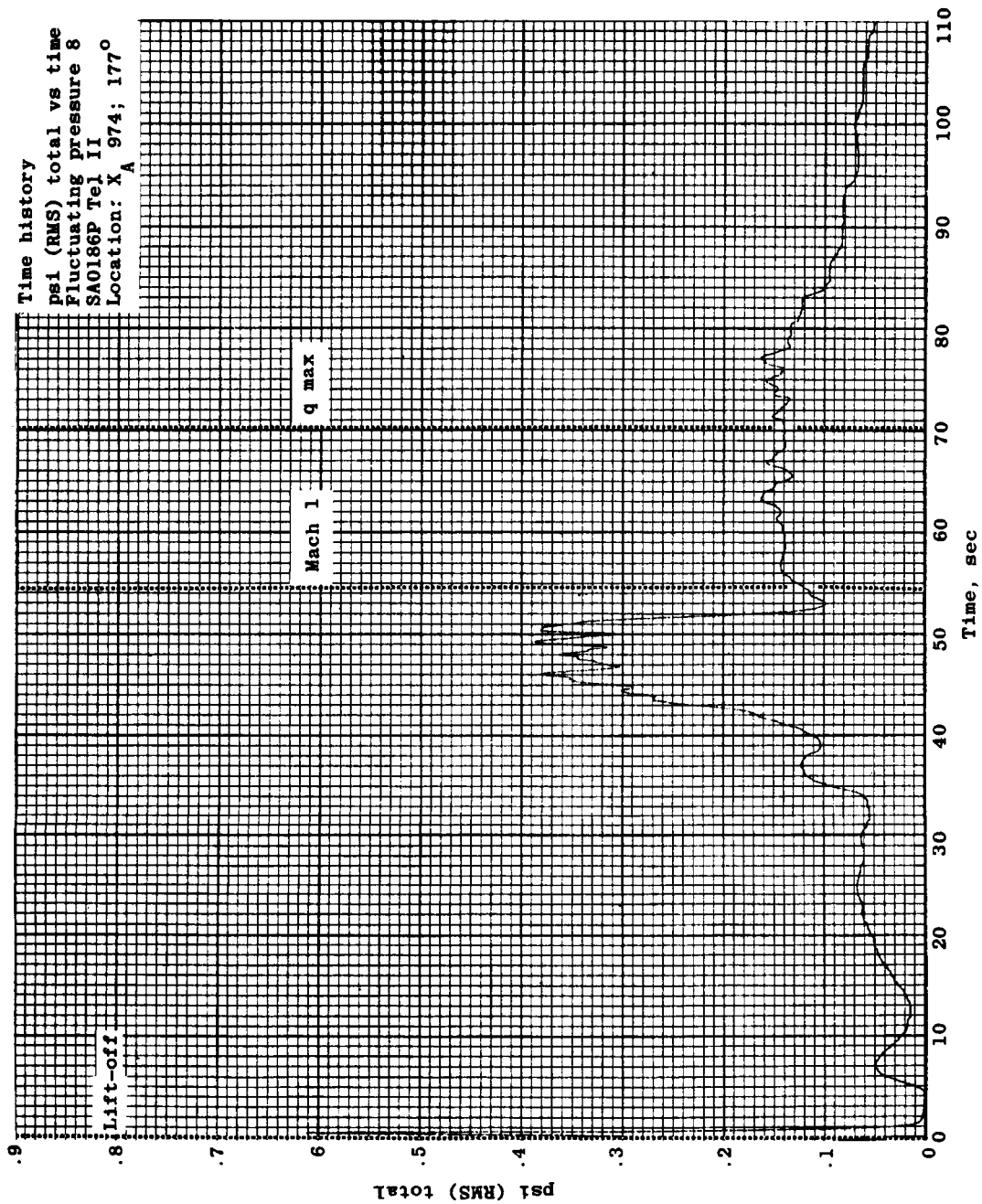
(e) Fluctuating pressure 6 (SA0184P)

Figure 4.6-22.- Continued.



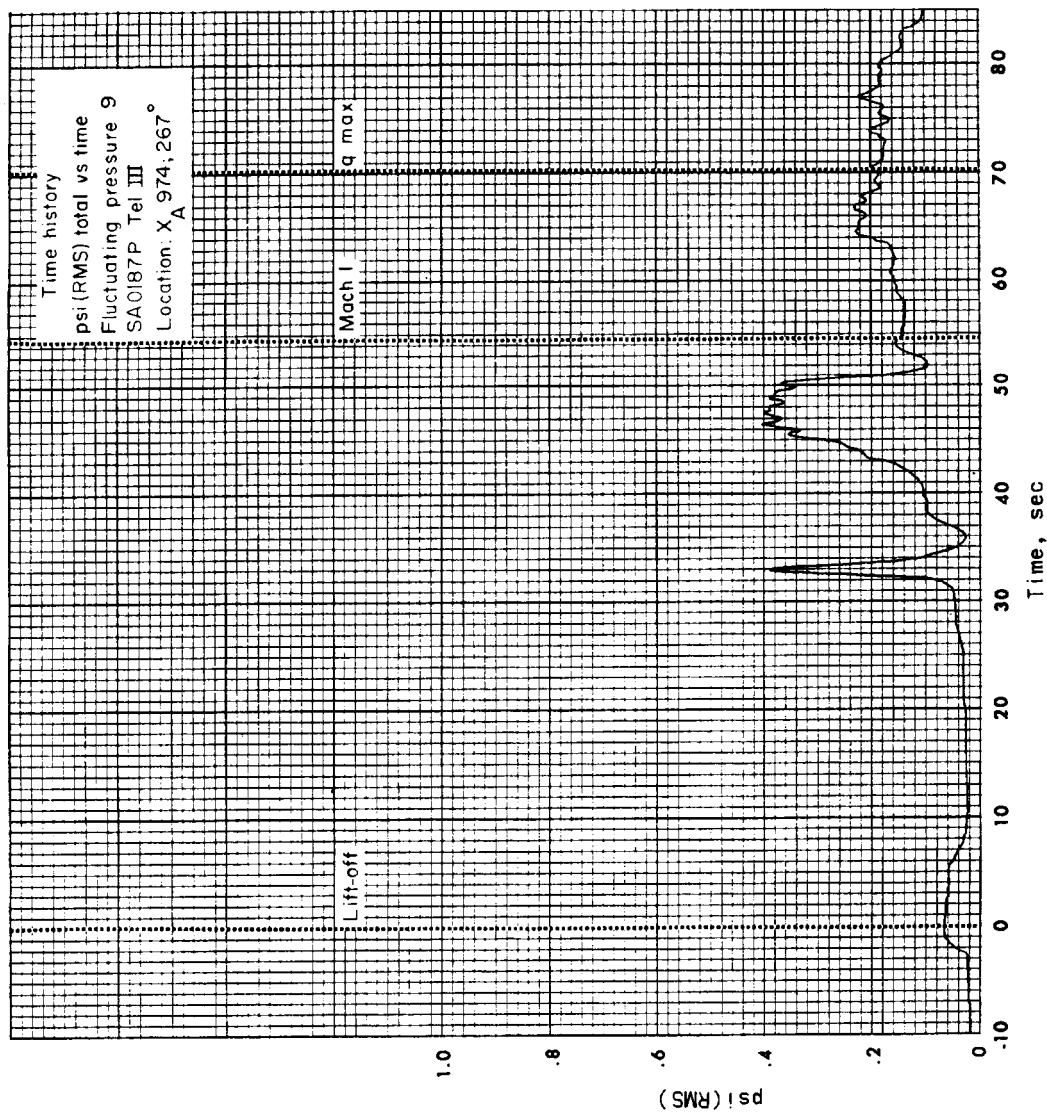
(f) Fluctuating pressure 7 (SA0185P)

Figure 4.6-22.- Continued.



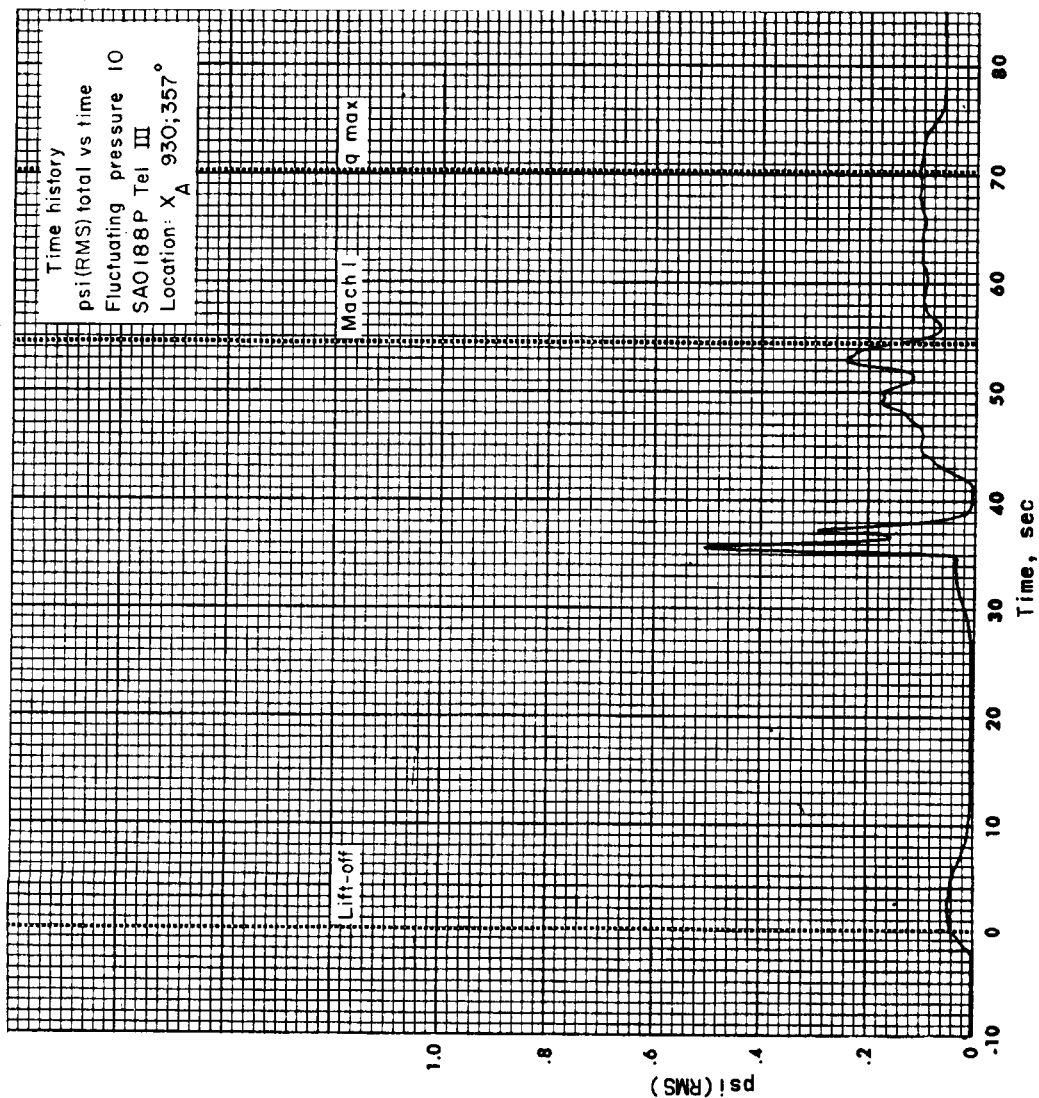
(g) Fluctuating pressure 8 (SA0186P)

Figure 4.6-22.- Continued.



(h) Fluctuating pressure 9 (SA0187P)

Figure 4.6-22.- Continued.



(1) Fluctuating pressure 10 (SAO188P)

Figure 4.6-22.- Concluded.

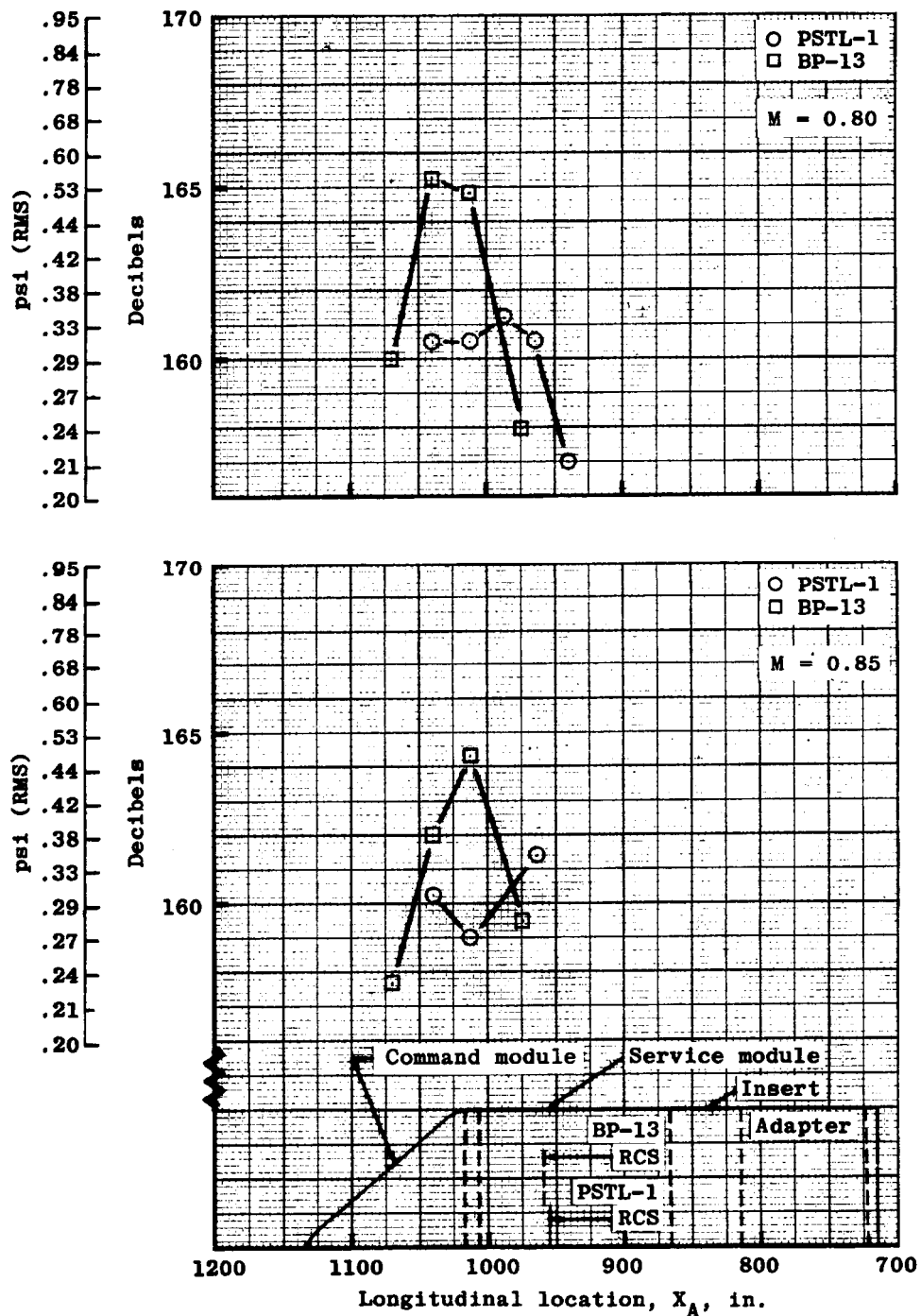
(a) $M = 0.80$ and $M = 0.85$

Figure 4.6-23.- Comparison of BP-13 spacecraft fluctuating pressures for longitudinal locations at 357° with wind tunnel data using model PSTL-1 (ref. 1).

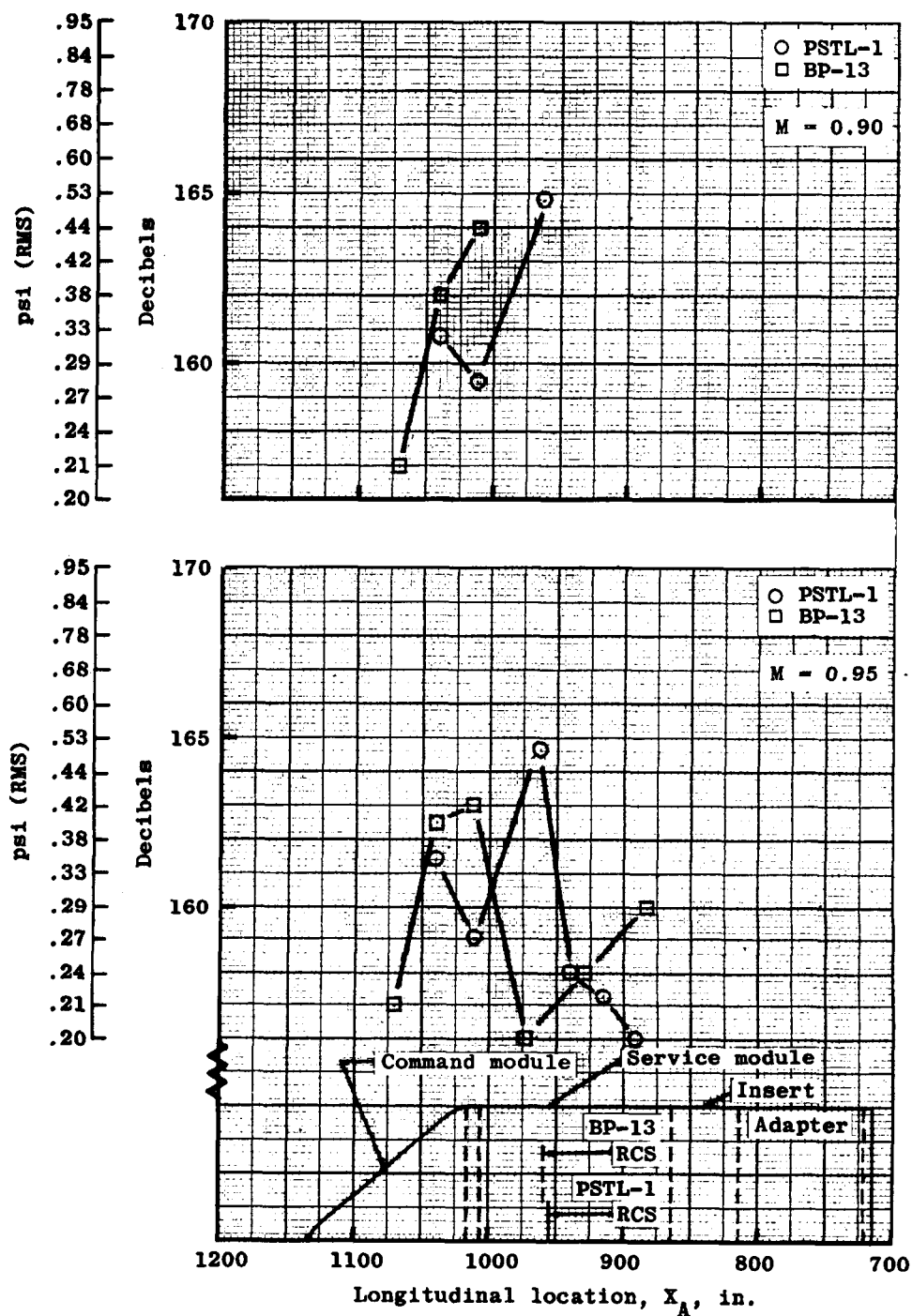
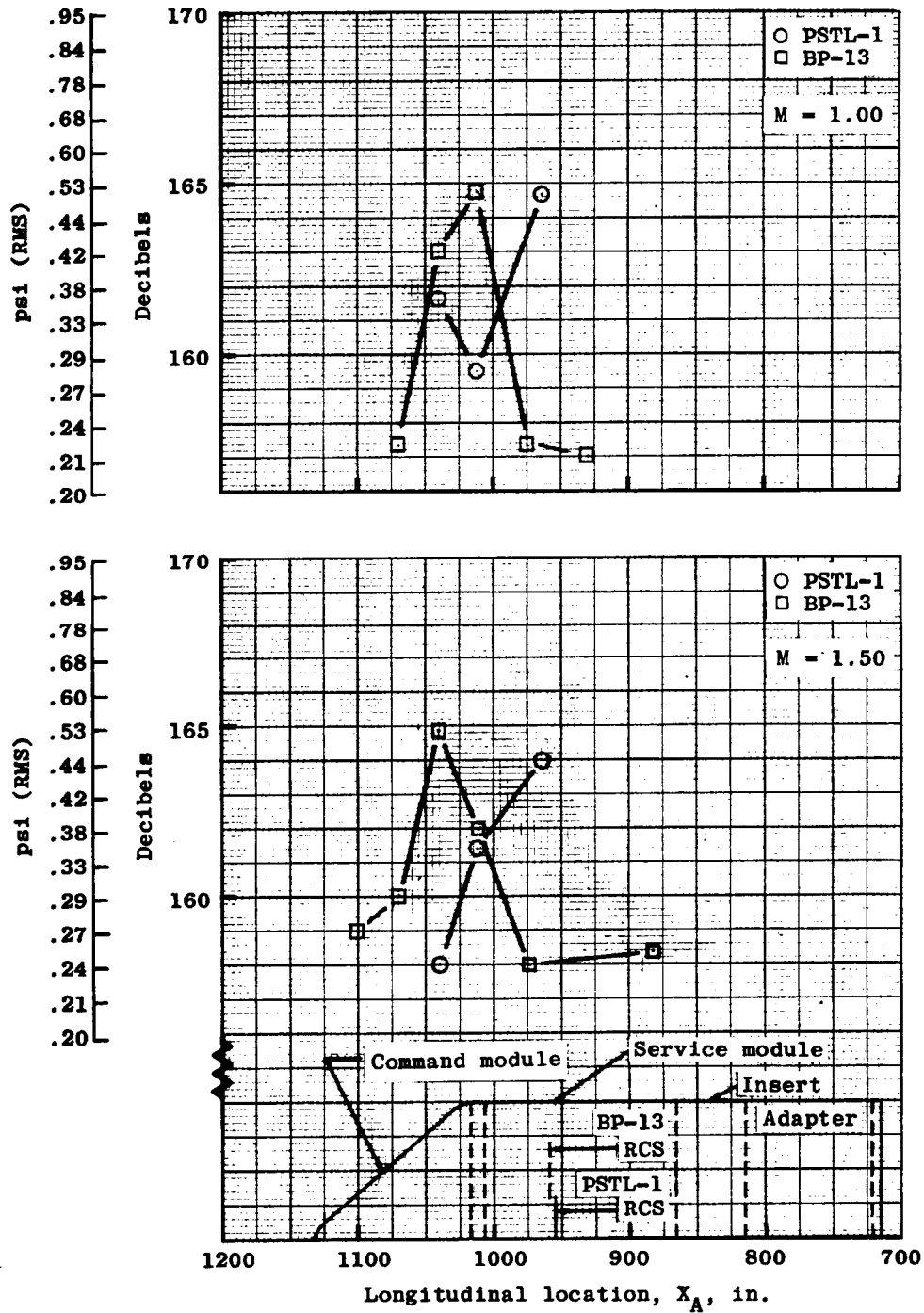
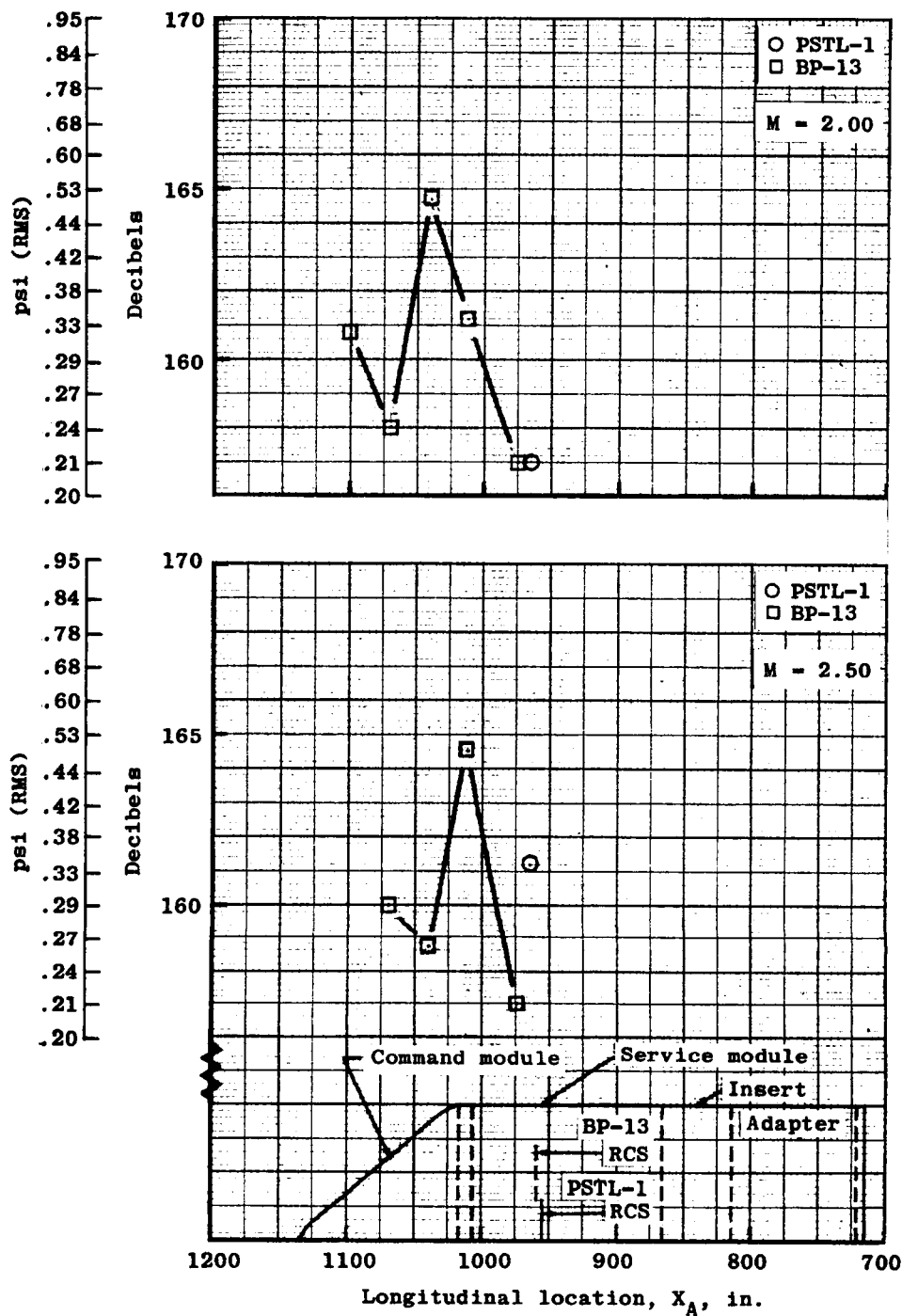
(b) $M = 0.90$ and $M = 0.95$

Figure 4.6-23.- Continued.



(c) $M = 1.00$ and $M = 1.50$.

Figure 4.6-23.- Continued.



(d) $M = 2.00$ and $M = 2.50$.

Figure 4.6-23.- Concluded.

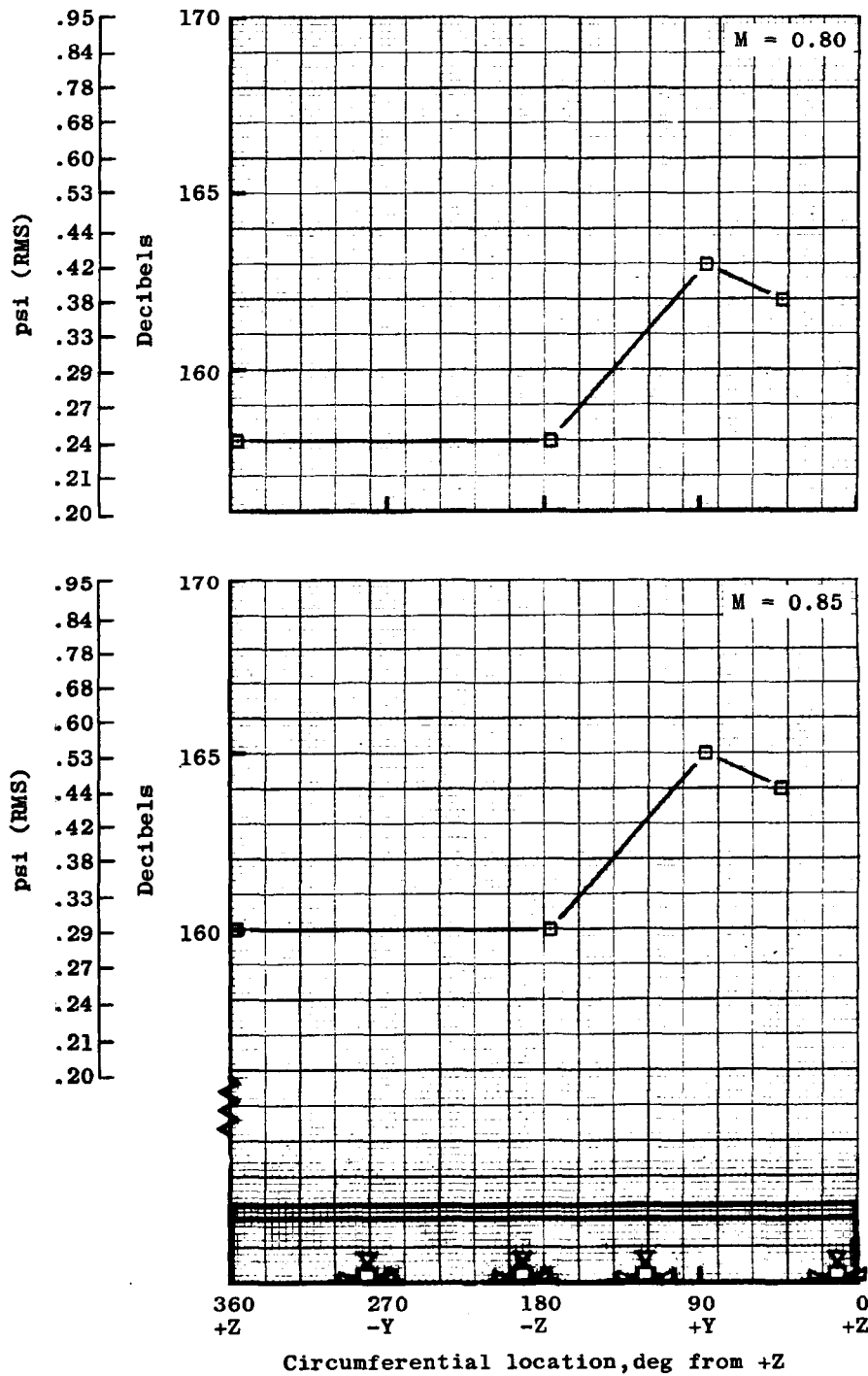
(a) $M = 0.80$ and $M = 0.85$.

Figure 4.6-24.- Fluctuating pressure trends for circumferential locations on BP-13 spacecraft service module at $X_A 974$.

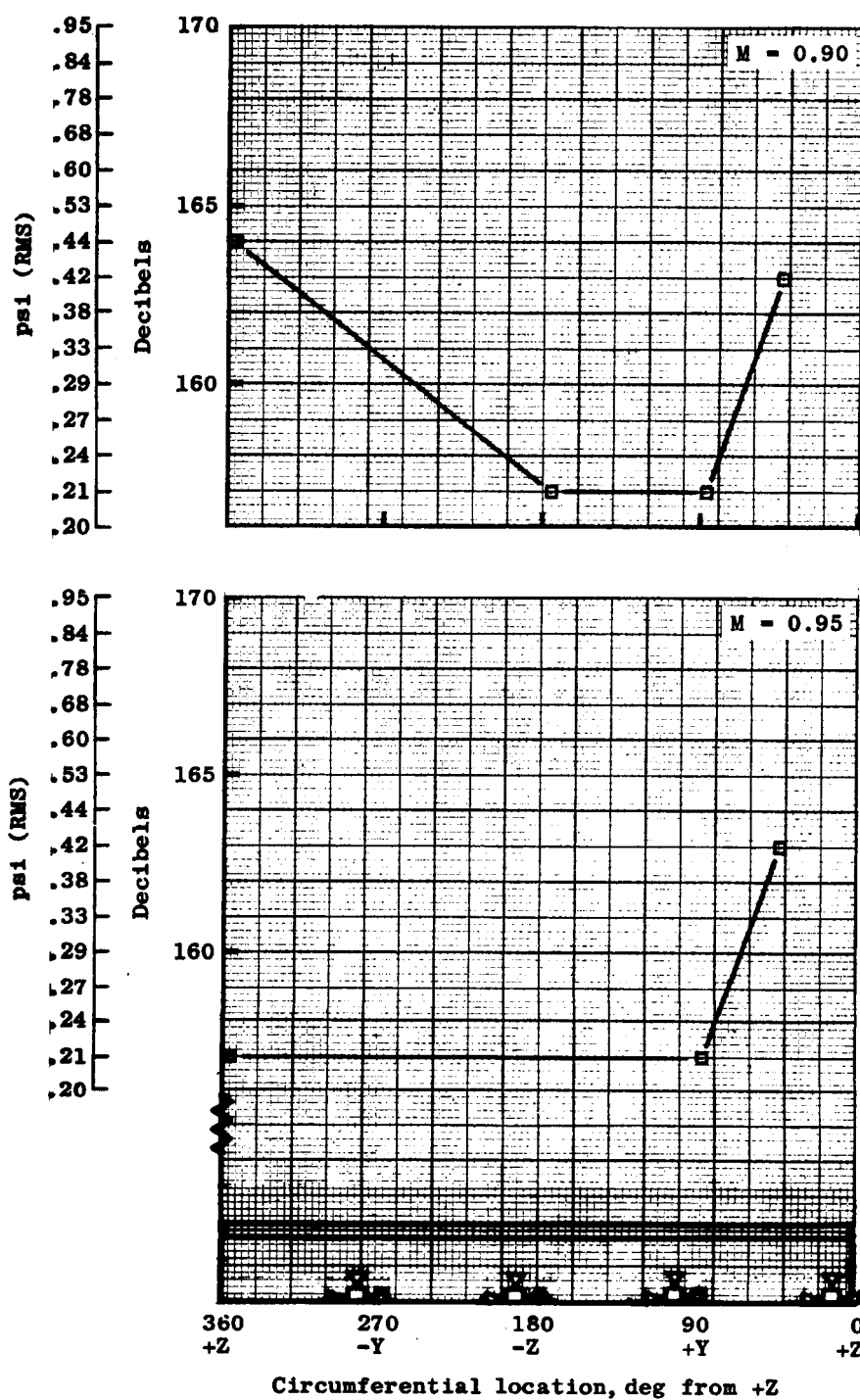
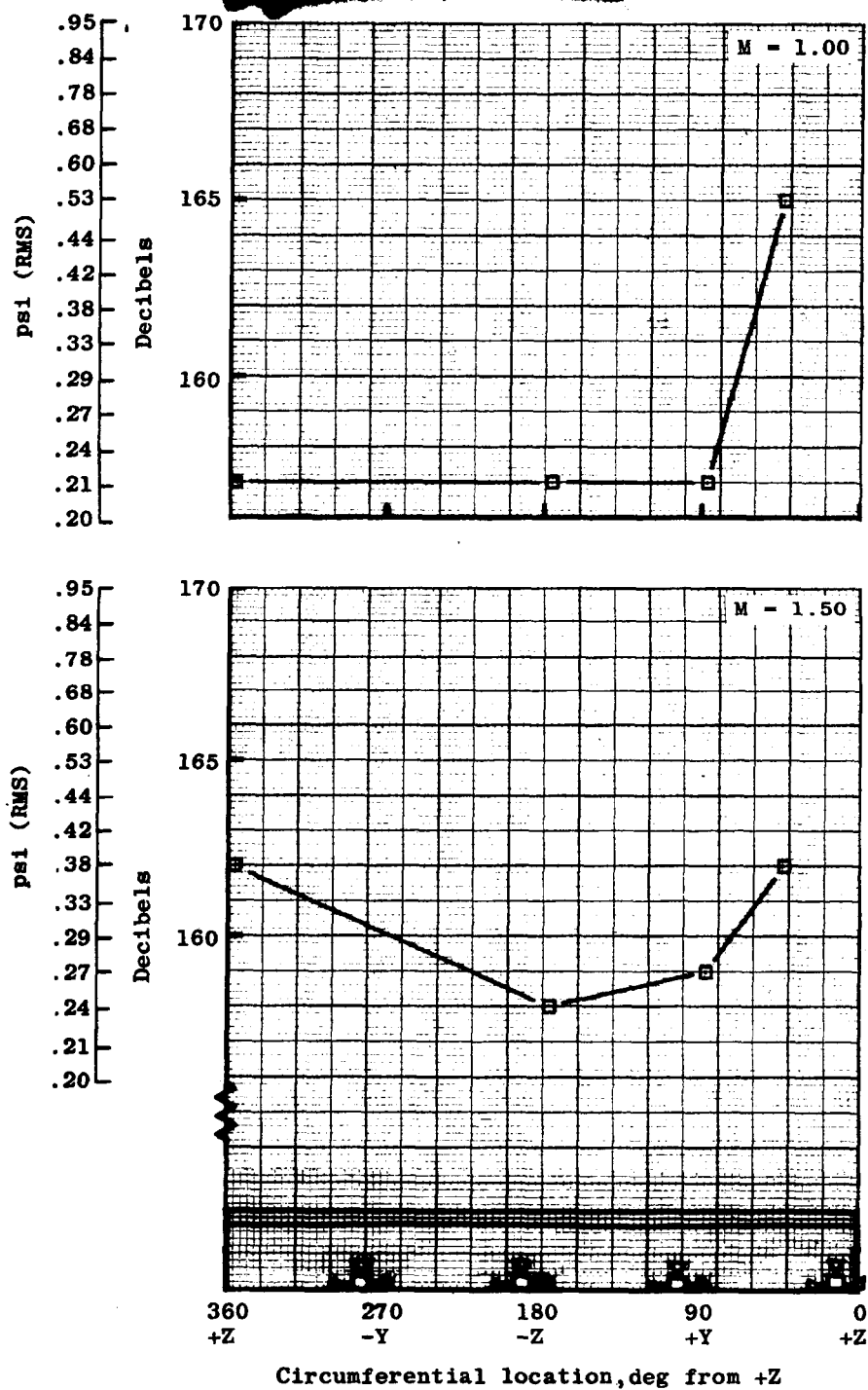
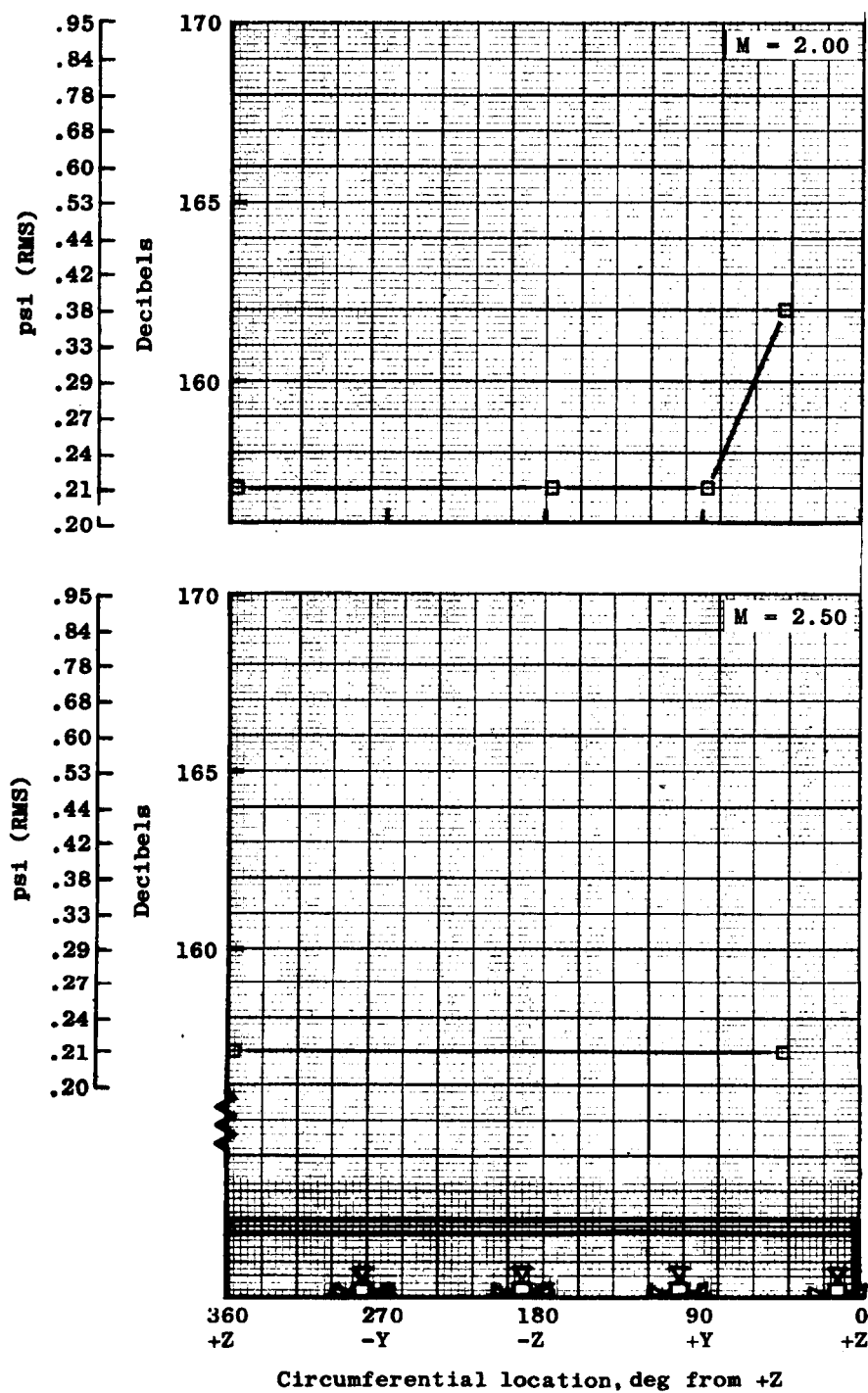
(b) $M = 0.90$ and $M = 0.95$.

Figure 1.6.24. Continued.



(c) $M = 1.00$ and $M = 1.50$.

Figure 4.6-24.- Continued.



(d) $M = 2.00$ and $M = 2.50$.

Figure 4.6-24.- Concluded.

Spectrogram
 Fluctuating pressure no. 4
 SA0182p
 Location: X_C 12; 357°
 ΔT= 45 to 50 sec
 Writing speed 80 mm/sec
 Paper speed 10 mm/sec
 TM data received at Tel III

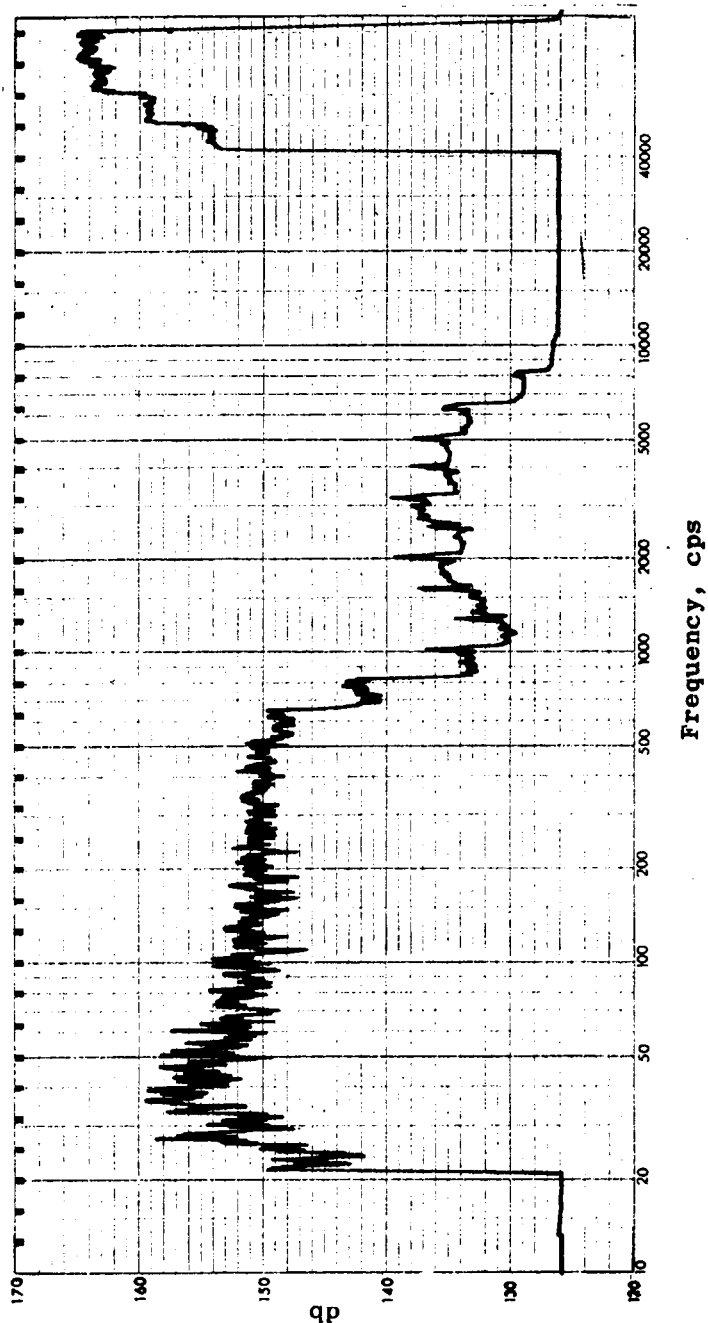


Figure 4.6-25.- Spectrogram of BP-13 spacecraft service module fluctuating pressures ($\frac{1}{3}$ octave band analysis).

TABLE 4.6-I.- FLIGHT LOADS COMPARISON

Location, X _A , in.	Time from lift-off, sec	Bending moment, in.-lb	Axial force (compression), lb	Source
a ₇₂₂	50	732,000	51,900	Flight measured parameters and predicted angle of attack for T-0 winds.
		1,755,000	52,200	Flight measured parameters and flight measured Q-ball angle of attack.
		856,000	53,400	Preflight calculations with programed angle of attack with no winds.
a ₇₂₂	60	1,550,000	73,000	Flight measured parameters and predicted angle of attack for T-0 winds.
		2,570,000	74,000	Flight measured parameters and flight measured Q-ball angle of attack.
		2,100,000	73,000	Preflight calculations with programed angle of attack with no winds.
a ₇₂₂	70	4,360,000	92,100	Flight measured parameters and calculated angle of attack for T-0 winds.
		6,380,000	94,400	Preflight calculations with programed angle of attack with no winds.
		4,160,000	78,000	Preflight calculations with programed angle of attack with no winds.
a ₇₂₂	72	5,570,000	94,200	Flight measured parameters and calculated angle of attack for T-0 winds.
b _{1008.5}	72	311,000	88,000	Flight measured parameters and calculated angle of attack for T-0 winds.
c ₁₀₈₄	72	205,000	18,000	Flight measured parameters and calculated angle of attack for T-0 winds.

a_{X_A} Sta. 722 - Adapter-IU interfaceb_{X_A} Sta. 1008.5 - CM-SM interfacec_{X_A} Sta. 1084 - LES-CM interface

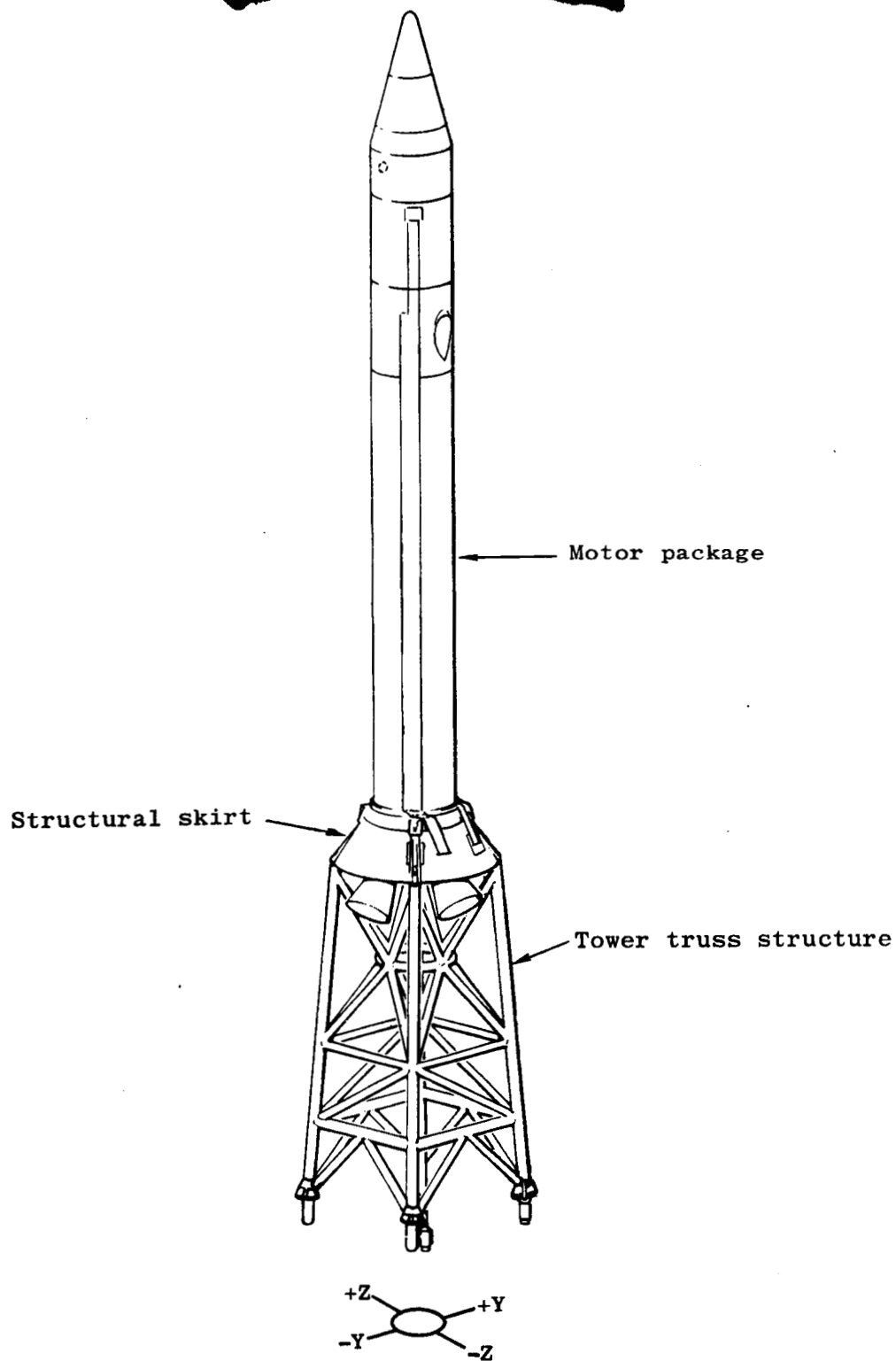


Figure 4.6-1.- Apollo BP-13 spacecraft launch escape subsystem structure.

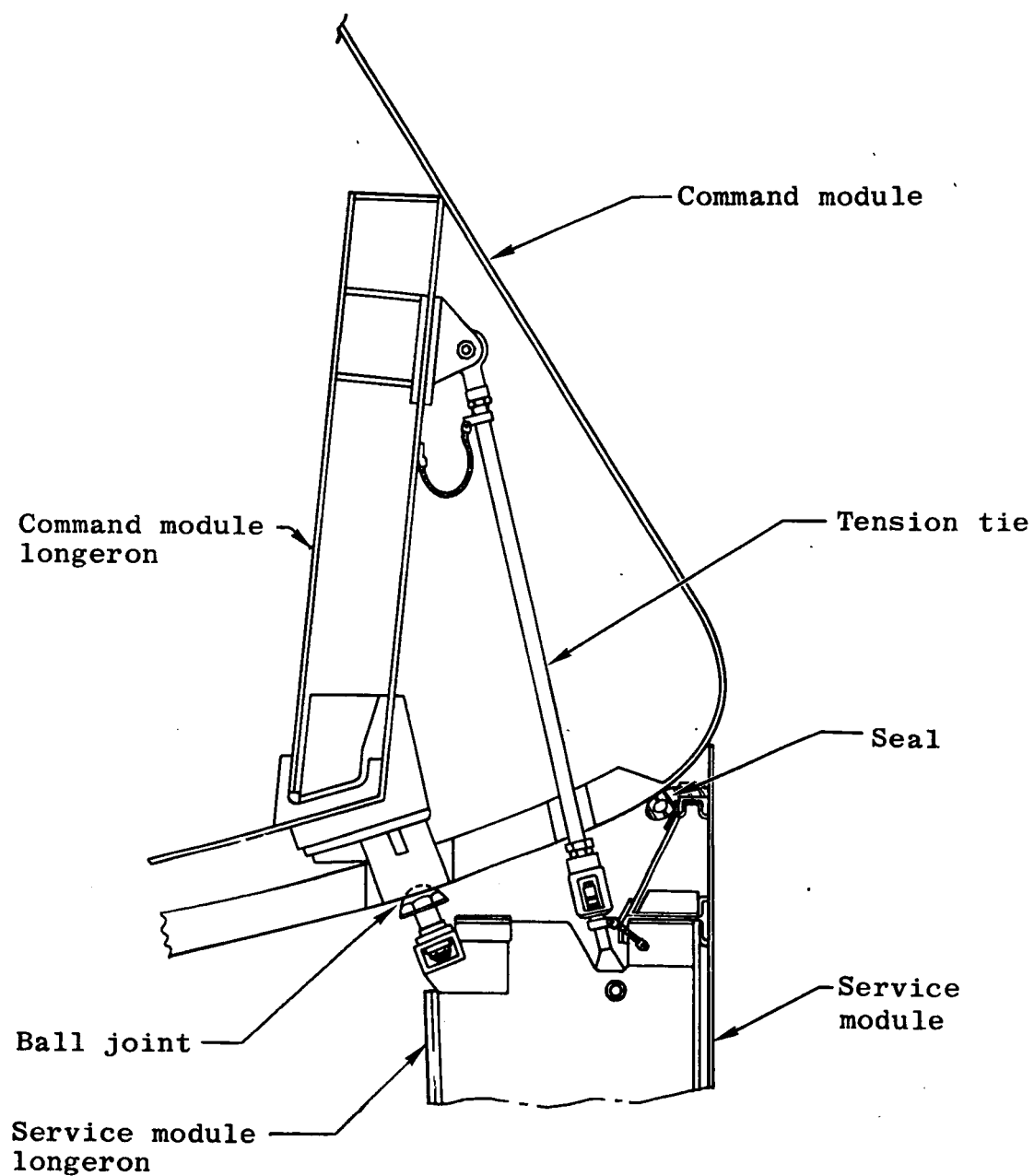


Figure 4.6-2.- Detail of command module-service module interface (BP-13 spacecraft).

4-64

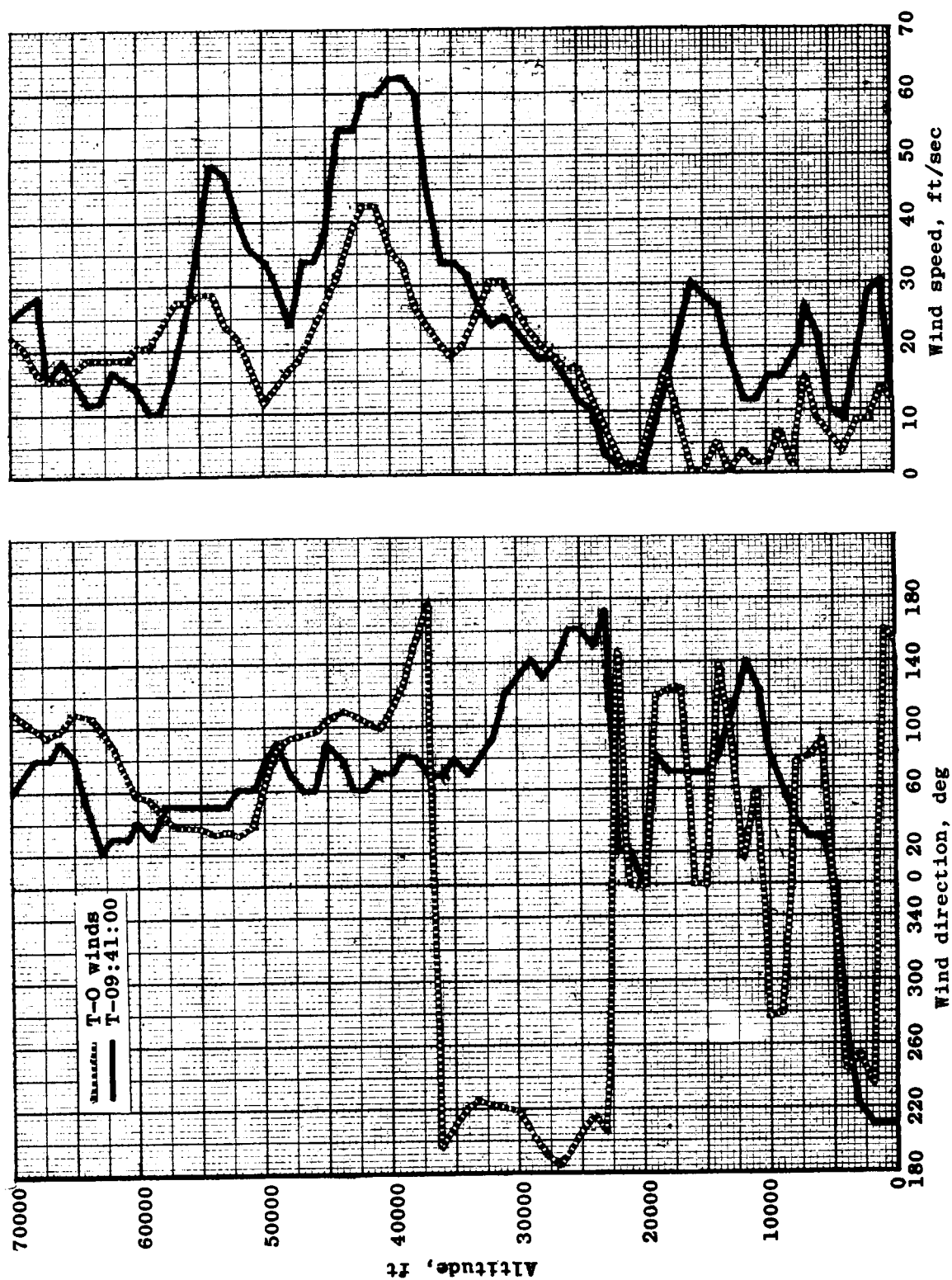


Figure 4.6-3.- Rawinsonde atmospheric wind data at Cape Kennedy, Fla., May 28, 1964.

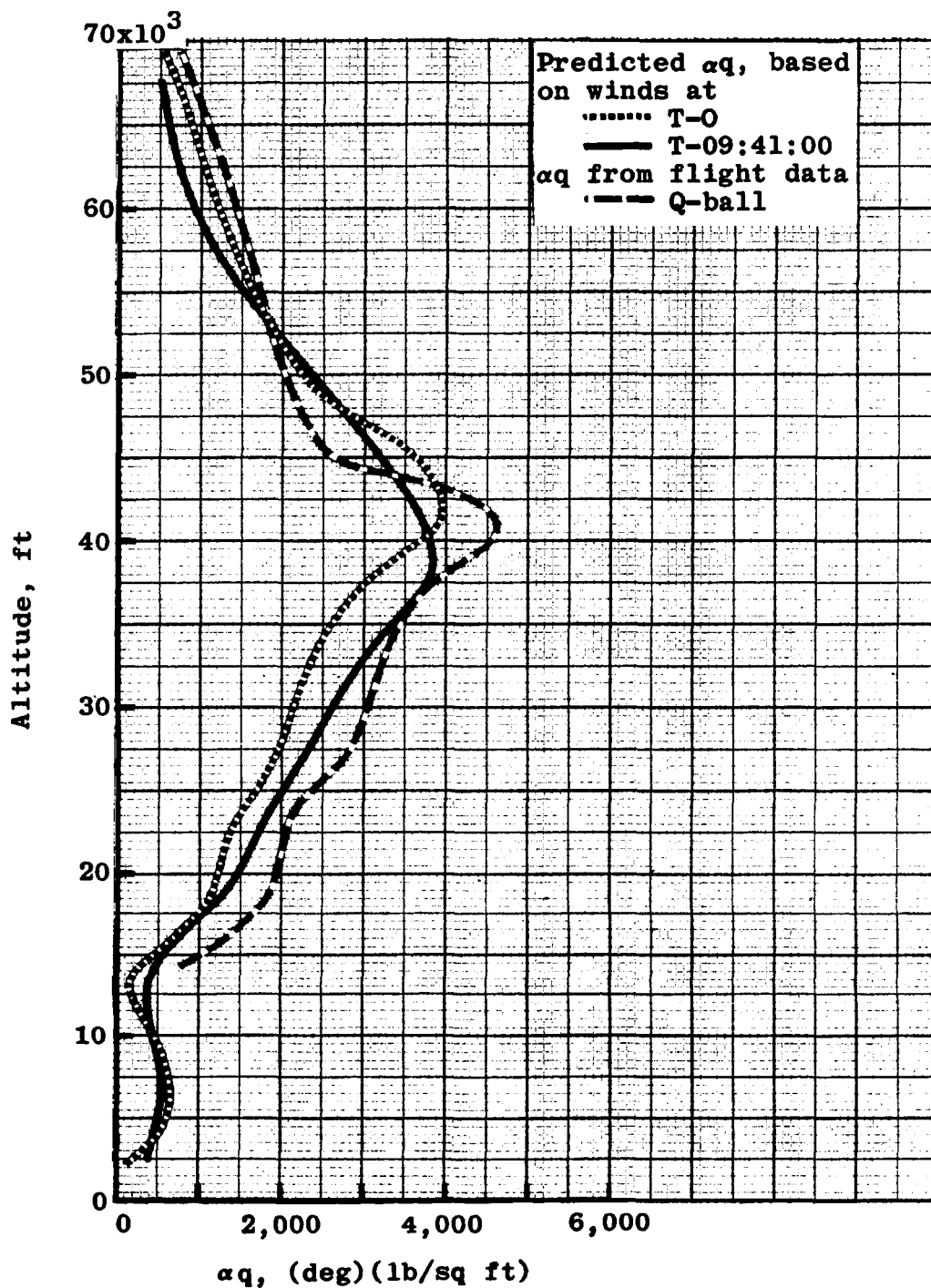


Figure 4.6-4.- Comparison of predicted αq and Q-ball αq (Apollo mission A-101).

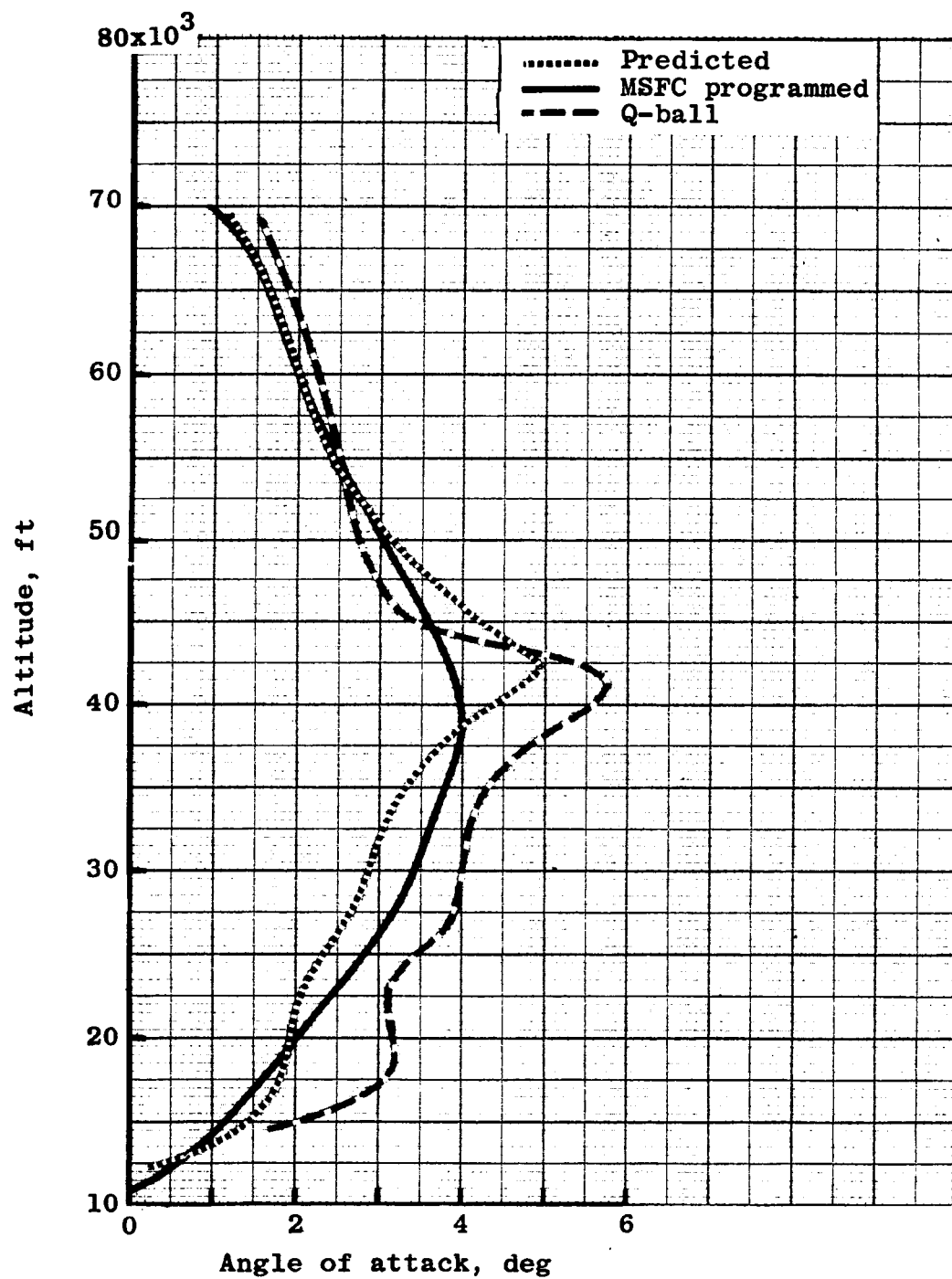


Figure 4.6-5.- Variation of angle of attack with altitude (Apollo mission A-101).

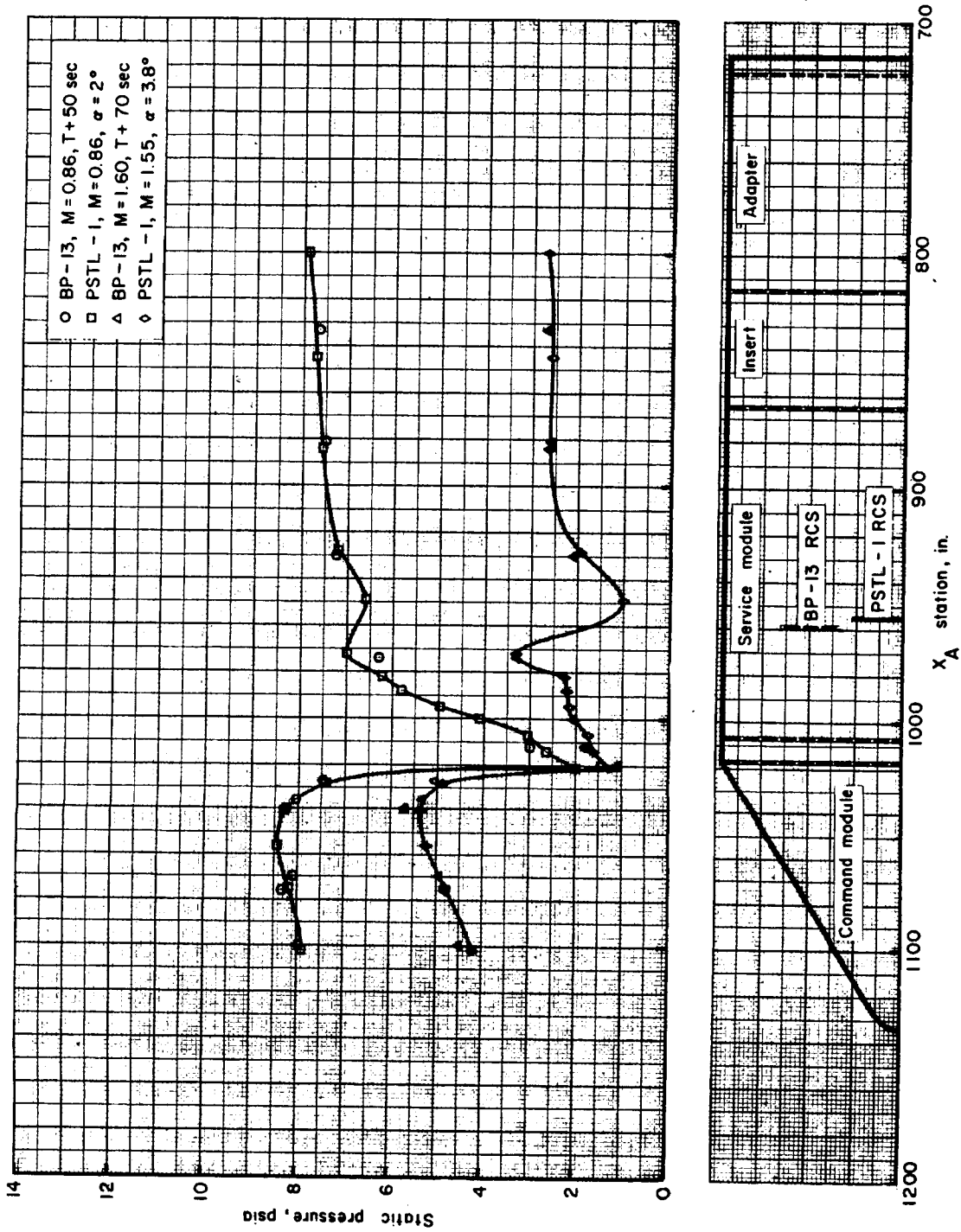
(a) $\phi = 0^\circ$

Figure 4.6-6.- Static pressure flight measurement on BP-13 spacecraft compared with wind-tunnel measurements on model PSTL-1 (ref. 1).

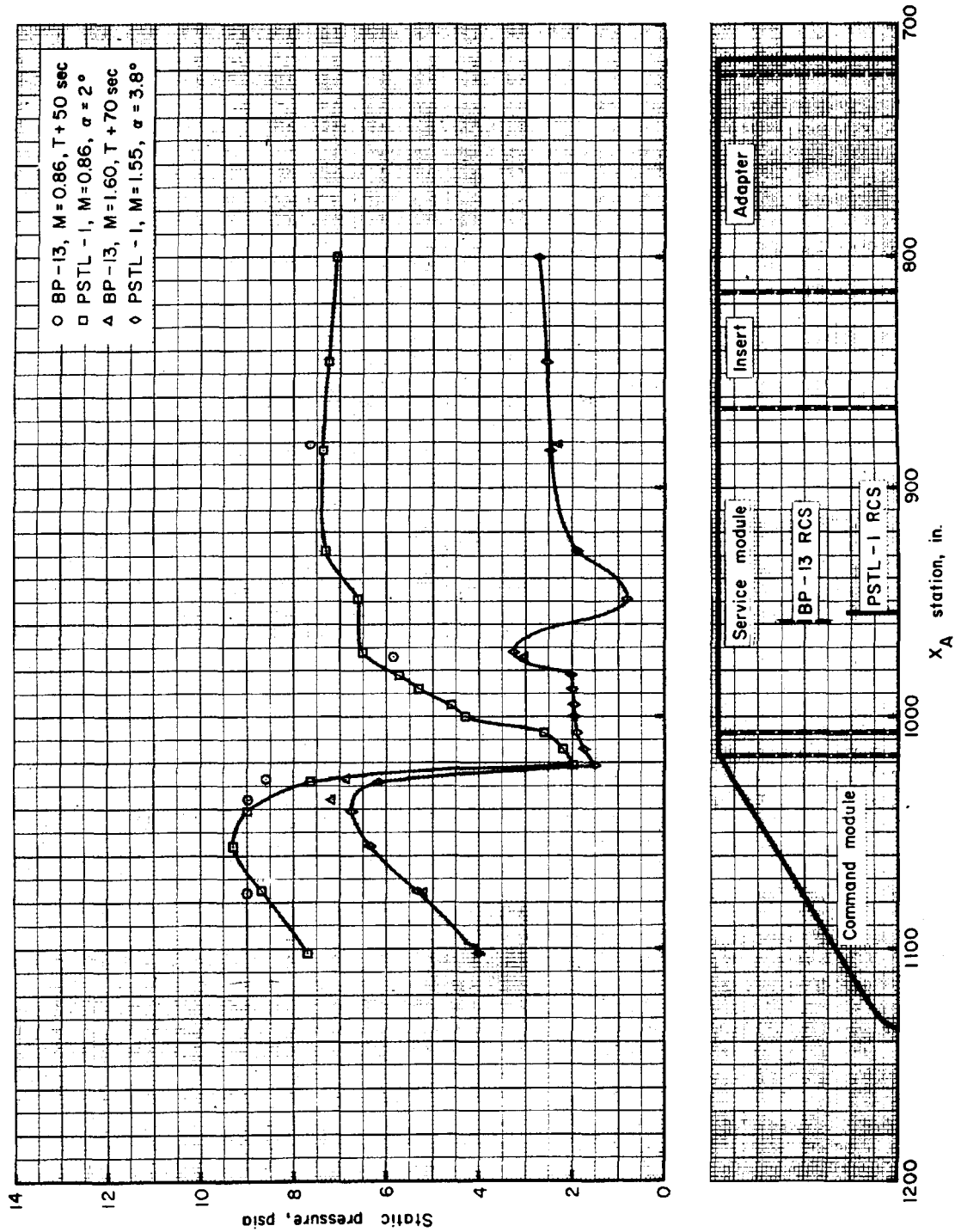
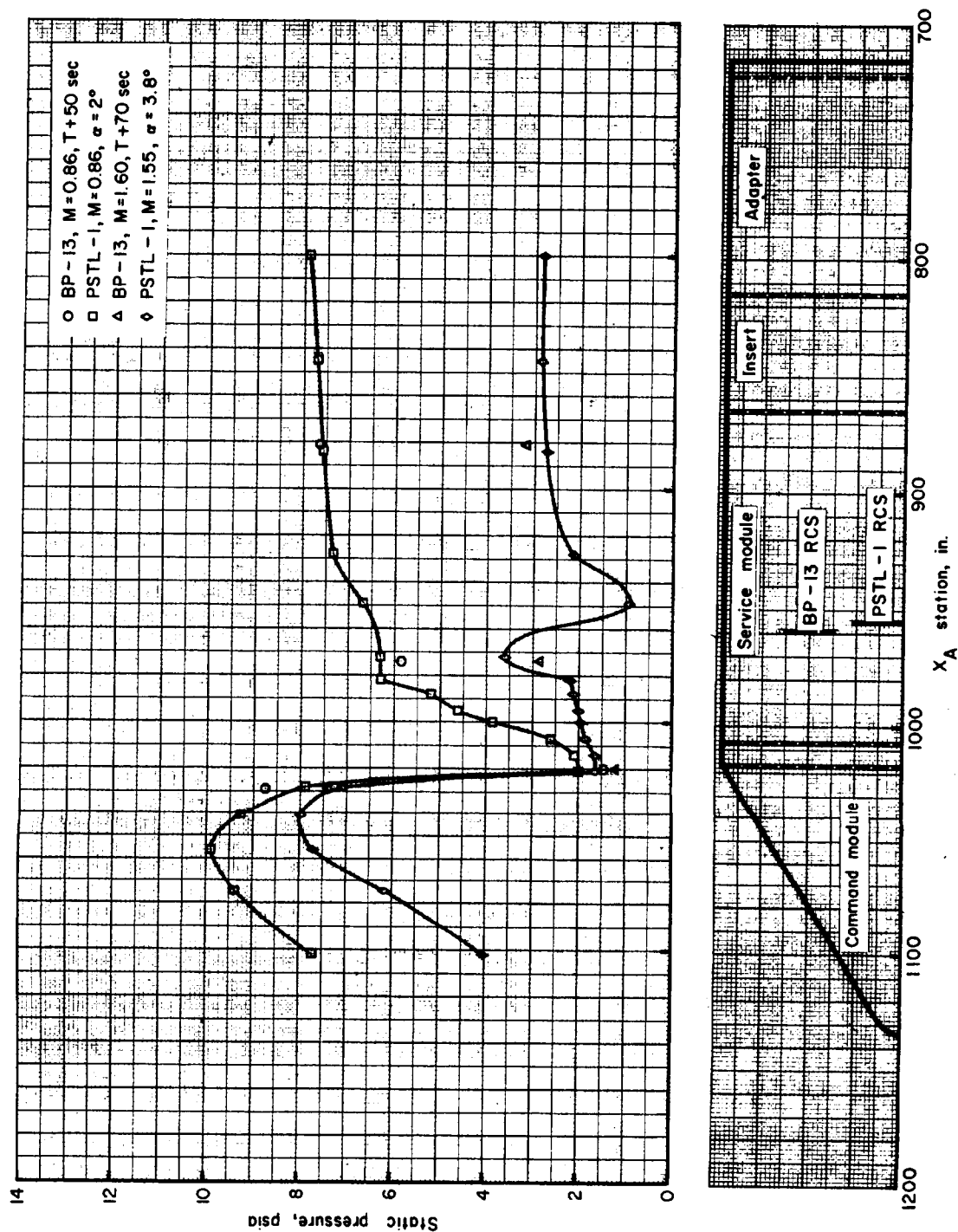
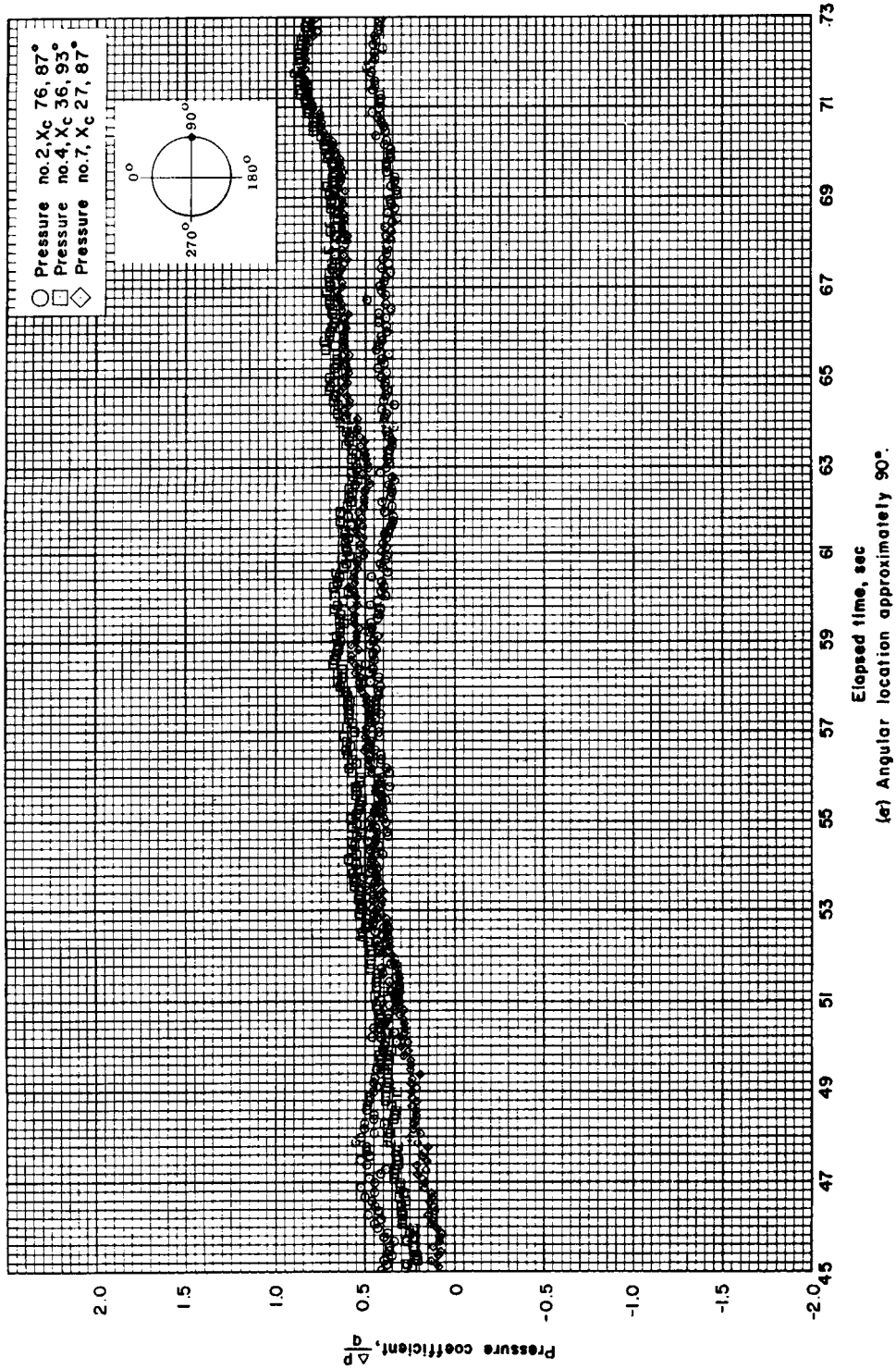
(b) $\phi = 90^\circ$

Figure 4.6-6.- Continued.



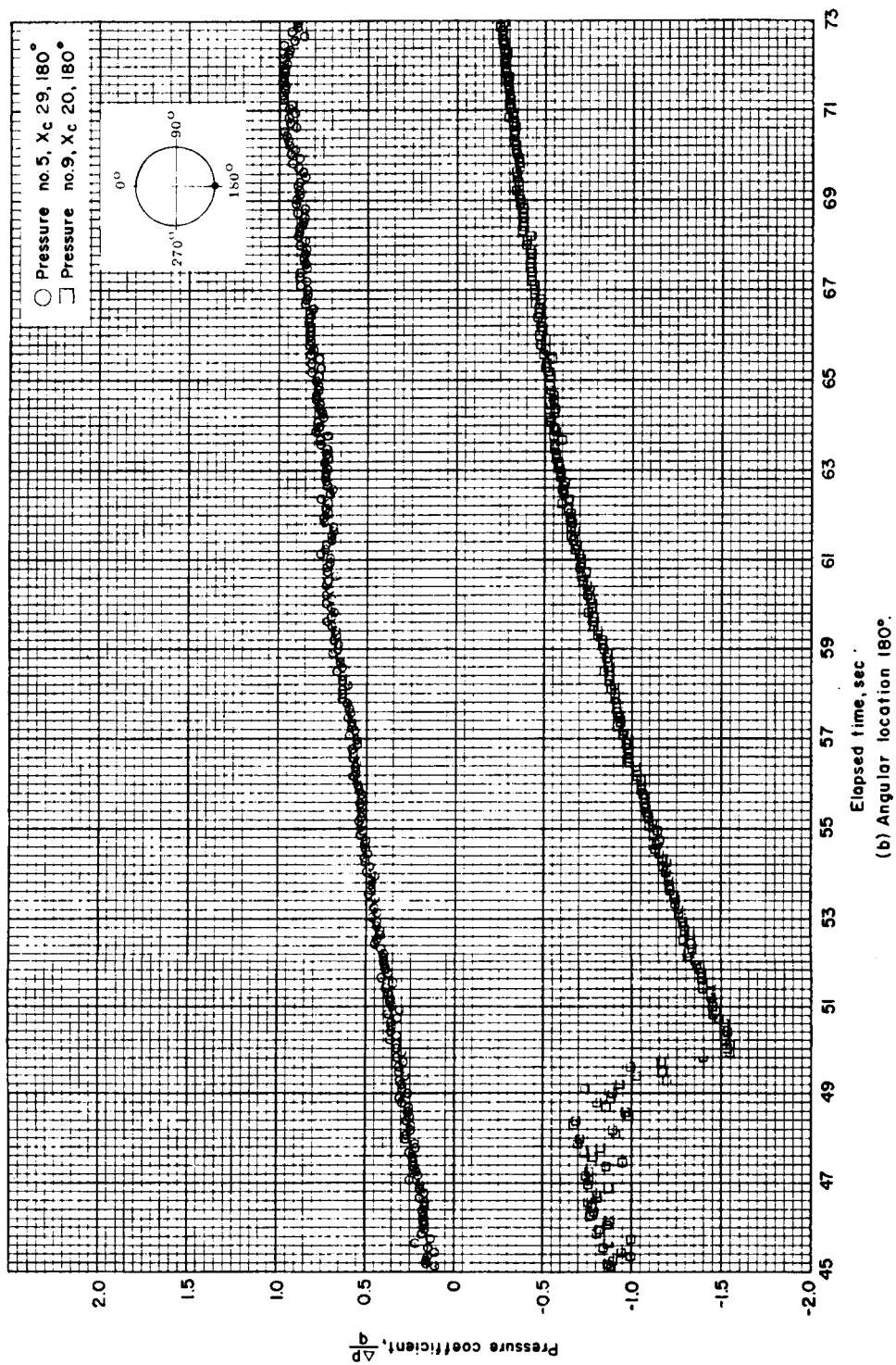
(c) $\phi = 180^\circ$

Figure 4.6-6.- Concluded.



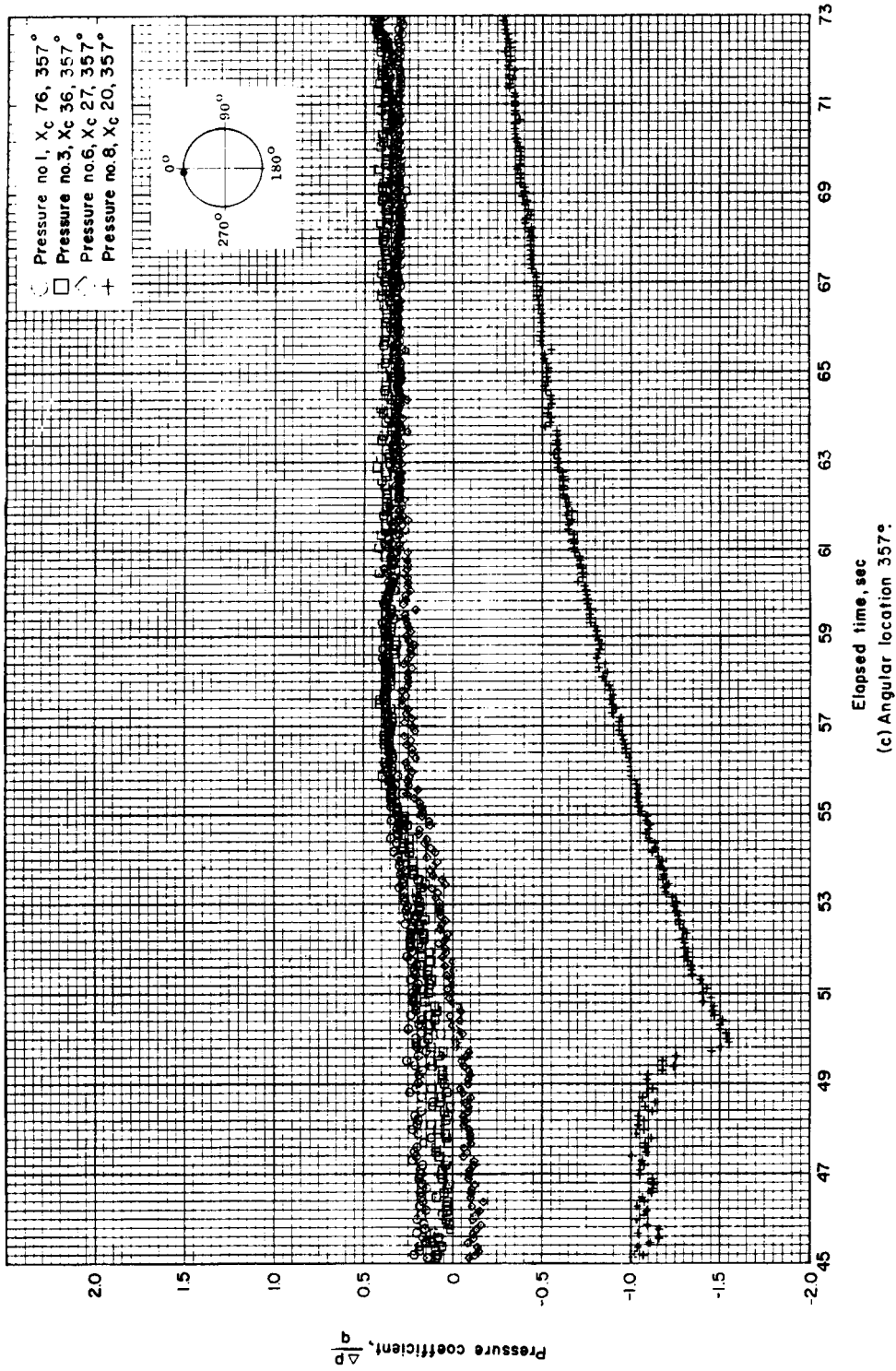
(a) Angular location, approximately 90°

Figure 4.6-7.- Static pressure coefficient over the command module conical surface (BP-13 spacecraft).



(b) Angular location, 180°

Figure 4.6-7.- Continued.



(c) Angular location, 357°

Figure 4.6-7.- Concluded.

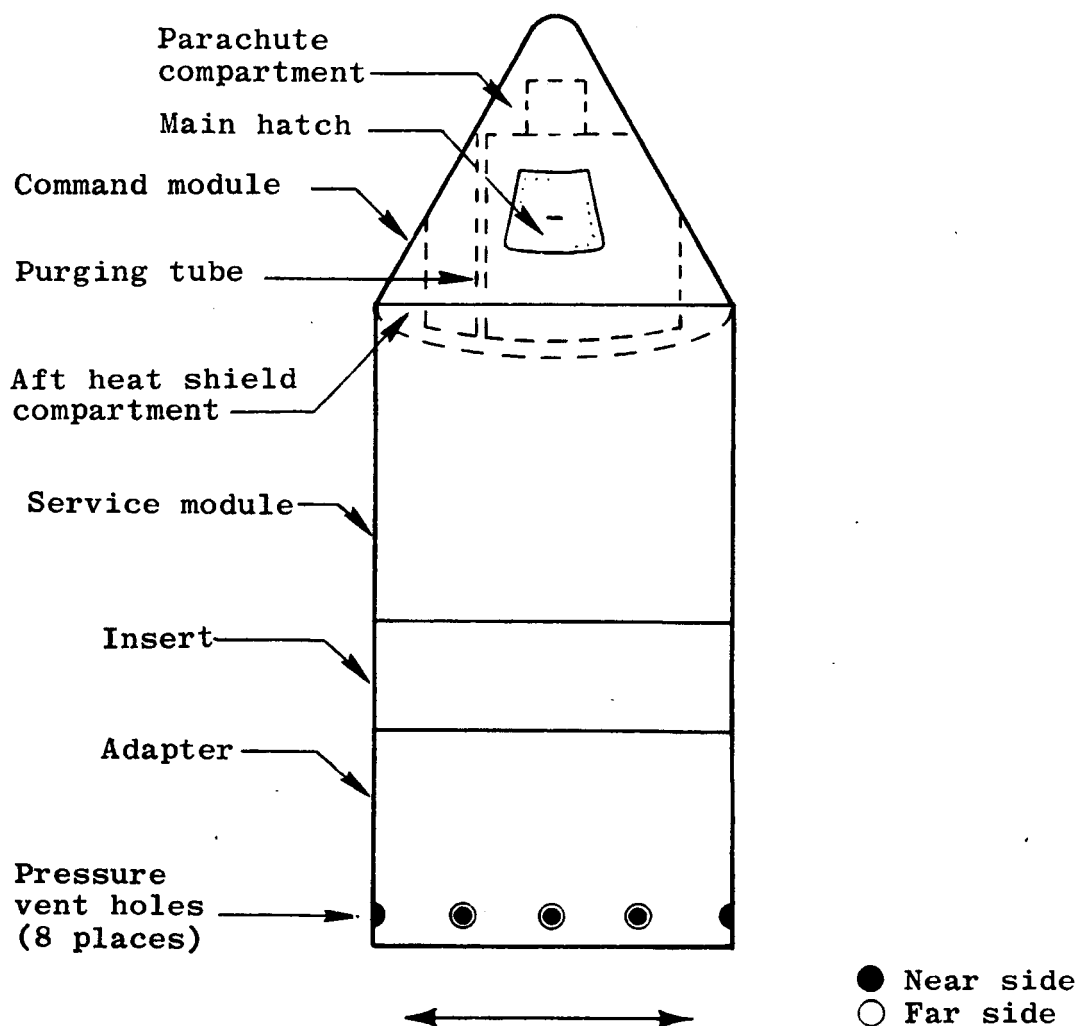


Figure 4.6-8.- Pressure venting scheme for BP-13 spacecraft service module, insert, and adapter compartment.

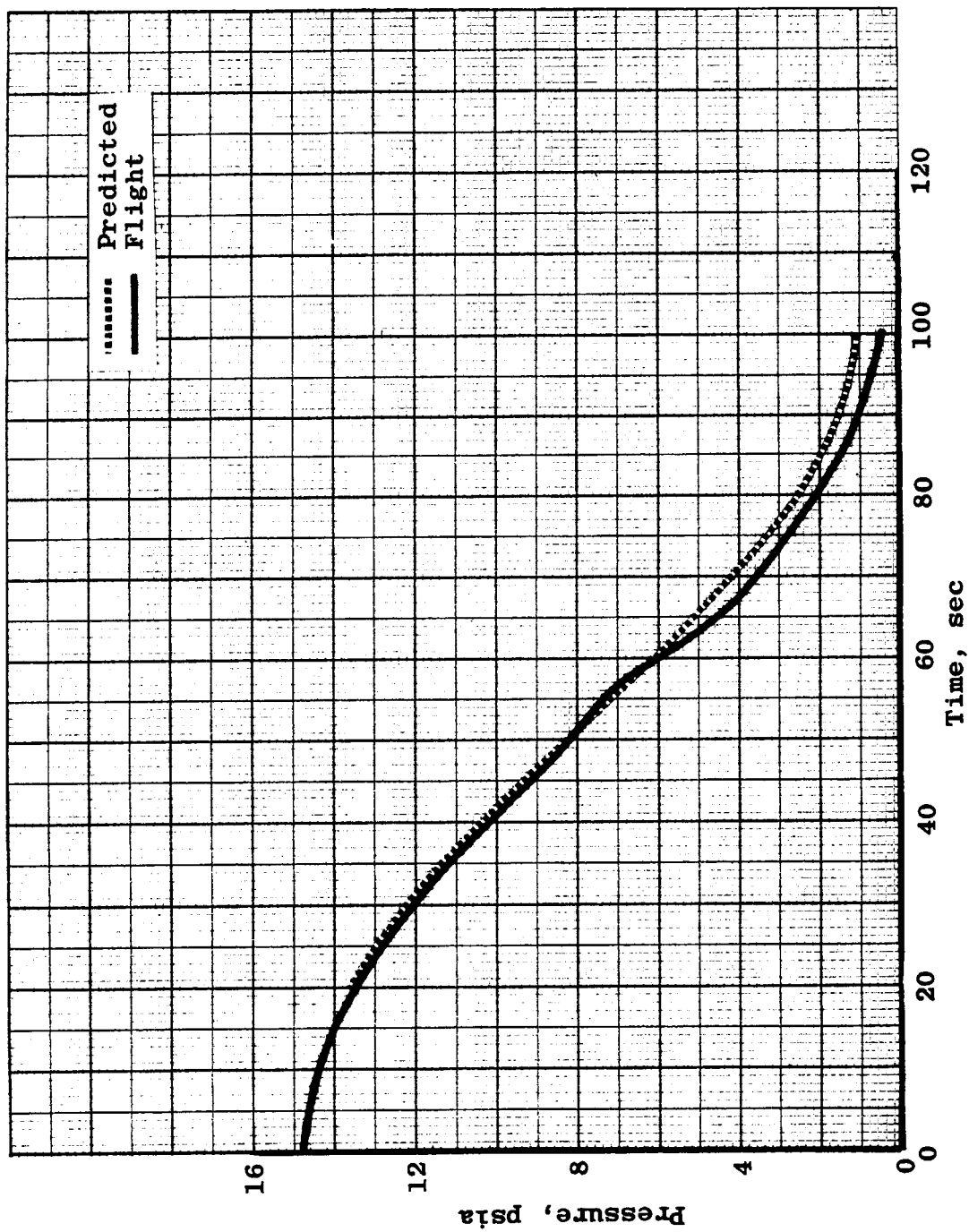


Figure 4.6-9.- Service module internal pressure (BP-13 spacecraft).

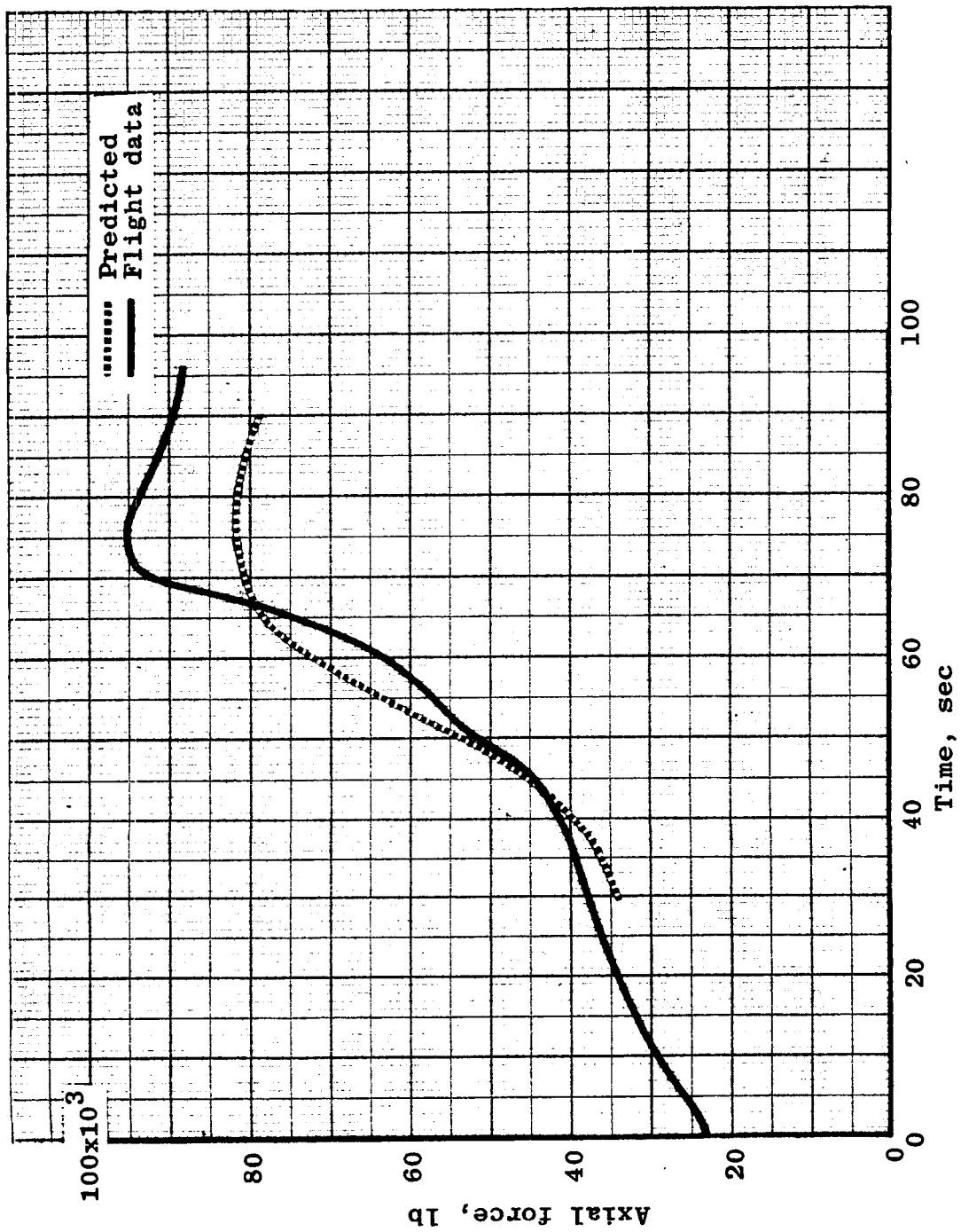
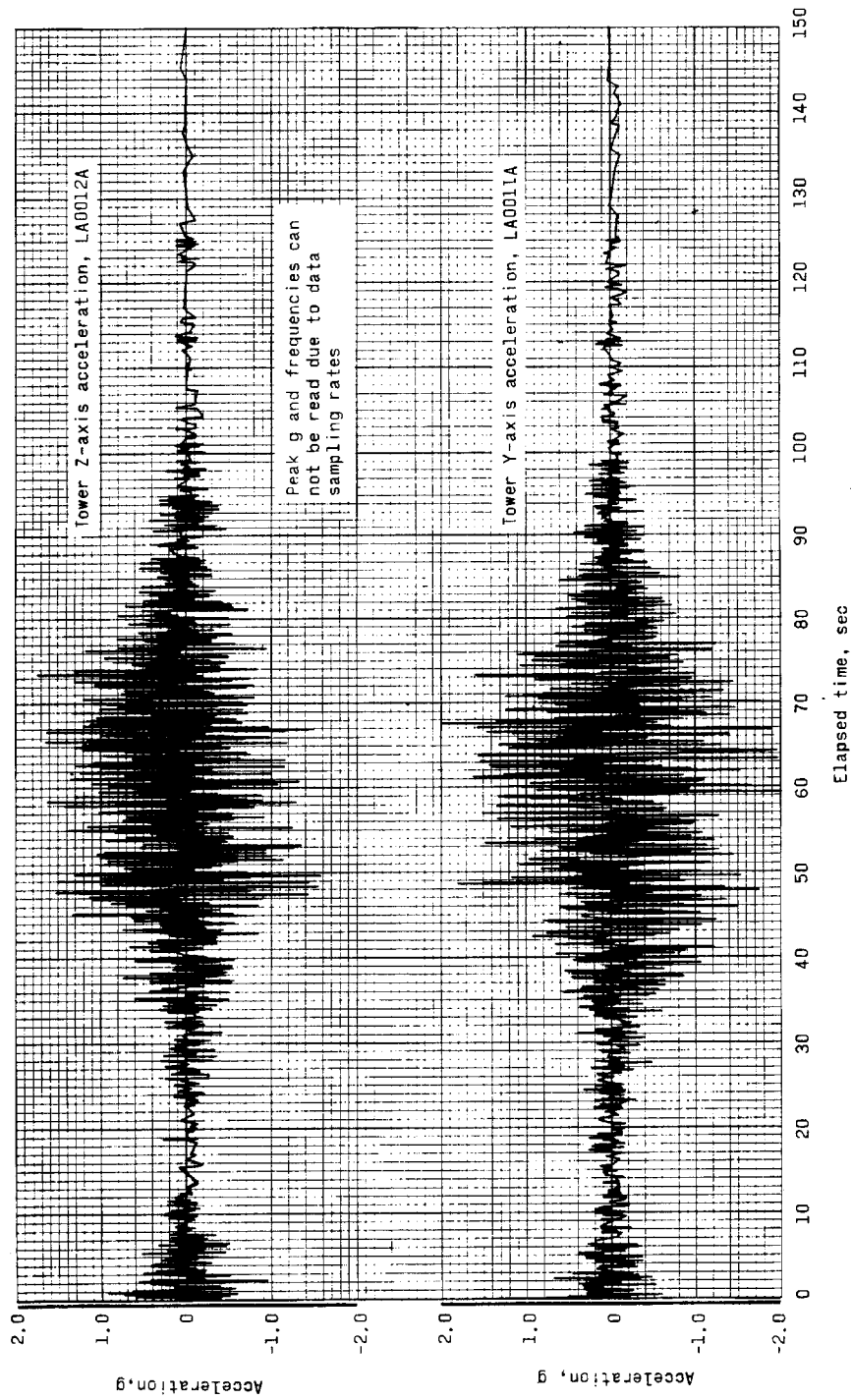
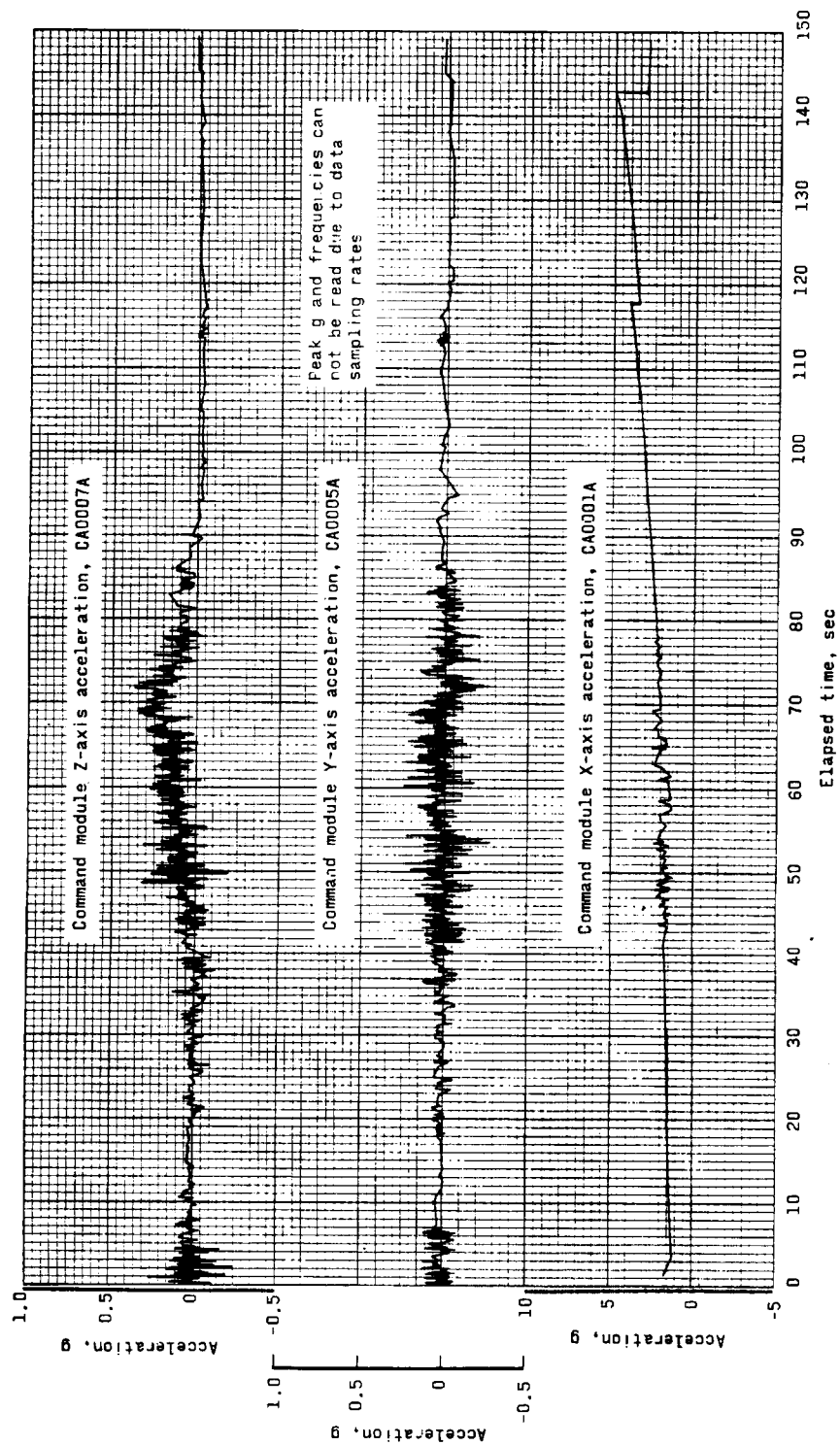


Figure 4.6-10.- Axial force (compression) at interface of BP-13 spacecraft adapter and Saturn SA-6 instrument unit (station $X_A 722$).



(a) Launch-escape subsystem at Q-ball interface.

Figure 4.6-11.- Flight measured acceleration (BP-13 spacecraft).



(b) Command module.

Figure 4.6-11.- Concluded.

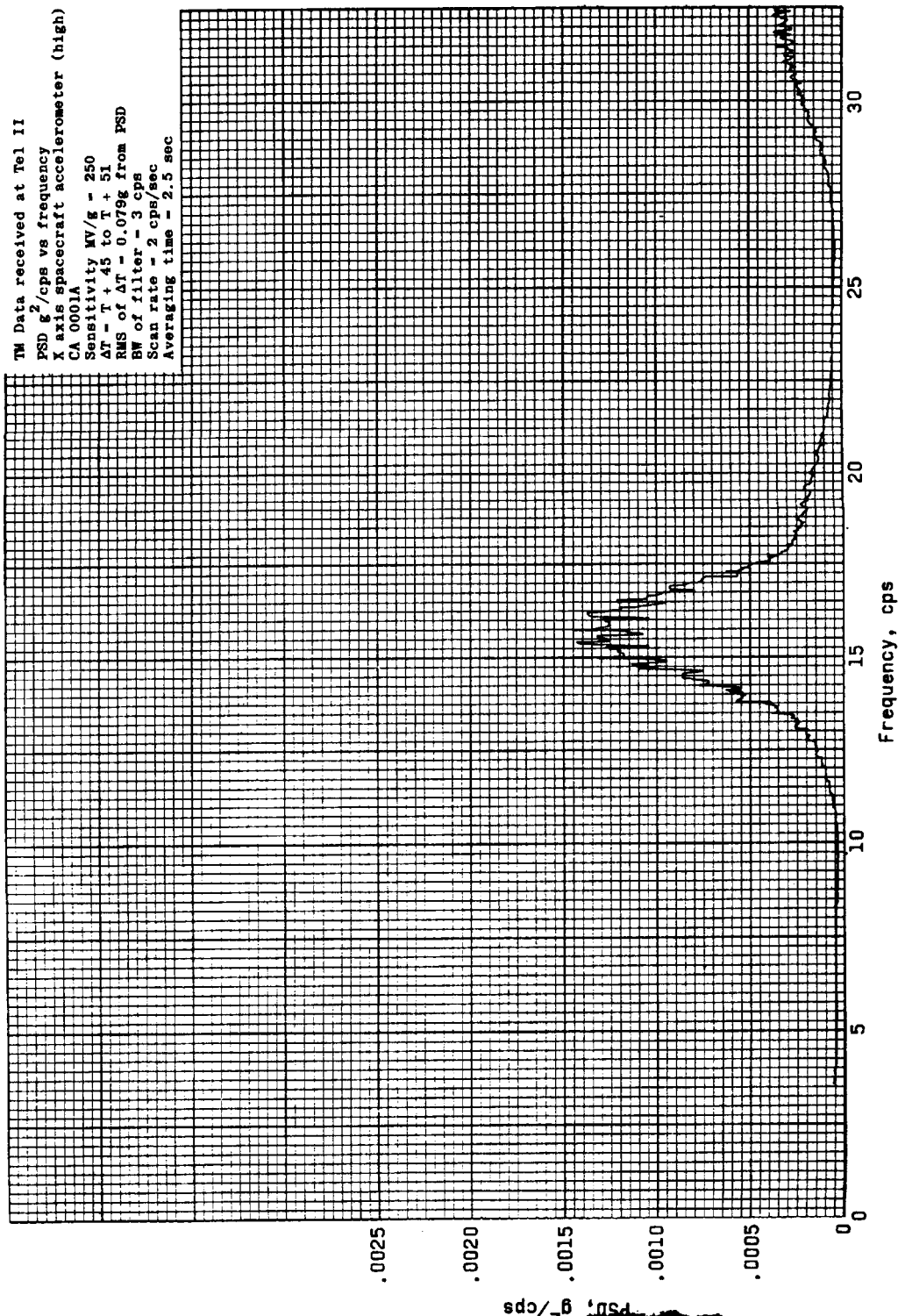
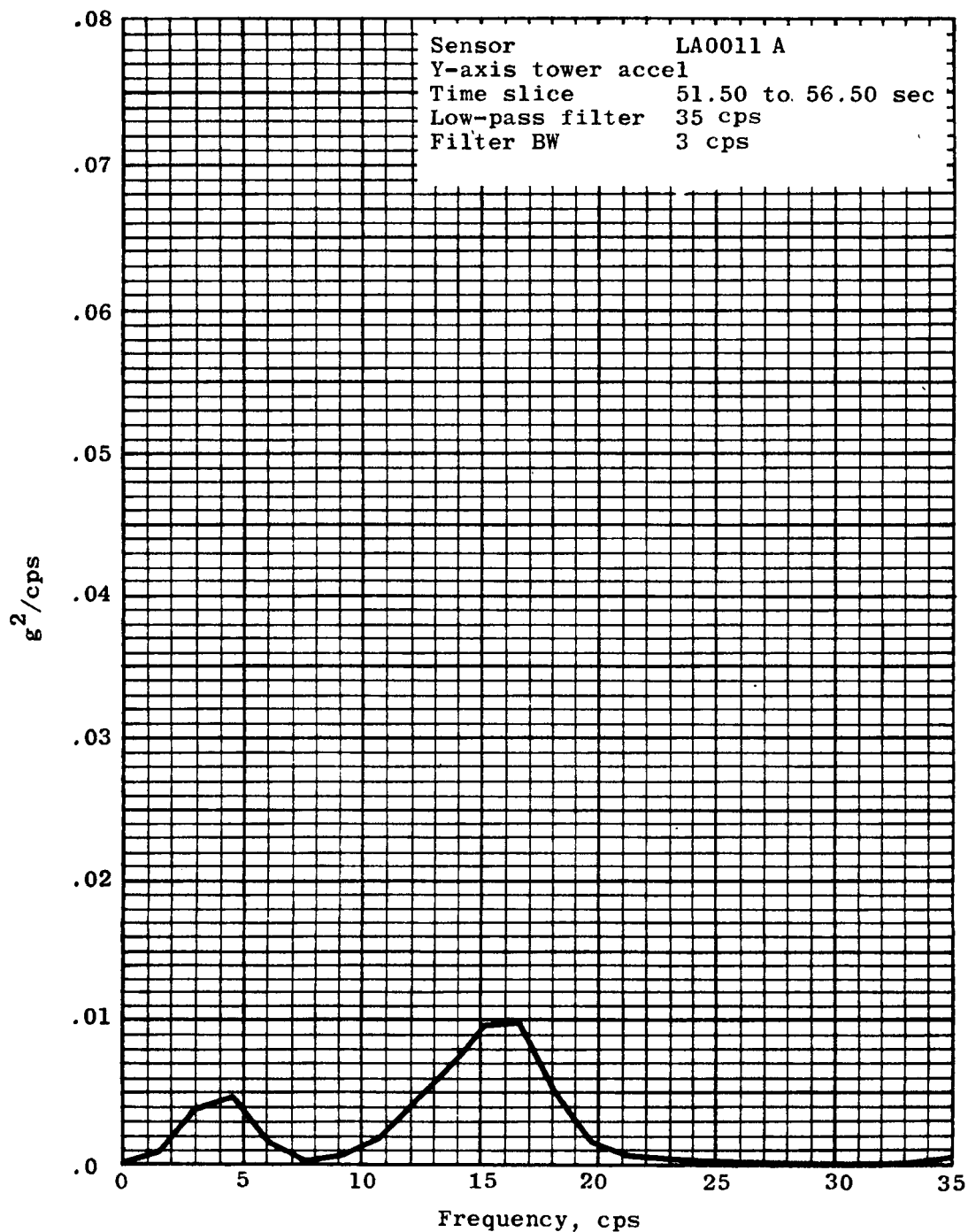
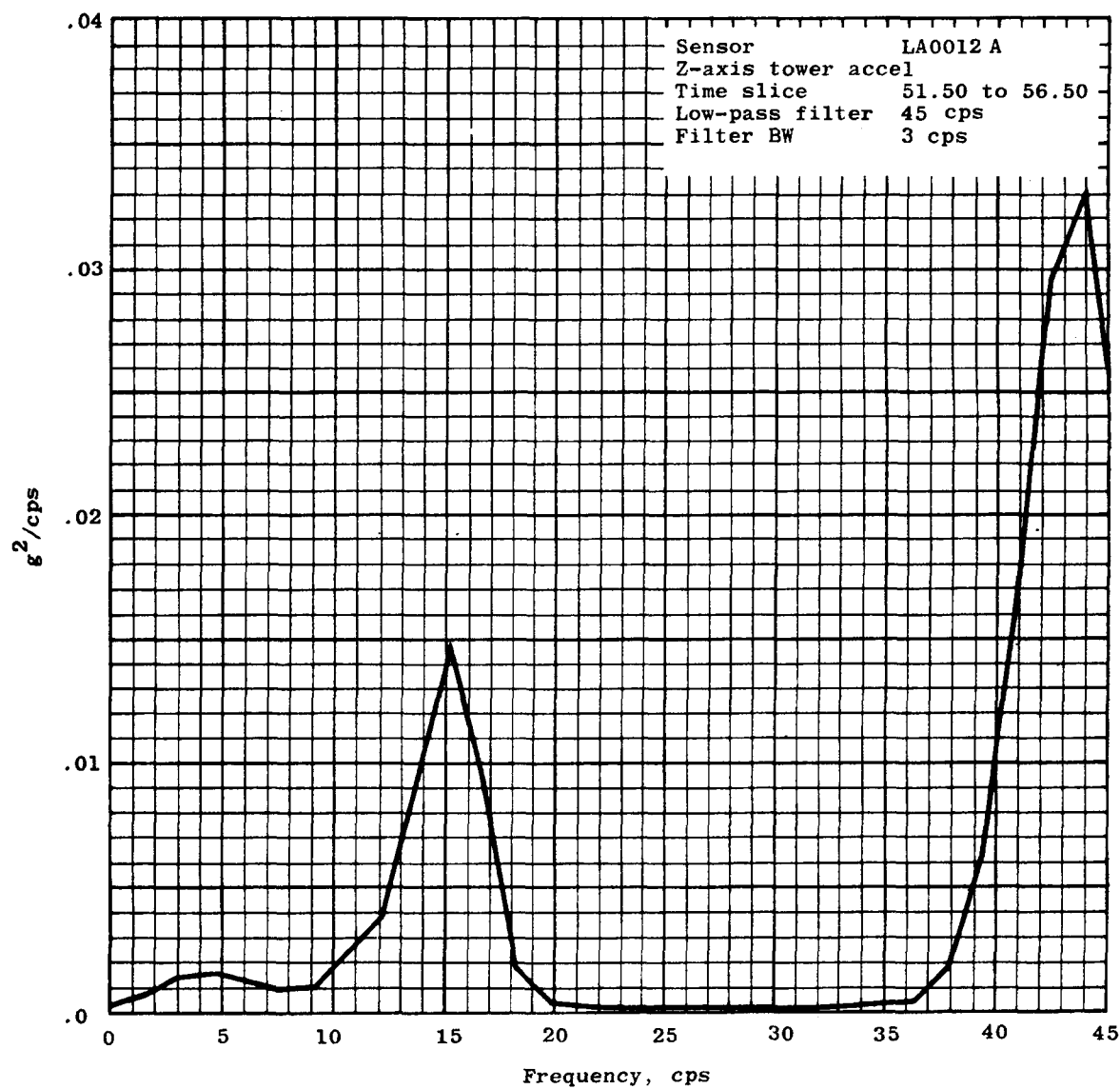


Figure 4.6-12.- Digital spectrum estimation of X-axis acceleration (BP-13 spacecraft).



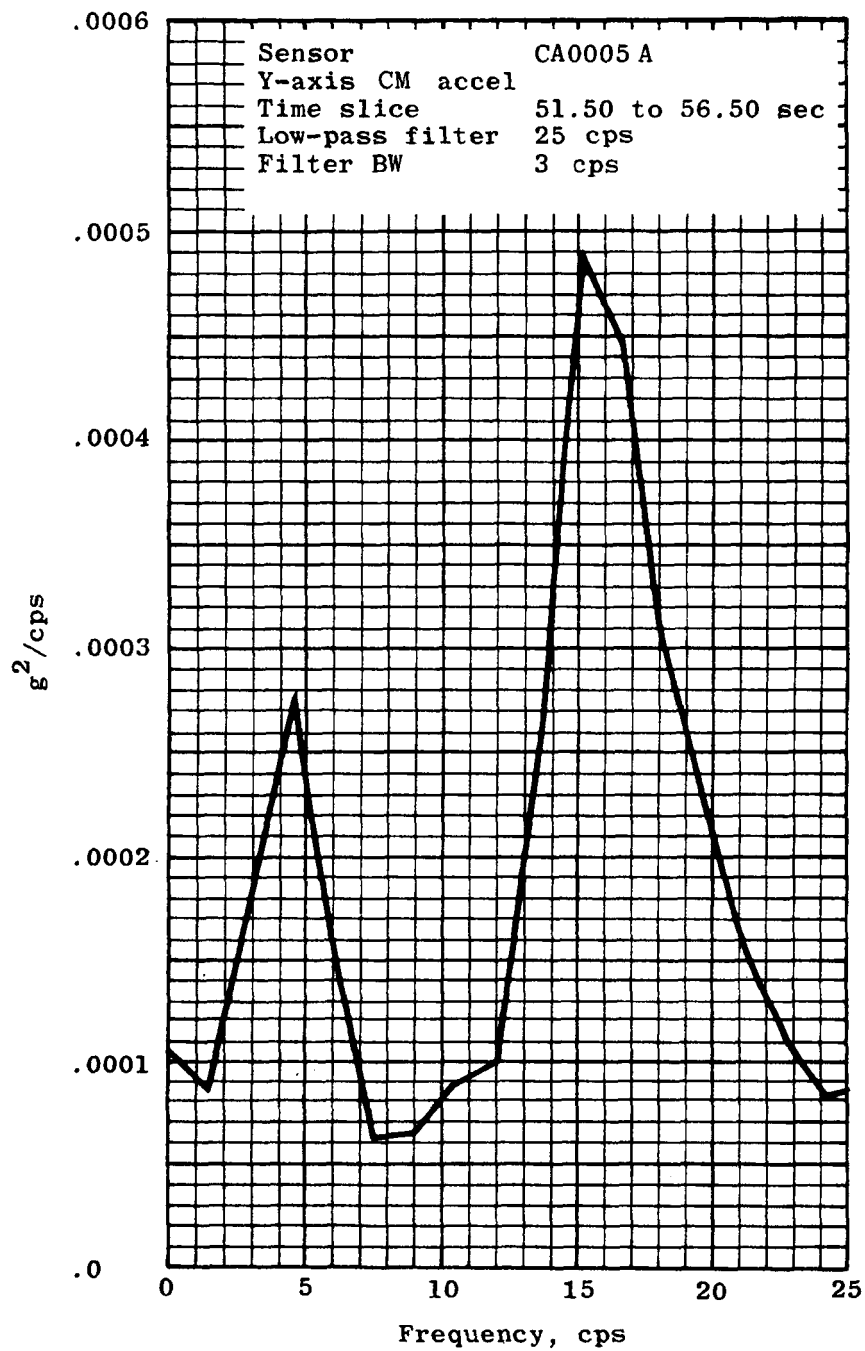
(a) LES Y-axis at Q-ball interface

Figure 4.6-13.- Digital spectrum estimation of lateral bending acceleration (BP-13 spacecraft).



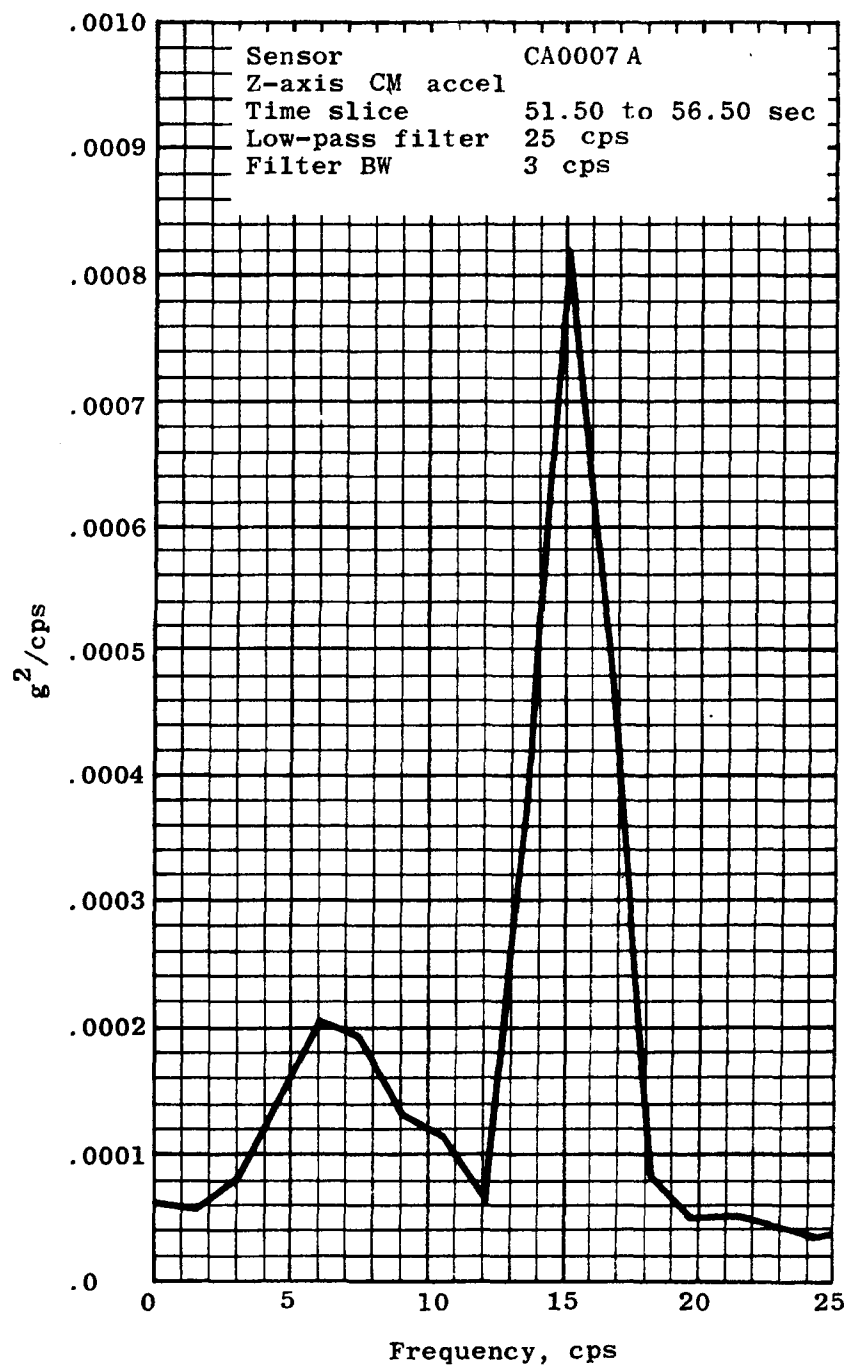
(b) LES Z-axis at Q-ball interface.

Figure 4.6-13.- Continued



(c) Command module Y-axis.

Figure 4.6-13.- Continued.



(d) Command module Z-axis.

Figure 4.6-13.- Concluded.

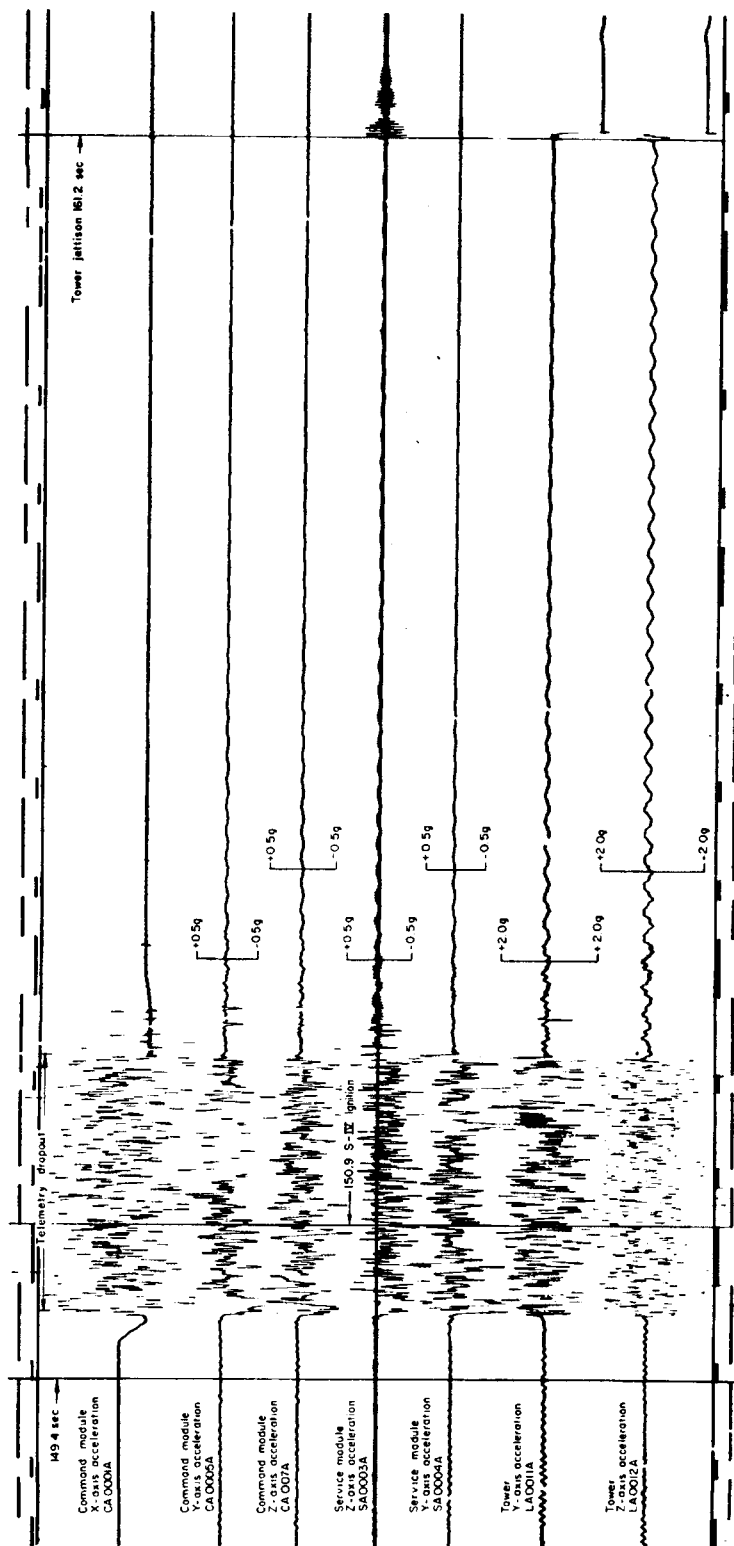
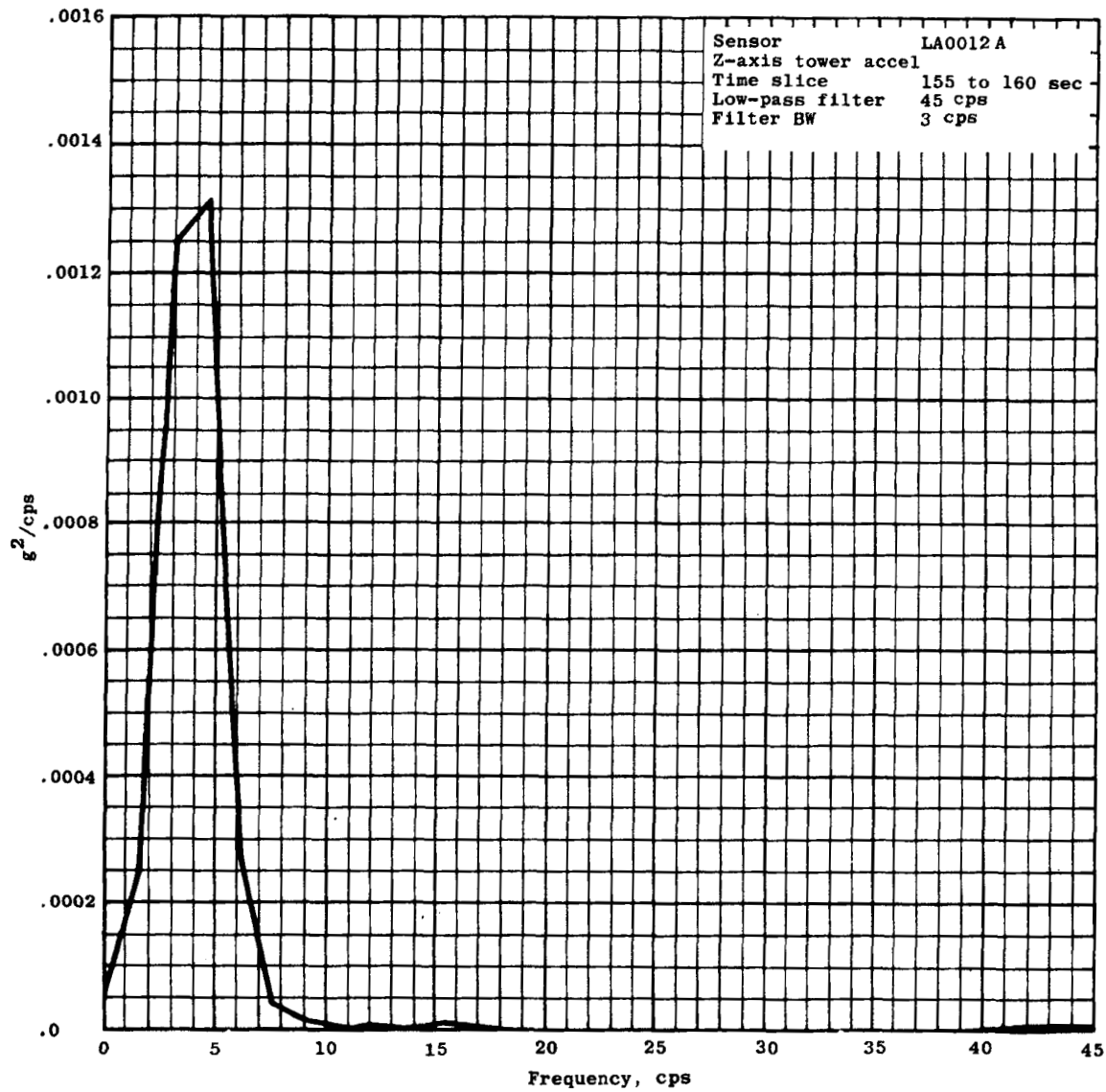
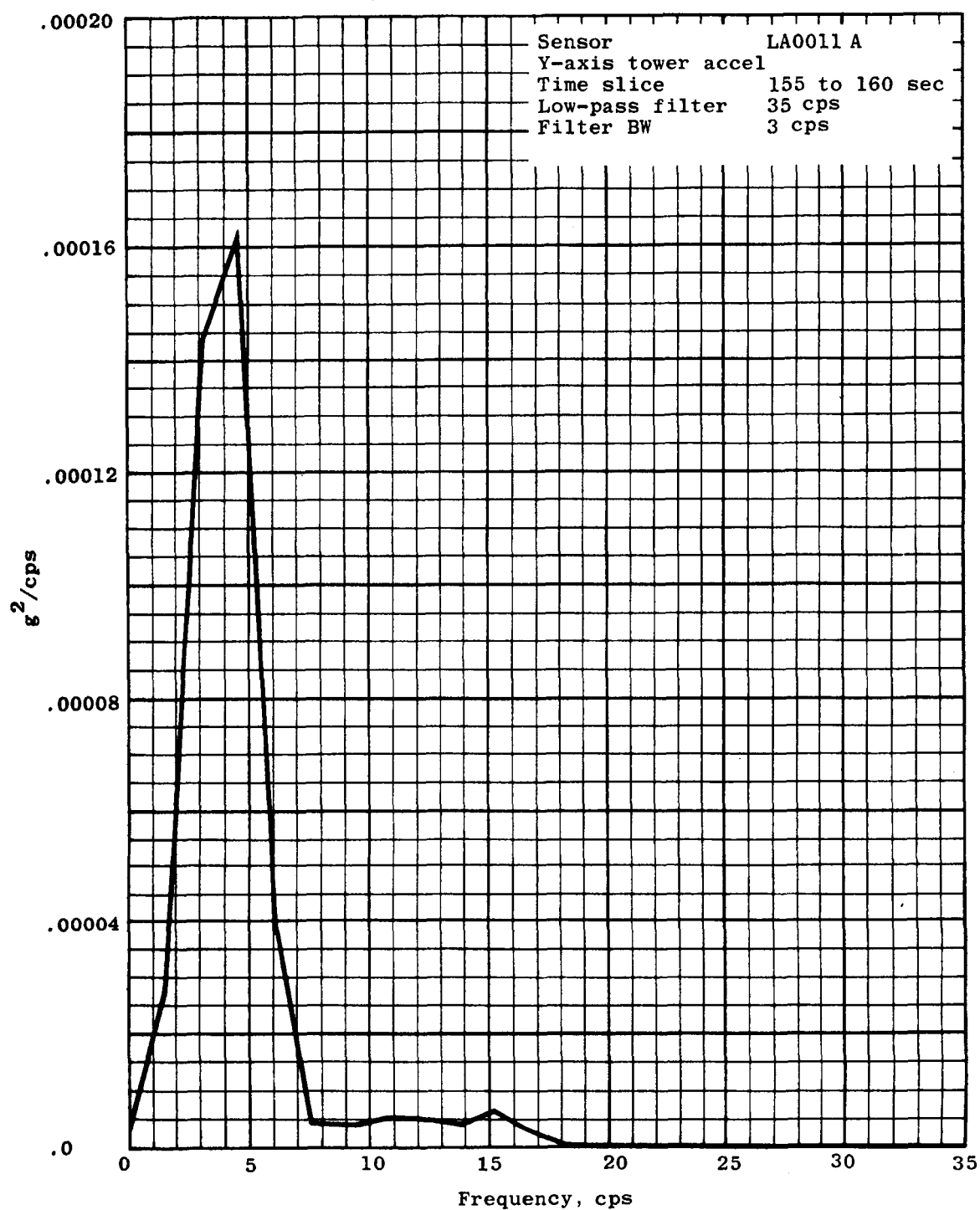


Figure 4.6-14.- First bending mode acceleration of BP-13 spacecraft at ignition of S-IV stage.



(a) LES Z-axis at Q-ball interface

Figure 4.6-15.- Digital spectrum estimation of first bending mode acceleration of BP-13 spacecraft after ignition of S-IV stage.



(b) LES Y-axis at Q-ball interface.

Figure 4.6-15.- Concluded.

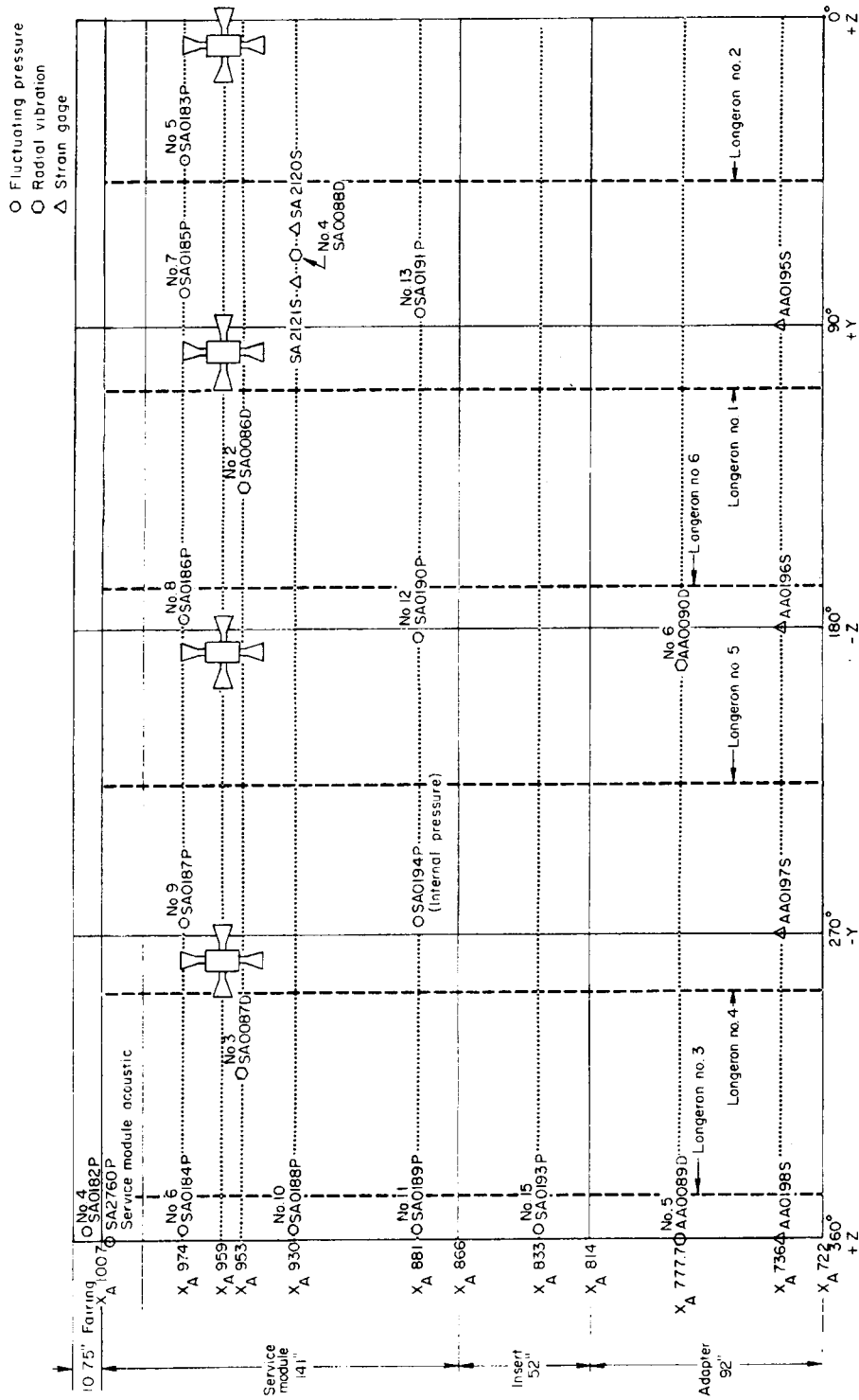


Figure 4.6-16.- Development view of BP-13 spacecraft service module, insert, and adapter wall showing transducer locations.

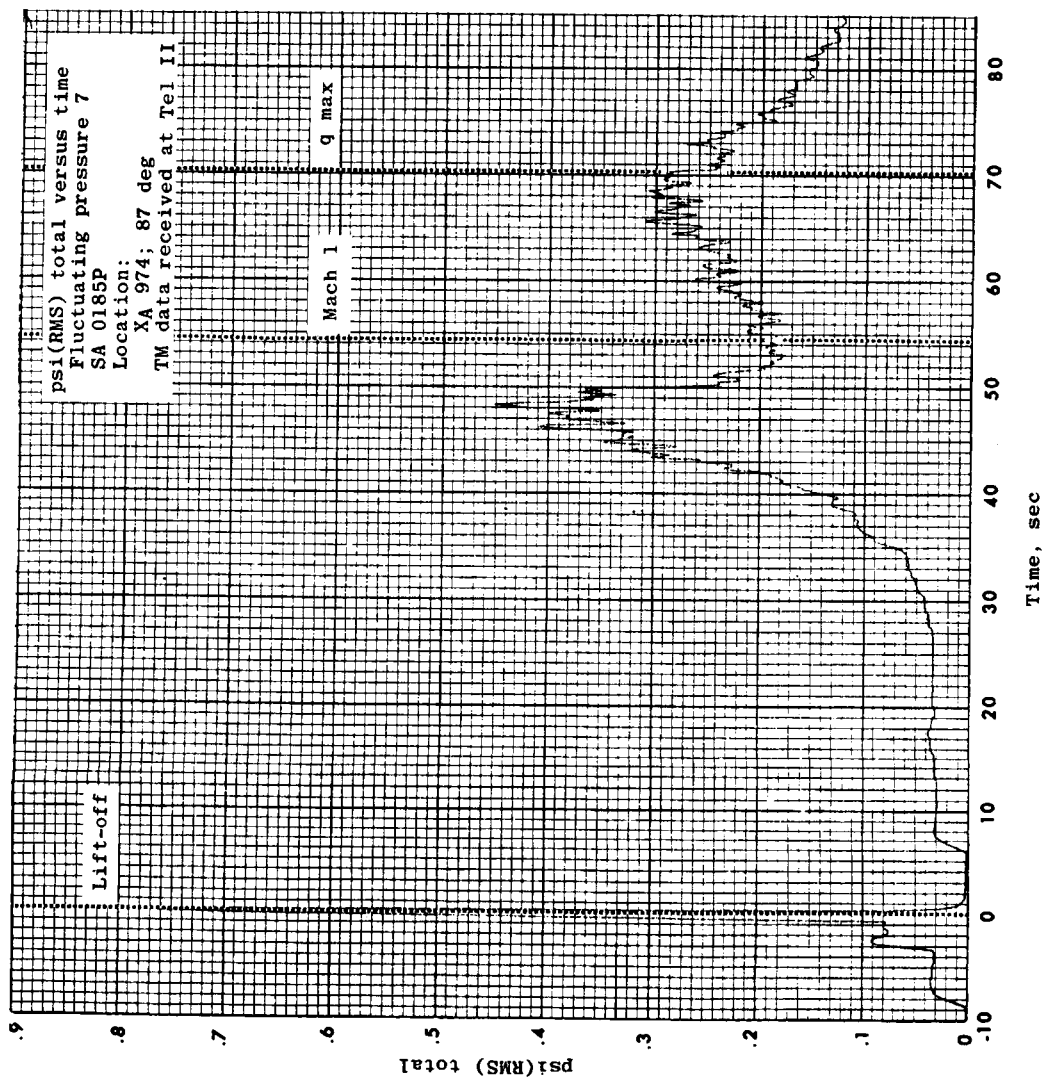


Figure 4.6-17.- RMS of fluctuating pressure no. 7 on BP-13 service module.

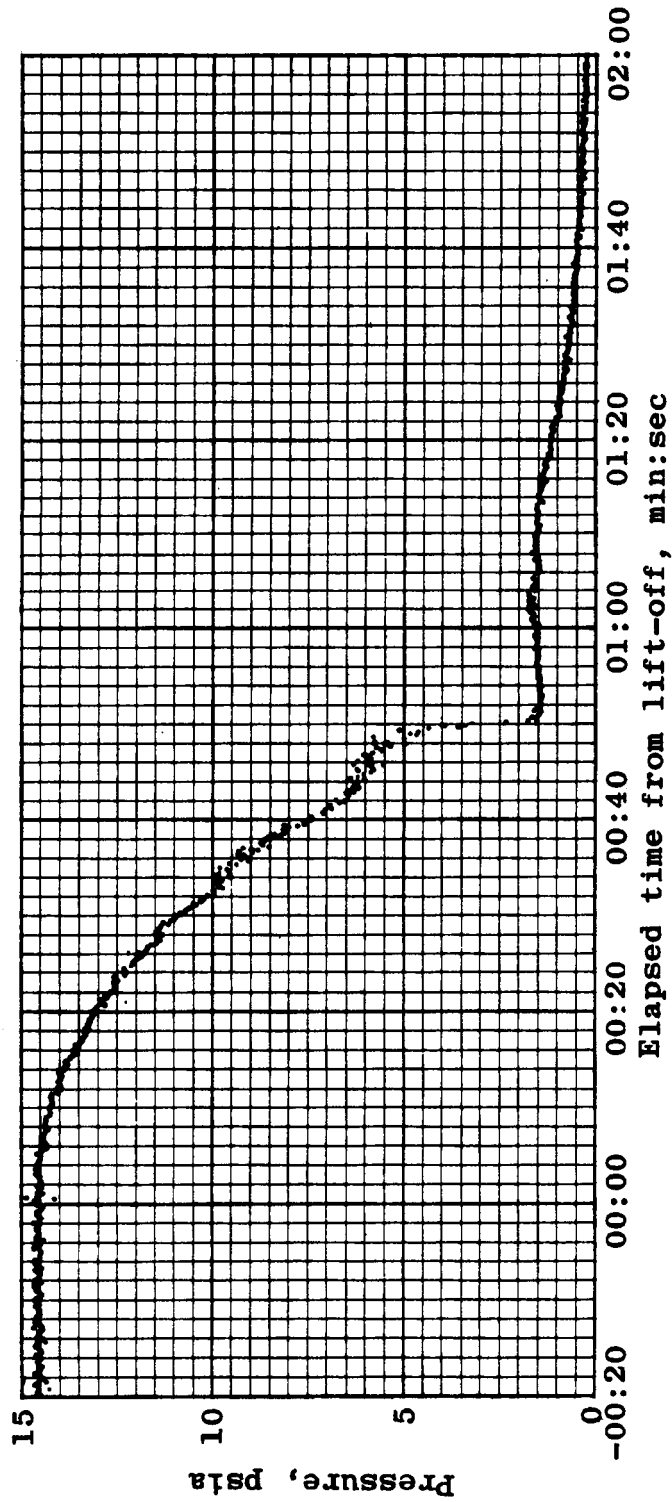


Figure 4.6-18.- Static pressure at BP-13 spacecraft CM-SM shoulder.

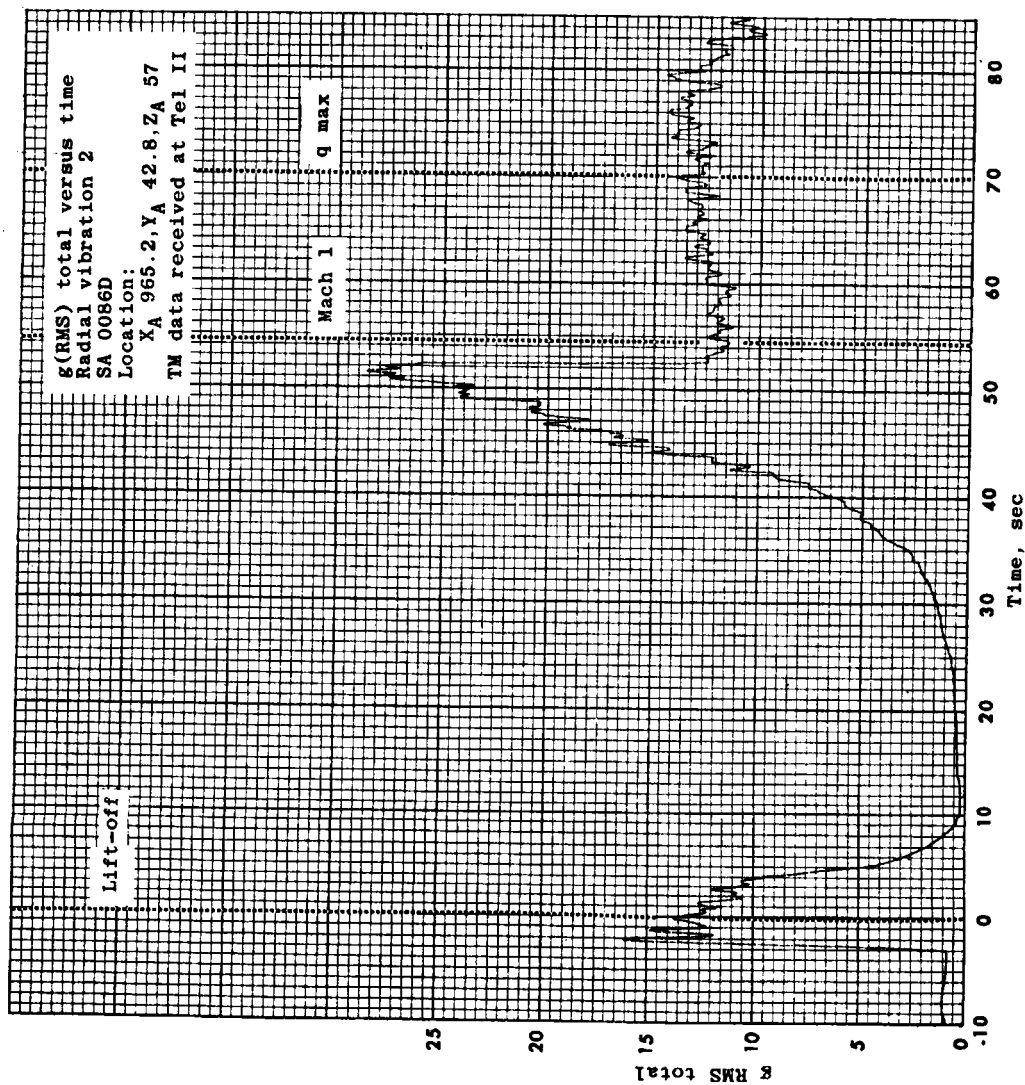
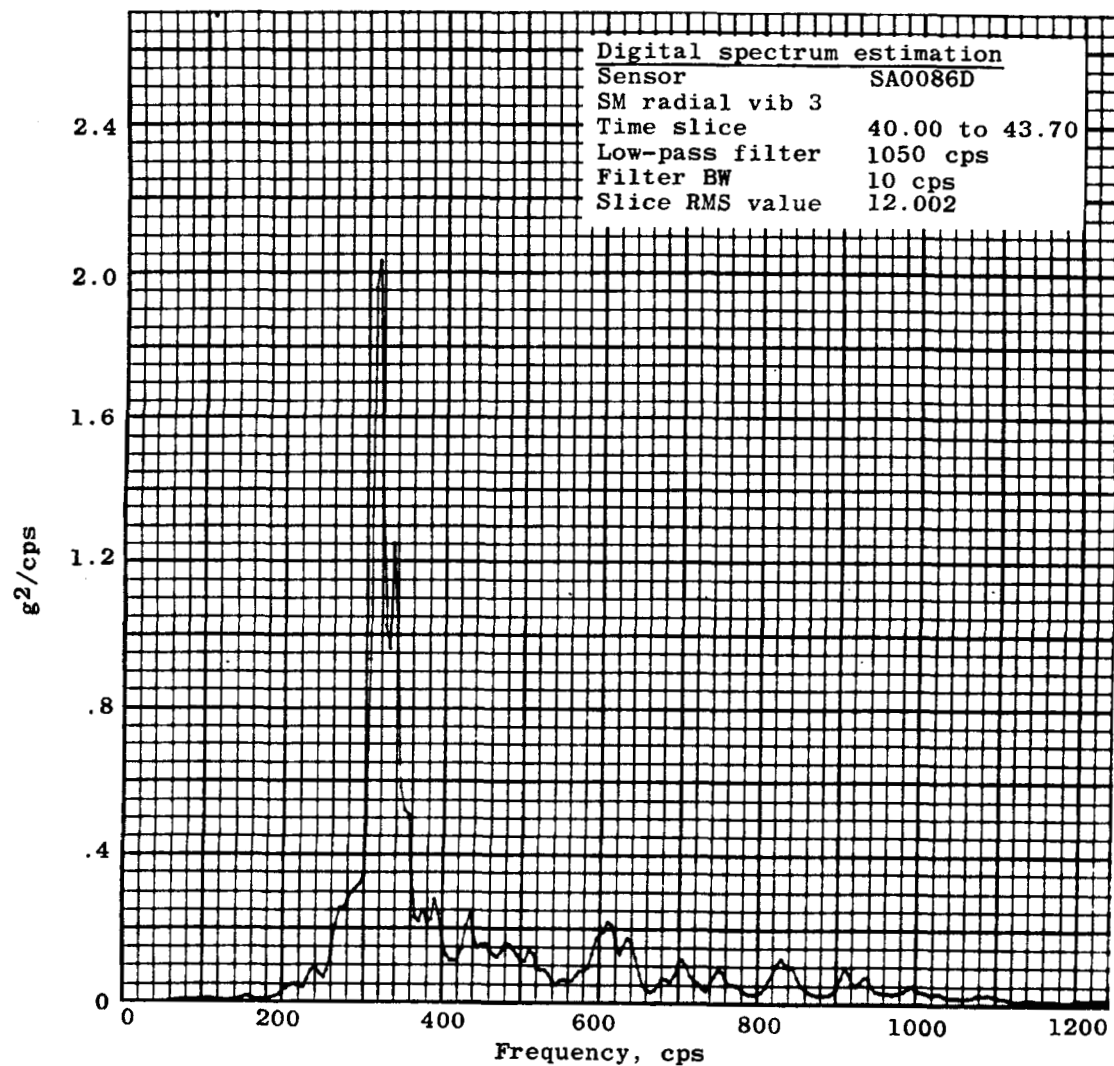
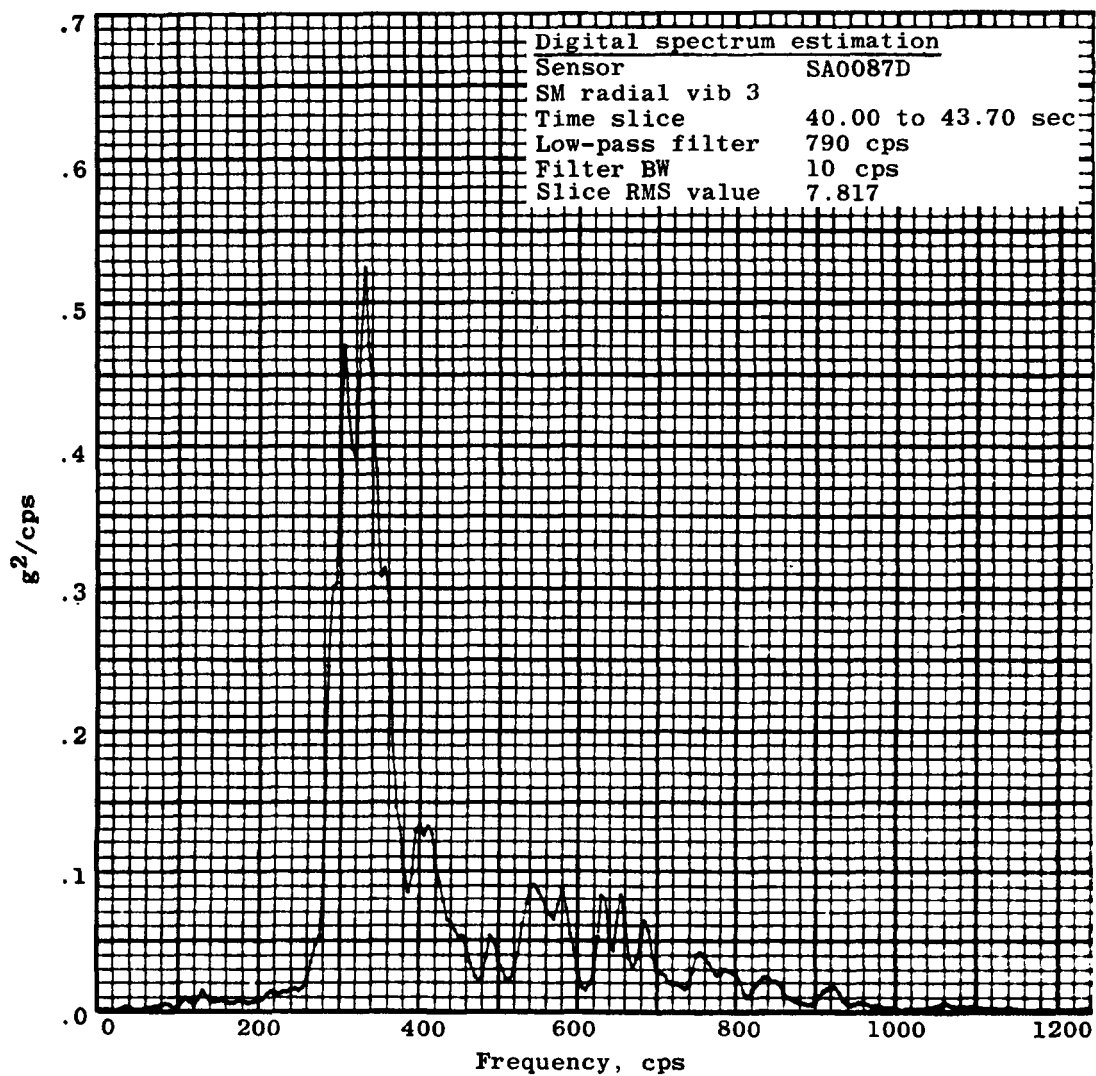


Figure 4.6-19.- RMS estimation of BP-13 spacecraft service module radial vibration.



(a) Instrument SA0086D

Figure 4.6-20.- Digital spectrum estimation of BP-13 spacecraft service module radial vibration.



(b) Instrument SA0087D

Figure 4.6-20.- Concluded.

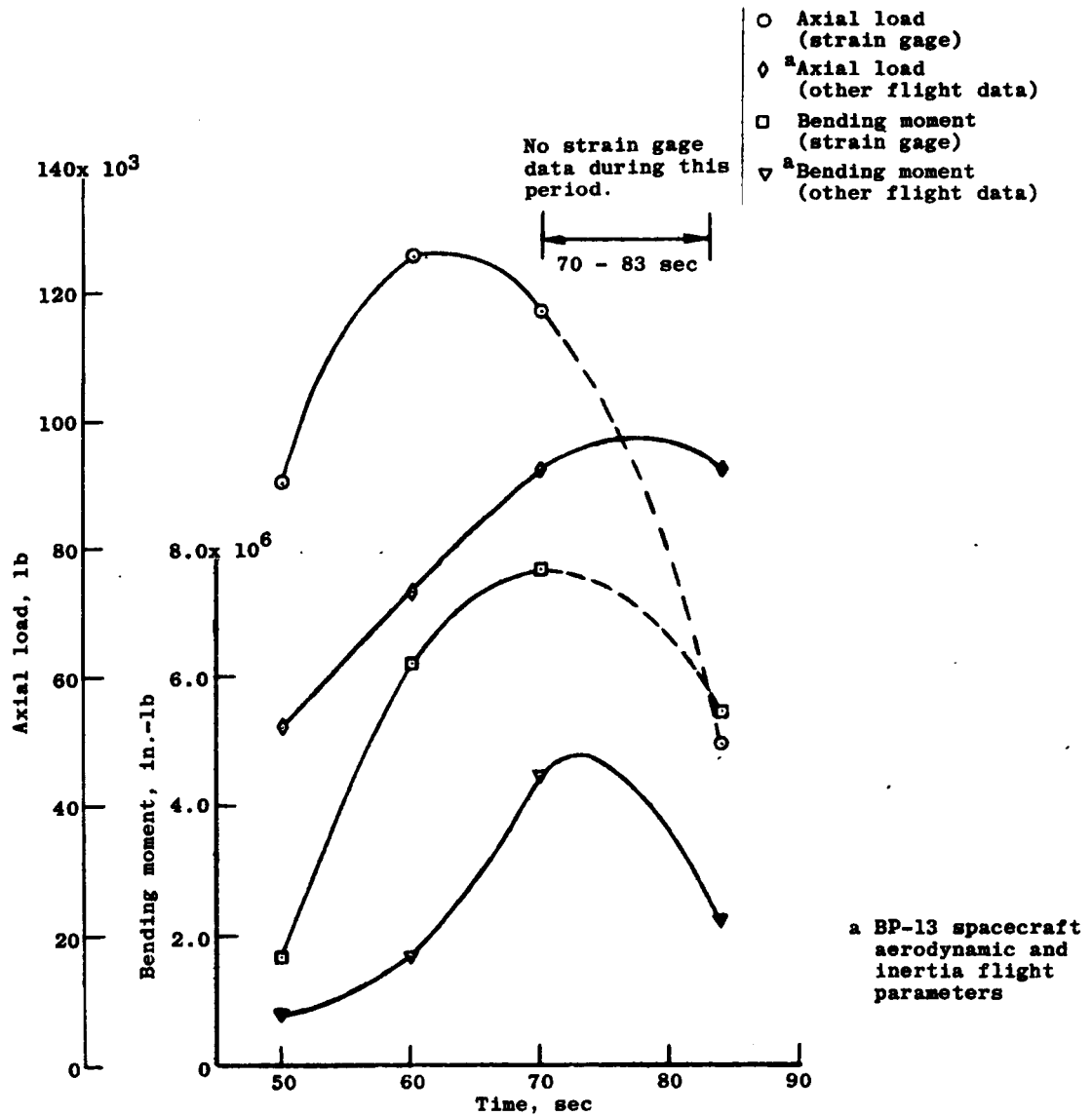
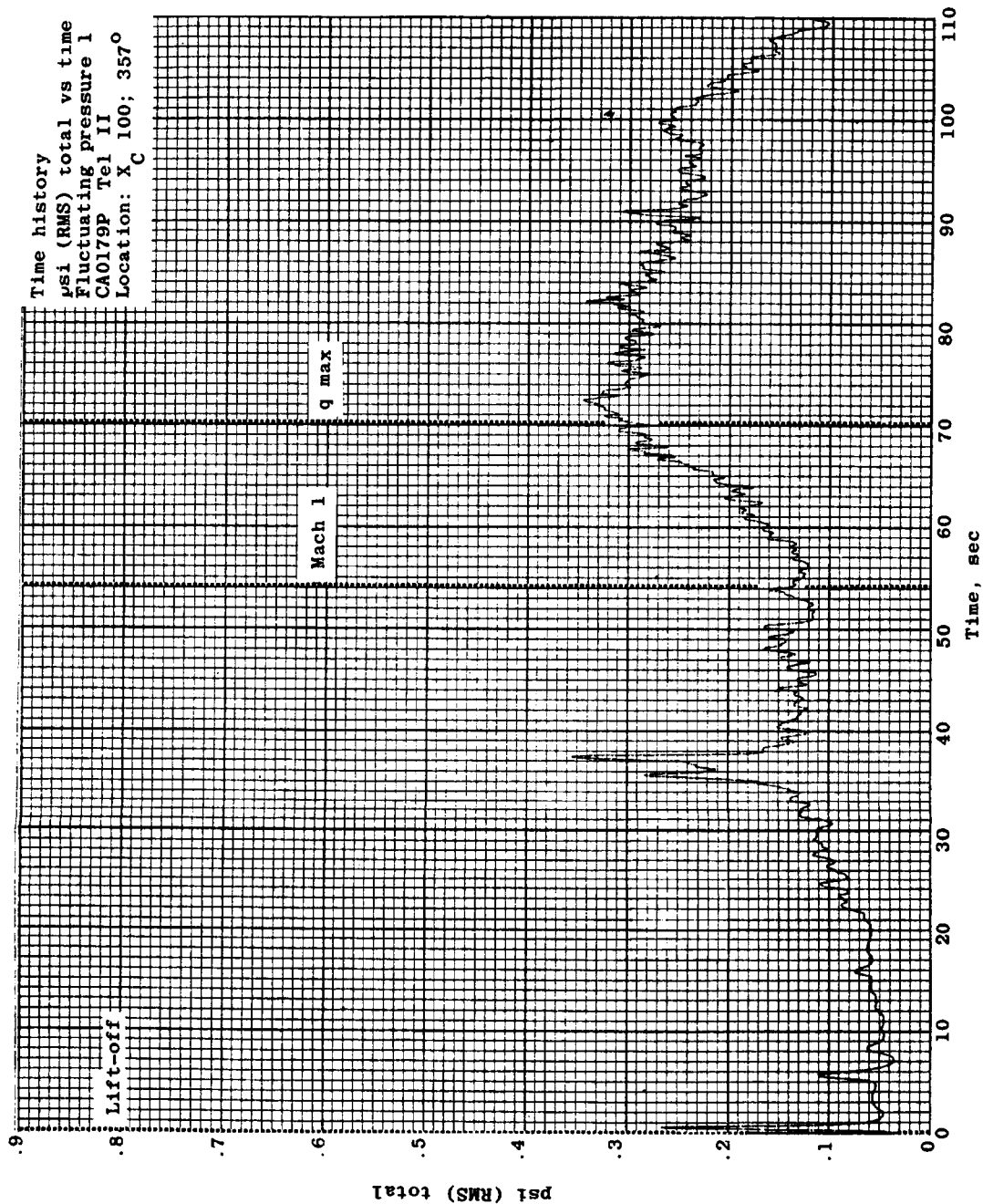
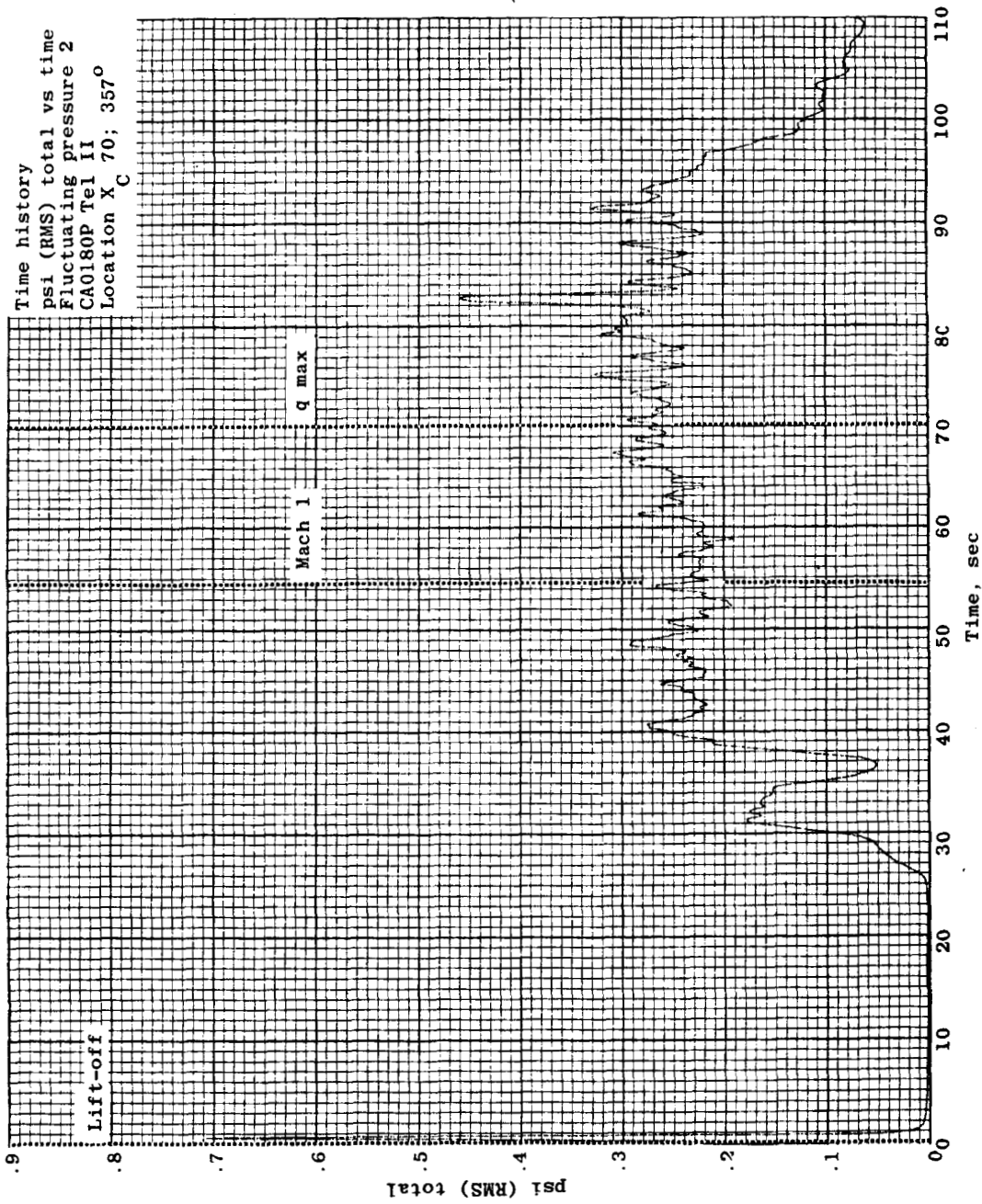


Figure 4.6-21.- BP-13 spacecraft adapter load trend comparison.



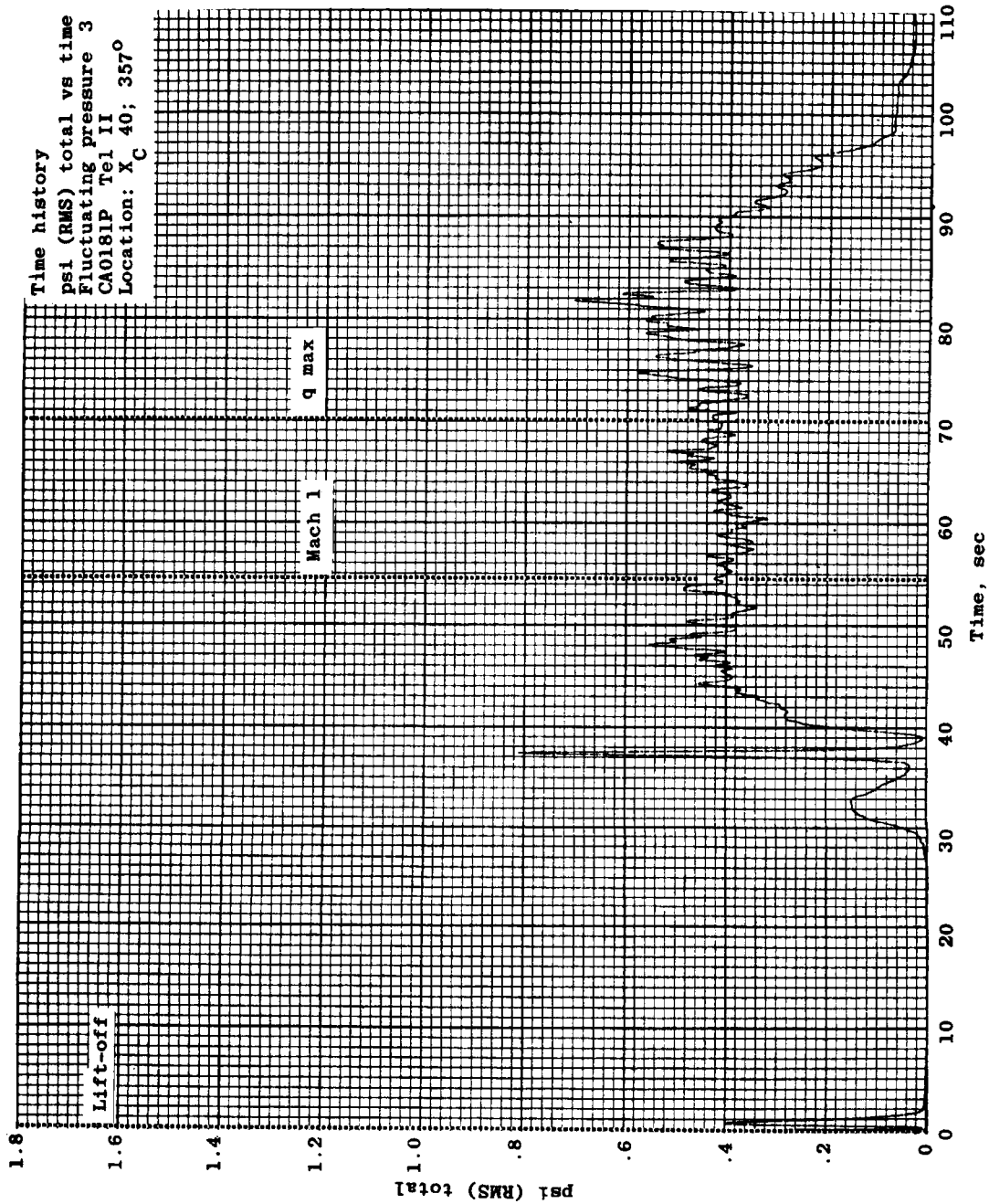
(a) Fluctuating pressure 1 (CA0179P)

Figure 4.6-22.- RMS of fluctuating pressures over BP-13 spacecraft.



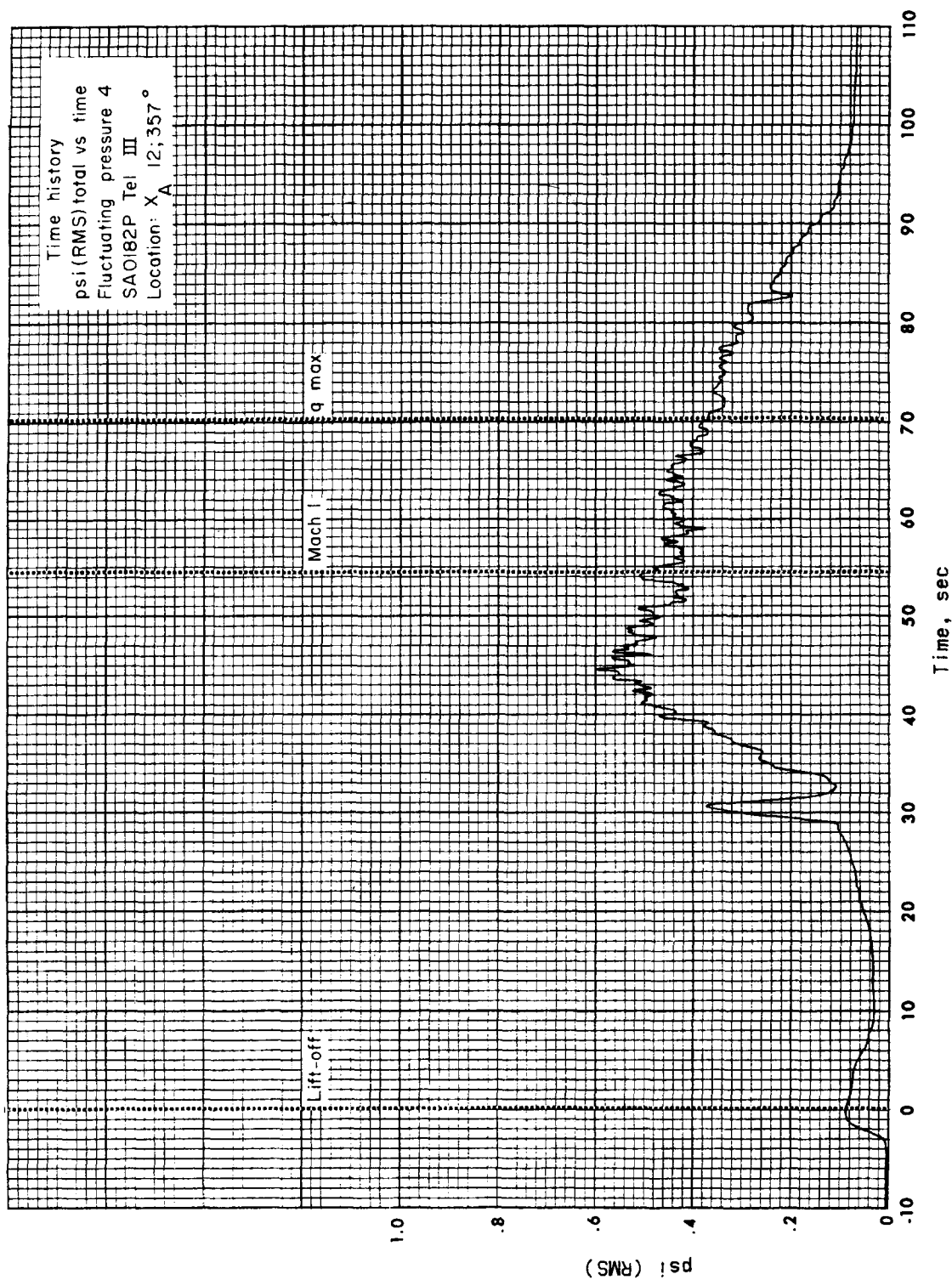
(b) Fluctuating pressure 2 (CA0180P)

Figure 4.6-22.- Continued.



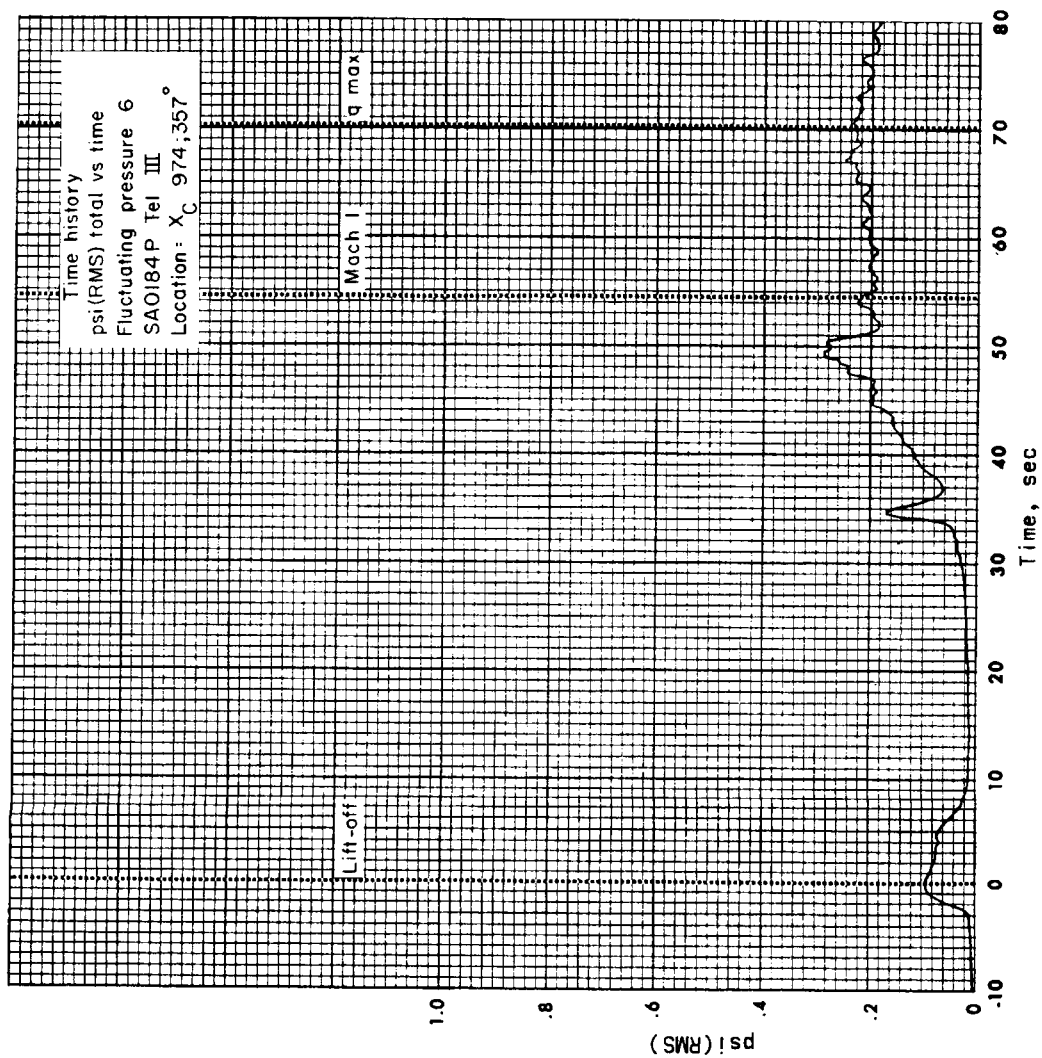
(c) Fluctuating pressure 3 (CA0181P)

Figure 4.6-22.- Continued.



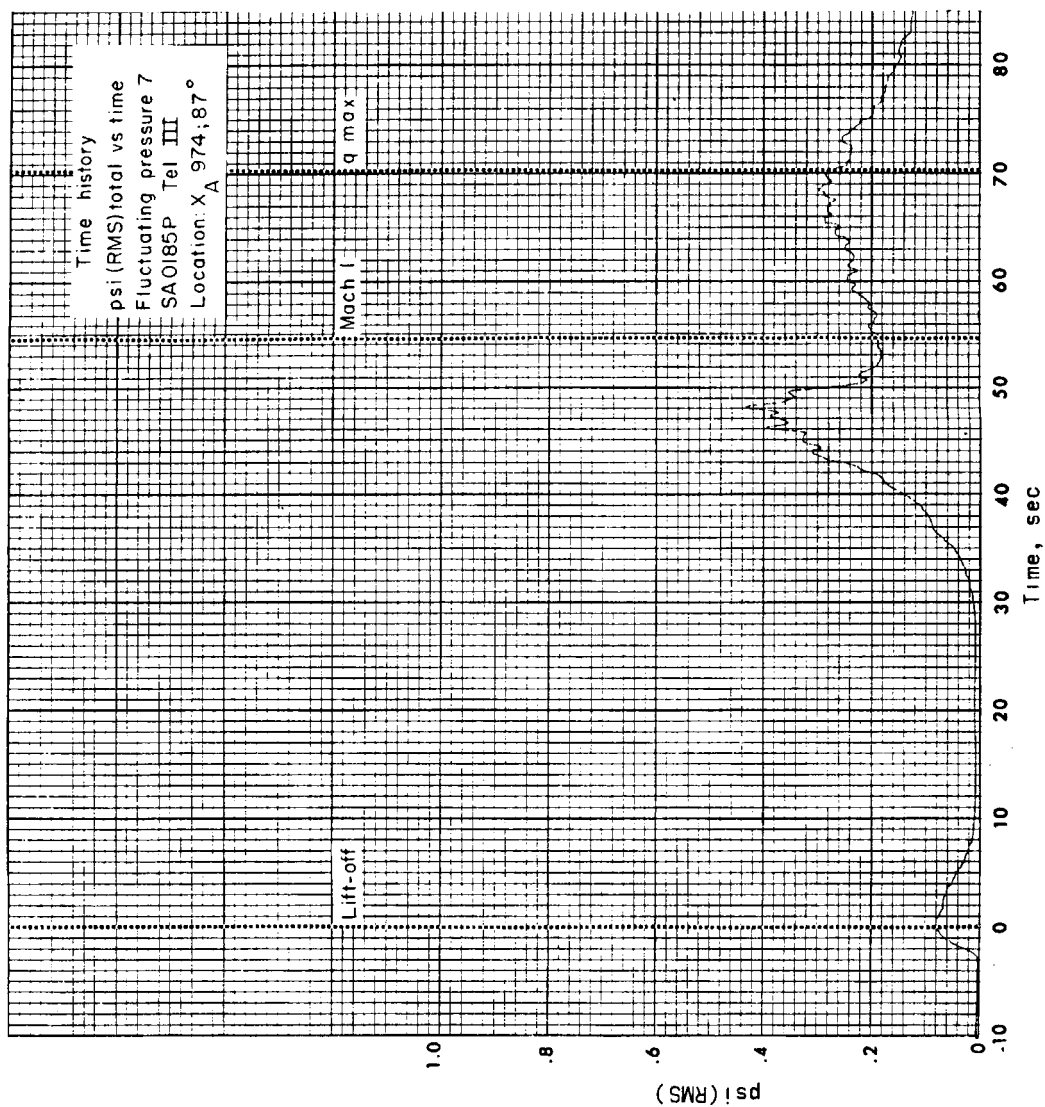
(d) Fluctuating pressure 4 (SA0182P)

Figure 4.6-22.- Continued.



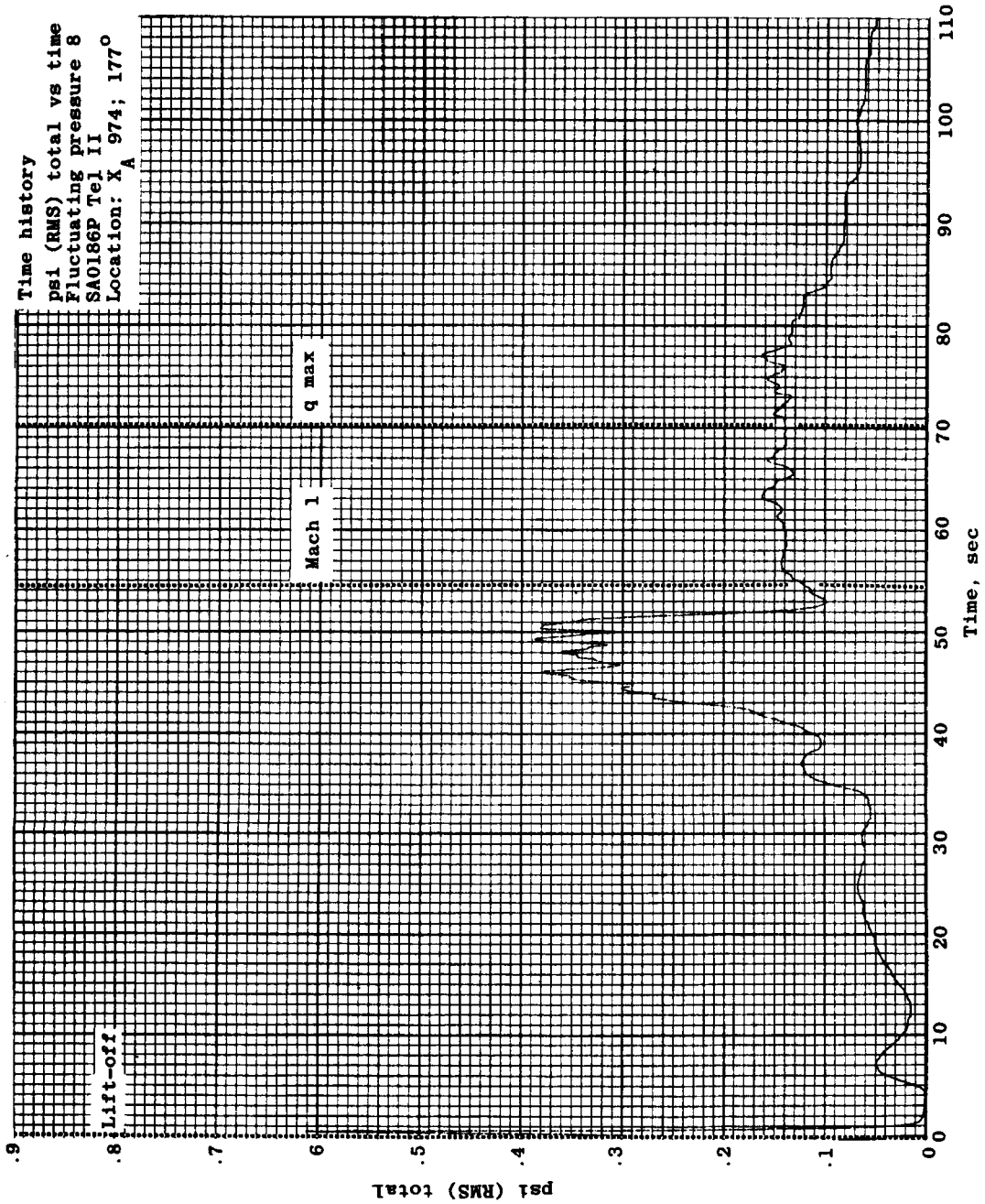
(e) Fluctuating pressure 6 (SA0184P)

Figure 4.6-22.- Continued.



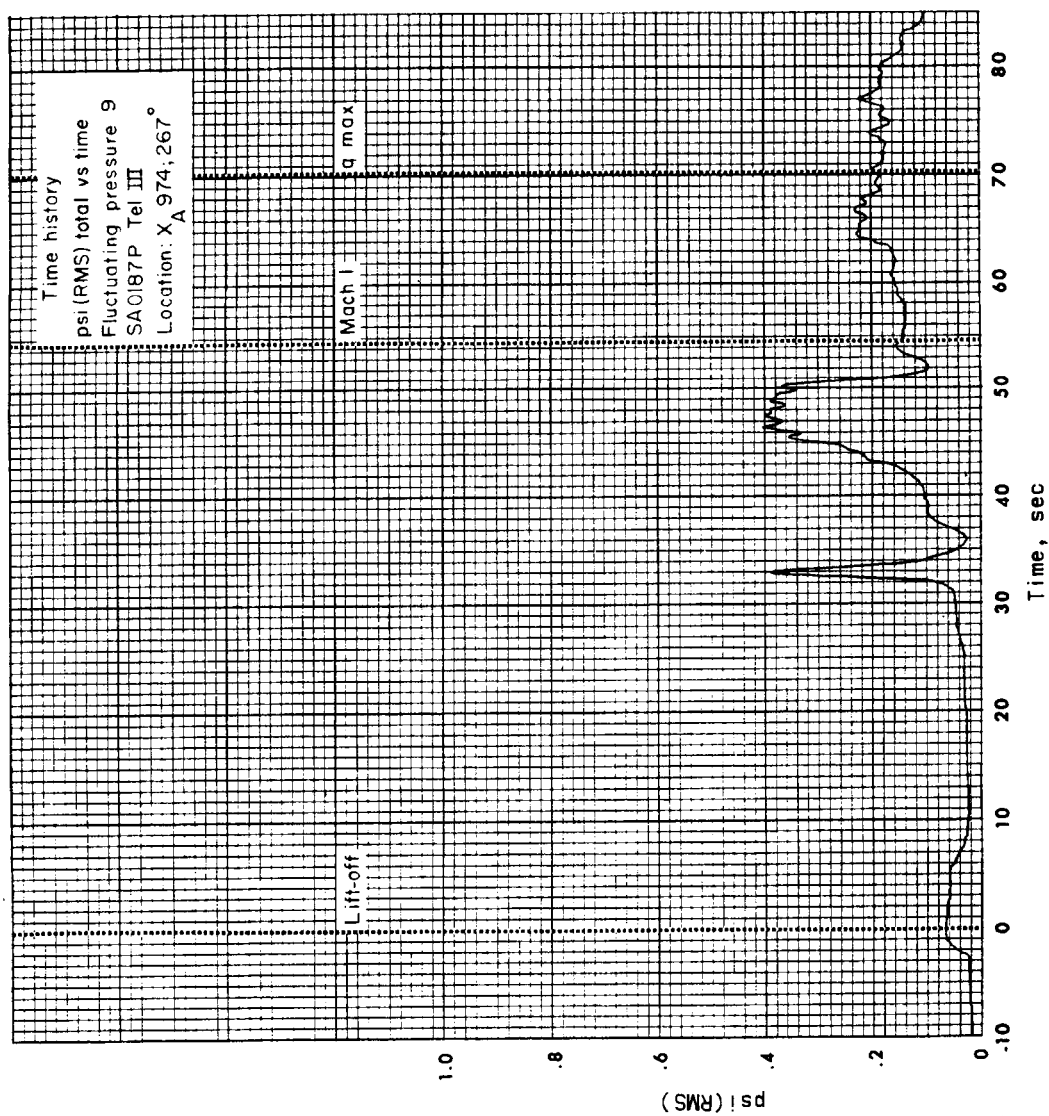
(f) Fluctuating pressure 7 (SA0185P)

Figure 4.6-22.- Continued.



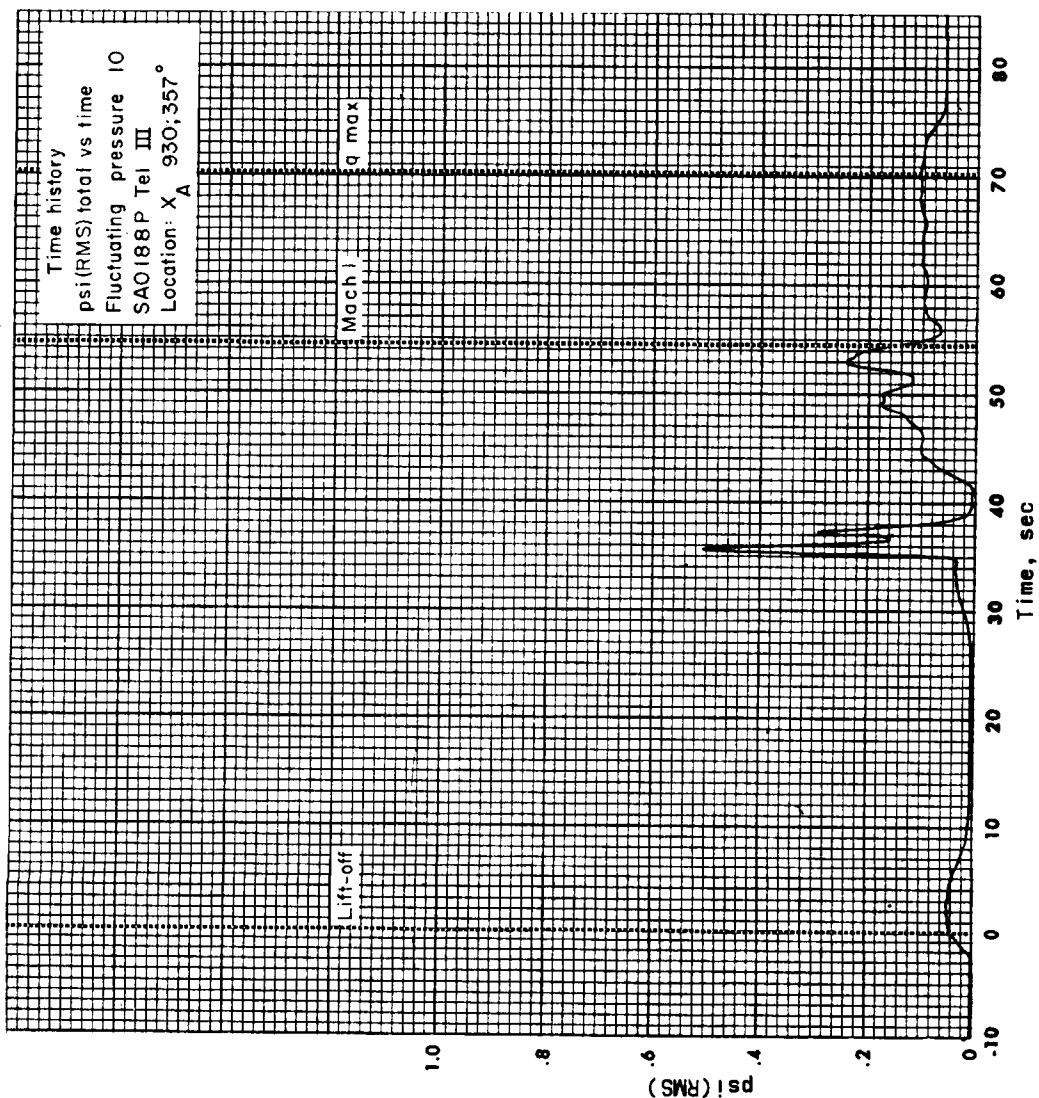
(g) Fluctuating pressure 8 (SA0186P)

Figure 4.6-22.- Continued.



(h) Fluctuating pressure 9 (SA0187P)

Figure 4.6-22.- Continued.



(1) Fluctuating pressure 10 (SAO188P)

Figure 4.6-22.- Concluded.

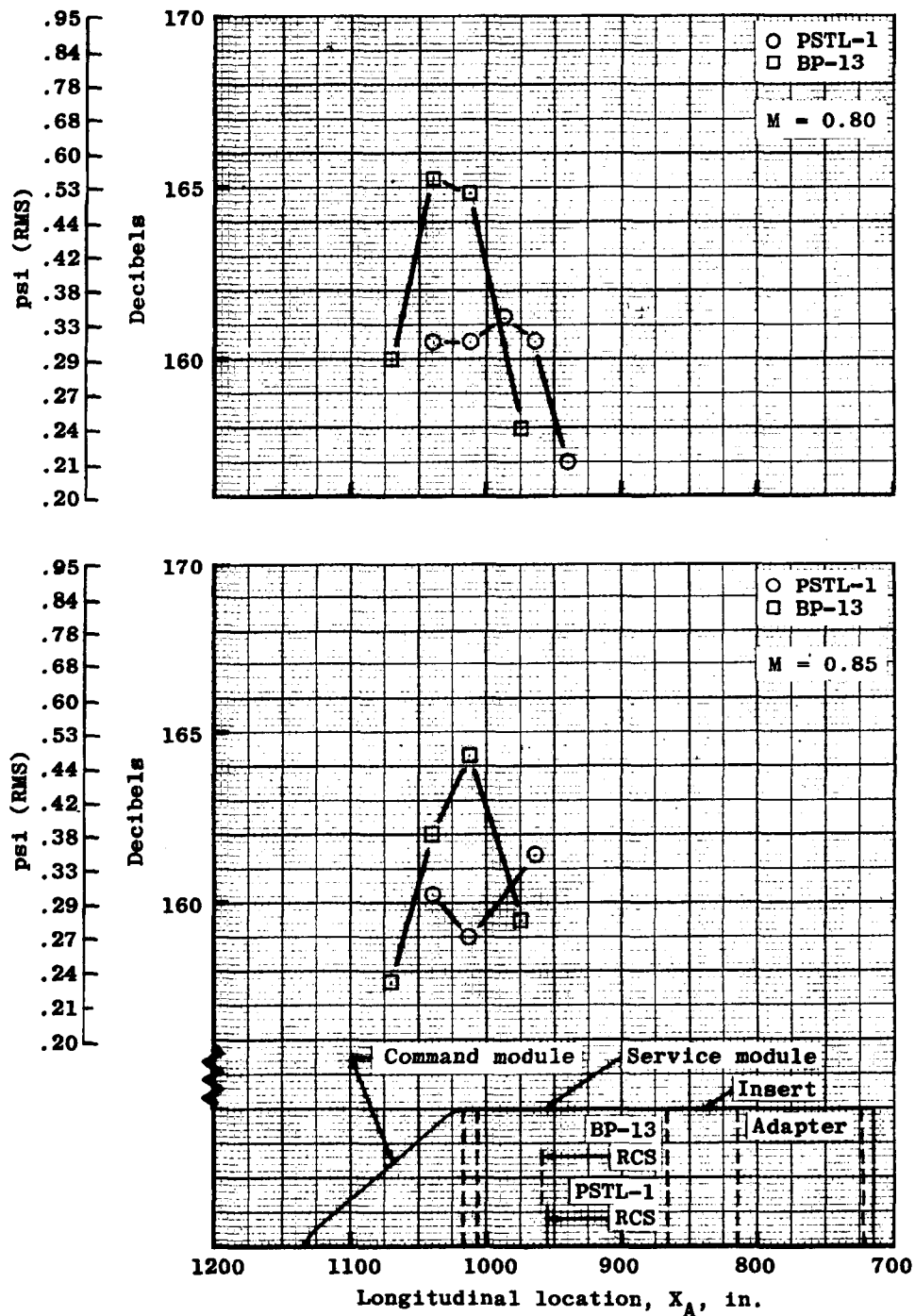
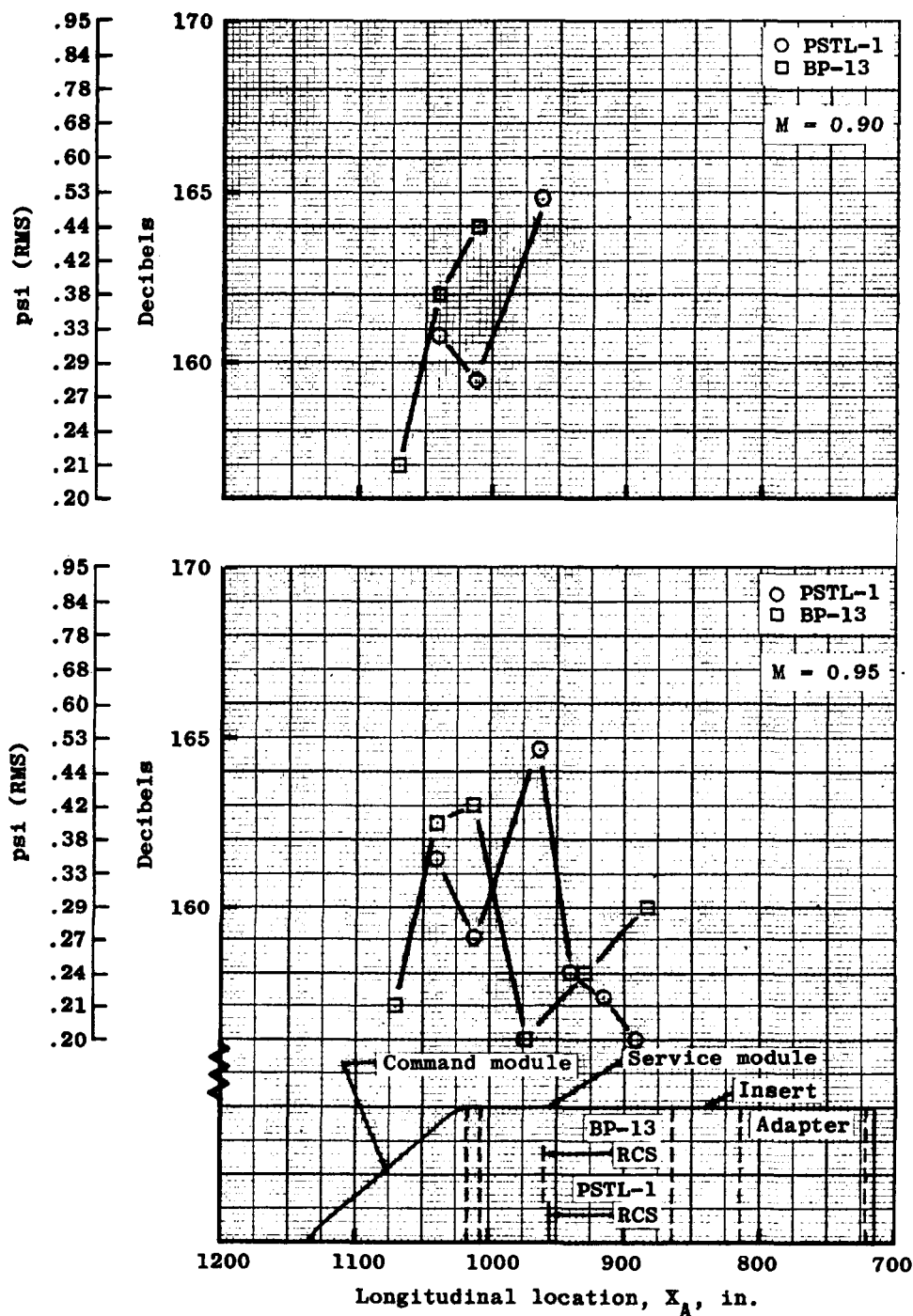
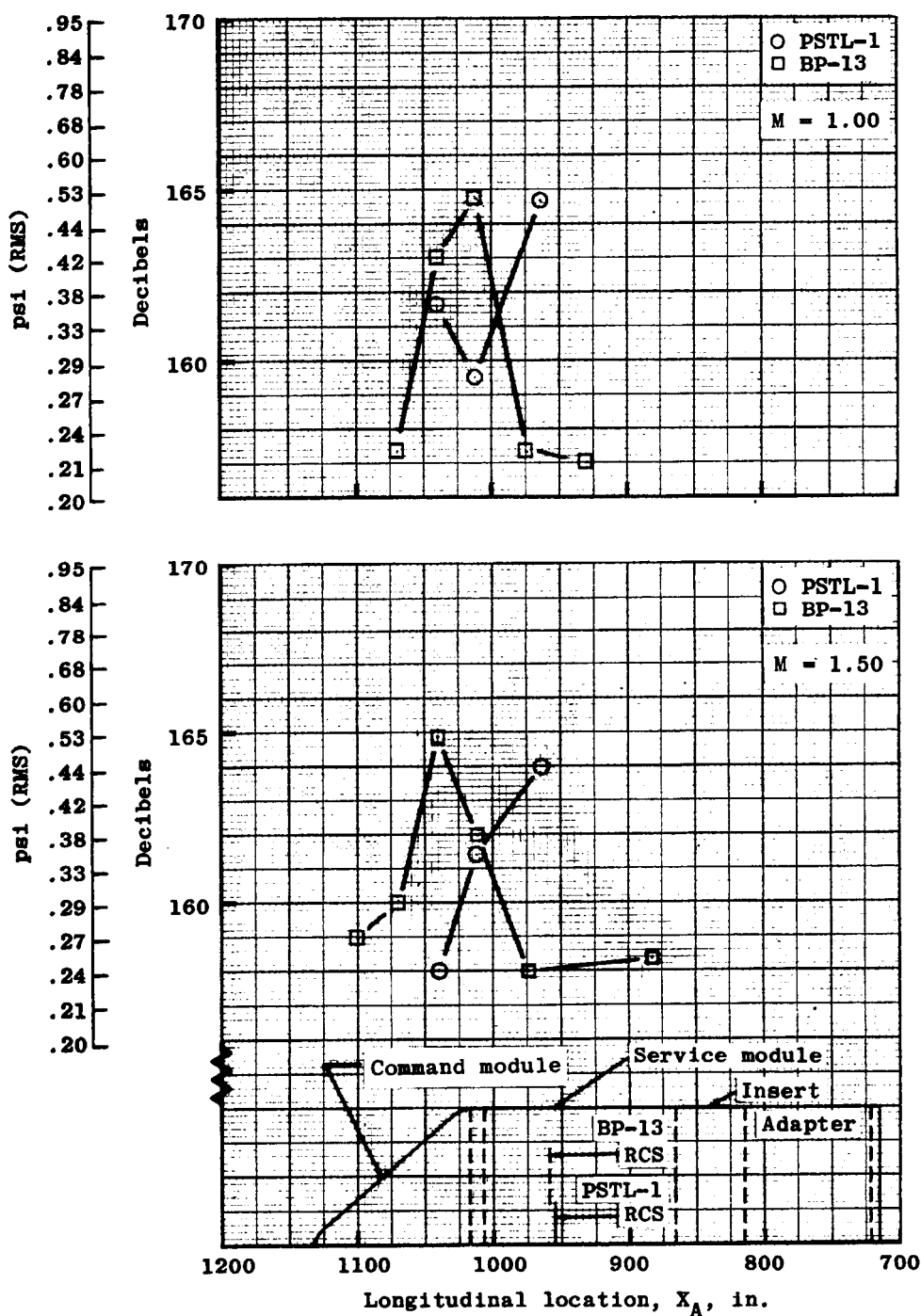
(a) $M = 0.80$ and $M = 0.85$

Figure 4.6-23.- Comparison of BP-13 spacecraft fluctuating pressures for longitudinal locations at 357° with wind tunnel data using model PSTL-1 (ref. 1).



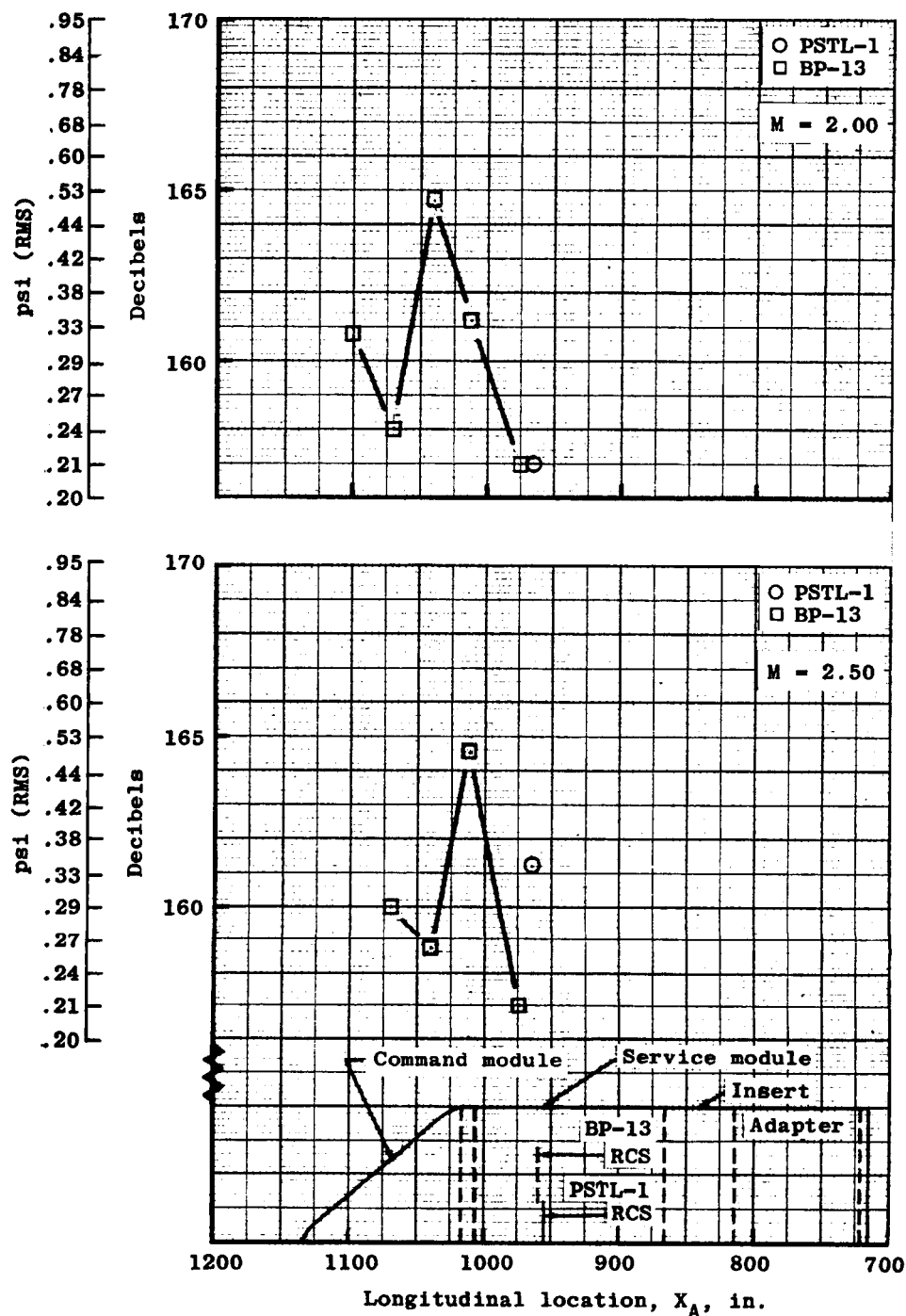
(b) $M = 0.90$ and $M = 0.95$

Figure 4.6-23.- Continued.



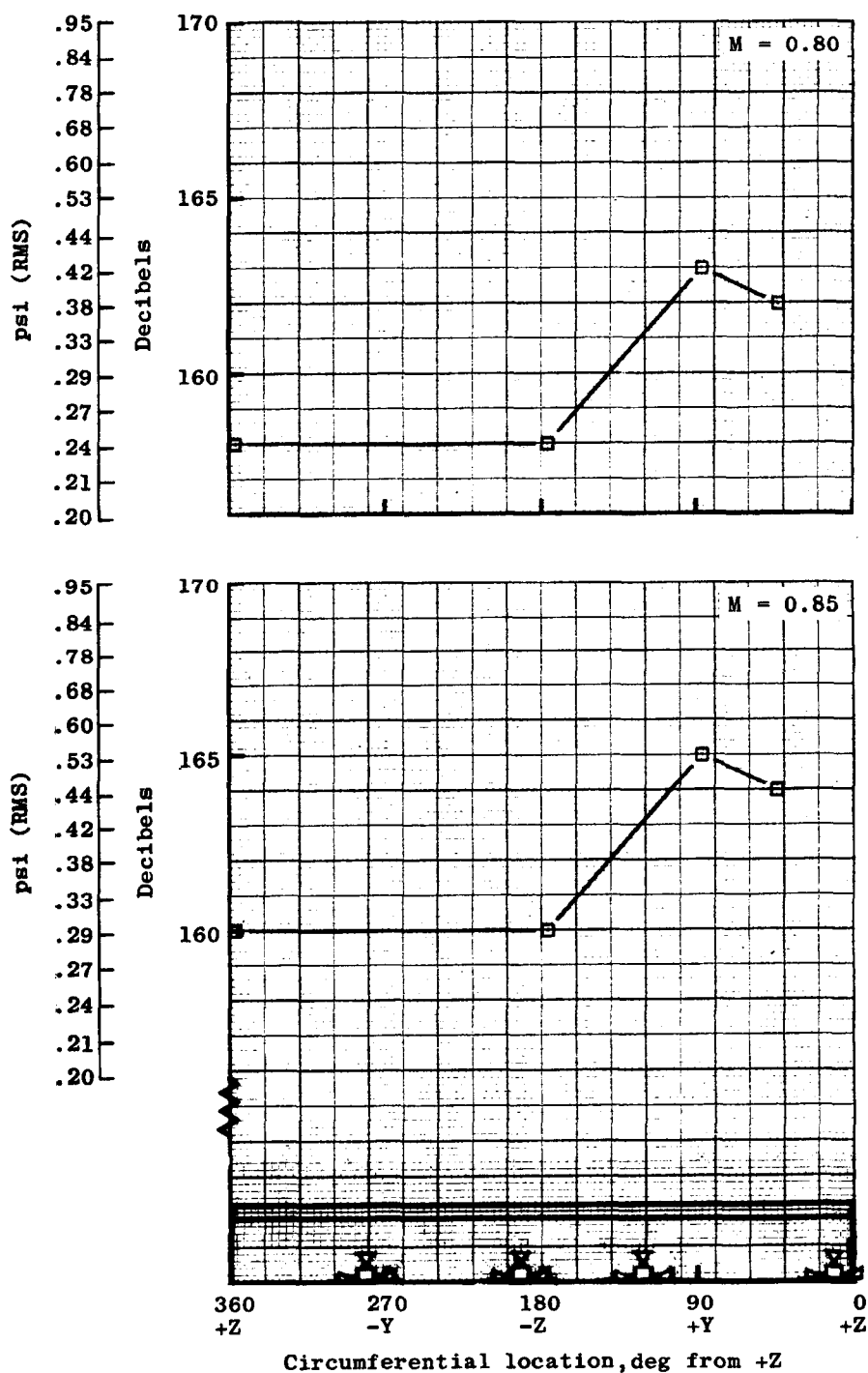
(c) $M = 1.00$ and $M = 1.50$.

Figure 4.6-23. - Continued.



(d) $M = 2.00$ and $M = 2.50$.

Figure 4.6-23.- Concluded.

(a) $M = 0.80$ and $M = 0.85$.Figure 4.6-24.- Fluctuating pressure trends for circumferential locations on BP-13 spacecraft service module at $X_A 974$.

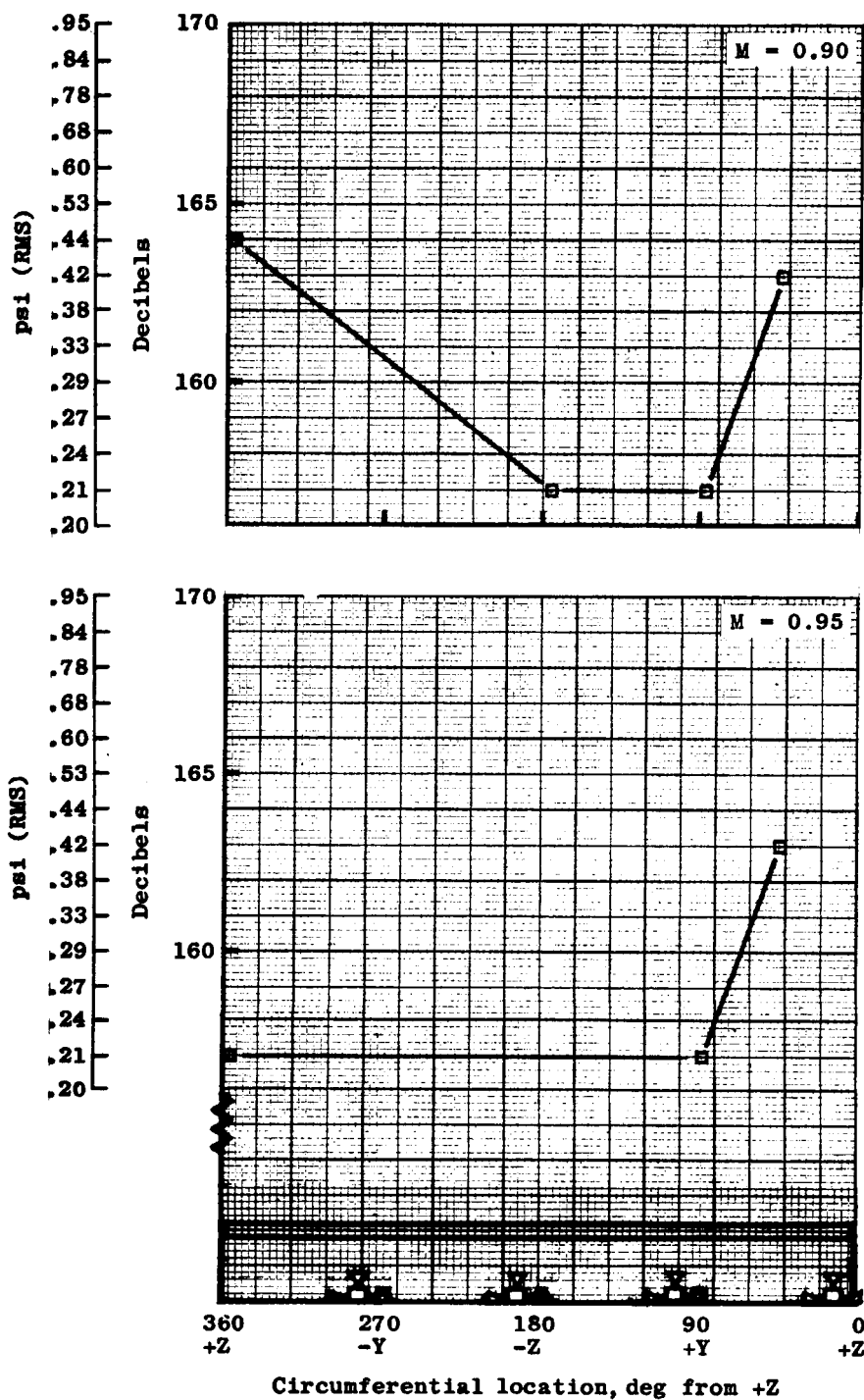
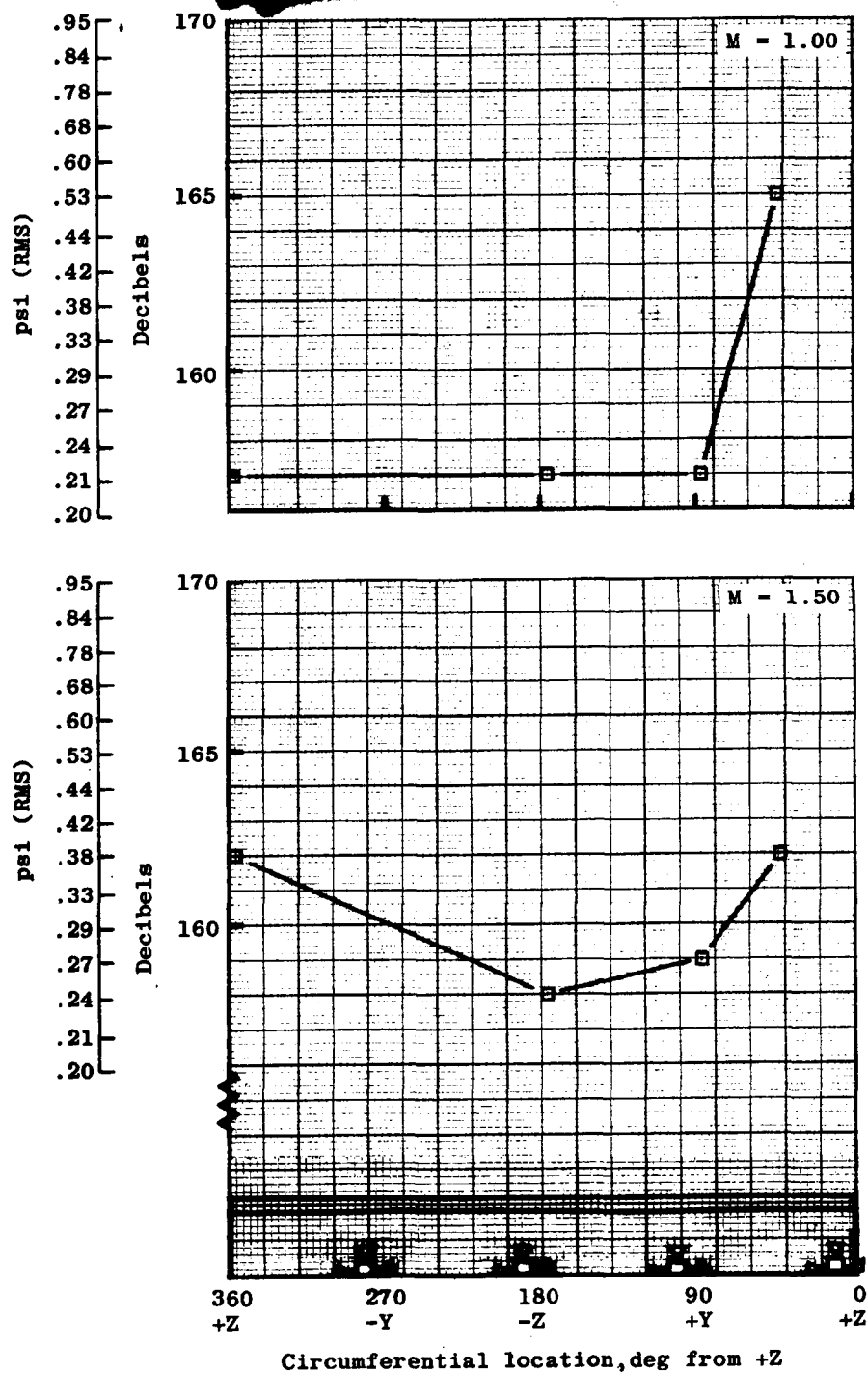
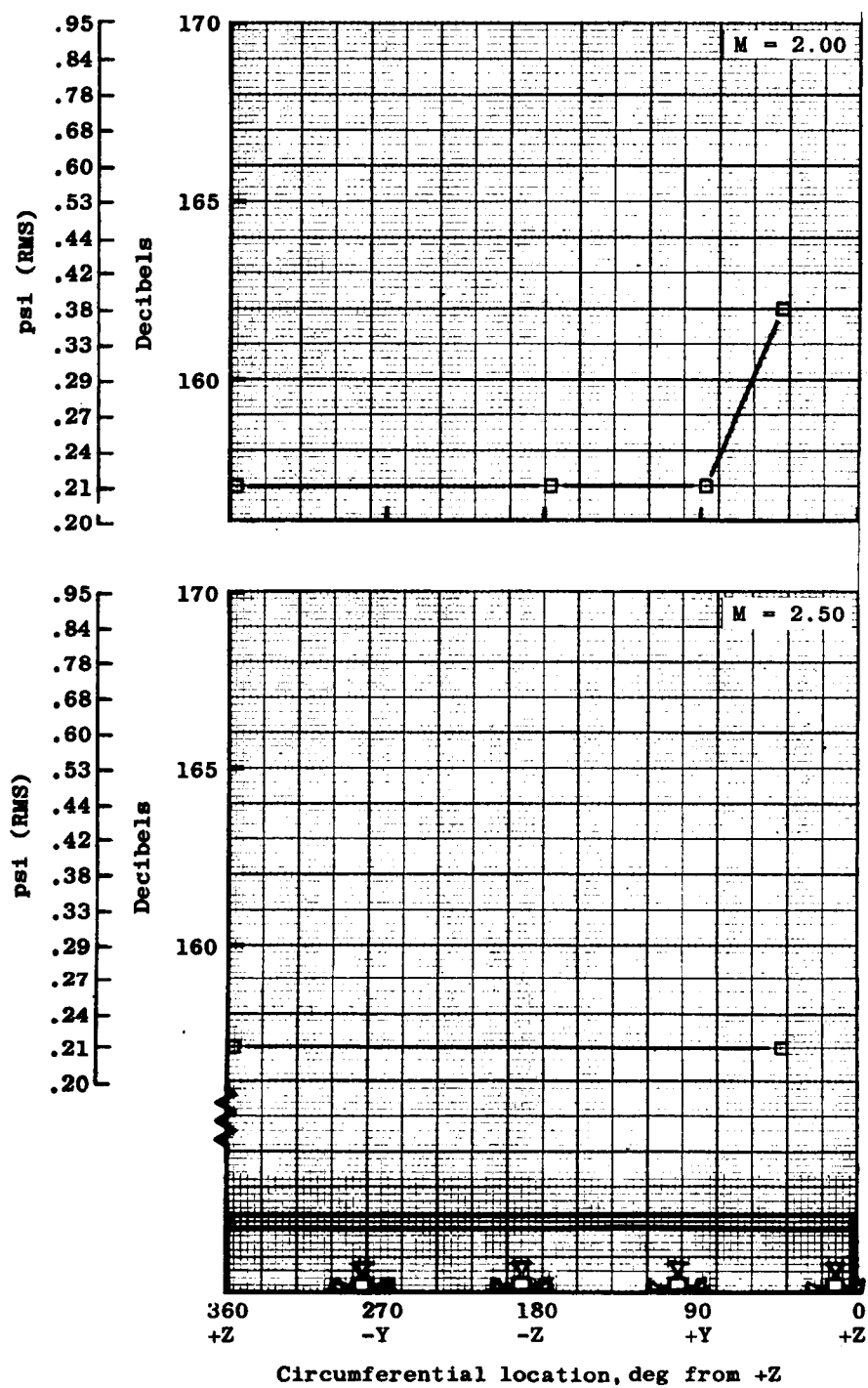
(b) $M = 0.90$ and $M = 0.95$.

Figure 1.6-24. Continued.



(c) $M = 1.00$ and $M = 1.50$.

Figure 4.6-24.- Continued.



(d) $M = 2.00$ and $M = 2.50$.

Figure 4.6-24. - Concluded.

Spectrogram
Fluctuating pressure no. 4
SA0182p
Location: X_C 12; 357°
Δ T= 45 to 50 sec
Writing speed 80 mm/sec
Paper speed 10 mm/sec
TM data received at Tel III

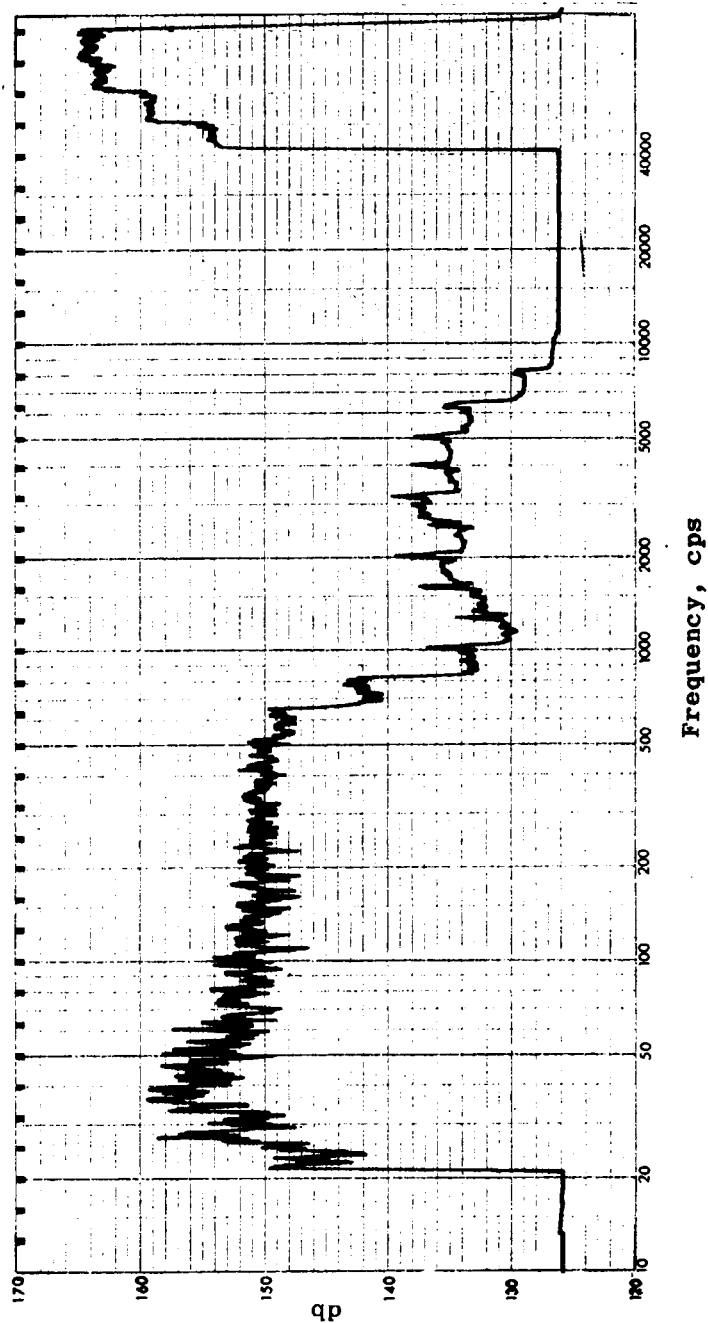


Figure 4.6-25.- Spectrogram of BP-13 spacecraft service module fluctuating pressures ($\frac{1}{3}$ octave band analysis).

4.7 Heat Protection

The heat protection on BP-13 consisted of an epoxy-impregnated cork covering the forward section of the command module and Buna-N rubber covering the truss members of the launch escape subsystem.

The forward section of the boilerplate command module was covered with varying thicknesses of cork thermal insulation required to prevent the command module aluminum skins from exceeding the design temperature of 250° F during the powered-flight phase of the mission. The thicknesses of cork on the command module are shown in figure 4.7-1. No thermal insulation was required between $X_C = 115.94$ and $X_C = 133.72$ because of the ablative qualities of the fiber-glass radome. The aft heat shield was not exposed to the launch environment and did not require heat protection.

No temperature measurements were made of the command module skin. Calorimeters were used to measure launch heating rates, and a description of the launch heating environment is covered in section 4.8, Aerothermodynamics.

The heat protection for the launch escape subsystem consisted of Buna-N rubber (60-percent silica filled) covering the truss members. Several plies of rubber were wound eccentric to the structural tube with the maximum thickness in the region of highest heating. Truss members perpendicular to the flow were protected by a maximum thickness of 0.375 inch of rubber, and the parallel and diagonal members were protected by a maximum of 0.3 inch of rubber. Figure 4.2-7 shows the launch escape tower truss members and the location of the temperature sensors.

Figure 4.7-2 shows the measured temperatures at the interface of the rubber and the metal surface (bond line) during powered flight. The figure indicates that at tower jettison the maximum bond-line temperature was 96° F on the diagonal member. Both instrumented truss members which were perpendicular to the air flow indicated a maximum temperature of 88° F. The bond-line temperatures of the members parallel to the air flow did not exceed 87° F.

Aerodynamic heating produced a maximum truss-member bond-line temperature which was less than 20 percent of the design limit (550° F). The thickness of the ablative material necessary to maintain the design limit temperature was calculated for the most severe thermal conditions that the launch escape subsystem might experience. This condition would occur if the tower were exposed not only to aerodynamic heating during the powered flight phase but also enveloped by the launch escape rocket plume with its heating and erosion during an abort. Since there was no abort during the A-101 mission, the truss members reached temperatures appreciably below the structural design limit.

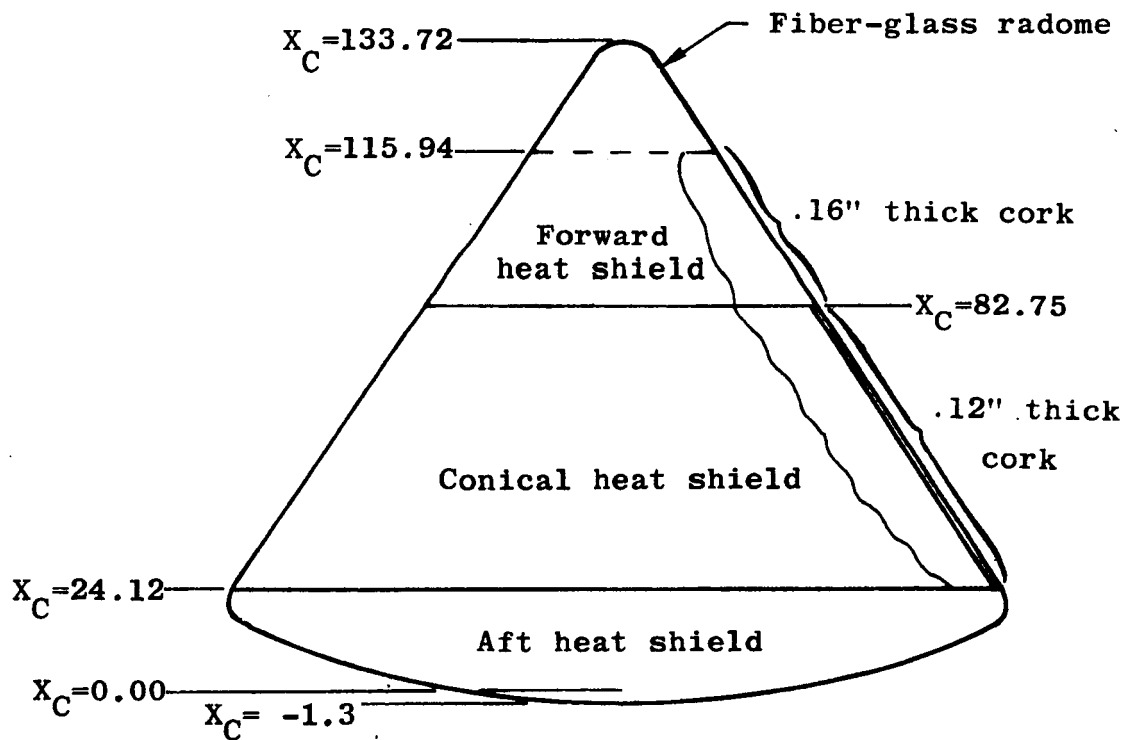


Figure 4.7-1.- Command module heat protection for BP-13 spacecraft.

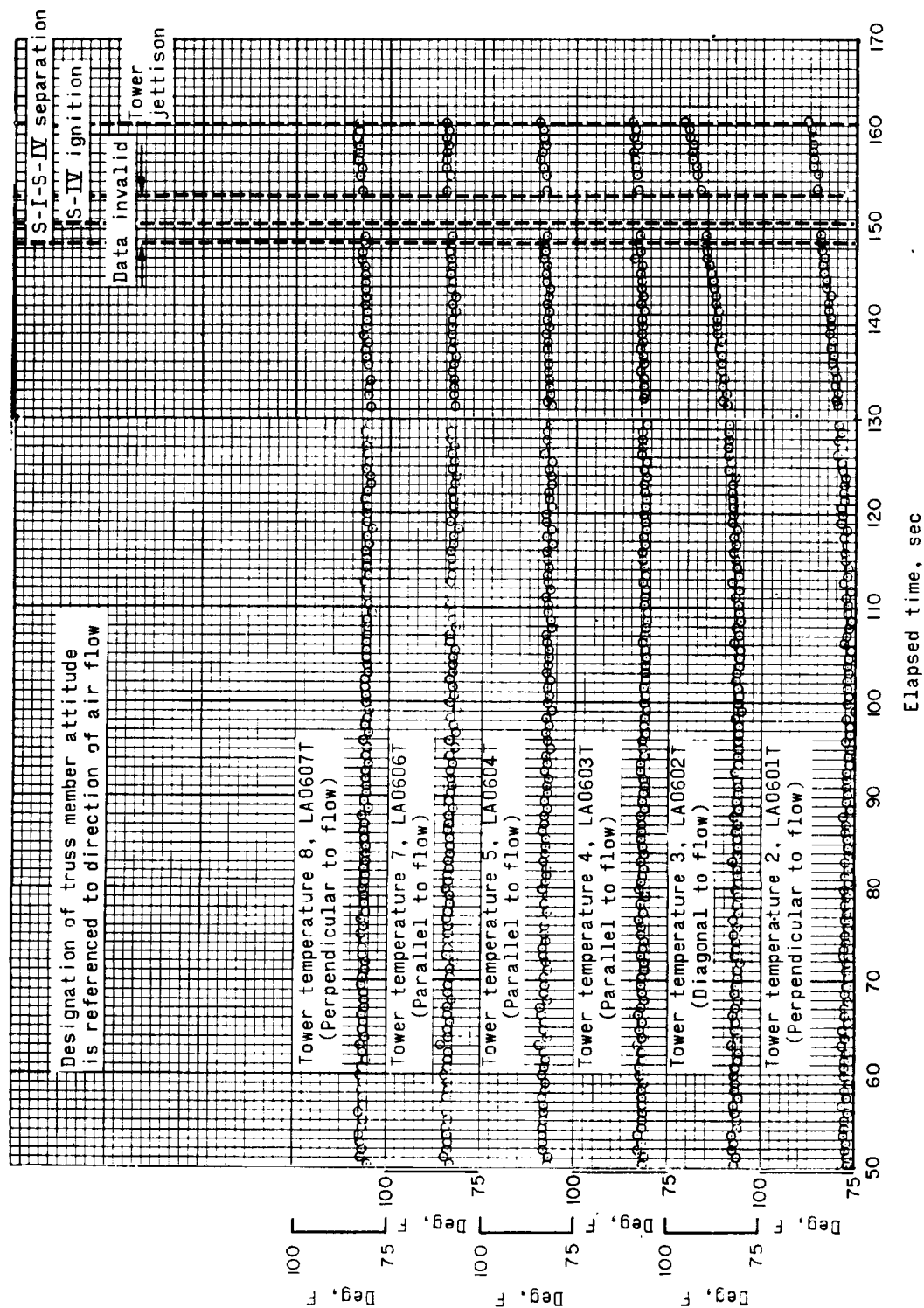


Figure 4.7-2.- Bond-line IES tower temperatures measured during flight (BP-13 spacecraft).

4.8 Aerothermodynamics

The aerothermodynamic instrumentation in the BP-13 spacecraft consisted of 20 asymptotic calorimeters, 12 of which were located on the conical surface of the command module in the various locations shown in figure 4.8-1. Eight calorimeters were located on the service module and adapter section as shown in figure 4.8-2. Each of the command module calorimeters had a range of 0 to 25 Btu/ft²/sec, while the remaining eight had a range of 0 to 5 Btu/ft²/sec. All the calorimeter units were equipped with thermocouples so that a correction for any change in calorimeter body temperature could be applied to the measured heat transfer rate.

The flight instrumentation was designed to provide information necessary to define the aerodynamic heating encountered during the launch phase of the trajectory. Instrumentation locations adjacent to and downstream of the various surface irregularities were chosen to establish the effect of the irregularities upon the local heat transfer rates. Measurements were made at these locations to correlate actual flight data with heating rate predictions based on data gathered in various wind-tunnel tests. For the smooth body without protuberances, a maximum heating rate of 6.2 Btu/ft²/sec was predicted for the command module and 0.60 Btu/ft²/sec was predicted for the service module. The heating rates measured during flight were in reasonable agreement with these predictions.

At the time of launch, 19 of the calorimeters appeared to be functioning normally. The output of calorimeter 17, located at X_S338 (just aft of the CM-SM interface), was oscillating at this time, and no data were obtained at this location. A preliminary study of the telemetry data revealed that calorimeters 13 and 20, both located at X_S305 (under and to the right, respectively, of the reaction control system (RCS) nozzle), failed to respond to the main heat pulse at approximately T + 60 seconds.

The BP-13 actual flight trajectory environment is shown in figure 4.8-3. The Reynolds number, based on maximum body diameter, ranged from greater than 10⁷ down to 5 × 10⁴ at staging. Hence, turbulent flow was expected throughout that portion of the trajectory during which heating occurred. A Mach number of 9.0 was reached at the time of staging. The peak heating rates were generally attained at a Mach number of 3.5 and a Reynolds number of 7 × 10⁶.

[REDACTED]

An estimate of the heat transfer rates over the command module were obtained from wind-tunnel data by plotting measurements made at a particular Mach number and body location against Reynolds number, so that the results could be extrapolated to the Reynolds number encountered at that Mach number during flight. Wind-tunnel tests of the Apollo launch configuration have been conducted for a range of Mach numbers from 2.0 to 10 and a range of Reynolds numbers (based on the maximum diameter) for the command module from 0.06×10^6 to 3.40×10^6 . Models with and without the tower and models with simulated RCS packages, scimitar antenna, umbilical fairings, and air vents have been tested to determine the effect upon the flow of adding these to the basic configuration.

The heating-rate time histories, as recorded by the calorimeters located on the command module, are shown in figures 4.8-4. Surface irregularities on the body had a large effect on the heating rates. The data from calorimeters 1, 5, and 6 show a smooth variation with time as indicated in figures 4.8-4(a) and 4.8-4(b). These measurements were obtained in areas in which the local flow was not disturbed by surface irregularities, that is, "clean" areas. This smooth variation with time was not present in the heating rates recorded at locations on the hatch or downstream of the tower leg wells, as may be seen in figures 4.8-4(b) and 4.8-4(c). It should be noted that in most instances, the duration of the heating was approximately 80 seconds ($T + 60$ to $T + 140$), although the total heat load varied widely at various locations.

Heating-rate time histories are shown in figure 4.8-5 for the three calorimeters located at X_{C74} to compare the circumferential variation of the data. The curves were obtained by fairing lines through the data in a manner intended to best represent the entire range of measurements. It is noted that the three curves are similar until $T + 90$ seconds, at which time the calorimeter located on the hatch cover ($\phi = 180^\circ$) shows a rapidly decreasing heating rate, and then a second peak 20 seconds later. The calorimeter located downstream of the tower leg well ($\phi = 319^\circ$) indicated similar heating rates, except that a second peak was not experienced at this location. Data from calorimeter 1 obtained in the "clean" area ($\phi = 3^\circ$) compared favorably with the predicted heat-transfer rates. The angle of attack during the time of heating was less than 1° , which should cause only a very small asymmetry of the flow.

Heating-rate histories are shown in figure 4.8-6 for six calorimeters located at X_{C52} to compare again the circumferential variation of heating rates and to determine the effect of surface irregularities ahead of the calorimeter location. The heating rates were also similar

[REDACTED]

[REDACTED]

during the initial phase of heating until $T + 90$ seconds, at which time they begin to differ. Calorimeter 8, located on the target side of the strake stub (see fig. 4.8-1), indicates a relatively low peak heating rate. Calorimeters 6 and 7, located on the other side of the strake stub, were not influenced in the same manner, in that the peak heating rates are higher than those at calorimeter 8. Calorimeter 4, located on the hatch cover ($\phi = 180^\circ$), showed quite a different pattern in that a definite second peak was experienced. The effect of the tower leg well at calorimeter 9 ($\phi = 319^\circ$) was apparent in both the peak heating rate and the total heating, and again a second peak was experienced. The measurement obtained in the area that was free from the influence or irregularities (calorimeter 5 at $\phi = 3^\circ$) followed the trend predicted by wind-tunnel tests.

Further aft on the command module, at X_{c27} , the effect of surface irregularities was less pronounced (fig. 4.8-7). Calorimeter 11, located below the hatch ($\phi = 180^\circ$), and calorimeter 12, below the tower leg well ($\phi = 319^\circ$) indicated heating rates which varied smoothly with time and which were in reasonable agreement with wind-tunnel measurements.

Some of these same curves are plotted in a different manner in order to compare the variation of heating rates at several locations downstream of surface irregularities. The heating rates recorded by calorimeters 2 and 4, located on the command module hatch, are shown in figure 4.8-8. It should be noted that the pattern in heating rate variation was similar at both locations. The effect of moving further downstream from the leading edge of the hatch cover is apparent in the curve for calorimeter 11, which showed no second peak.

The heating rates at several locations downstream from the tower leg wells ($\phi = 319^\circ$) are shown in figure 4.8-9. The effect of the wells is seen to be dependent upon the downstream distance. The occurrences after $T + 95$ seconds are not readily explainable from the amount of data available.

The heat transfer rates measured just ahead of the dummy scimitar antenna are compared to other measurements made at the same radial location in figure 4.8-10. A higher heating rate was expected at this longitudinal location on the command module. The additional heating rate due to flow characteristics ahead of the protuberance was indicated by the second peak.

Heating-rate time histories for the calorimeters located on the service module are shown in figure 4.8-11. As mentioned previously, three units failed to operate properly, leaving five good measurements: four aft of the RCS package and one ahead. The failure of calorimeter 13,

[REDACTED]

[REDACTED]

located under the RCS nozzle, is believed to be particularly unfortunate in that wind-tunnel tests have indicated maximum interference heating factors (ratio of heating with and without protuberance, respectively) in this vicinity. The loss of calorimeter 20 resulted in a lack of data at a point where the interference heating was due to the umbilical fairing as well as the RCS package. The heating at this location, based on wind-tunnel results, was expected to be generally about 1.2 times the value which would have been measured had there been no protuberance on the body. The failure of calorimeter 17 resulted in the loss of heating rate data for the SM fairing area between the umbilical and the air duct.

The heating rates measured in the vicinity of the RCS package were in agreement with wind-tunnel test data. As shown in figure 4.8-2, four calorimeters (which functioned) were in the vicinity of the RCS package. Calorimeter 16, at X_{S267} and $\phi = 145^\circ$, was unaffected by protuberances, therefore the heating rates measured at this location can be regarded as the clean body value. The increase in heating, above the clean body value, measured at calorimeter 14 ($\phi = 160^\circ$) was due primarily to the presence of the umbilical fairing in the flow. The peak value indicates an interference heating factor of about 1.3 at this location.

The heating rates measured immediately aft of the RCS package at calorimeter 15, $\phi = 183^\circ$, are also shown in figure 4.8-11. Wind tunnel tests have indicated that the interference heating factor at this location due only to RCS package is increased by 20 percent with the addition of the air duct, scimitar, and umbilical fairing to the configuration. The maximum heating rate measured during flight at this location was about 1.25 times the clean body value. The single heating-rate time history obtained ahead of the RCS package in the vicinity of a nozzle is shown in figure 4.8-11. The interference heating factor in this area due to the RCS package alone is 1.5, which is increased by 30 percent with the addition of the protuberances on the command module. The peak heating measured at this location during flight was $1.1 \text{ Btu/ft}^2/\text{sec}$, which represents an interference heating factor of nearly 2.0. This measurement was the highest heating rate measured on the service module, but, as mentioned earlier, higher values were expected at calorimeter 13, which failed to operate.

Heating rates of 3 to 3.5 times the clean body value have been observed in wind-tunnel tests at locations on the service module which were under and adjacent to the RCS nozzles.

Aft of the service module, on the adapter section, a peak heating rate of $0.6 \text{ Btu/ft}^2/\text{sec}$ was measured, as shown in figure 4.8-12.

[REDACTED]

[REDACTED]

This measurement was expected to be only slightly different from the clean body heating rate because it was relatively far behind the RCS package, whose effect on the local flow was greatly reduced at this distance.

In summary, local heating rates of 7 Btu/ft²/sec were measured on the conical portion of the command module during launch. These heating rates, in both peak and duration, were greatly influenced by surface irregularities. Heating rates on the service module were observed to be 0.6 Btu/ft²/sec in the absence of protuberances. The presence of the RCS package increased the heating rate at a particular location by a factor of 1.3. However, interference heating factors of 3.0 to 3.5 were predicted from wind-tunnel tests for some areas. Unfortunately, no data were obtained from the calorimeter located in these areas. The heating-rate predictions based on wind-tunnel data were in reasonable agreement with the flight measurements.

[REDACTED]

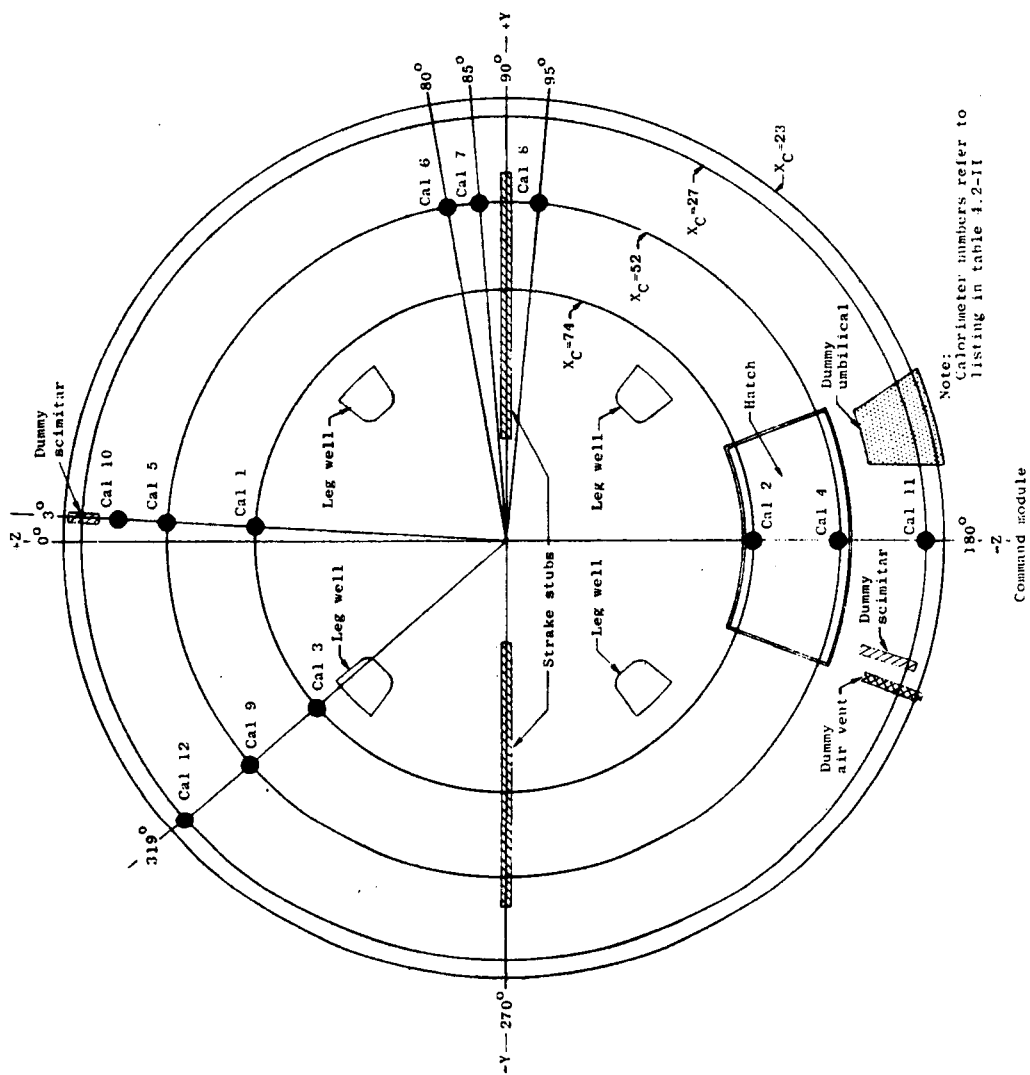


Figure 4.8-1.- Top view of BP-13 spacecraft command module showing calorimeter locations.

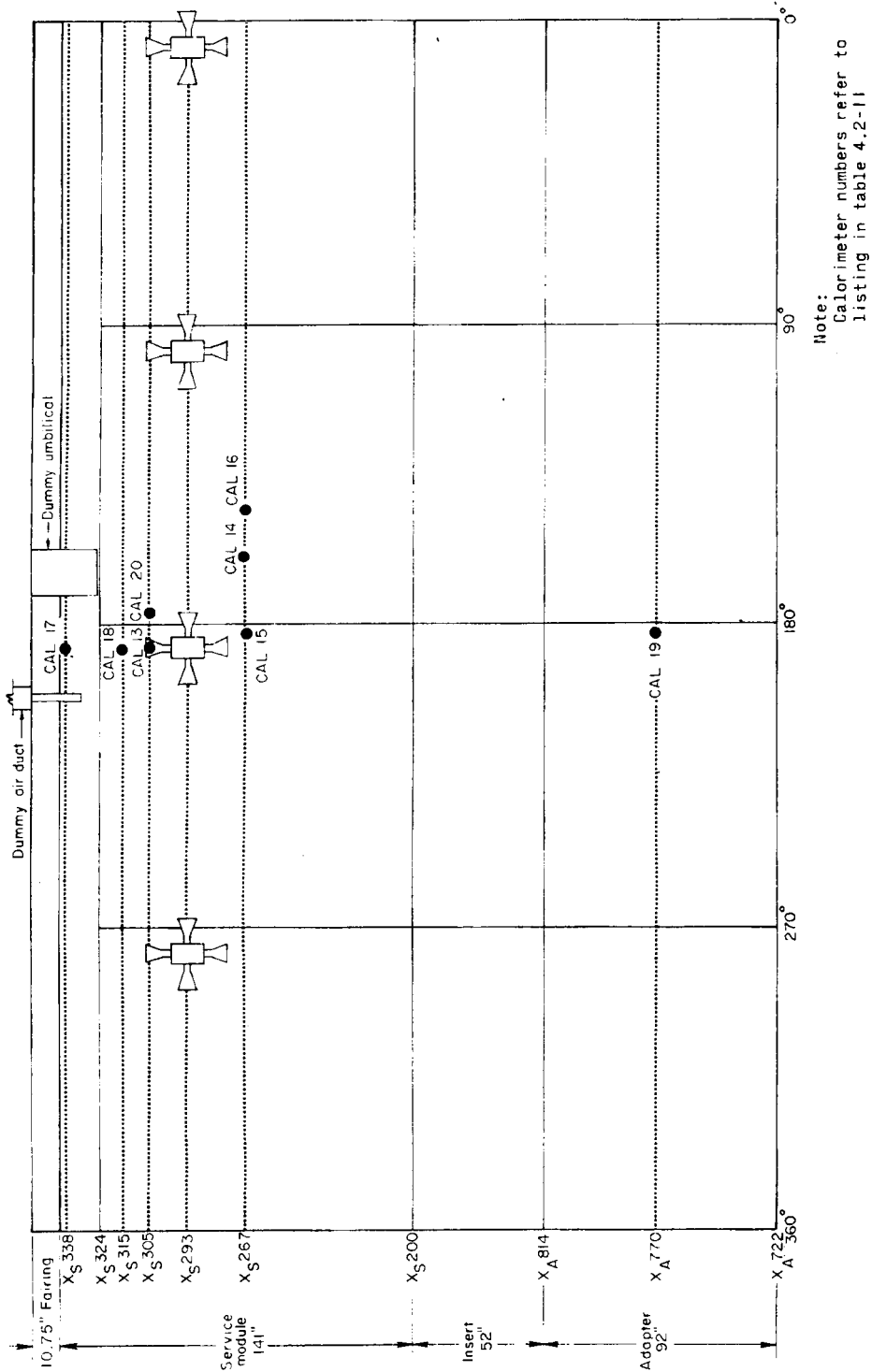


Figure 4.8-2.- Development view of BP-13 spacecraft service module, insert, and adapter compartment showing calorimeter locations.

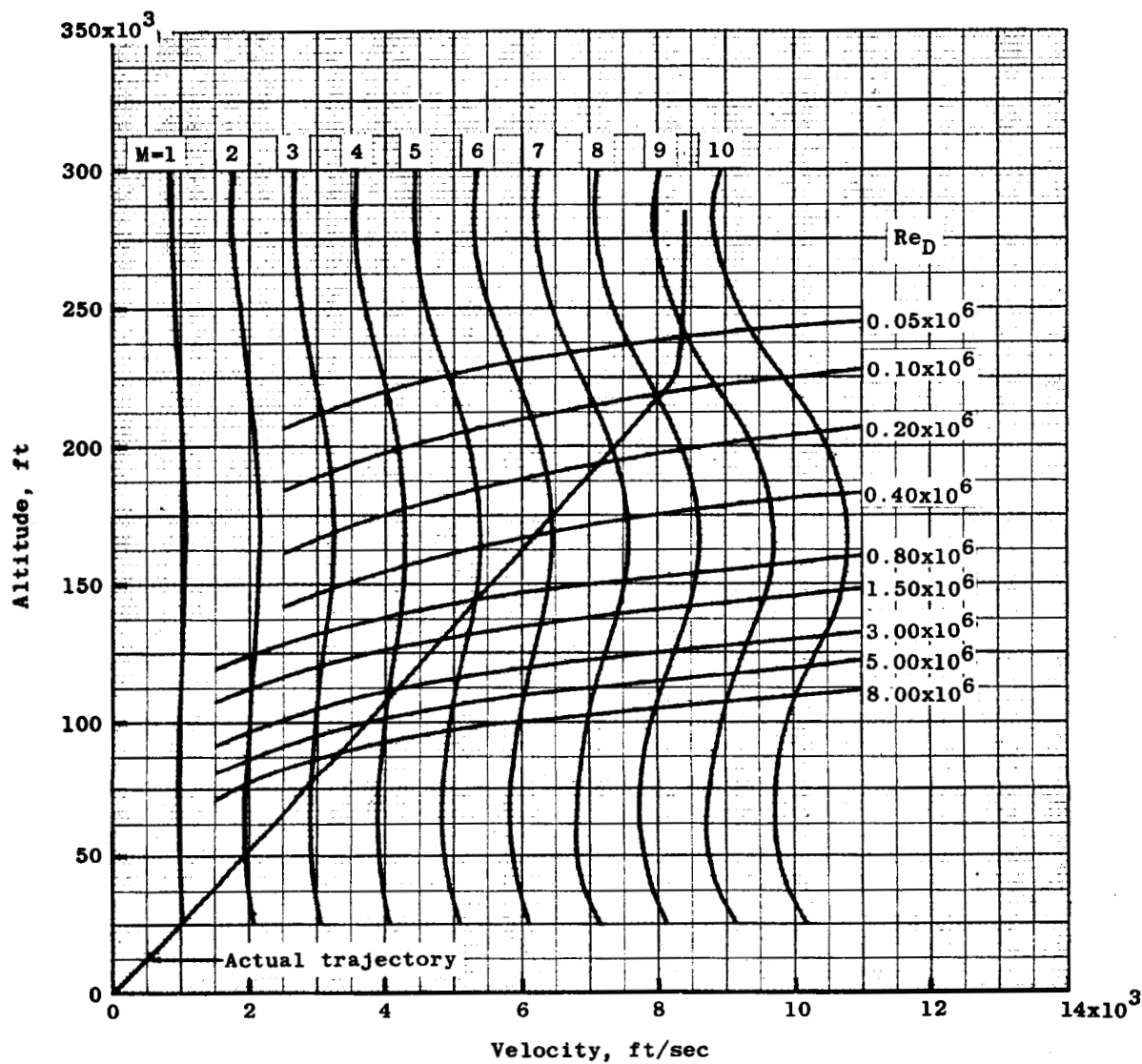
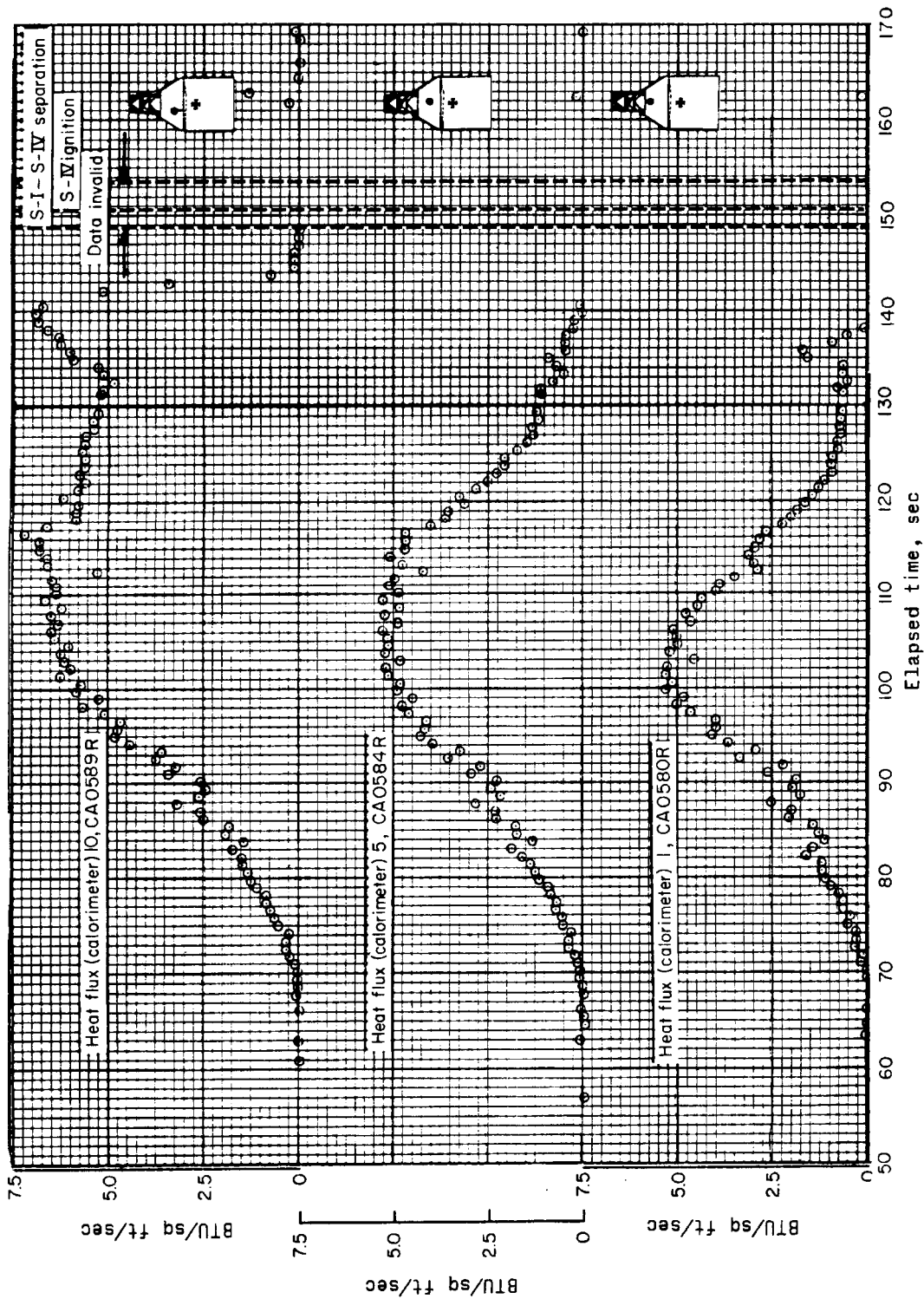
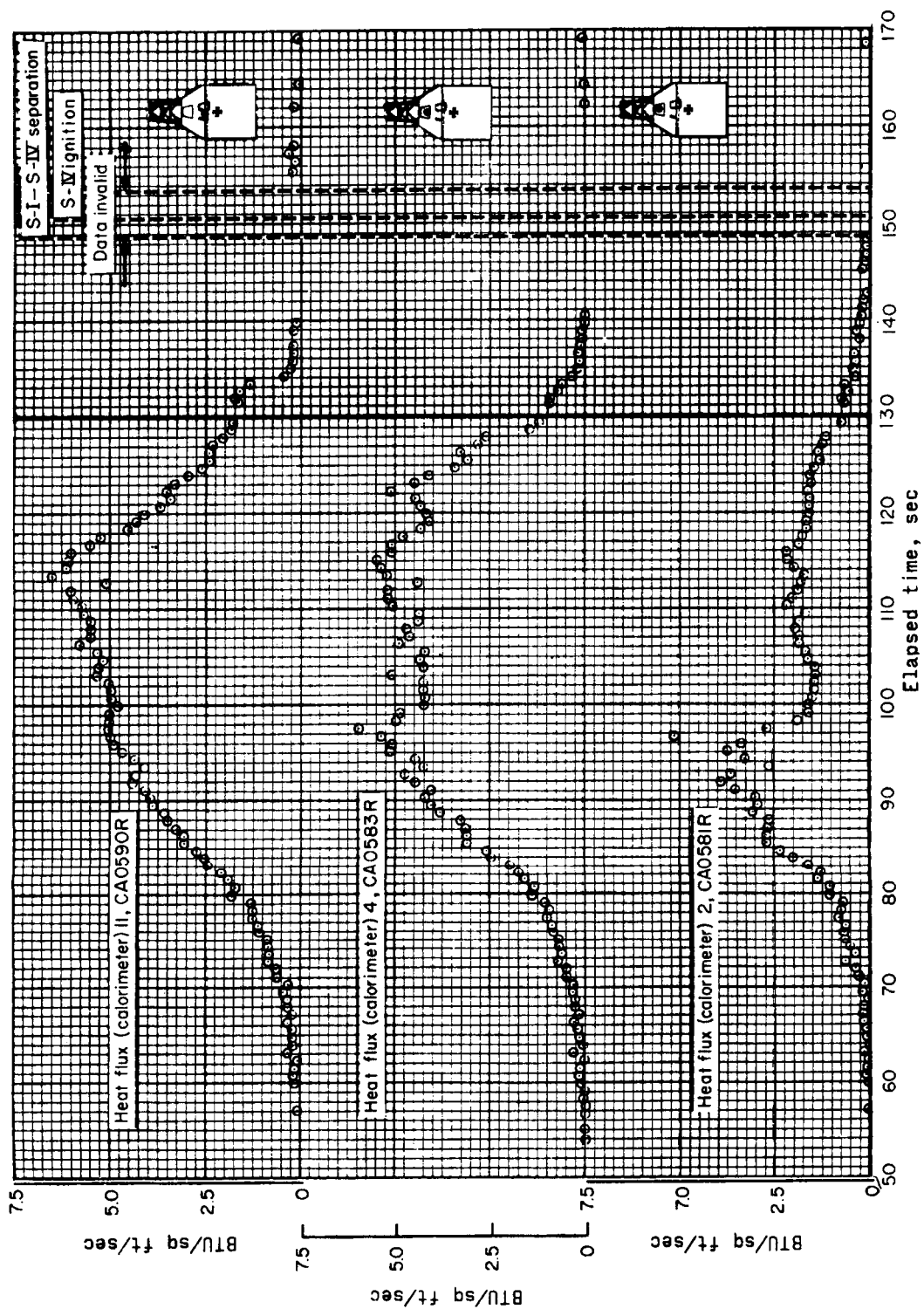


Figure 4.8-3.- Launch configuration environment in terms of Mach number (M) and Reynolds number (Re_D) for BP-13 spacecraft.



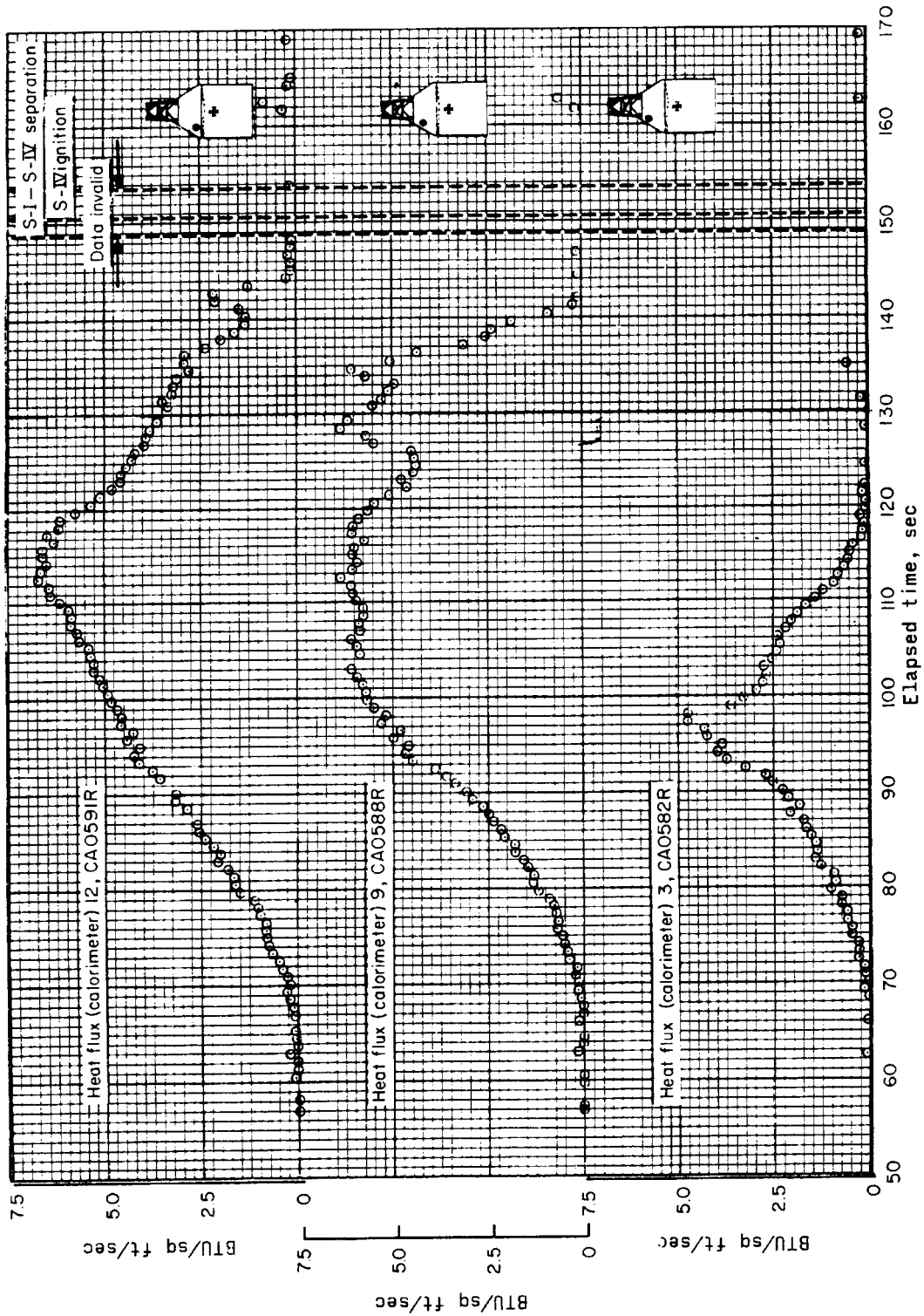
(a) Calorimeters 1, 5, and 10.

Figure 4.8-4.- Heating rates measured on BP-13 spacecraft command module during flight.



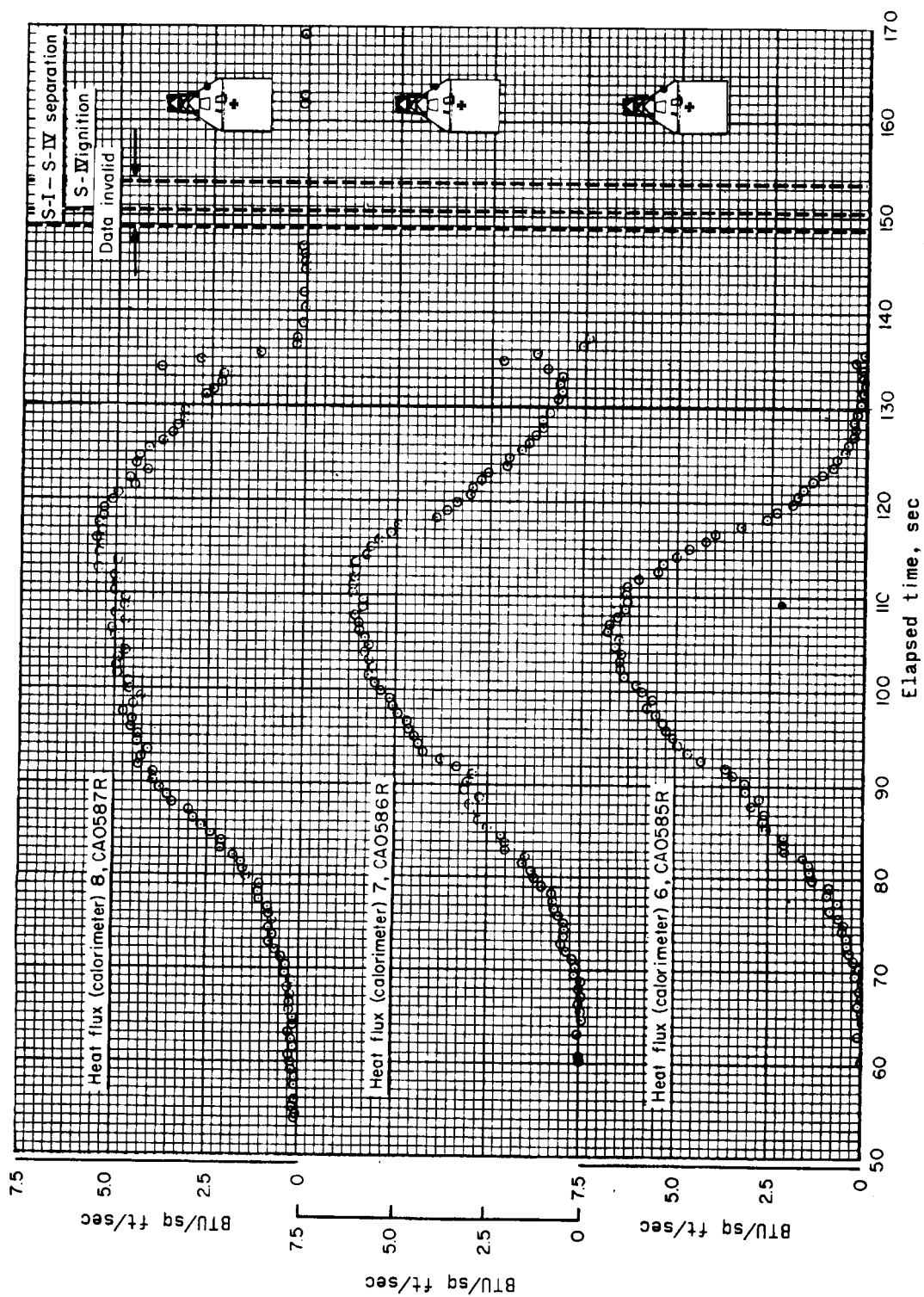
(b) Calorimeters 2, 4, and 11.

Figure 4.8-4.- Continued.



(c) Calorimeters 3, 9, and 12.

Figure 4.8-4.- Continued



(d) Calorimeters 6, 7, and 8.

Figure 4.8.4. - Concluded

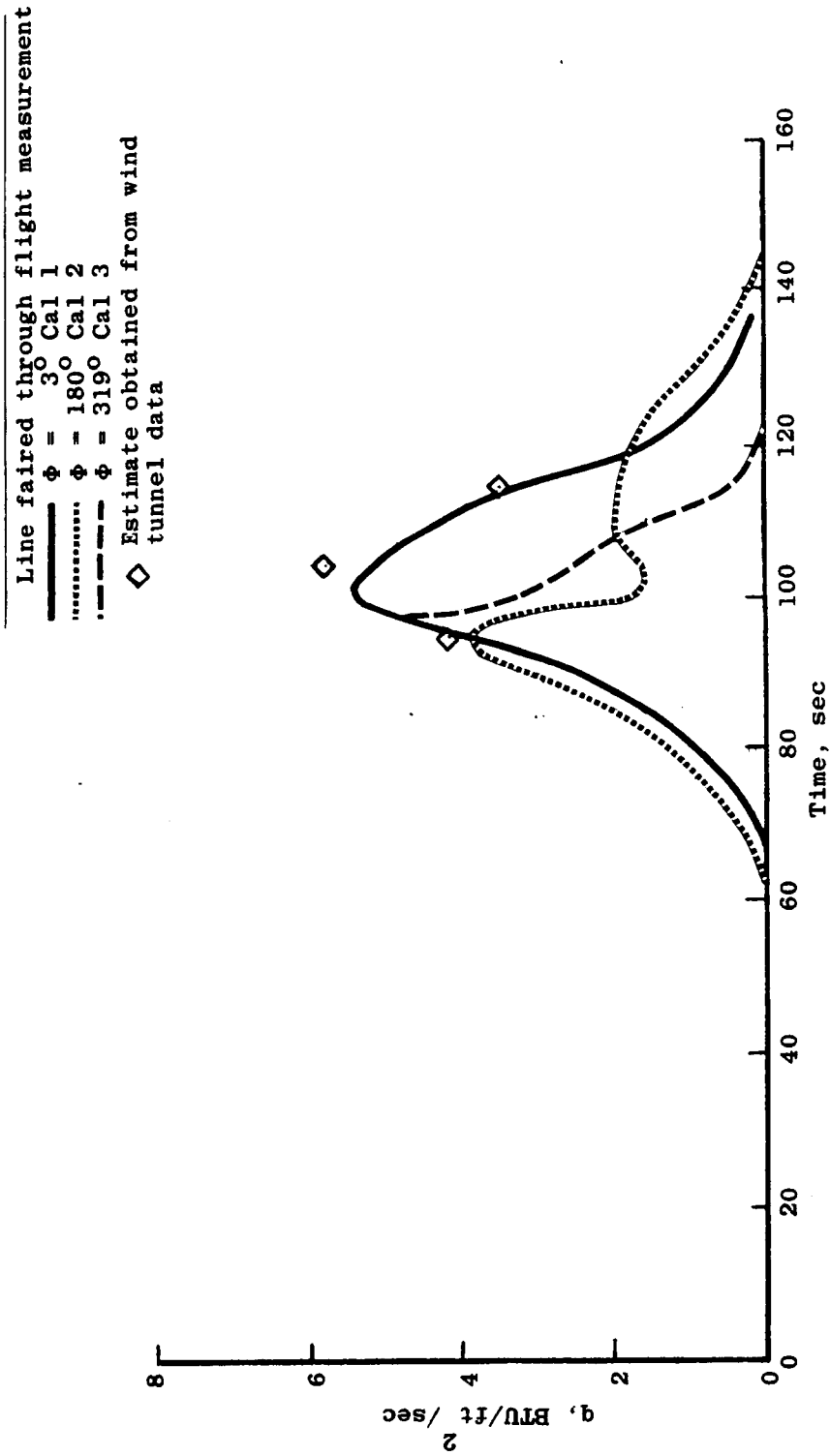


Figure 4.8-5.- Comparison of heating rate histories at $X_C = 74$ for three circumferential locations on BP-13 spacecraft.

Line faired through flight measurements

— $\theta = 95^\circ$ Cal 8

..... $\theta = 319^\circ$ Cal 9

- - - $\theta = 85^\circ$ Cal 7

- - - $\theta = 3^\circ$ Cal 5

- - - $\theta = 180^\circ$ Cal 4

- - - $\theta = 80^\circ$ Cal 6

◇ Estimate obtained from wind tunnel data

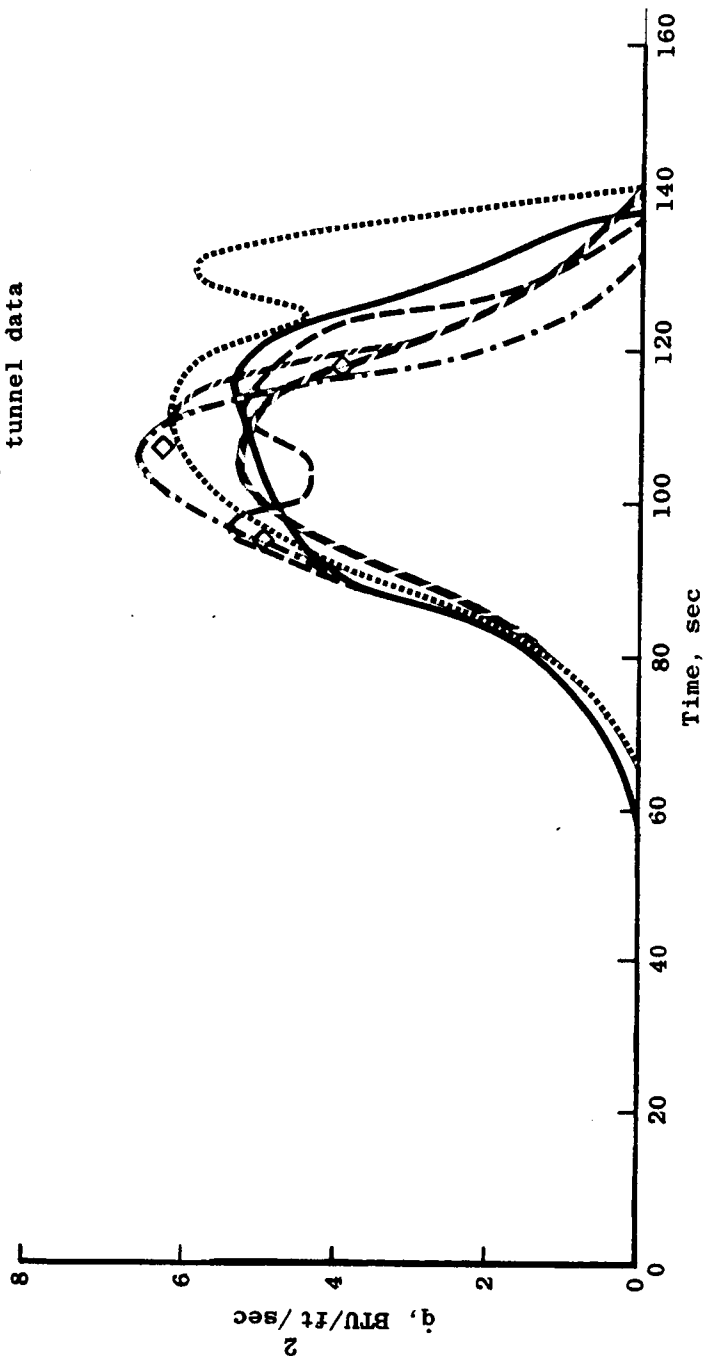


Figure 4.8-6.- Comparison of heating rate histories at $X_C = 52$ for six circumferential locations on BP-13 spacecraft.

Faired through flight measurements
 — $\phi = 319^\circ$ Cal 12
 $\phi = 180^\circ$ Cal 11
 \diamond Estimate obtained from wind
 tunnel data

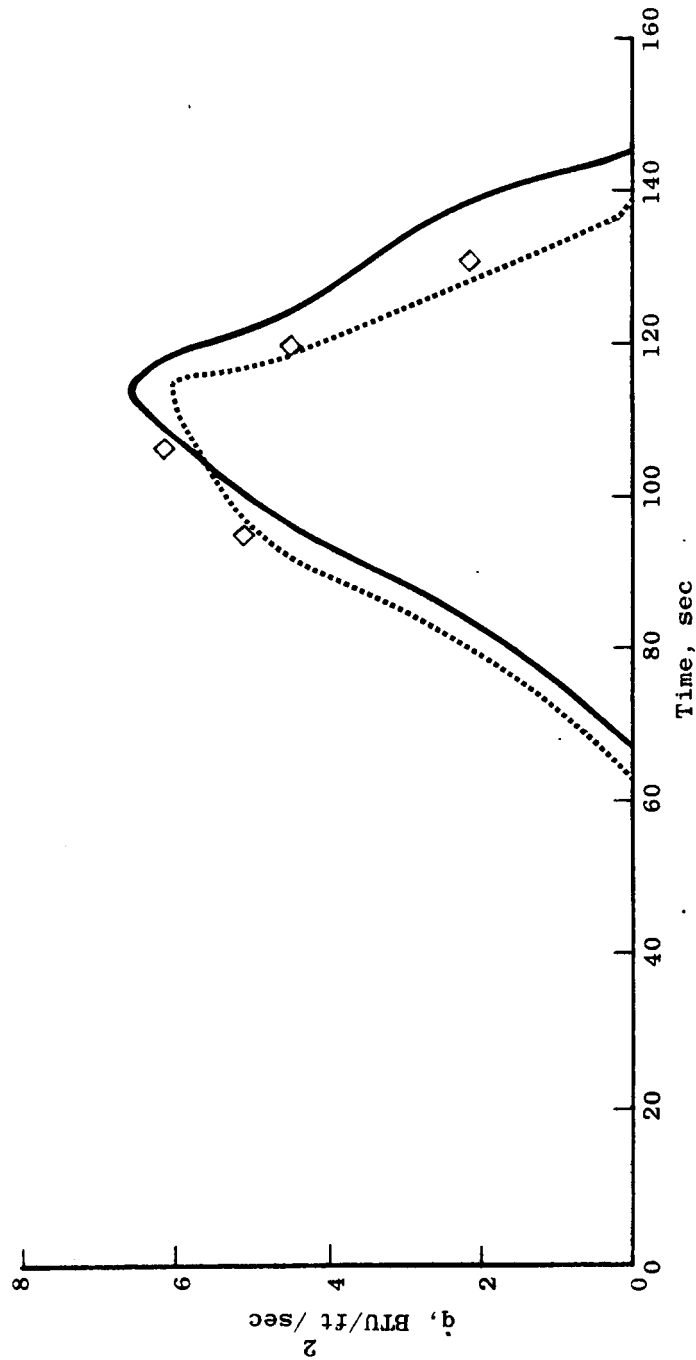


Figure 4.8-7.- Comparison of heating rate histories at $X_G = 27$ for two circumferential locations on BP-13 spacecraft.

— $X_C = 52$ Cal 4
 $X_C = 27$ Cal 11
 - - $X_C = 74$ Cal 2

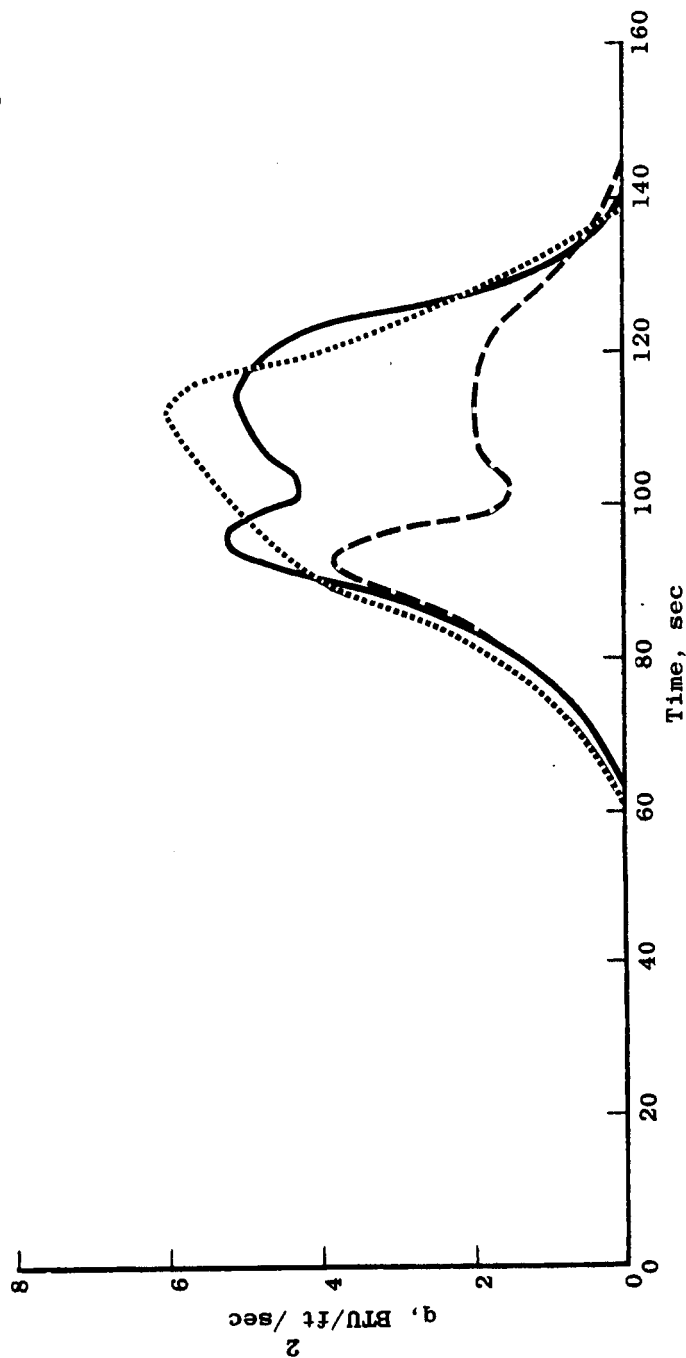


Figure 4.8-8.- Comparison of heating rate histories at $\phi = 180^\circ$ for three longitudinal locations on BP-13 spacecraft.

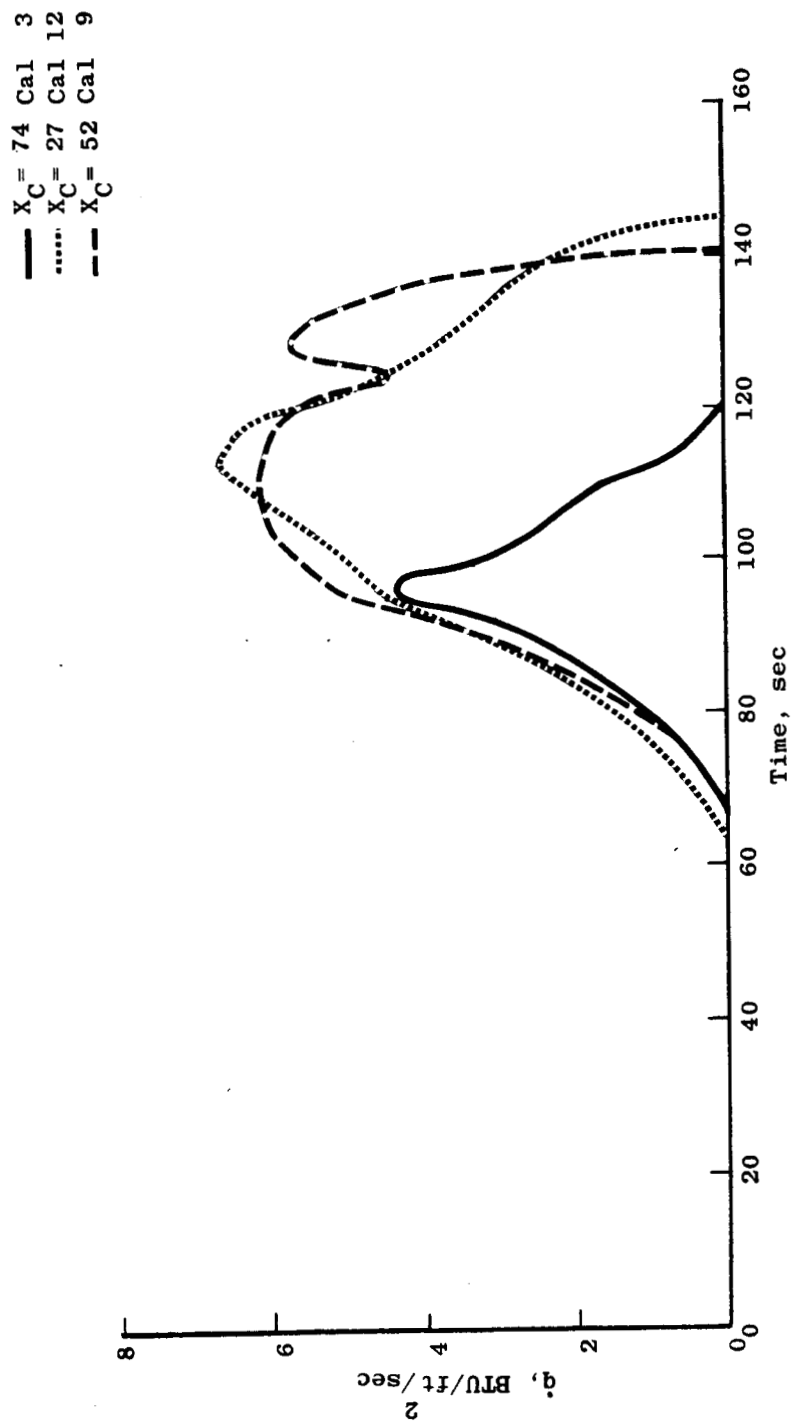


Figure 4.8-9.- Comparison of heating rate histories at $\phi = 319^\circ$ for three longitudinal locations on BP-13 spacecraft.

— $X_C = 42.65$ Cal 10
 $X_C = 74$ Cal 1
 - - - $X_C = 52$ Cal 5

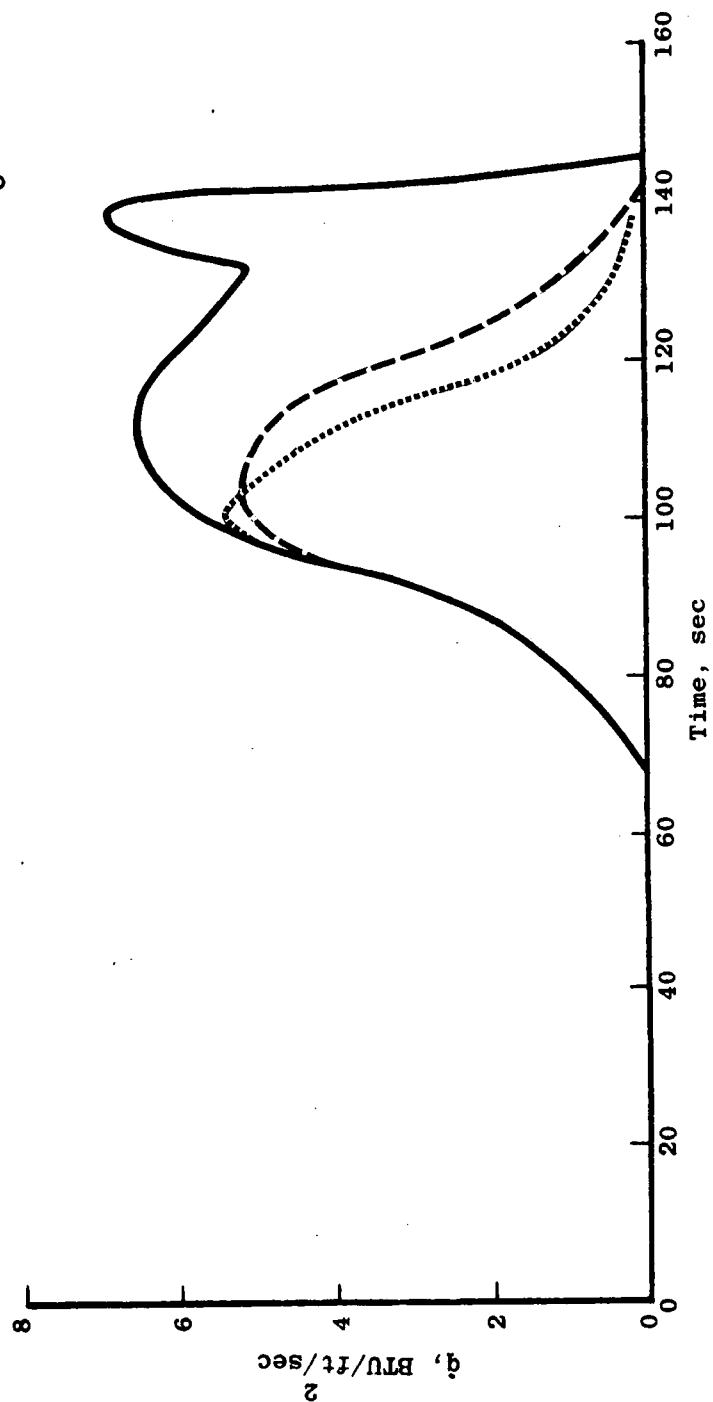


Figure 4.8-10.- Comparison of heating rate histories at $\phi = 3^\circ$ for three longitudinal locations on BP-13 spacecraft.

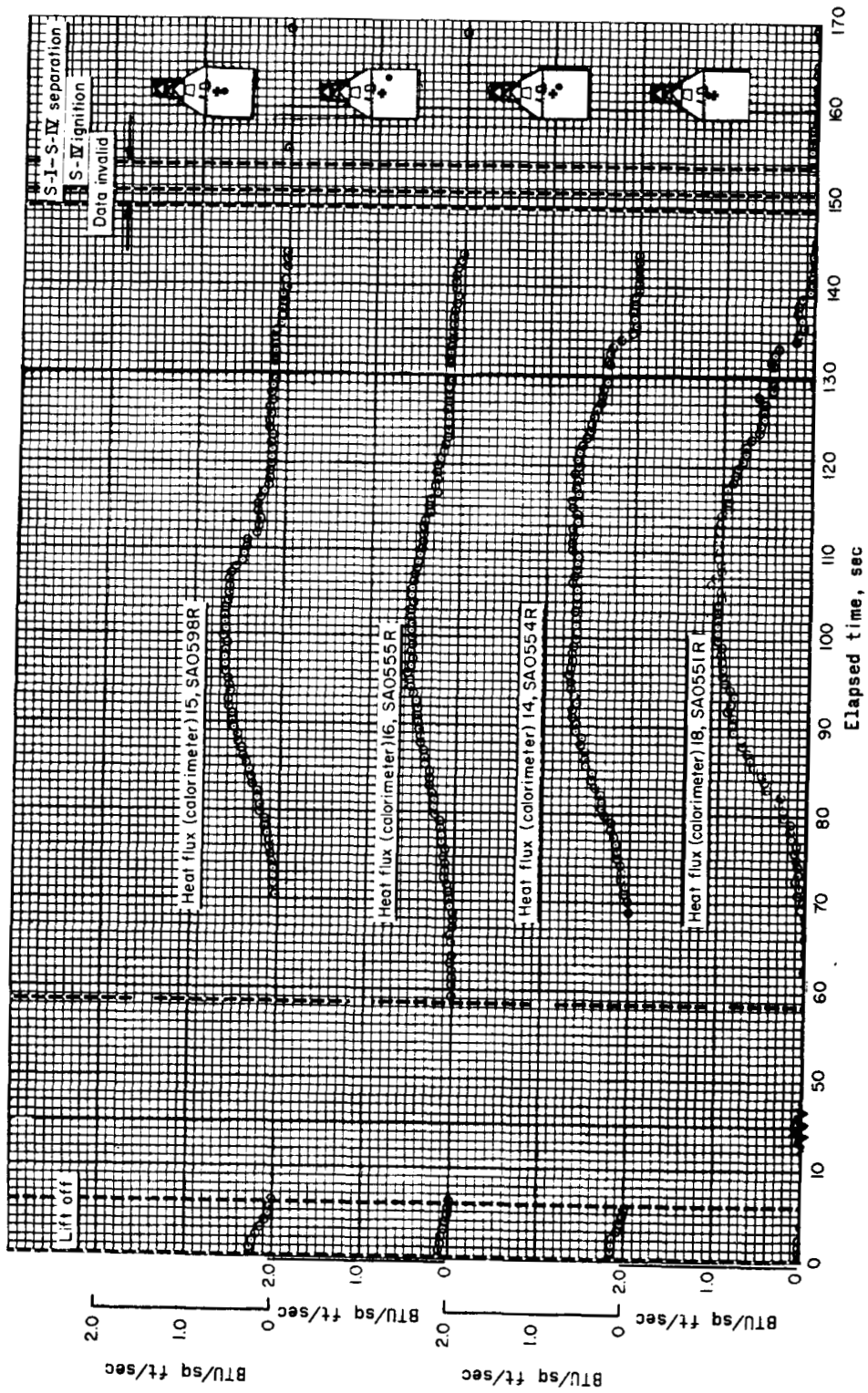


Figure 4.8-11.- Heating rates measured on the BP-13 spacecraft service module during flight.

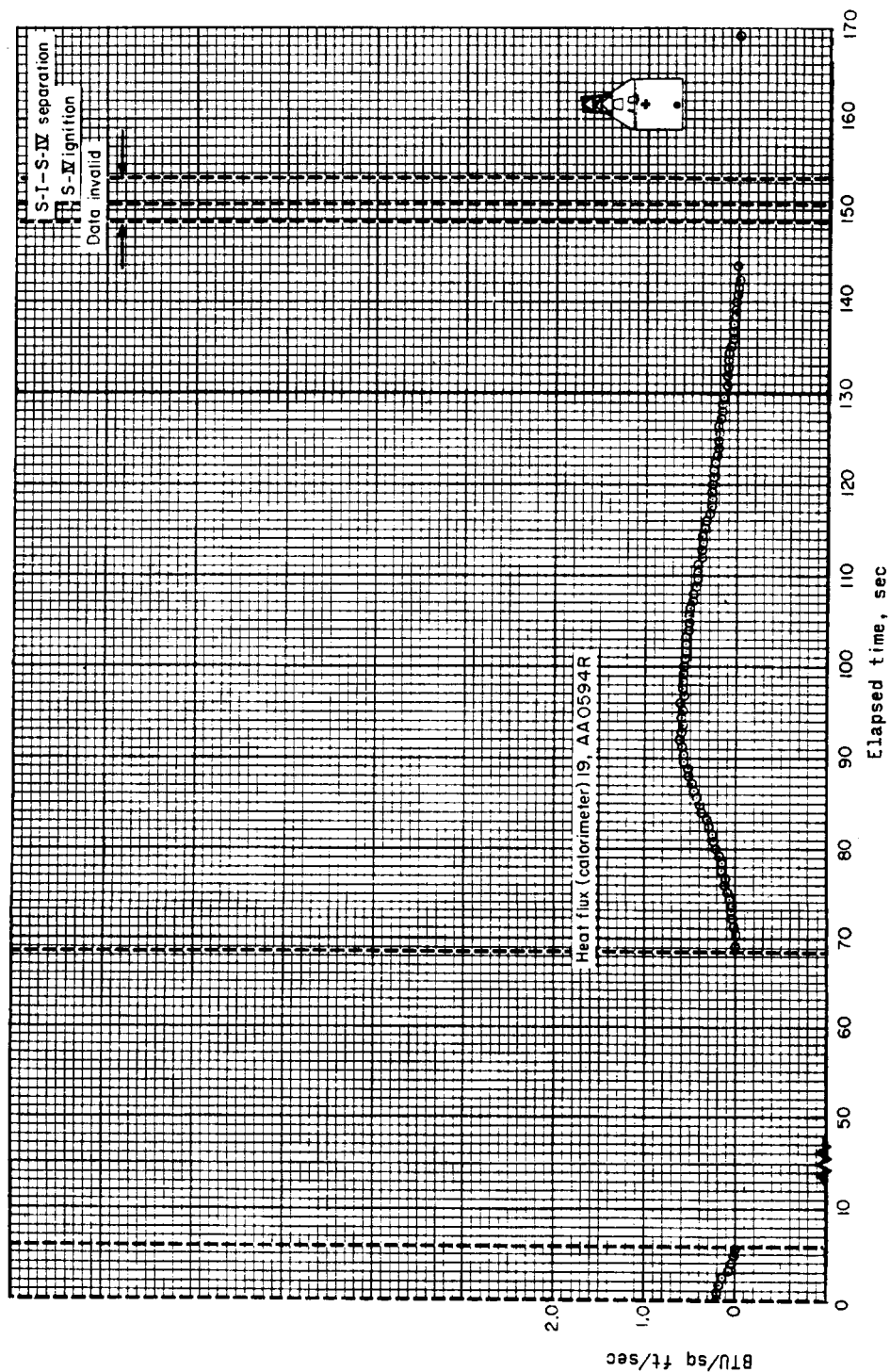


Figure 4.8-12. - Heating rates measured on the BP-13 spacecraft adapter during flight.

4.9 Equipment Cooling

Environmental control subsystem description. - The environmental control subsystem (ECS) shown in figures 4.1-5, 4.1-6 and 4.9-1 was a closed-loop water-glycol cooling subsystem located in the command module. The coolant mixture used in the subsystem was 40-percent water and 60-percent glycol. The subsystem was designed to provide cooling for the command module electronic equipment during ground operations and during flight and to cool the cabin air during launch countdown. The major components of the airborne subsystem were the 250-pound-capacity water-glycol tank, coolant pump, heat exchanger and fan, accumulator, thermal control valve, and five coldplates.

Prior to flight, the entire subsystem was filled with the water-glycol mixture from the ground support equipment (GSE) through the spacecraft umbilical. The temperature of the water-glycol mixture in the onboard tank was lowered to the proper preflight temperature by circulating the water-glycol mixture through the GSE refrigeration system and back to the spacecraft tank. This process continued throughout the countdown and terminated with spacecraft umbilical ejection. After spacecraft umbilical ejection, the coolant tank served as a heat sink and was designed to provide cooling for the launch phase of the flight.

The spacecraft electronic equipment was cooled by pumping the cold water-glycol mixture through the coldplates. The coldplates were designed to maintain the temperature of the electronic equipment at less than 150° F with a maximum coolant temperature of 45° F.

The automatic temperature control valve adjusted the amount of cold water-glycol from the coolant tank to mix with the recirculating coolant to maintain a coldplate inlet temperature of $40 \pm 5^\circ \text{F}$. When the coldplate inlet temperature dropped below 35° F, the temperature control valve cut the coolant tank out of the coldplate circuit. When the temperature of the coolant in the tank rose above 45° F, the thermal control valve opened to direct all flow through the tank. The fan circulated cabin air through the heat exchanger. When the pressure in the command module dropped to 5.45 ± 5 psia during launch, the fan and fan inverter were cut off by a barostat switch.

Environmental control subsystem performance during countdown. - The measurements of the cooling subsystem parameters shown in table 4.9-I were obtained only by umbilical hardline. The readings at the time of umbilical ejection indicate that all ECS temperatures were well within specification limits at the time of launch even though the low differential pressure (4 psi) and abnormally high currents (table 4.9-II) indicate that the ECS pump was not operating properly. A sectional view of the ECS pump is shown in figure 4.9-2.

[REDACTED]

The first indication that the pump was operating improperly was observed 11 hours 51 minutes before launch when the fan and pump were first turned on during the final count. At this time, the sound of the pump changed from its usual smooth whine to a sound characteristic of a rough-running pump. The differential pressure at this time was noted to be normal (approximately 10 psi). During the next 2 hours and 52 minutes, the pump was turned on three times, each time with the same symptom of rough running. The differential pressure was normal in each case. When the pump was turned on for the fourth time with 8 hours 59 minutes until launch, it again exhibited rough running, but in addition, a drop in differential pressure and a higher than normal current were observed. Also, there were fluctuations in the differential pressure and current. The pump was turned on two more times before launch, and each time a lower than normal differential pressure, higher than normal currents, and fluctuating pressures and currents were observed. The differential pressure appeared to decrease while the pump was running. When the pump was turned on just 9 minutes before launch, the differential pressure was approximately 8 psi. At umbilical ejection, the differential pressure had dropped to 4 psi, and the total current was 55 amperes, an increase of 12 amperes above normal.

The pump problem experienced on launch day in the BP-13 spacecraft is the first of its kind to be noted during the testing of the BP-13 spacecraft. At the contractor's plant and at Cape Kennedy, another problem was encountered with a number of these pumps, including the one which was used in the BP-13 spacecraft. This problem exhibited itself as an initial surge of current when the pump was turned on after a relatively long period of inactivity. When the pump was used frequently, this condition did not occur. A malfunction investigation at Cape Kennedy on two other pumps found corrosion on moving parts in the pump. It was decided that with a preventative maintenance program consisting of frequent starts (every third or fourth day), the pump in the BP-13 spacecraft would be satisfactory for flight. The flight pump was installed in the BP-13 spacecraft on May 1, 1964, after the factory installed pump had been removed for failure analysis of the current surge phenomenon. After the pump used for the flight was installed in the spacecraft, two initial current surges were noted. From that time until launch, the pump was started 45 times for a total operating time of 17.5 hours of its 1,000-hour design operating life. On no other occasion did the pump give any indication of abnormal operation until launch day. The current surge problem is not known to be related to the pump problem which occurred on launch day.

Environmental control subsystem flight performance. - Table 4.9-II indicates that during the powered flight phase, the cabin fan was turned off by the barostat switches at T + 231 seconds at a cabin pressure of

[REDACTED]

[REDACTED]

5.4 psia. This actuating pressure is within specification. Cutoff of the fan was verified by a drop of approximately 8 amperes in total d-c current at T + 231 seconds.

The total d-c current (table 4.9-II) and telemetry package temperature data indicate that the pump continued to operate through the first orbital pass.

The cooling system was required to maintain the telemetry package temperature below 150° F through the first orbital pass and to maintain the cabin air temperature below 100° F during the countdown operation. The temperature of the electronics packages was held below the 150° F maximum for the life of the pump power supply, which was approximately two orbital passes (table 4.3-I and fig. 4.9-3); and, with scheduled intermittent operation of the pump, the cabin air temperature was held well below the 100° F maximum during the launch countdown.

The cabin was designed to have a maximum rate of leakage equivalent to a leakage area between 0.25 sq in. and 0.50 sq in. In figure 4.9-4 the pressure decay calculated for leakage areas of 0.25, 0.50, and 1.00 sq in. are compared with the decay of cabin pressure in BP-13 during flight.

[REDACTED]

TABLE 4.9-I.- COOLING SUBSYSTEM PARAMETERS

Parameter	Actual value	Specifications
CM air temperature, °F	56	100 (maximum)
Coldplate inlet temperature, °F	41	40 ± 5
Coldplate outlet temperature, °F	45	None
Tank outlet temperature, °F	21	70 (maximum)
Tank inlet pressure, psi	16.5	---
Pump outlet pressure, psi	20.5	---
Tank-pump differential pressure, psi .	4	normally 10
GSE water-glycol circulation rate, gal/min	2.5	---
GSE circulating water-glycol temperature, °F	18	---

TABLE 4.9-II.- DIRECT CURRENT SUMMARY

[Fan normally draws 7 amperes; pump normally draws 10 amperes]

Time	Expected total d-c current with pump on	Actual total d-c current	Differential current	Fan
T - 0	43	55	12	On
T + 231 sec	35	47	12	Off
T + 360 sec	35	46	11	Off
T + 524 sec	35	36	1	Off
T + 533 sec	35	44	9	Off
T + 549 sec	35	36	1	Off
T + 552 sec	35	44	9	Off
T + 676 sec	35	36	1	Off
T + 685 sec	35	44	9	Off
T + 896 sec	35	36	1	Off
T + 905 sec	35	44	9	Off
T + 98 min	35	42	7	Off

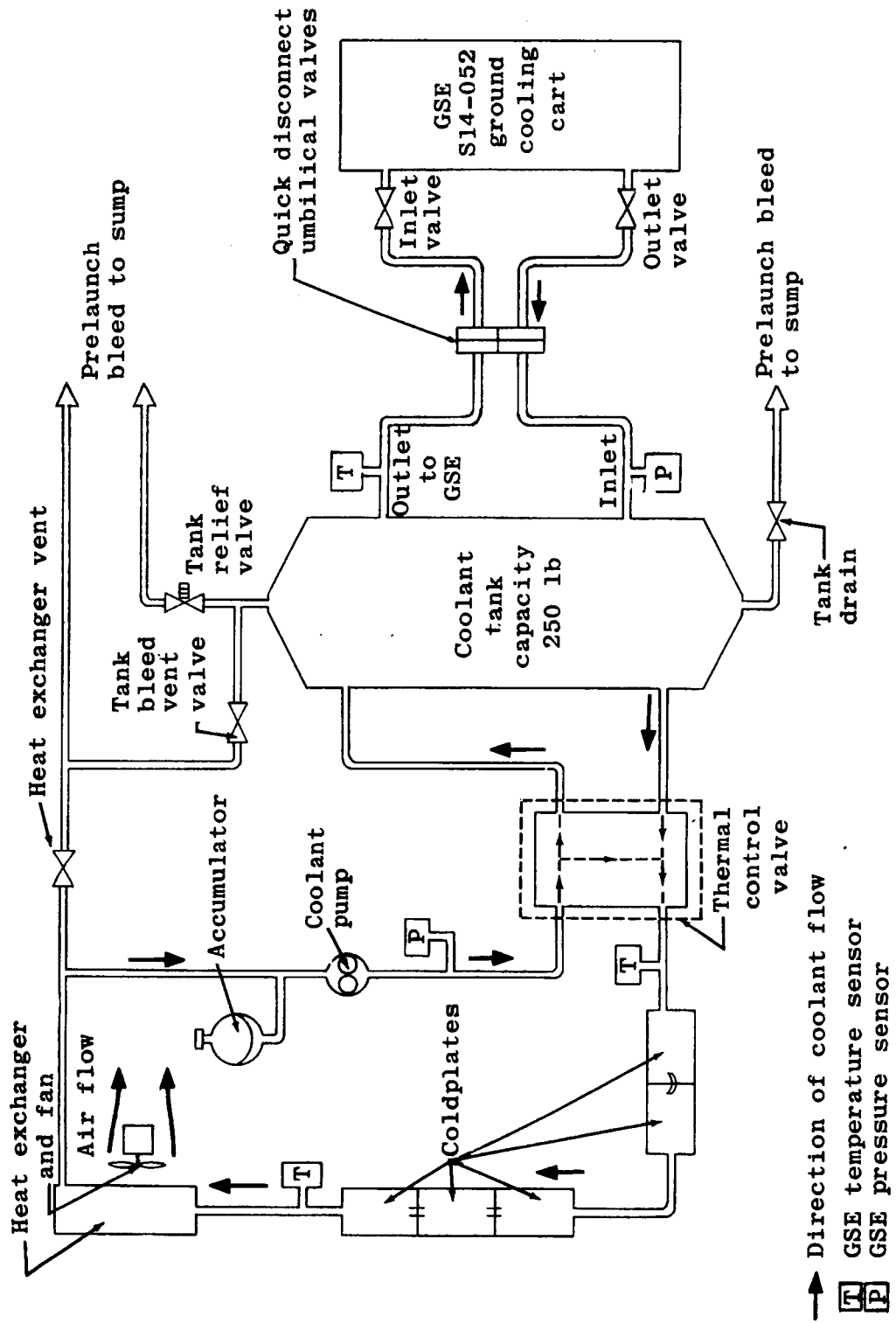


Figure 4.9-1.- Environmental control subsystem schematic for BP-13 spacecraft.

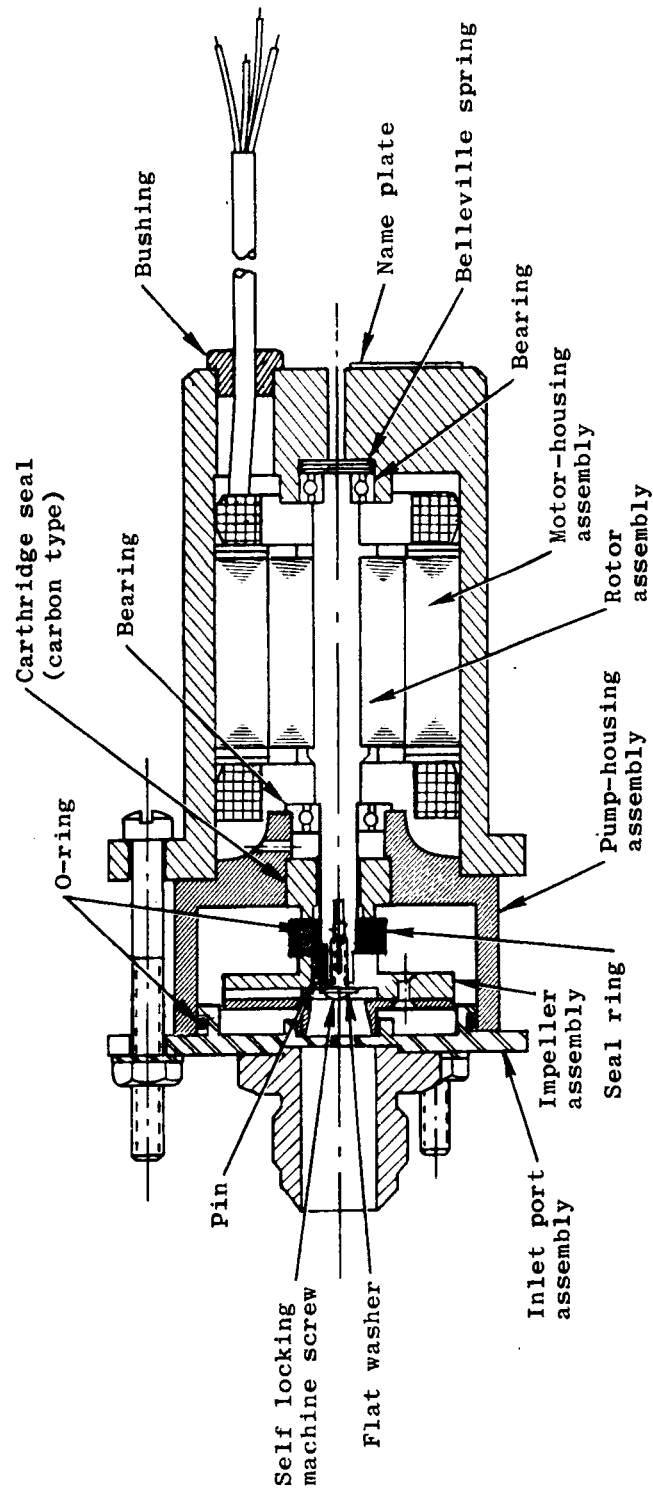


Figure 4.9-2.- Sectional view of coolant-pump assembly for BP-13 spacecraft.

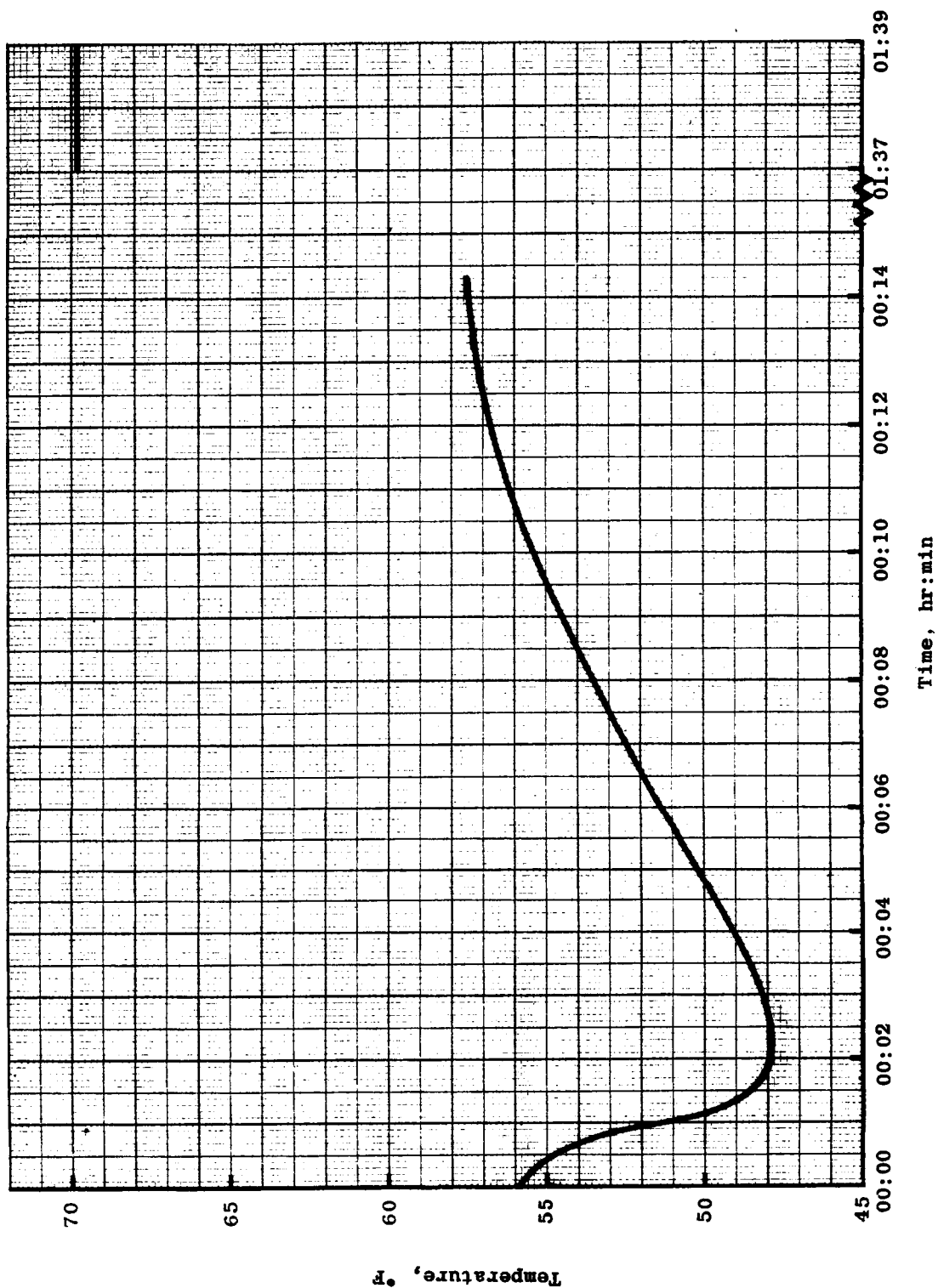


Figure 4.9-3. - Command module cabin air temperature (BP-13 spacecraft).

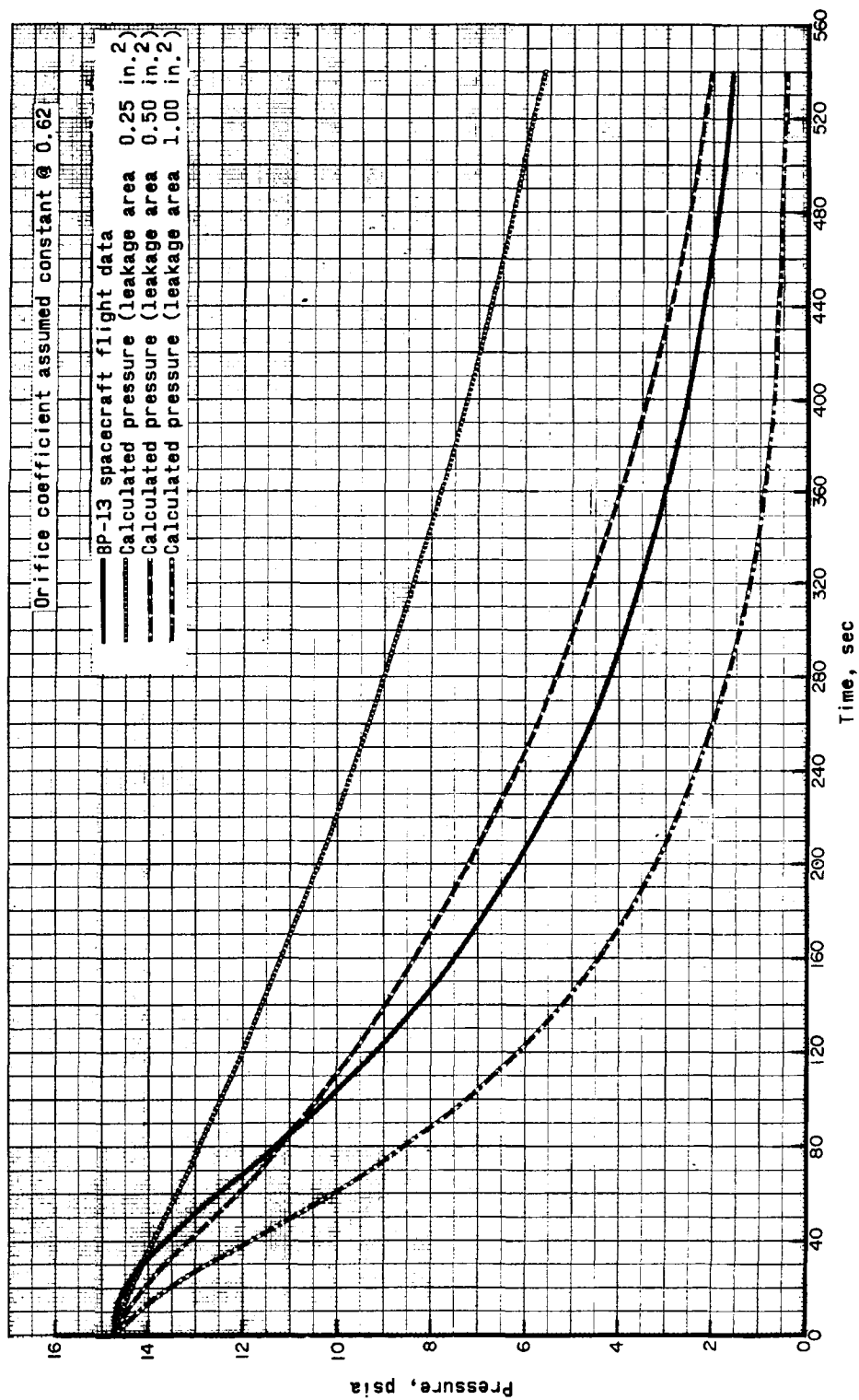


Figure 4.9-4.- Command module cabin pressure (BP-13 spacecraft).

4.10 Acoustics

An acoustic microphone (measurement SA2760Y, table 4.2-II) was installed flush with the exterior surface of the service module just below the shoulder of the command module (see fig. 4.6-16 for location) and within 8 inches of fluctuating pressure transducer SA0182P.

At the time of publication of this report adequate reduced data from this acoustic sensor had not been received. When these data are received, analyses will be made and the results published at a later date.

5.0 LAUNCH-VEHICLE DESCRIPTION AND PERFORMANCE

5.1 SA-6 Launch-Vehicle Description

The Saturn I is a two-stage launch vehicle consisting of stages S-I and S-IV, an instrument unit, and various fairings and adapters. The total vehicle length is approximately 190 feet, consisting of an 80.3-foot-long by 257-inch-diameter S-I stage, a 41-foot-long by 220-inch-diameter S-IV stage, a 4.8-foot-long by 154-inch-diameter instrument unit, and a 64.1-foot-long by 154-inch-maximum-diameter boilerplate spacecraft and launch escape subsystem (LES). Vehicle details and dimensions are presented in figure 5.0-1.

The S-I stage dry weight is 107,239 pounds with a propellant capacity of 850,000 pounds (lox and RP-1). Eight H-1 engines mounted in two clusters, four inboard and four outboard, produce a total sea-level thrust of 1.5 million pounds.

The S-IV stage dry weight is 13,960 pounds with a propellant capacity of 103,000 pounds (LH_2 and lox). The six RL10A-3 engines of the S-IV stage produce a combined thrust of 90,000 pounds.

The instrument unit (IU) contains most of the flight control equipment, including the vehicle inertial guidance and control system and the airborne hardware of six tracking and four telemetry systems. The IU also has an integral power supply and distribution system, cooling systems, and a gaseous nitrogen supply system. The IU begins to function prior to lift-off to command S-I start sequencing and to maintain programming, sequencing, and flight control through S-I and S-IV stage operation.

Vehicle telemetry systems are provided for each stage and the instrument unit which include six airborne systems and one digital data acquisition system for preflight checkout in the S-I stage, three systems in the S-IV stage, and four systems in the instrument unit.

5.2 Preliminary Flight Performance

After a brief period (about 8 sec) of vertical flight, the launch vehicle started to roll to the proper flight azimuth (105° East of North) and completed this maneuver at $T + 12.2$ seconds. At $T + 15.2$ seconds, the preprogramed pitch attitude profile was initiated and continued until $T + 134.2$ seconds, at which time a constant vehicle

[REDACTED]

attitude was maintained until the initiation of active guidance at 18.6 seconds after separation of the S-I and S-IV stages. The flight performance of the launch vehicle was near nominal until T + 116.9 seconds when the inboard engine no. 8 shut down 23.2 seconds prematurely. Proper flight control was maintained, and the reduced total propellant flow rate of the remaining seven engines produced a longer than nominal burn time before the propellant-level sensors initiated the shutdown sequence. The increase in burning time was also partly due to lower flow rates throughout S-I flight. The entire shutdown and staging sequence was consequently 2.7 seconds later than planned, and the trajectory parameters as compared to nominal at S-I stage shutdown were about 330 ft/sec, 0.8° , and 1,110 feet low in space-fixed velocity, space-fixed flight-path angle, and altitude, respectively. Ullage rocket and S-IV ignition and ullage rocket and LES jettison were also 2.7 seconds later than nominal since these sequences were based on a time after separation. One ullage rocket failed to jettison. The additional 70 pounds of ullage rocket hardware carried into orbit and the center-of-gravity offset had little effect on the flight performance. Launch escape subsystem jettison had no disturbing effect on the vehicle flight dynamics. Following initiation of closed-loop guidance, the vehicle was steered into a nearly nominal orbit after S-IV shutdown. A higher than nominal S-IV stage thrust resulted in a burn time that was 4.0 seconds less than nominal.

The SA-6 flight performance was acceptable for meeting the required spacecraft test objectives relevant to flight compatibility and exit environment. The SA-6 engine anomalies produced no degradation of spacecraft test objectives.

Except for the early shutdown of the S-I engine no. 8, the S-I stage performed as expected. The S-I stage thrust and propellant flows were slightly lower than nominal but within tolerance. Residual propellants at separation were 6,062 pounds of lox and 775 pounds of fuel compared with the predicted 200 pounds of lox and 1,874 pounds of fuel. This difference in residual was primarily due to off loading propellants and a less than predicted lox density. Lox temperature was 2.5° F warmer than predicted.

The premature shutdown has been isolated to a failure in the no. 8 engine turbopump assembly. Preliminary results indicate that the probable cause was bearing seizure or gear failure. The Mark III turbine assembly was flown for the last time on SA-6, and the improved version of the Mark III (Mark III H) assembly will be flown on SA-7 and subsequent Saturn I missions.

[REDACTED]

[REDACTED]

Preliminary results indicate that the thrust controller for the no. 4 engine had malfunctioned and was in the fully closed position, which would account for the higher chamber pressure observed in the no. 4 engine. Because of higher no. 4 engine thrust, the S-IV stage acceleration was high throughout the entire flight. The thrust controller malfunction also caused a higher than predicted propellant flow rate to engine no. 4.

Satisfactory performance was achieved from the ullage rockets; however, the empty rocket no. 4 was not jettisoned, although the exploding bridgewire (EBW) apparently operated properly. The probable cause has not been determined.

The guidance and control system performed satisfactorily. There was no appreciable effect on the control system due to the premature shutdown of the S-I engine no. 8. The resulting velocity deficit at separation and the higher acceleration of the S-IV stage were compensated for during closed-loop guidance, and the vehicle was steered to the proper cutoff conditions (see section 3.0).

The major transients observed included a roll-attitude deviation of 3° during S-I stage operation resulting from an aerodynamic moment caused by the unsymmetrical arrangement of the turbine exhaust ducts on the S-I stage. The aerodynamic moment was partially counteracted by a small bias in the roll attitude due to a small effective thrust misalignment of the S-I engine thrust vector. There were only very small transients during the S-IV flight due to separation and LES jettison. Switchover of attitude signal from the ST-90S platform to the ST-124 platform was satisfactorily accomplished 14 seconds after separation. Guidance was introduced 4.6 seconds later and resulted in a pitch command peak transient of 3.3° (nose up) and a yaw command peak transient of 5.9° (nose right).

Overall performance of the launch-vehicle telemetry instrumentation system was good, with only 8 of 1,196 measurements having failed completely.

A complete detailed evaluation of the performance of the launch vehicle is given in reference 2.

[REDACTED]

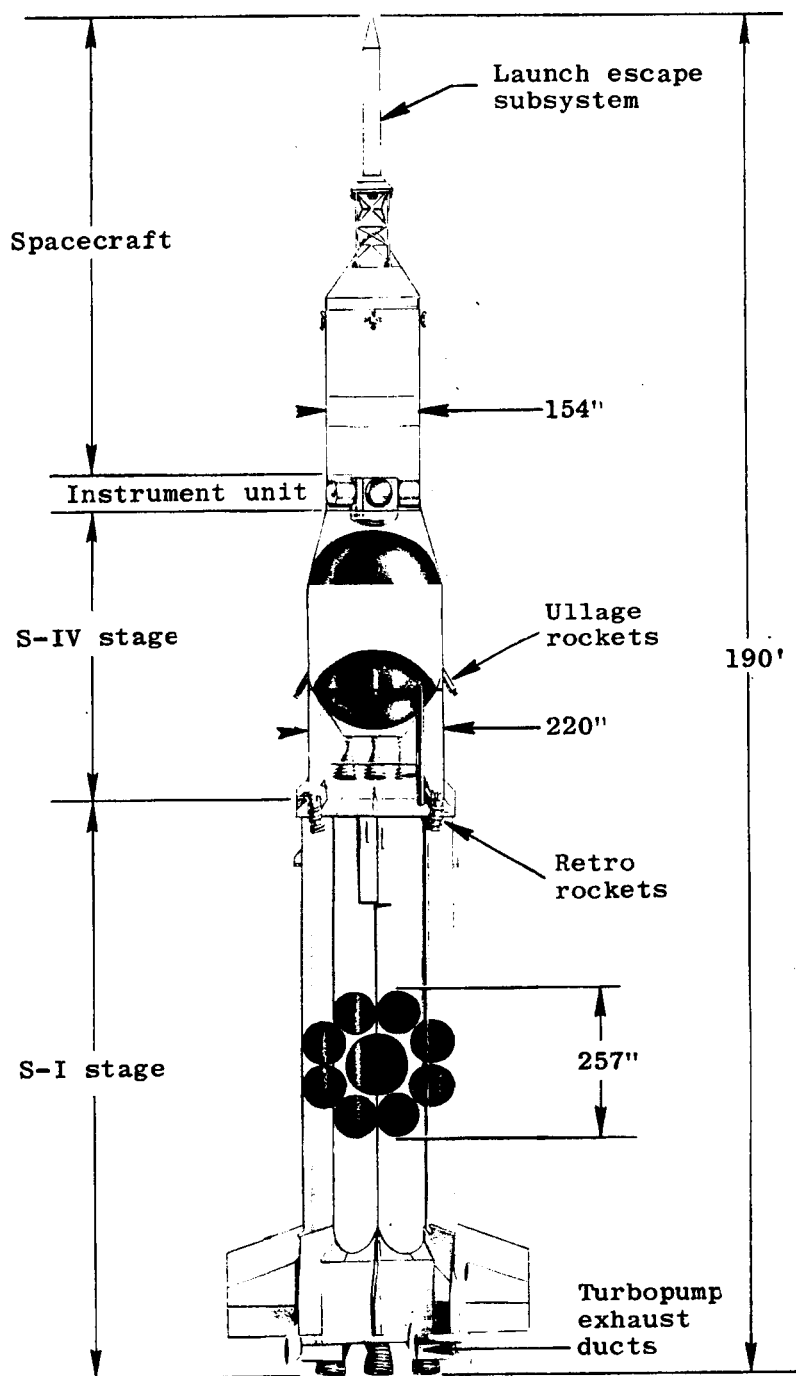


Figure 5.0-1.- Apollo mission A-101 space vehicle showing cutaway views of launch vehicle.

6.0 MISSION OPERATIONS

6.1 Prelaunch Operations

Initial checkout of the Apollo spacecraft was accomplished in the Apollo Test and Operations (ATO) area at the contractor's facility at Downey, California. Final checkout terminated at Cape Kennedy with the launch operation.

The major tests and operations performed on the spacecraft or in conjunction with spacecraft operations were conducted in accordance with the detailed Operational Test Procedures (OTP). These procedures define the step-by-step operations to be performed and the normal response to be expected, where applicable. The OTP's were used throughout the checkout operations at Downey, California (ATO) and at the Hangar AF and launch complex 37B facilities at Cape Kennedy, Florida. See tables 6.1-I and 6.1-II.

On November 13, 1963, the service module, insert, adapter, and launch escape tower were transferred to ATO from the manufacturing facilities. The command module was transferred to ATO on November 20. The schedule of milestone events for the BP-13 spacecraft during the ATO period is given in figure 6.1-1.

A modification period for the various spacecraft assemblies was scheduled from November 13 to December 3, 1963. During the manufacturing phase of the BP-13 spacecraft, it was recognized that the ground support equipment (GSE) required for the spacecraft subsystems checkout would not be available in time to support the ATO checkout schedule. As a result, Special Measuring Devices (SMD) and Special Adapter Devices (SAD) were furnished to accomplish the subsystems checkout, and the GSE units were furnished for the final subsystems integrated tests. Prior to shipment, the spacecraft subsystems were to be checked out with the GSE to be used at the launch site.

A spacecraft work and modification period was scheduled for the period from December 21, 1963, through January 23, 1964. During this period mass characteristics were determined individually for the CM, SM, insert and adapter; the spacecraft assemblies were mated and aligned in the Navajo tower in preparation for the integrated system test; and the following modifications were completed:

- (1) ECS heat exchanger in the CM replaced by a redesigned unit
- (2) Cap strip reinforcement added to six ring frames in the SM

[REDACTED]

- (3) Two strain gages added in the SM
- (4) Tower strain gages removed
- (5) Calorimeters in the SM and adapter relocated
- (6) Acoustic transducer in the SM added
- (7) Two vibration transducers in the adapter changed
- (8) Wiring for launch vehicle telemetry installed
- (9) Changes resulting from the BP-13 spacecraft Design Engineering

Inspection incorporated

- (10) Main battery bracket mounting modified
- (11) Electrical power portion of the ECS modified
- (12) RCS mountings in the SM reworked
- (13) SM fluctuating pressure transducer mounts changed
- (14) The $90 \times 1\frac{1}{4}$ low level commutator and associated wire harness

installation modified

- (15) Structural rework and initial fit checks of the dummy scimitar antennas, umbilical fairing, and air vent

When the required GSE was received and integrated as part of the test complex, design deficiencies and incompatibilities were found that required modifications to several of the units. These modifications were made and checked out between January 24 and 29.

The integrated system test using GSE began on January 30 and was successfully completed on February 6. From February 7 to 17, the spacecraft was demated and prepared for shipment. Between February 13 and 19, the spacecraft assemblies and most of the GSE were transported on three airplane shipments to the MSC Florida Operations facility at Cape Kennedy, Florida. The more critical GSE and the launch escape tower were shipped by an Air Force C-124; the SM, insert/adapter and the associated handling GSE by B-377PG (Guppy); and the command module and most of the remaining GSE by an Air Force C-133B.

[REDACTED]

[REDACTED]

Boilerplate 13 spacecraft operations at Cape Kennedy, Florida, began with the receiving inspection of the GSE and spacecraft assemblies in Hangar AF. Details of the Hangar AF schedule milestones for the BP-13 spacecraft are given in figure 6.1-2. The receiving and inspection of the spacecraft assemblies were completed between February 17 and 22; GSE receiving inspection, installation, and checkout were completed between February 15 and March 5. No significant discrepancies were found during the inspection period. A spacecraft work period, mating and alinement, in preparation for testing continued from February 21 to March 4 (fig. 6.1-3).

Hangar AF complex compatibility tests were conducted from March 7 to 10. These tests were followed by a work period, extending from March 11 to March 20, required to update the GSE and spacecraft in preparation for the integrated system test, which was conducted on March 24 and 25.

The following day, March 26, GSE was moved from Hangar AF to complex 37B; installation at complex 37B was completed on March 30. Concurrently, the spacecraft was being prepared, single-point weighed, and loaded on the vertical transport in preparation for mating with the launch vehicle. The spacecraft and LES were transported to the pad and mechanically mated with the launch vehicle, the Saturn SA-6, on the scheduled day of April 2 (fig. 6.1-4).

The BP-13 launch complex schedule milestones are given in figure 6.1-5.

After the GSE had been installed at the launch complex, electrical interface incompatibilities with the complex wiring delayed the start of the GSE Integrated Test for 3 days. These were corrected by Kennedy Space Center (KSC), and the GSE integrated test was conducted on April 3 and 4. Between April 3 and April 18, independent spacecraft tests were conducted prior to electrical mating with the launch vehicle. The tests included a spacecraft integrated systems test with the launch-vehicle simulator unit. Two interim mission sequencers were used for these tests.

The interim mission sequencer was a nonflight item that was identical to the flight unit. Two major redesign efforts caused the delivery of a flight qualified sequencer to be delayed. The first redesign eliminated the integral bias batteries and replaced them with R-C filters and self-biasing transistor stages. The second redesign eliminated the low-level latching circuit and added a relay with a coil in parallel with the motor switch driver circuit input and with contacts in series

[REDACTED]

[REDACTED]

with the motor switch driver output. This change was the result of a single point failure analysis. The flight mission sequencer was installed and satisfactorily tested in the spacecraft on April 25, 1964.

The spacecraft-launch-vehicle integrated tests began with the electrical mate and interface checks on April 20 and were successfully completed on May 20 with the final spacecraft-launch-vehicle simulated flight test. During the course of the integrated tests, the RF compatibility and the electrical interface signals and commands were demonstrated with the service structure in place and removed, and with the umbilicals installed and ejected. Also, approximately midway through this test period (May 3, 1964), the pyrotechnic substitute unit was determined to be unacceptable as a valid checkout unit. This unit was replaced by a fuse/real time recorder test setup that monitored the pyrotechnic lines for transients and firing signals.

A flight readiness review, conducted on May 19, 1964, established that the BP-13 spacecraft was acceptable for launch.

[REDACTED]

TABLE 6.1-I. - OPERATIONAL TEST PROCEDURES AT DOWNEY (ATO)

OTP	Title	Began	Completed
P-0003	Integrated system checkout	Jan. 30	Feb. 6
P-1012	Activation and charging of batteries	(a)	(a)
P-1047	Electrical subsystem checkout using SMD	Dec. 3	Dec. 7
P-1048	LES checkout using SMD	Dec. 18	Dec. 18
P-3013	LES-CM mate, demate	Jan. 11 Feb. 7	Jan. 12 Feb. 7
P-3014	CM-SM mate, demate	Jan. 8 Feb. 7	Jan. 10 Feb. 8
P-3015	SM-insert mate, demate	Jan. 7 Feb. 8	Jan. 8 Feb. 9
P-3028	CM weight and center-of-gravity determination	Dec. 28	Dec. 29
P-5022	ECS service and checkout using SMD	Dec. 7	Dec. 11
P-8023	VHF omniantenna (telemetry) checkout	Dec. 13	Dec. 13
P-8071	C-band antenna checkout	Dec. 14	Dec. 14
P-8102	Telemetry and instrumentation subsystem checkout using SMD	Dec. 13	Dec. 18
P-8103	C-band subsystem checkout using SMD	Dec. 16	Dec. 17

^a72 hours per battery

TABLE 6.1-I. - OPERATIONAL TEST PROCEDURES AT DOWNEY (ATO) - Concluded

OTP	Title	Began	Completed
^b P-9019	GSE integrated checkout	Jan. 20	Jan. 23
P-9102	SMD/SAD integrated checkout	Nov. 22	Nov. 22
P-10002	Test configuration checklist	(c)	(c)
P-10003	Test configuration checklist using SMD	(c)	(c)

^bIndividual GSE units checkout according to OTP's 9003, 9004, 9005, 9011, 9013, 9014, 9015, 9016, 9017, 9022, 9032, 9034, 9035, 9039, 9103, 9104, 9105, and 9192.

^cUsed for checking test cabling and setup.

TABLE 6.1-II. - OPERATIONAL TEST PROCEDURE
AT FLORIDA OPERATIONS

OTP	Title	Duration (1964)	
		Began	Completed
C-0003	Integrated systems checkout with simulator in Hangar AF	Mar. 25	Mar. 25
C-0004	Electrical interface checks with launch vehicle	Apr. 20	Apr. 20
C-0005	Integrated systems checkout with launch vehicle simulator (launch complex)	Apr. 9	Apr. 13
C-0006	Spacecraft-launch-vehicle overall test 1 ("plugs in")	Apr. 30	Apr. 30
	Spacecraft-launch-vehicle overall test 1 (rerun)	May 4	May 4
C-0007	Launch countdown (canceled)	May 25	May 25
	Launch countdown	May 27	May 28
C-0009	Spacecraft-launch-vehicle RFI test	Apr. 23	Apr. 24
C-0021	Spacecraft-launch-vehicle overall test 2	May 4	May 5
C-0028	Spacecraft-launch-vehicle overall test (final simulated flight at launch complex)	May 20	May 20
C-0030-2	Spacecraft complex compatibility	Mar. 9	Mar. 10
C-0031	Launch-vehicle sequencer malfunction - spacecraft monitor test	Apr. 21	Apr. 21
C-0032	Spacecraft-launch-vehicle simulated flight with swing arm test	Apr. 28	Apr. 28

TABLE 6.1-II. - OPERATIONAL TEST PROCEDURE
AT FLORIDA OPERATIONS - Continued

OTP	Title	Duration (1964)	
		Began	Completed
C-1012A	Electrical subsystem - Activation and charging of spacecraft battery	May 20	May 25
C-3044A	LES weight and center-of-gravity determination	Mar. 19	Mar. 23
C-3045	LES build-up	Feb. 25	Mar. 9
C-3063	Spacecraft off-loading	Feb. 19	Feb. 20
C-3065	Transportation of spacecraft to launch pad and mating of spacecraft to instrument unit	Mar. 31	Apr. 3
C-3071	Mate CM to SM (run 1)	Mar. 2	Mar. 2
	Mate CM to SM (run 2)	Mar. 3	Mar. 3
C-3073-2	Mate forward heat shield to CM	Feb. 29	Feb. 29
C-3074-1	Demate forward heat shield from CM	Mar. 20	Mar. 20
C-3075A	Transportation of LES to pad and mating of LES to CM	Apr. 2	Apr. 3
C-3080	Spacecraft adapter-instrument unit fit check	Feb. 20	Feb. 20
C-3081	Air conditioning barrier installation	Mar. 26	Mar. 31
C-4057-1	Rocket motor receiving and inspection	Feb. 14	Mar. 4
C-4058A-1	Pyrotechnic receiving and inspection	Mar. 26	Mar. 26
C-5024A-1	ECS service	Apr. 3	Apr. 8

TABLE 6.1-II. - OPERATIONAL TEST PROCEDURE
AT FLORIDA OPERATIONS - Concluded

OTP	Title	Duration (1964)	
		Began	Completed
C-5025A	ECS drain and purge	Apr. 7	Apr. 9
C-8114A	Antenna voltage standing wave ratio (VSWR)	May 4	May 4
C-9003	Pyrotechnic substitute unit validation	Feb. 14	Feb. 29
C-9006	Auxiliary crane control checkout	Apr. 6	Apr. 6
C-9019-1	GSE integrated checkout - Hangar AF	May 4	May 4
C-9033-3	Hookup and aline umbilical disconnect set	Apr. 13	Apr. 13
C-9036-2	Water-glycol unit checkout - launch complex	Mar. 4	Mar. 6
C-9037-1	GSE integrated and umbilical checkout - launch complex	Apr. 3	Apr. 3
C-9106	GSE receiving and inspection	Feb. 14	Feb. 14
C-9107	Water-glycol - complex check-out	Mar. 5	Mar. 5
C-9114	Facility checkout - GSE (hangar)	Jan. 17	Mar. 5
C-10000-2	Hangar checklist	Mar. 23	Mar. 24
C-10001	Pad checklist	Apr. 22	Apr. 28
ICL-1-13	Receiving inspection checklist	Feb. 18	Feb. 26

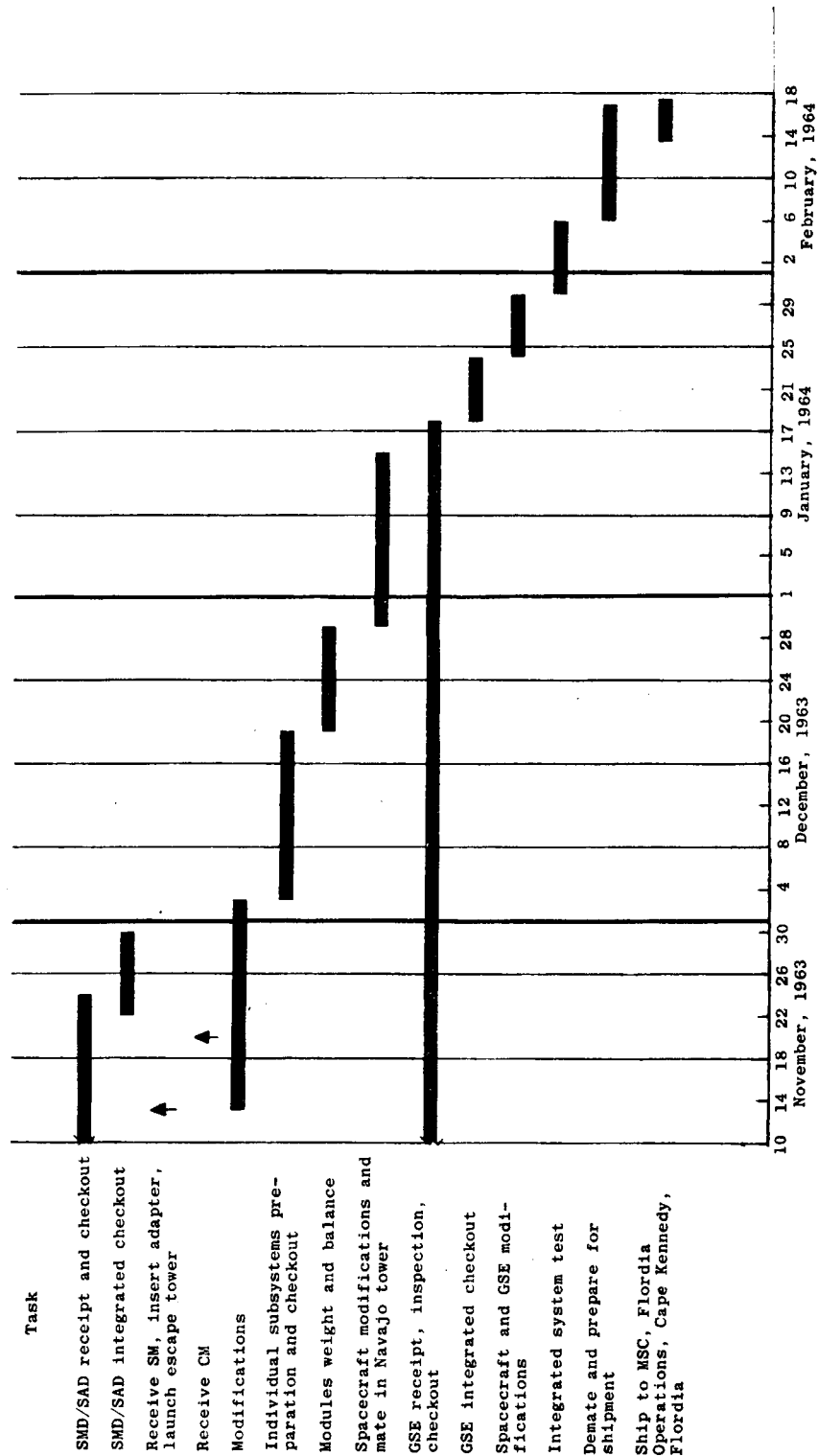


Figure 6.1-1.- Schedule milestones for BP-13 spacecraft at Downey, California, ATO.

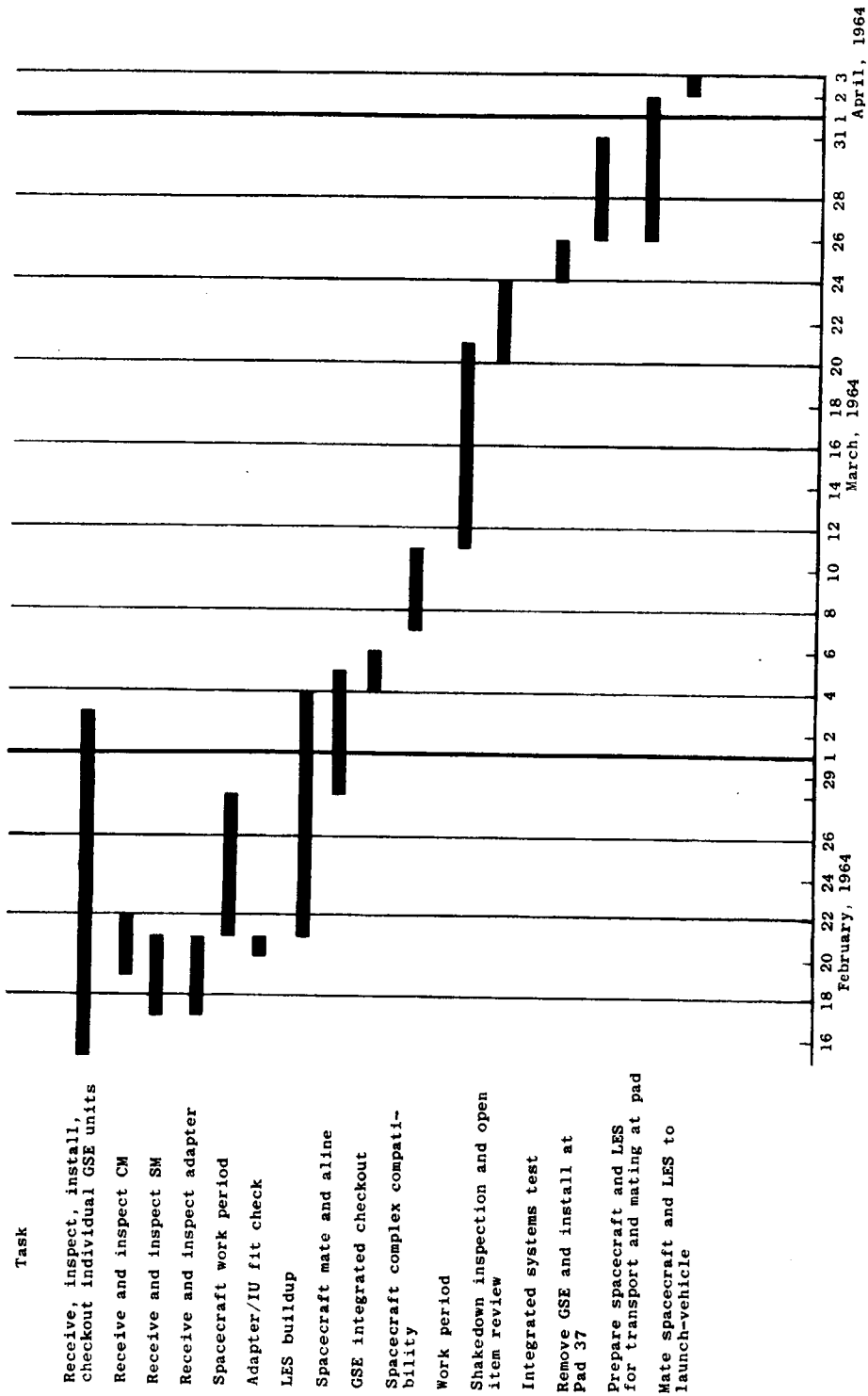


Figure 6.1-2.- Schedule milestones for BP-13 spacecraft in Hangar AF, Cape Kennedy, Florida.

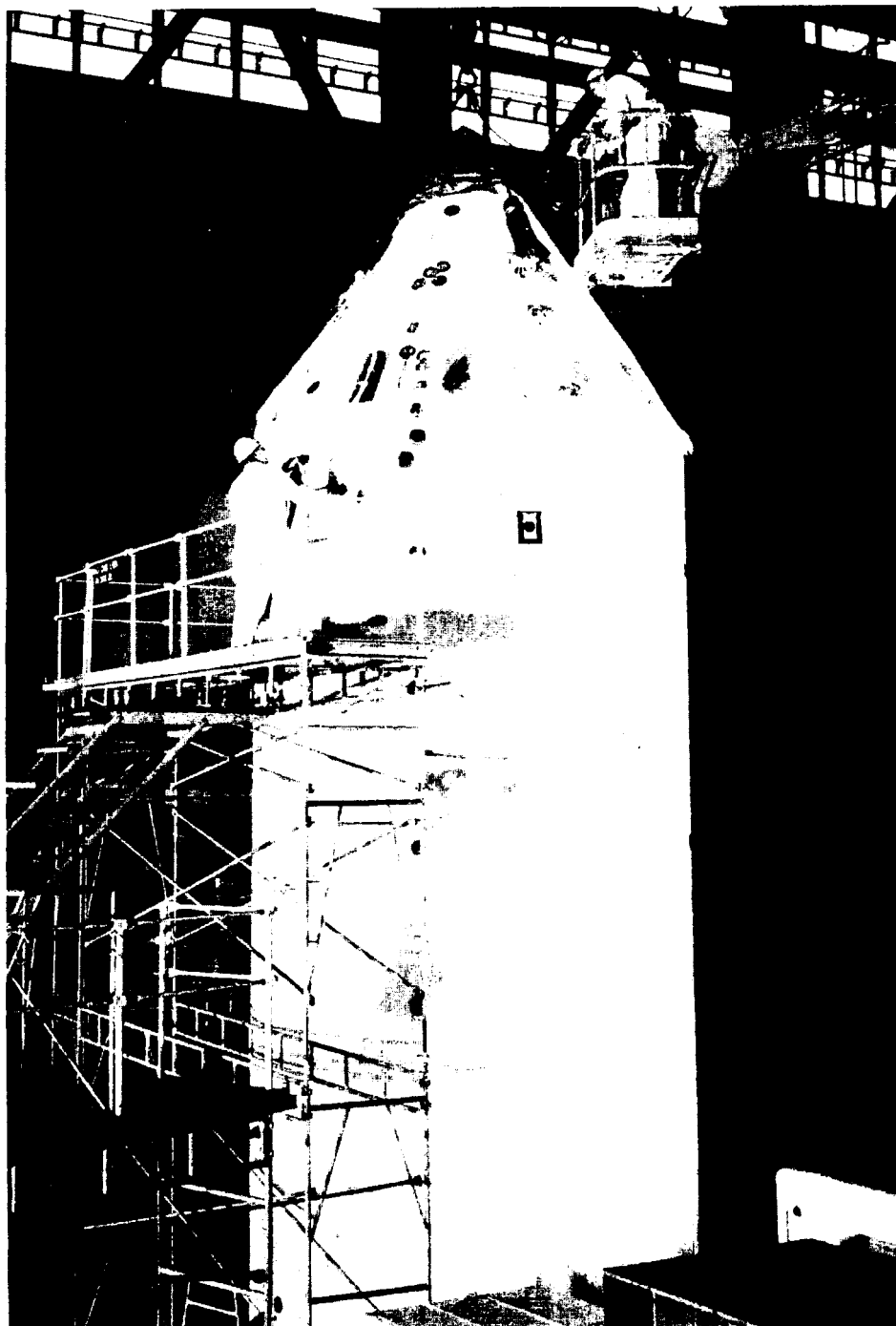
~~CONFIDENTIAL~~

Figure 6.1-3.- BP-13 spacecraft mating in Hangar AF,
Cape Kennedy, Florida.

~~CONFIDENTIAL~~

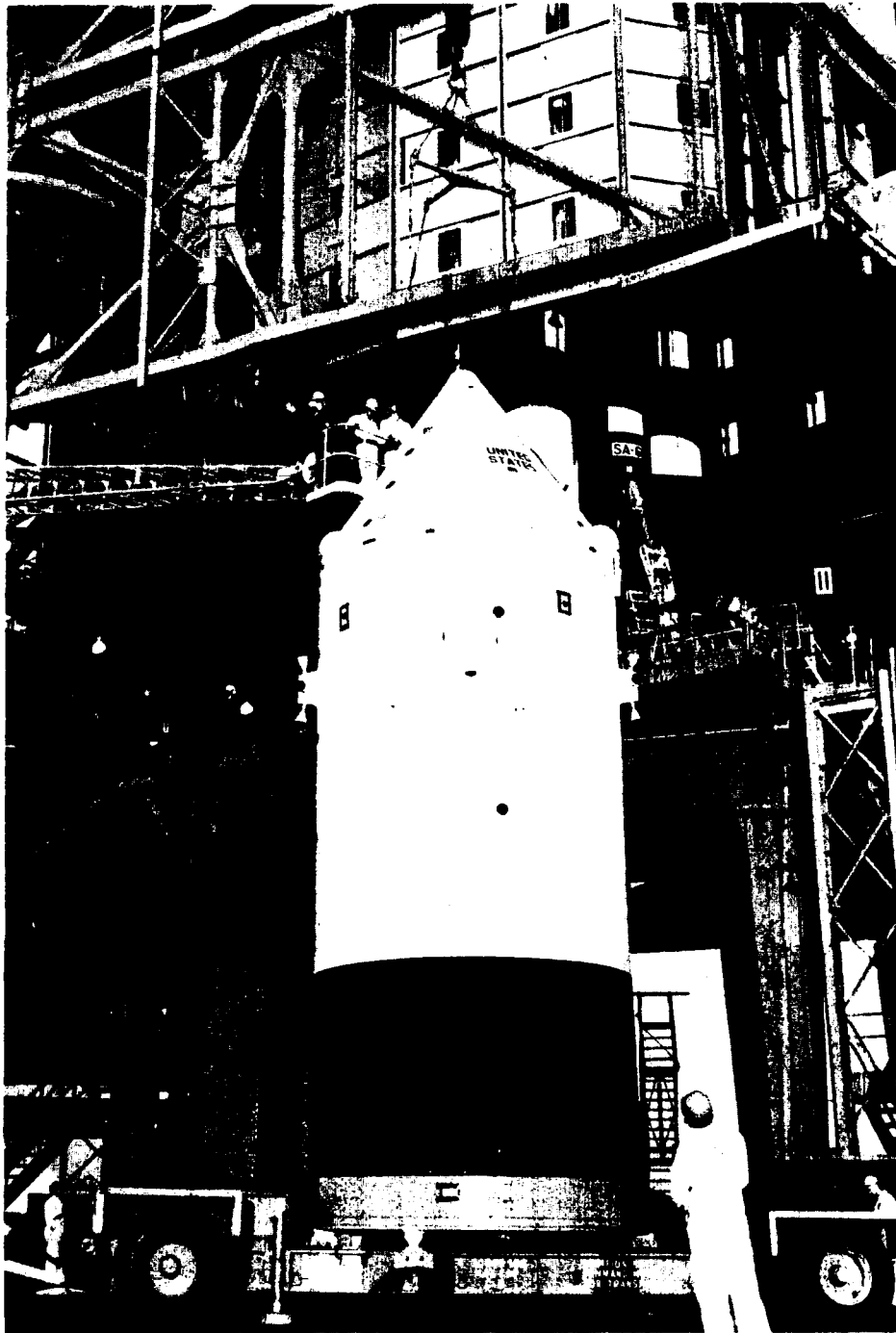


Figure 6.1-4.- BP-15 spacecraft loaded on vertical transport prior to mating with the launch vehicle.

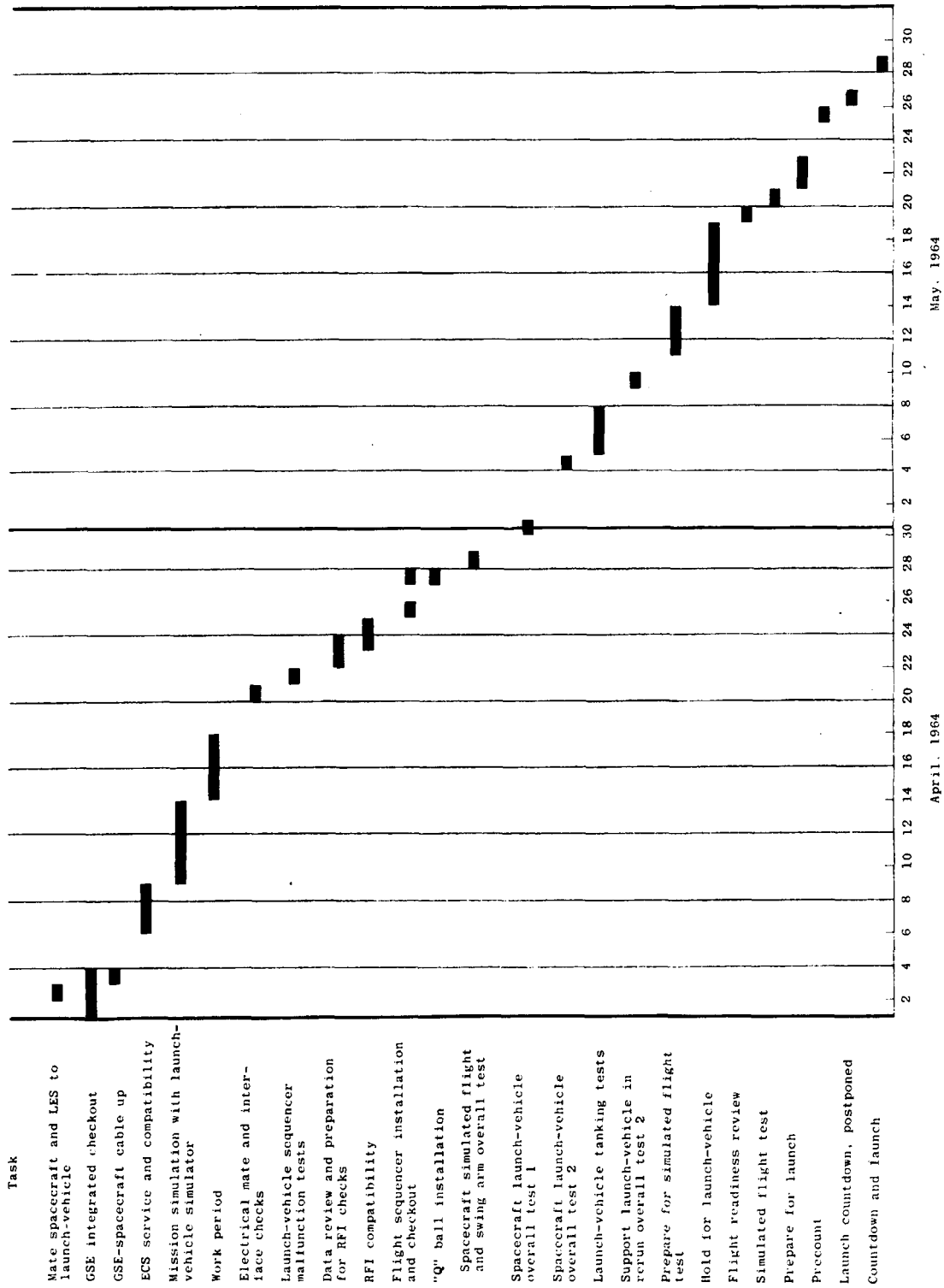


Figure 6.1-5.- Schedule milestones for BP-13 spacecraft at launch complex 37B, Cape Kennedy, Florida.

6.2 Launch Operations

The launch countdown was planned to require 17 hours and 15 minutes to complete. A rest period of 12 hours and 15 minutes was provided for the launch team by dividing the count into two portions consisting of a precount (F-1 day) of 8 hours and 10 minutes and a final count (F day) of 9 hours and 5 minutes.

The F-1 precount began as scheduled on May 25, 1964, at T-1035 minutes (3:50 a.m. e.s.t.) and proceeded normally until a launch-vehicle hold was called at T-795. (Refer to fig. 6.2-1.) Spacecraft ordnance work continued during this time and was completed before the count was resumed at 10:00 a.m. e.s.t. At the direction of the Eastern Test Range (ETR) Range Safety Officer, post-installation resistance measurements of the initiators were rescheduled for the hold period at T-545 minutes, when the launch complex could be cleared of all personnel except the seven members of the spacecraft ordnance team.

The final count on F day began approximately 20 minutes late on May 26, 1964, as a result of a failure of "critical" power at the blockhouse. (Refer to fig. 6.2-2.) Spacecraft testing proceeded normally, and the operations were essentially completed 23 minutes early at T-293 minutes. Failure of the launch-vehicle environmental control subsystem (ECS) compressor caused the countdown to be postponed at T-115 minutes (9:40 a.m. e.s.t.), after a hold of 2 hours and 10 minutes. Spacecraft recycling operations consisted of hatch removal, battery disconnect, and disarming of the launch escape subsystem (LES) initiator. In addition, the nitrogen bottles used for command module purging were refilled, the instrumentation batteries were recharged and makeup electrolyte added, new hatch screws were obtained and the hatch secured and sealed, placing the spacecraft in the correct configuration to begin the countdown again at T-545 minutes.

The launch countdown began again on May 27, 1964, at T-545 minutes (11:55 p.m. e.s.t.). (Refer to fig. 6.2-3.) When the onboard ECS pump was initially activated at T-522 minutes, it was noisy but was otherwise normal. The time required to change this pump was estimated to be 8 hours, and the decision was made to continue the count but to monitor closely the communications package temperatures.

Spacecraft testing operations were normal and were completed 13 minutes early at T-283 minutes. Holds for the launch vehicle of 37 minutes at T-95 minutes, and 61 minutes at T-70 minutes did not affect spacecraft operations. The terminal count was normal until "cutoff" was given in the launch-vehicle count at T-41 seconds (10:37 a.m. e.s.t.), causing a recycle to T-15 minutes. The spacecraft LES was disarmed,

[REDACTED]

the power was transferred to external power for battery conservation, and the communications systems were shut down to reduce the heat load. After a 74-minute hold, the launch count was resumed at 11:52 a.m. e.s.t., and it proceeded normally to the launch at 12:07 p.m. e.s.t. on May 28, 1964.

[REDACTED]



Figure 6.2-1.- Apollo mission A-101 precount activities on F-1 day, May 25, 1964.

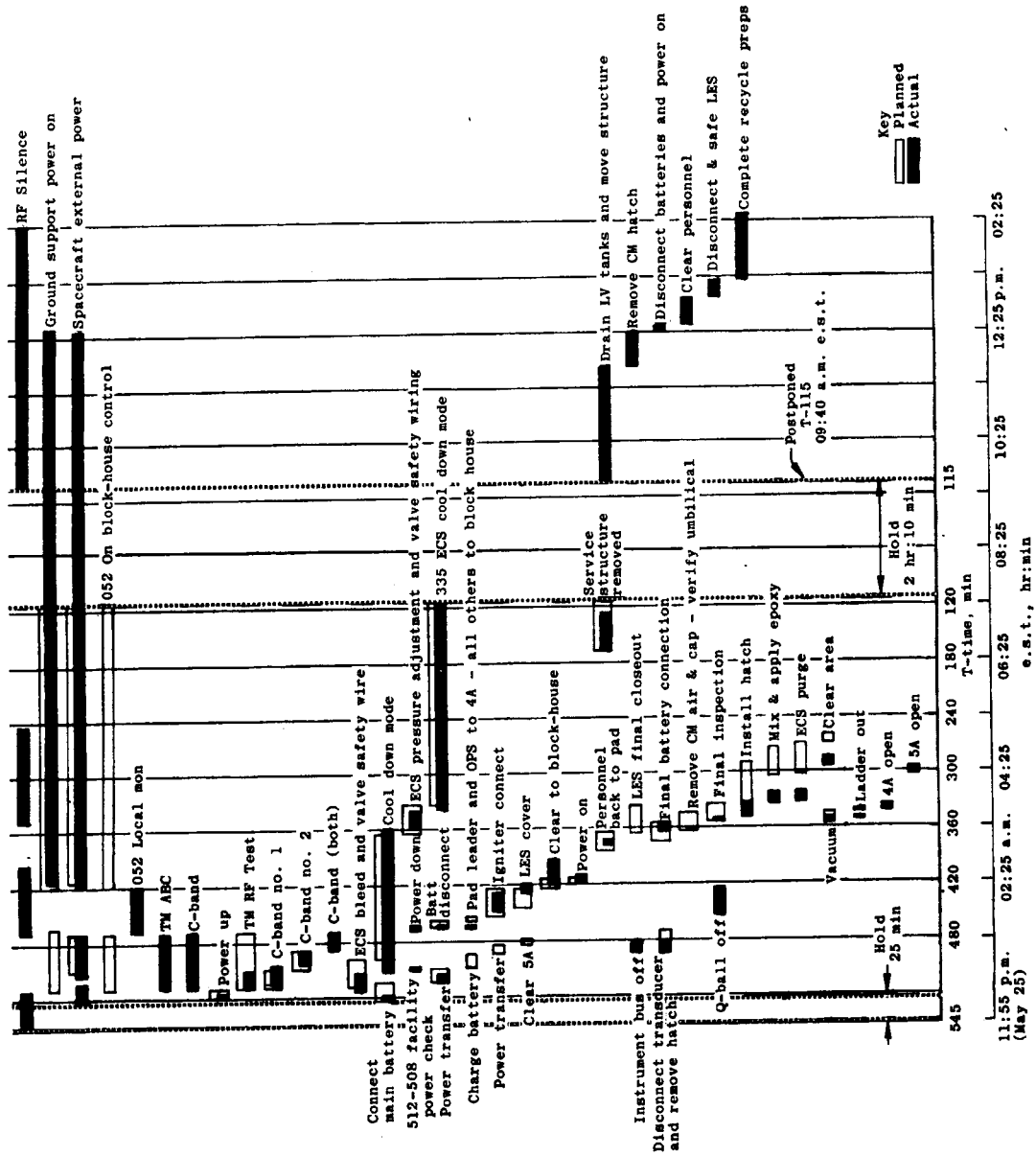


Figure 6.2-2.- Apollo mission A-101 countdown activities on postponed launch day, May 26, 1964.

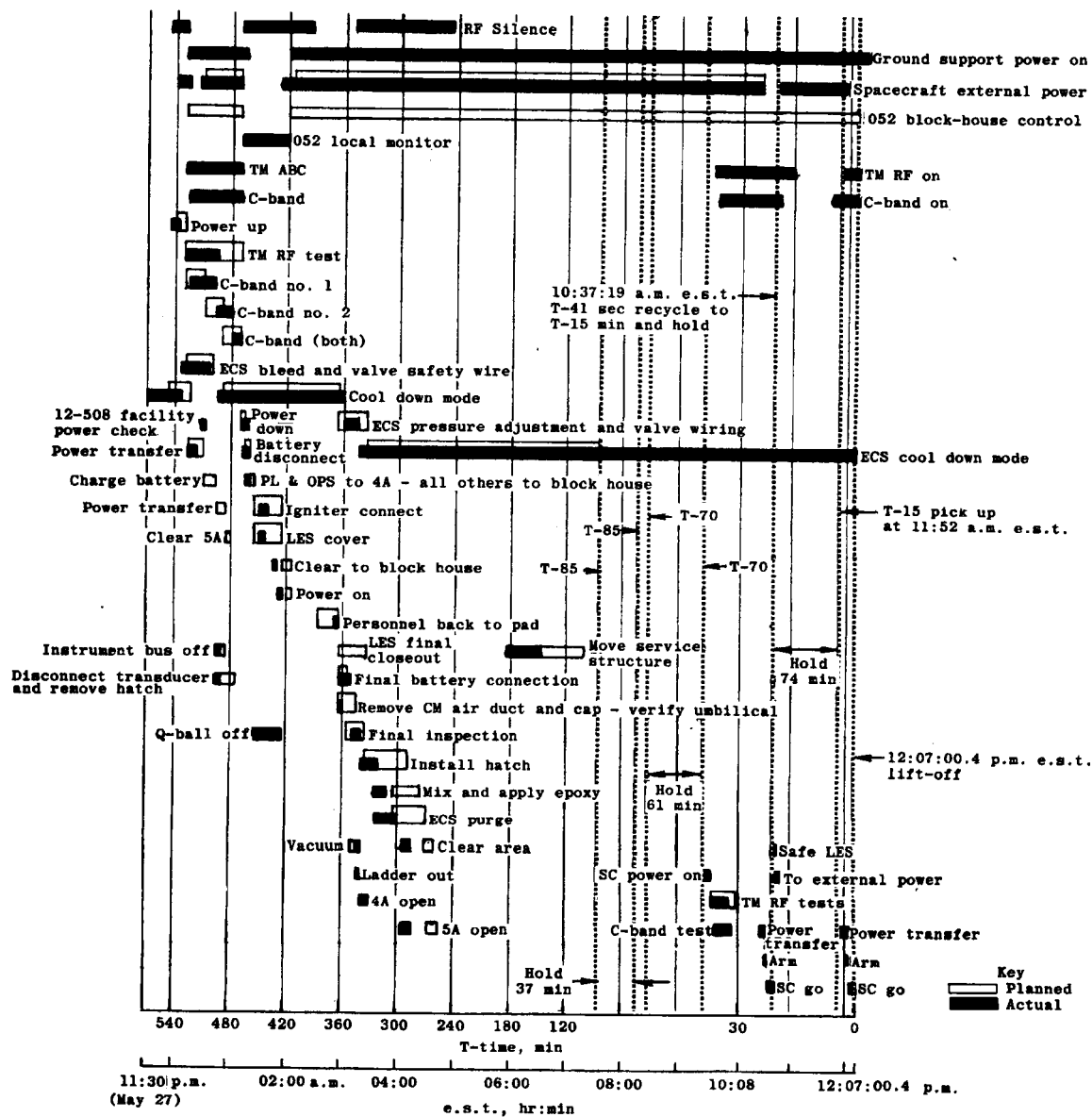


Figure 6.2-3.- Apollo mission A-101 final countdown activities, F day, May 28, 1964

6.3 Range Operations

The network which provided telemetry and radar support for the mission consisted primarily of stations of the Eastern Test Range, augmented by Department of Defense and NASA stations. The coverage provided by the stations is shown in table 6.3-I. The instrumentation of these stations was committed to support the mission with the exception of the FPS-16 radars at Bermuda and Hawaii which were being modified for Gemini program support.

During the countdown, the California and Grand Turk stations reported malfunctions. California replaced a defective tube in the parametric amplifier power supply in the FPS-16 radar at T-250 minutes. Grand Turk reported a complete power failure for 60 seconds at T-15 minutes with no apparent damage to the TPQ-18 radar or other systems. At lift-off, no major problems existed at any of the network stations.

During the mission, telemetry coverage was obtained on the first three orbital passes and part of the fourth. Radar transponder tracking was obtained during the first full orbital pass and nearly all of the second pass, after which no further signals were received from the transponders. After the transponder stopped operating, many of the stations skin tracked the vehicle throughout its lifetime of 54 orbital passes.

The times of acquisition and loss of telemetry reception for each station are given in table 6.3-I. In general, each station reported horizon-to-horizon reception on all three spacecraft links. The last station to report reception of links A and B was Pretoria, South Africa, on the fourth pass. Loss of signal was recorded at 05:21:02 g.e.t. The next station in view, Hawaii, searched from 05:53:00 to 06:07:00 g.e.t. but was unable to detect any trace of a signal. The last station to receive link C was California on the second orbital pass. Loss of signal was recorded at 03:06:26 g.e.t. No station reported reception of link C telemetry after this time.

The only known telemetry anomaly occurred at the Cape Kennedy Telemetry Station 2 on both the launch phase and the first orbital pass. Rather severe spiking was noted on several of the continuous channels on all three links, but the most severe was on link C. Spiking was noted on the oscillograph records made from the Cape Kennedy Telemetry Station 3 tape, but it was not nearly as severe as that noted in the Telemetry Station 2 data. The problem is presently being fully investigated at Telemetry Station 2.

The times of acquisition and loss of C-band radar reception are presented in table 6.3-II. The last station to report tracking of the C-band transponders was White Sands during the second orbital pass. Loss of C-band reception occurred at 03:08:36 g.e.t., which is approximately the

same time that the loss of signal from the link C telemetry occurred.

The following anomalies were noted in the performance of the network radar:

(1) At White Sands Missile Range, New Mexico, on the first orbital pass, the FPS-16 transmitter failed at the point of closest approach, which was attributed to a power surge.

(2) At Eglin Air Force Base, Florida, on the first orbital pass, severe countdown was experienced on the transponder reply which resulted in a loss of $2\frac{1}{2}$ minutes of valid tracking.

(3) Antigua Island, on the second orbital pass, did not acquire track although it received the transponder reply. Possibly, side-lobe returns prevented lock-on.

(4) California, on the second orbital pass, did not acquire valid track due to a 50-percent reduction in transmitter power, which was caused by an operator error in properly positioning a switch.

The network stations that reported skin tracking of the vehicle at various times throughout its orbital lifetime included Patrick Air Force Base, Florida; Grand Turk Island; Antigua Island; Ascension Island; Pretoria, South Africa; Carnarvon, Australia; California; White Sands Missile Range, New Mexico; and Eglin Air Force Base, Florida. Carnarvon reported the most extensive coverage, having skin tracked the spacecraft on passes 1, 12, 13, 14, 15, 16, 26, 27, 28, 29, 30, 31, 42, 43, 44, 45, 46, and 47.

TABLE 6.3-1 - TELEMETRY COVERAGE

[All times are ground elapsed time]

Station	Launch phase and first pass			Second pass			Third pass			Fourth pass		
	Acquisition	Duration of signal, hr:min:sec	Loss	Acquisition	Duration of signal, hr:min:sec	Loss	Acquisition	Duration of signal, hr:min:sec	Loss	Acquisition	Duration of signal, hr:min:sec	Loss
Eastern Test Range												
Cape Kennedy, Telemetry 2	00:00:00	00:09:46		01:35:50	01:41:55							
Cape Kennedy, Telemetry 3	00:00:00	00:10:00		01:35:35	01:42:20							
Grand Bahama Island	00:00:58	00:10:08										
San Salvador Island	00:01:57	00:11:00		01:39:30	01:47:42							
Antigua Island	00:05:48	00:14:33										
Ascension Island	00:20:35	00:28:40		02:05:42	02:12:39		^a 03:39:28	^a 03:47:22		^a 05:12:39	^a 05:21:02	
Pretoria, South Africa	00:32:20	00:40:20										
Manned Space Flight Network												
Carnarvon, Australia	00:49:44	00:59:40										
Bermuda	00:03:28	00:11:50										
Department of Defense Range Stations												
Hawaii	01:16:52	01:24:20		02:51:21	~2:57:10		^a 04:24:56	^a 04:31:35				
California	01:29:44	01:37:00		02:59:30	03:06:26							
White Sands Missile Range, N. Mex.	01:29:44	01:37:00										
Eglin Air Force Base, Fla.	01:33:57	01:41:13										

^a A and B links only

TABLE 6.3-II.- C-BAND RADAR COVERAGE

[All times are ground elapsed time]

Station	Launch phase and first pass			Second pass			Third pass		
	Duration of signal, hr:min:sec	Acquisition	Loss	Duration of signal, hr:min:sec	Acquisition	Loss	Duration of signal, hr:min:sec	Acquisition	Loss
Eastern Test Range									
Cape Kennedy	00:00:00	00:00:00	00:08:56	01:37:00	01:42:20				
Patrick Air Force Base	00:00:00	00:00:00	00:07:20						
Grand Bahama Island	00:01:09	00:01:09	00:09:28						
San Salvador Island	00:02:10	00:02:10	00:11:06						
Grand Turk Island	00:03:40	00:03:40	00:11:40						
Antigua Island	00:07:02	00:07:02	00:14:21						
Ascension Island	00:21:28	00:21:28	00:27:42						
Pretoria, South Africa	00:32:07	00:32:07	00:39:53	02:06:30	02:13:11				
Manned Space Flight Network									
Carnarvon, Australia	00:52:07	00:52:07	00:59:36						
Department of Defense Range Stations									
California	01:28:40	01:28:40	01:33:40	03:05:22	03:08:36				
White Sands Missile Range, N. Mex.	01:31:35	01:31:35	01:33:24						
Eglin Air Force Base, Fla.	01:34:08	01:34:08	01:35:21						

6.4 Data Coverage and Availability

Data for evaluation of the Apollo A-101 test mission included pre-launch hardline to ground, telemetry, radar, optical, meteorological, and environmental information (table 6.4-I). These data were obtained from both the Eastern Test Range and the Manned Space Flight Network through the Goddard Space Flight Center (GSFC) and through the Kennedy Space Center (KSC). Data were also provided by the U. S. Weather Bureau.

The recorded data were reduced at Cape Kennedy Telemetry Station 2, Manned Spacecraft Center Computation and Analysis Division in Houston, Texas, Marshall Space Flight Center in Huntsville, Alabama, and the contractor's facility at Downey, California.

The Operations Support, Plans, and Programs Office (OSPPO) of MSC-Florida Operations provided active liaison support for data reduction and data evaluation.

The delivery of many data items to OSPPO was delayed, as indicated in table 6.4-I, because of the new logistics channels established for this specific mission. The data liaison support by OSPPO caused no delay. For a complete outline of coverage planned from the range, see references 3 to 5.

The data listed in table 6.4-I will be on file at the Manned Spacecraft Center, Houston, Texas. Requests may be addressed to the Manager, Apollo Spacecraft Program Office.

Eastern Test Range and Kennedy Space Center.- Data were delivered to OSPPO and the evaluation team from ETR and from KSC via the KSC Data Coordination Office. Oscillograph charts and magnetic tape recordings of telemetry received at Cape Kennedy were made available approximately 3 hours after lift-off. Quick-look 4020 plots were provided in 35mm film format in T+8 hours. Quick-look trajectory tabulated data were obtained by MSC on the day after launch, and the first part of the final trajectory data was available in 4 calendar days. Magnetic tape recordings of telemetry received for orbital passes were available in 4 to 6 days after launch. First signal strength records from Cape Kennedy were received 7 days after the flight.

Engineering sequential film was planned for support of the mission from three fixed cameras and four tracking cameras. They were to provide 16mm and 35mm photographic coverage of the BP-13 spacecraft. Only the film from three of the tracking cameras was available for study by the evaluation team, the other four engineering sequential film being missent to another organization. The Vero Beach ROTI tracking film did not provide coverage of tower jettison as requested. However, good quality coverage of the spacecraft was provided prior to and following tower jettison.

Goddard Space Flight Center. - The GSFC network stations recorded telemetry data and tracked the spacecraft during the mission. Tracking data from the Bermuda network station were used in calculating orbital trajectory data and insertion parameters. Corrected trajectory data were presented from calculations made at Greenbelt, Maryland, and were made available in 2 days after launch. The first signal strength and telemetry (magnetic tapes) from down range stations arrived at MSC-Florida Operations 6 days after the flight.

MSC Houston. - Spacecraft telemetry data were processed by the Computation and Analysis Division, MSC, Houston, with support from Instrumentation and Electrical Systems Division, MSC, Houston. A tape copy from Telemetry Station 2 (Tel II) was received in Houston at T + 10 hours, and a copy from Antigua, at T + 20 hours. The first package of engineering analysis plots from these data tapes was provided to the evaluation team at T + 4 days. The package contained time-history data of accelerations, electrical information, temperatures, heat flux, strain gages, and RMS of low-frequency accelerations, fluctuating pressures, and radial vibrations. These data were reduced by using telemetry tapes from both Tel II and Antigua. The second package, which was available within 5 calendar days, contained the time histories of conical pressure coefficients and power spectral density (PSD) of low-frequency accelerations, strain gages, and radial vibrations. The pressure coefficients were determined by using the measured conical surface pressure and the dynamic pressure based on the measured atmospheric density at the time of launch. The PSD was plotted by using the Tel II and Antigua tapes and was produced by a digital-computer process. The third package, which was available within 7 days after launch, contained PSD plots of the same parameters included in the second package. The PSD was plotted by using the Tel II and Antigua tapes and was produced by an analog process with equipment operated by the General Instrumentation Branch of the Instrumentation and Electrical Systems Division.

Lift-off (T-0) was established as 12:07:00:42 a.m. e.s.t. (17:07:00:42 G.m.t.). Prelaunch R and Z calibration values, which were recorded for the continuous and high-level commutator parameters, were within 1 percent of the orbital values. No corrections were made as a result of R and Z calibration changes because the change to the data would not have been significant. The changes from the original R and Z calibration values were also checked for the low-level commutator and were found to be greater than 1 percent. However, because of the type of calibration circuit utilized, no changes were made to the calibration curves to correct for the R and Z calibration changes.

All pressure measurements were biased to read ambient pressure at launch, and the accelerations were biased to read 1g on the X-axis and zero-g on the Y- and Z-axes.

[REDACTED]

In processing the BP-13 data, an edit routine was used to determine changes of 2 percent or greater of telemetry full scale in the commutator data and 3 percent or greater of telemetry full scale in the continuous data. In addition to the data being tabulated and plotted at a basis rate, a point was tabulated and plotted for each change greater than the predetermined values of 2 and 3 percent.

Telemetry tape from Tel II was used for reduced data from T + 400 seconds through insertion. The Tel II tape showed the 2.7-second dropout at the time of launch-vehicle staging. Reasons for the dropout are discussed in section 4.2, Instrumentation. The values printed for all parameters during this time were considered to be invalid. None of the available telemetry tapes provided data for this 2.7-second period.

The engineering scales were established for most of the plots to be in accordance with the calibrated instrument range and to provide a reading accuracy of approximately 2 percent of telemetry full scale. Tabulation and plots were produced for all parameters that were planned before the flight, except for those parameters whose instruments failed to operate properly. These failures are discussed in section 4.2, Instrumentation.

Data were processed from the Antigua tape for the second pass; that is, as the spacecraft began its second pass and was within telemetry contact. No other orbital data processing was planned to support this report, but supplemental processing will be done to include orbital-pass data at a later date.

The data reduction operation was planned to provide data to the analysts as rapidly as possible by utilizing high-speed reproduction methods. Special plots requested during the evaluation and report-writing period were provided after the system analysts had reviewed data initially processed.

Additional copies of the engineering plots processed by MSC Houston are available through the Apollo Spacecraft Program Office.

Data transmitted by the launch-vehicle telemetry from instrumentation in the spacecraft were processed by MSFC in accordance with previous arrangements made between MSC and MSFC. IBM compatible tape copies were forwarded to MSC Houston and reduced engineering plots to the test evaluation team at MSC FO at T + 13 days.

Engineering plots received from MSFC included adapter radial vibrations, service module acoustic, Q-ball, and launch vehicle attitude gyro data.

[REDACTED]

TABLE 6.4-I. - DATA AVAILABILITY

Data type	Presentation	Anticipated availability (a)	Date received (a)
Telemetry data			
Telemetry Building 2, recorder 3	$\frac{1}{2}$ -inch magnetic tape	4 H	5 H
Telemetry Building 3, recorder 3	$\frac{1}{2}$ -inch magnetic tape	4 H	4 CD
Grand Bahama Island, recorder 3	$\frac{1}{2}$ -inch magnetic tape	ASAP	4 CD
Antigua, recorder 3	$\frac{1}{2}$ -inch magnetic tape	ASAP	4 CD
Ascension, recorder 3	$\frac{1}{2}$ -inch magnetic tape	ASAP	6 CD
Pretoria, recorder 3	$\frac{1}{2}$ -inch magnetic tape	ASAP	6 CD
DOD Stations - Point Arguelo, Hawaii, Corpus Christi	1-inch magnetic tape	ASAP	X
DOD Station-Eglin Air Force Base	$\frac{1}{2}$ -inch magnetic tape	ASAP	8 CD
Composite recording of spacecraft links from all NASA stations	1-inch magnetic tape	ASAP	4 CD
Telemetry signal strength recordings from all ETR stations	Strip chart	2 CD	7 CD (Tel 3 at T + 9 CD)
Telemetry signal strength recordings from all non-ETR, DOD, and NASA stations	Strip chart	ASAP	7 CD
Telemetry data sheet (ETR)	Log sheet	2 CD	(b)
Telemetry data sheet all non-ETR, DOD, and NASA stations	Log sheet	ASAP	(b)
Preliminary estimate of data coverage	Sheet	2 H	4 CD
Preliminary telemetry messages	Sheet	ASAP	During and 1 hr after flight

^aKey:

H - Hour

CD - Calendar Day

ASAP - As soon as possible

WD - Working Day

^bData requested but not received during the postlaunch reporting period

TABLE 6.4-I.- DATA AVAILABILITY - Continued

Data type	Presentation	Anticipated availability (a)	Date received (a)
Telemetry data			
Real time recordings	Oscillograph rolls	3 H	3 H
	Magnetic tapes	8 H	6 H
Telemetry engineering data: Commutated channels	35mm film	8 H	8 H
	Plots	14 H	14 H
Continuous channels	35mm film	5 CD	5 CD
	Plots	5 CD	5 CD
Radar			
Impact predictor data (Special trajectory and aerodynamic parameters)	Tab printout computer output tape	1 CD	1 CD
		1 CD	(b)
Position data	Computer tape tab printout	3 WD	4 CD
		3 CD	4 CD
Velocity data	Computer tape tab printout	3 WD	4 CD
		3 CD	4 CD
Acceleration data	Computer tape tab printout	3 WD	4 CD
		3 CD	4 CD
Special trajectory parameters	Computer tape tab printout	3 WD	(b)
		3 WD	(b)
Attitude data	Tab printout	3 CD	(b)
Launch escape tower position and velocity	Tab printout	3 WD	(Requirement submitted too late to be supported by range)
Best estimate of trajectory	Tab printout	3 CD	(b)

^aKey:

H - Hour

CD - Calendar Day

ASAP - As soon as possible

WD - Working Day

^bData requested but not received during the postlaunch reporting period

TABLE 6.4-I. - DATA AVAILABILITY - Continued

Data type	Presentation	Anticipated availability (a)	Date received (a)
Radar			
Final calculations of position and velocity from insertion to completion of first pass	Tab printout Tape	3 CD 3 CD	(c) (c)
Final calculations of special trajectory items from insertion to completion of first pass	Tab printout Tape	3 CD	(c)
Orbital flight parameters (per letter from MSC/FO to GSFC, 1-15-64)	Teletype message	ASAP	3 H
Radar beacon log Cape Kennedy	Log format	1 CD	4 CD
Radar data sheet (uprange ETR)	Log format	1 CD	6 CD
Radar data sheet (downrange ETR)	Log format	4 CD	6 CD
Radar data sheet all non-ETR, DOD, and NASA stations	Log format	ASAP	7 CD
Radar event record (uprange ETR)	Strip chart	1 CD	6 CD
Radar event record (downrange ETR)	Strip chart	6 CD	(b)
Plotting board charts (copies of charts made by KSC from station 1 and LCC 37)	Chart	3 H	Sta. 1-4H LCC-37-4H
Plotting board charts (downrange)	Chart	2 CD	7 CD
Aerodynamic parameters (velocity of sound, dynamic pressure, Mach number, Reynolds number)	Tabular	3 CD	Working paper not submitted in time for computer programming; should be available by June.
Radar event record from all non-ETR, DOD, and NASA stations	Strip chart	ASAP	7 CD

^aKey:

H - Hour

CD - Calendar Day

ASAP - As soon as possible

WD - Working Day

^bData requested but not received during the postlaunch reporting period^cInitial trajectory conditions only have been received to perform analysis for section 3.

TABLE 6.4-I. - DATA AVAILABILITY - Continued

Data type	Presentation	Anticipated availability (a)	Date received (a)
Radar			
Radar function record (uprange ETR)	Strip chart	4 CD	6 CD
Radar function record (downrange ETR)	Strip chart	4 CD	(b)
Radar function record from all non-ETR, DOD, and NASA stations	Strip chart	ASAP	(b)
Optical data			
Sequential events (times derived from optics from lift-off, S-I burnout, S-IV ignition, and LES jettison)	Tab printout	1 CD	1 CD
Spacecraft umbilical disconnect	Engineering prints 16mm	5 CD	(b)
Structural surveillance of spacecraft during launch	Engineering prints 16mm	5 CD	(b)
Lift-off and early flight	Engineering prints 16mm	5 CD	(b)
Long focal length optical tracking	16mm - Vero Beach engineering print 16mm - Melbourne Beach engineering print	5 CD	6 CD
Meteorological data			
Weather forecasts: Forecasts will be made by Space Flight Weather (U.S. Weather Bureau assigned to NASA)		Preflight and launch	As required
Surface weather observation for T-O (temperature, pressures, R.D., wind direction, and velocity and density)	Tabular	1 CD	8 H
Cloud coverage and visibility from T-O (uprange)	Tabular	1 CD	8 H

^aKey:

H - Hour

CD - Calendar Day

ASAP - As soon as possible

WD - Working Day

^bData requested but not received during the postlaunch reporting period

TABLE 6.4-I. - DATA AVAILABILITY - Concluded

Data type	Presentation	Anticipated availability (a)	Date received (a)
Meteorological data			
Cloud coverage and visibility for T-0 (downrange)	Tabular	1 CD	4 CD
Upper air weather observation for T-0 (temperature, pressure, R.H., wind direction, and velocity and density). (Both uprange and downrange)	Tab printout computer output tapes	1 CD	Cape - 2 CD Other - 6 CD
Prelaunch upper air observation (temperature, pressure, R.H., wind direction and velocity). (Uprange and downrange) surface to 40 km	Tab printout	4 H (after release)	2 CD
Prelaunch upper air observations (temperature, pressure, density, wind direction and velocity) (Uprange and downrange 25 to 90 km)	Tab printout	4 H (after release)	(b)
Ground and environmental measurements			
Flash reports from ground and environment (G and E) measuring program	Report	As available	(b)
Ground and environmental (G and E) measuring numbers			
12CD3-Water-glycol inlet temperature	Strip chart		4 CD
12CD4-Water-glycol outlet temperature	Strip chart		4 CD
12CD5-Air temperature at 268-ft level	Strip chart		4 CD
13CD9-Air temperature at 188-ft level	Strip chart		4 CD
22C29-Vibration deck 188-ft level vertical	Strip chart		(b)
22C30-Vibration deck 188-ft level (58-238 deg)	Strip chart		(b)
22C31-Vibration deck 188-ft level (148-328 deg)	Strip chart		(b)
25C11-Acoustic at 188-ft level umbilical tower	Strip chart		(b)

^aKey:

H - Hour

CD - Calendar Day

ASAP - As soon as possible

WD - Working Day

^bData requested but not received during the postlaunch reporting period

7.0 CONCLUDING REMARKS

All of the spacecraft test objectives for the Apollo mission A-101 were fulfilled:

1. The boilerplate spacecraft BP-13 mated satisfactorily with the SA-6 launch vehicle and all systems and interfaces were compatible under preflight, launch, and orbital conditions.
2. Satisfactory engineering data covering designated parameters of spacecraft launch environment were obtained for use in verifying or determining spacecraft design criteria for Apollo earth orbital missions.
3. The launch environment conditions measured did not exceed the criteria used in the design of the boilerplate spacecraft.
4. The tower jettison motor propelled launch escape subsystem clear of the spacecraft as required.
5. The launch escape subsystem structure performed satisfactorily under flight loading conditions.
6. Ground support handling equipment and procedures were used successfully during prelaunch and countdown operations.

The flight trajectory of the mission provided the launch environment required.

Spacecraft subsystems including instrumentation, performed the functions required for a satisfactory mission.

8.0 REFERENCES

1. Anon.: An Investigation of Aerodynamic Noise Measured on a 0.055-Scale Apollo/Saturn Vehicle in the NASA Ames 14-Foot Transonic and 9 x 7-Foot Supersonic Wind Tunnels. SID 63-1480 [NAS 9-150], North American Aviation, Inc., Dec. 31, 1963. [PSTL-1]
2. Staff of Saturn Flight Evaluation Working Group: Results of the Sixth Saturn I Launch Vehicle Test Flight. NASA George C. Marshall Space Flight Center.
3. Anon.: Data Acquisition Plan for Apollo Mission A-101 (SA-6/BP-13). NASA Manned Spacecraft Center, Florida Operations, May 15, 1964.
4. Anon.: Saturn Launch (Test Code B). Operations Directive no. 2400, Air Force Missile Test Center, Nov. 1, 1963 (supersedes OD 2400, Sept. 19, 1961.)
5. Anon.: Orbital Tracking and Data Acquisition Saturn SA-6. Operations Directive no. 2460, Air Force Missile Test Center, May 4, 1964.